EPRI
Electric Power
Research Institute

Keywords:
Circuit Breakers
Gas-Blast Interrupters
$SF_6$

EPRI EL-3100
Project 478
Final Report
May 1983

EPRI-EL--3100

DE83 902190

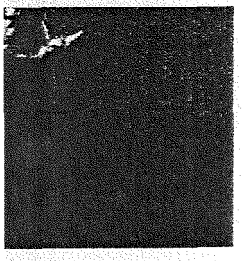

# High-Capacity Single-Pressure $SF_6$ Interrupters

Prepared by
Westinghouse Electric Corporation
Trafford, Pennsylvania

## DISCLAIMER

# High-Capacity Single-Pressure $SF_6$ Interrupters

EL-3100
Research Project 478

Final Report, May 1983

Prepared by

WESTINGHOUSE ELECTRIC CORPORATION
Power Circuit Breaker Division
Forbes Road
Trafford, Pennsylvania 15085

Authors
J. R. Rostron
L. E. Berkebile
H. E. Spindle



Prepared for

Electric Power Research Institute
3412 Hillview Avenue
Palo Alto, California 94304

EPRI Project Manager
N. G. Hingorani

Consultant
G. Bates

Transmission Substations Program
Electrical Systems Division

## ORDERING INFORMATION

Requests for copies of this report should be directed to Research Reports Center (RRC), Box 50490, Palo Alto, CA 94303, (415) 965-4081. There is no charge for reports requested by EPRI member utilities and affiliates, U.S. utility associations, U.S. government agencies (federal, state, and local), media, and foreign organizations with which EPRI has an information exchange agreement. On request, RRC will send a catalog of EPRI reports.




Prepared by
Westinghouse Electric Corporation
Trafford, Pennsylvania

## ABSTRACT

The object of this project was to design and develop a high-voltage, single-pressure, $SF_6$ interrupter with an interrupting capability of 120 kA at 145 kV with a continuous current rating of 5000 A and an interrupting time of 1.5 cycles or less. A second objective of 100 kA at 242 kV was added during the project. Mathematical models were used to extrapolate design requirements from existing data for 63 and 80 kA. Two model puffers, one liquid and the other gas, were designed and tested to obtain data at 100 kA. An interrupter, optimized on the basis of total prospective breaker cost, was designed using the mathematical models. A study was made of the construction materials to operate under the high-stress conditions in this interrupter. Existing high-speed movies of high-current arcs under double-flow conditions were analyzed to obtain more information for modeling the interrupter. The optimized interrupter design was built and tested. The interrupting capability confirmed calculations of predicted performance near current zero; however, the dielectric strength after interrupting these high-current arcs was not adequate for the 145-kV or the 242-kV ratings. The dielectric strength was reduced by hot gases flowing out of the interrupter. In conclusion, valuable data have been obtained for modeling the $SF_6$ puffer interrupter for high currents. A model is needed that will predict performance in the critical post-interruption period when hot gases reduce the dielectric strength of the interrupter.

## EPRI PERSPECTIVE

### PROJECT DESCRIPTION

Electric utilities need equipment with a high level of reliability, and new technologies that promise considerable improvement in reliability as well as reductions in cost must be constantly pursued. The use of $SF_6$ gas for arc interruption has gained wide acceptance in circuit breakers that use a two-pressure gas system to provide the necessary gas flow for arc interruption. However, circuit breakers that use a single-pressure $SF_6$ system are more desirable; they would not require the compressor systems, the high-pressure reservoirs with their gas heaters, and the controls associated with the two-pressure gas system and thus would inherently be more reliable and less costly. In single-pressure breakers, the $SF_6$ gas could be used in the gaseous state such as in puffer-type or liquid-state breakers. While the puffer breaker technology was not new, it had not been sufficiently developed to permit design of interrupters having the interrupting current and voltage ratings that would meet the forecasted requirements. The amount of work that had been done on liquid interrupters was quite limited.

System growth is demanding higher interrupting duties and voltage, and continuous current ratings are increasing. These facts make it desirable to increase the interrupter voltage-handling capability so as to keep the number of interrupters per pole to a minimum, which would improve reliability and reduce cost. The higher continuous current rating makes higher operating temperatures desirable; therefore, materials normally used had to be investigated to determine their performance in the environment that is associated with $SF_6$ interrupters at higher temperatures.

### PROJECT OBJECTIVE

This project (RP478) initially was a 39-month investigation conducted to design, build, and test a single-pressure $SF_6$ interrupter with an interrupting rating of 120 kA at 145 kV with a continuous current rating of 5000 A. The project was later changed to have a dual rating goal of 120 kA at 145 kV or 100kA at 242 kV.

PROJECT RESULTS

An initial study was made to determine if high-pressure $SF_6$ puffer or liquid $SF_6$ technology should be used to achieve the goals of this project. Model interrupters of each type were built and tested up to 100kA, and their performance was compared. On the basis of comparative test performance of the model interrupters and upon evaluation of cost, reliability, and maintainability of breakers utilizing the two-interrupter concepts, a decision was made to develop the puffer-type interrupter. The test data on the model interrupter were promising and resulted in a decision to go ahead with the dual rating with an $SF_6$ fill pressure of 75 psig.

At the same time, work was done to evaluate materials for use in high-duty interrupters that used $SF_6$. This study revealed that many of the materials already in use for $SF_6$ interrupters could be used at the higher temperatures desired.

The prototype interrupter was designed, built, and tested, but it fell short of achieving the ratings set as goals. The failures were dielectric in nature, and the prototype failed at values near 100 kA for long arcing times. There was adequate initial thermal recovery, but failure occurred in the downstream region as delayed dielectric breakdowns due to recovery voltage. Due to a decrease in interest in very high-current interrupters, an effort was not made to solve the problem, and the work was stopped. The necessary know-how had been developed for present needs and it was demonstrated that the puffer-type interrupter can be designed for higher current and voltages than had been available previously. It was also determined that materials could be operated at the higher temperatures necessary for higher continuous current ratings. There are always side benefits to projects of this type, as knowledge can be used in the development of lower rated interruptors.

Narain Hingorani, Project Manager
Electrical Systems Division

ACKNOWLEDGMENT

The authors wish to acknowledge the contribution made to this project by many individuals within Westinghouse. In particular Zeno Neri and Stan Billings contributed to the solution of dielectric problems. Don Fahrnkopf worked diligently to obtain high power tests at current levels higher than ever made before in his laboratory. Bill Fischer designed an excellent liquid $SF_6$ interrupter that performed very well. Kue Yoon carried out the materials study. Charles Cromer contributed many useful ideas for the interrupter designs. Sam Kolocouris patiently made the hundreds of charts and curves and illustrations used during the project and many included in this report. Finally many of the scientists at the Westinghouse R&D Center contributed ideas, calculations and analyses for this project. Among those contributors were; L. S. Frost, B. Swanson, J. Lowkay, T. Dakin and A. Lee.

CONTENTS

ILLUSTRATIONS

TABLES

# SUMMARY

## 1. INTRODUCTION

This report describes work that was done on an EPRI funded project to advance the state of the art of $SF_6$ circuit interrupters. In 1975 with the increasing power system generating capabilities it was evident that the need for both higher voltage and current ratings per interrupter would become more prevalent, networks would become more intricate and the reliability, as well as the speed with which interruption takes place and the service restored would have to increase. The major determining factor of power circuit breaker product cost was the number of arc interrupters and the mass of the moving parts. With the cost of materials rising very rapidly and the need for miniaturization in Gas-Insulated-Substations, there was a strong need for major improvement in interrupter capability. Other needs were also apparent having to do with the changing sociological conditions in the United States. Power circuit interrupters were needed which:

a. Interrupt more current.
b. Withstand more voltage (per unit interrupter).
c. Operate faster (system stability, limitation of current damage).
d. Are more reliable (fewer parts, components).
e. Are compact.
f. Are ecologically compatible.
g. Cost less.

This program was formulated to meet these needs.

## 2. OBJECTIVE

The objective of this project was to design and develop a high voltage single pressure, $SF_6$ interrupter with an interrupting capability of 120 kA for a single break per phase, for a 145 kV system with a continuous current rating of 5000 Amps and an interrupting time of 1.5 cycles or less.

## 3. ANALYSIS

Mathematical models for puffer type circuit breakers have been developed and refined over the past several years. In this project a computer was used to model the masses and flexibility of the complete circuit breaker, the mechanism driving forces and the pressure forces developed by the interrupter.

Background information was available as high speed arc photographs taken from an interrupter with mirrors to photograph two axies of the arc simultaneously. In this project the photographs and corresponding electrical data were compiled into a report. Analysis of the data showed that the arc light intensity was proportional to the arc conductance during the 100 micro-seconds preceding current zero. The region downstream of the interrupter nozzle throat looses conductance most rapidly and hence was shown to be very effective in the interrupting process.

The environment of high temperatures, high pressures, and arc products expected in a high performance interrupter could overstress materials that were used in the past. Materials limitations prior to this work were 105°C for insulating materials and 130°C for structural and conductor materials. In this project insulator materials were tested at 135°C and structural and conductor materials were tested at 150°C.

Most of the fourteen insulating materials tested were unchanged by the tests. Nylon was appreciably degraded by the test conditions whereas teflon and Kel-F had no apparent change. Metal surfaces showed only a slight hardness increase for eight types of steel, copper, and aluminum alloys. Highly stressed metal samples showed no relaxation of stress due to exposure to arc products. Copper finger contact systems showed no appreciable degradation while silver plated aluminum contacts showed serious deterioration at 150°C in arced $SF_6$.

Measurement of interrupter pressure and contact travel are important in analyzing and improving interrupter performance. This data is difficult to obtain due to the electrical interference present during high current high power tests. A new approach was taken to make mechanical measurements more reliable and accurate. First pressure transducers and travel indicators were selected then a fiber optic signal transmission link was designed and built for this project.

## 4. MODEL SELECTION

After the analysis of existing data it was decided that better data was required to permit the adequate design of an interrupter. The decision was made to build and test model interrupters using both liquid and high pressure gas to obtain test data at about 100 kA. With this data then it would be possible to extrapolate by only 20% to reach the project goal.

Two model double flow interrupters were designed using a teflon nozzle downstream and a metal nozzle in the moving contact. The design parameters were differential pressure at current zero, nozzle diameter, and arc length. There is a critical relationship between the puffer velocity, gas fill pressure, nozzle area and current. Gas flow through the nozzle including partial blocking of the nozzle by the arc determines the maximum pressure that can be achieved at current zero. The length of the interrupter gap is critical to the ability to withstand maximum recovery voltages. Liquid interrupters differ from gas interrupters only in that different techniques are used for generating pressure. Since the temperature of the arc is thousands of degrees Kelvin and the liquid temperature is of the order of 300°K, there is gaseous $SF_6$ between the arc and the liquid. The arc interruption process is quite similar to that of a gas interrupter for identical conditions. Therefore, the same criteria should be used for both liquid and gas.

The liquid $SF_6$ puffer interrupter used two high speed pump cylinders to force the liquid $SF_6$ at 1500 psig around the arc. A novel feature of the liquid interrupter was an accumulator which reduces pressure variations produced by the high current arc in the interrupter nozzles. The net effect is that the pressure at current zero is doubled.

The high pressure gas puffer interrupter was designed to operate at 300 psi fill pressure.

## 5. MODEL TESTS

Mechanical, dielectric and interrupting tests were made with the liquid and high pressure puffer interrupters.

Mechanical tests were made to adjust the mechanical system for each model for interrupting tests. Dielectric tests of the liquid model were rather extensive because little data was available for liquid gaps with interrupter components and

no data was available for the dielectric strength of combined gas and liquid in the gap. These tests showed that a liquid interrupter required a gas gap in series with the liquid to obtain the dielectric strength required for this application.

In interrupting tests of both the liquid and gas puffer interrupters the pressure required for interruption was significantly less than calculated using the computer interrupter model. The liquid interrupter was able to interrupt the bus fault and short line fault requirements for a 100 kA 145 kV rating over a short range of arcing times. The gas interrupter achieved interruption with fill pressures lower than the anticipated 300 psig. The fill pressure was reduced in steps to determine the minimum fill pressure that could be used for this interrupter. It interrupted 80% short line faults and bus faults for the 100 kA rating with 125 and 75 psig fill pressures respectively. These results were so encouraging that it was decided to expand the scope of the project to include a 242 kV 100 kA rating for a single interrupter.

## 6. PROTOTYPE SELECTION

Based on the results of these tests the liquid interrupter was dropped from further consideration. Maintaining liquid level in the interrupter would require cooling in the summer and heating in the winter. This over-shadowed any advantages of the higher pressures that could be developed.

## 7. DESIGN OF THE PROTOTYPE INTERRUPTER

The computer model was improved and the higher current test data provided better guidelines for extrapolation to 120 kA. The basis for optimization was reviewed and the components of circuit breaker cost were evaluated. The components evaluated were the breaker tank, heating the gas to prevent liquifiaction, the mechanism and line to ground capacitors.

Two novel methods for achieving high differential pressures were considered and compared with the simple puffer. Since the simple puffer was cheaper and the driving requirements were similar it was selected for prototype development.

Computer analysis lead to the selection of a puffer piston diameter of 9.75 inches with a stroke of 6.5 inches. This provides adequate dielectric strength for the 242 kV rating and when operated at 30 feet per second provides the dielectric strength required for interrupting line charging currents.

## 8. DESCRIPTION OF PROTOTYPE TESTS

The test program planned for the prototype consisted of:

a. 242 kV line dropping (capacitor switching)
b. 120 kA - 145 kV 85% short line fault (i.e. 102 kA)
c. 100 kA - 242 kV bus fault
d. 120 kA - 145 kV bus fault
e. 100 kA - 242 kV 90% short line fault

The interrupter successfully interrupted 200 ampere charging current when driven at design velocity. At 75% of design velocity the interrupter showed one reignition out of 16 tests. This would produce less than 1 per unit switching surge on a connected transmission line.

Seven tests were made for a 100 kA 242 kV bus fault. The first two tests were successful at arcing times of 7.5 and 9 ms. The third and subsequent tests showed dielectric breakdown inside the interrupter chamber. When the interrupter was opened and examined it was found that a shield had been blown off and the fiber glass test chamber had been carbonized.

After repair a second series of tests under bus fault conditions showed that the interrupter broke down at low voltage (100 kV) at long arcing times even though the interrupter and the test chamber withstood the full required test voltage at a lower current (20 kA).

It was concluded that the confined space of the insulating chamber was too small to permit mixing and cooling of the hot gases produced by the interrupter at long arcing times. Therefore a dead tank design with additional coolers and increased gas volume was recommended.

## 9. DEAD TANK PROTOTYPE

To provide the extra volume and cooling capacity an existing circuit breaker tank was adapted to the prototype. Additions clearance flow area for hot gases, a more effective cooler and a large plenum were provided. The high voltage connection to the interrupter was made through a cast epoxy bushing.

## 10. DEAD TANK PROTOTYPE TESTS

The first tests in this configuration were made at the 120 kA 145 kV 100% bus fault rating. These tests showed total failure at all arcing times. The next tests were made for the 145 kV 120 kA 85% SLF rating. These tests also resulted in failures.

The next test was made at the 242 kV 100 kA 90% SLF arcing. The interrupter worked at 14.5 ms arcing time and withstood the line side transient at 15.3 ms arcing time. However it broke down later at 90% of the recovery voltage. A second series of tests under the same conditions showed that the interrupter could withstand the line side transient at arcing times of 10 and 17.5 ms but it broke down at about 50% of the required recovery voltage.

## 11. CONCLUSIONS

The prototype interrupter developed during this project does not have the ability to interrupt the objective ratings. The interrupting chamber was shown to interrupt the full requirements for up 242 kV 100 kA only at short arcing times. The downstream flow region of the interrupter was not able to absorb all of the hot gases produced at long arcing times. Hot gases in the downstream region lead to delayed breakdown of the interrupter gap.

Materials have been verified for high temperature high stress interrupters. Virgin teflon and Kel-F, coated cast epoxy resin and coated glass reinforced epoxy resins were shown to be suitable for use at 135°C . Nylon reinforced polyesters and porcelain were shown to be unsuitable for this application. The common metals of construction were shown to operate safely at up to 150°C. Copper and silver contacts perform satisfactorily in this environment. Only silver plated aluminum contacts proved to be inadequate for this high stress application.

Computer models for circuit breakers have been improved in this project so that they can be applied regularly to the design of puffer circuit breakers for all ratings.

## 12. RECOMMENDATIONS

This project shows the need for further study of the flow and cooling of the hot gases produced by $SF_6$ interrupters. There is good test data for the characteristics of the upstream portion of $SF_6$ interrupters, where the initial energy balance interruption of current occurs. However the equally critical downstream portion of the interrupter where the hot arc gases can lead to dielectric failure has not been carefully studied. This project has shown that these factors are critical in very high current interrupters.

Therefore it is recommended that a study should be initiated to measure the flow patterns and cooling of exhaust gases from high current interrupters. This should include the development of efficient coolers and flow directors to control the hot gases.

Section 1

# PROJECT DESCRIPTION

## 1.1 BACKGROUND

Sulphur hexaflouride ($SF_6$) has been used, in gaseous form, as an insulating and interrupting medium in electrical apparatus for many years. The majority of early commercial $SF_6$ circuit breakers utilized two pressure interrupters. In these interrupters, $SF_6$ was stored at high pressure (180 to 280 psig) to provide gas blast for interruption and low pressure $SF_6$ (30 to 60 psig) was used for insulation. The two pressure system required auxiliary heaters to prevent liquification of the high pressure $SF_6$ gas at low temperatures and compressor to maintain the gas at high pressure.

Single pressure puffer and self generating circuit breakers were investigated early in the development of $SF_6$ circuit breakers but were not used for significant commercial production until recent years, because early single pressure breakers had low interrupting capability. Two pressure breakers, employing high pressure $SF_6$ for interruption provided higher interrupting capability during early $SF_6$ interrupter development. Two pressure breakers have high pressure $SF_6$ constantly stored at high pressure while single pressure breakers must develop the necessary interrupting pressure during their opening operation.

The best single pressure interrupter is the "puffer". This interrupter uses a single stroke compressor attached directly to the interrupters to produce a $SF_6$ gas blast for arc interruption. Nominal $SF_6$ gas pressure is usually 75 psig. Puffer circuit breakers are generally available 30 kA to 63 kA ratings.

However since the puffer can generate high pressure very quickly during the opening stroke it has the potential for developing much higher pressures than can be stored in a practical two pressure $SF_6$ circuit breaker. At the inception of this project it was assumed that these high pressures would be achieved by starting with a higher fill pressure of 200 to 300 psig or by starting with liquid $SF_6$ which is relatively incompressible and can therefore achieve much higher pressures.

Puffer circuit breakers have so many advantages over two pressure breakers that it is desirable to explore means of extending their interrupting rating to higher currents. These advantages include simplicity, and higher reliability, and fewer seals. An $SF_6$ gas compressor is not required. High pressure reservoirs and piping are eliminated. Blast valves, to control the high pressure gas blast at the interrupter, are not needed.

This research program was proposed to investigate the arc quenching and interrupting characteristics of high density gaseous $SF_6$ and liquid $SF_6$ leading to extremely high capacity single pressure interrupters. The initial goal was 120 kA, at 145 kV interrupter with 5 kA continuous current rating. This was later increased to 120 kA to 145 kV and 100 kA at 242 kV. The resulting circuit breaker would be faster than present day designs, smaller and more reliable at lower cost.

## 1.2 ORIGINAL PROJECT PLAN - FIVE TASKS

Task 1 was to perform preliminary research on liquid and high-pressure $SF_6$ for circuit interruption, determining physical properties and dielectric and arc interruption characteristics. From this background information, a prototype liquid $SF_6$ interrupter was to be designed and tested.

Task 2 was the identification of the parameters of $SF_6$ and other materials to be used in circuit breaker interrupters which may be affected by high temperature, high pressure, and high dielectric stress; and to determine the long-term effects of this environment on these same materials and $SF_6$, including arc-decomposed $SF_6$.

Task 3 was a study of previously-made high-speed photographic arc tests to determine parameters affecting arc interruption, design improved test models and perform photographic studies of power arcs under high-pressure gas flow conditions.

Task 4 was to develop concepts of a high-pressure $SF_6$ puffer interrupter which would produce 60 to 80 atmosphere interrupting pressure from a starting or fill pressure of 10 to 20 atmospheres and to design and prepare drawings of a prototype interrupter.

Task 5 was the comparative analysis of the liquid $SF_6$ and high-pressure $SF_6$ prototype interrupters and the selection of one of these two interrupters for

further development. The selected interrupter was to be manufactured, tested, and the results analyzed and a recommendation made for a follow-on project to design, manufacture, and test a complete three-pole circuit breaker.

## 1.3 PROJECT PLAN CHANGES

During the early stages of this project the plan was modified to expedite the development of a high current interrupter. Instead of the preliminary research on liquid and high pressure $SF_6$ in Part 1 and the further arc studies of Part 3, a full scale model liquid interrupter and a full scale model high pressure puffer interrupter were designed and built for interrupting tests in the 100 ka current range. Data obtained from tests on these models were used to extrapolate to the design of the 120 kA prototype interrupter in Part 4.

## 1.4 REVISED PROJECT PLAN

Part 1 consisted of preliminary research using available data to project the requirements and performance of high pressure liquid and gas $SF_6$ interrupters. Then two model interrupters were built and tested at currents up to 100 kA to develop interrupter design parameters for the 120 kA rating. The results of these preliminary model tests were very encouraging. The performance goals were increased to two different ratings for the same proposed interrupter; 120 kA at 145 kV and 100 kA at 242 kV.

Part 2 was unchanged.

Part 3 was limited to reporting the results of previously made high-speed photographic arc studies. No further photographic studies were planned. A summary and analysis of these photographic studies is presented in Appendix F.

Part 4 consisted of the development of concepts for both liquid and gas high pressure interrupters based on the results of the model tests in Part 1.

Part 5 was unchanged.

At the conclusion of the tests in Part 5 it was concluded that the interrupter did not meet the goals and that due to the limitations of funds the project should be terminated and the final report prepared.

Section 2

# MODEL INTERRUPTERS

Preliminary estimates of the high pressure interrupter parameters for double flow interrupters for 100 kA bus fault and 80% short line faults are shown in Figure 2-1. A double flow interrupter is assumed to be equivalent to two breaks for this nomograph because the arc is acted on by the two nozzles in series. Curve C shows that for double flow nozzles of approximately 1.5 inch diameter the required total interrupting pressure at current zero is about 900 psi for the gas interrupter and 1400 psi for the liquid interrupter where 3000 pF shunt capacitance would be used for the gas interrupter and 1000 pF would be used for the liquid interrupter. In both cases no shunt resistor would be required.

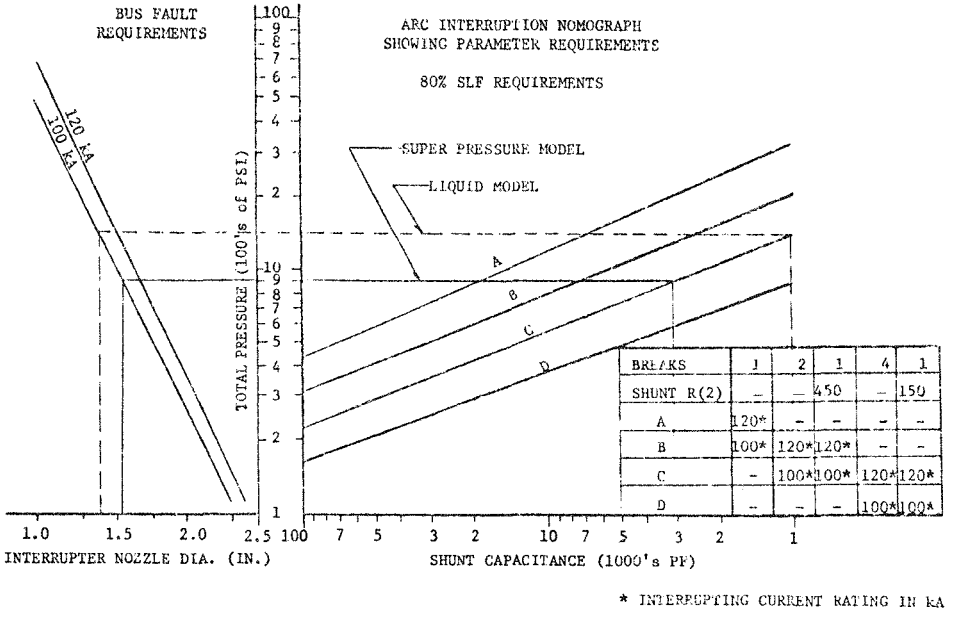


Figure 2-1 Arc Interrupting Nomograph Showing Parameter Requirements

Based upon previous experience the three critical performance requirements for $SF_6$ interrupters were known to be:

a. Interruption of bus faults which require the maximum currents with a relatively high rate of recovery of restored voltage across the interrupter.

b. Short line faults which produce the highest rates of rise of recovery voltage across the interrupter at currents from 70 to 90% of the maximum bus fault current.

c. Line dropping or capacitor switching where the interrupted current is quite low and the interrupter can break the current with almost no contact gap and must therefore withstand 2.4 p.u. 8.3 milliseconds after the contacts separate.

In order to design the model interrupters for interrupting currents of 100 kA in a 145 kV circuit it was necessary to extrapolate from data that had been acquired in the design and test of puffer circuit breakers for currents up to 63 kA and in the design and test of two pressure interrupters for up to 80 kA. It had been found that the interruption of bus faults required an high differential interrupter pressure that was closely related to interrupting nozzle diameter. The interruption of short line faults also required high differential interrupter pressures but the interrupter was much more sensitive to the actual rate of rise of recovery voltage and consequently the performance was easily modified by adding shunt capacitance or shunt resistance to the interrupter. Shunt capacitance is by far the most effective because it most effectively reduces the initial rate of rise of voltage which is the critical condition for $SF_6$ interrupters.

The interruption of line charging currents requires very little differential interrupter pressure however in order to withstand the full recovery voltage 8.3 milliseconds after contact part the interrupter contacts must be separated at sufficient speed to achieve the required withstand voltage capability.

The final consideration in the design and selection process was the selection of either a single or double flow interrupter. Double flow interrupters have gas flow through two interrupting nozzles with the arc drawn through both. Since there are two sections of the arc subject to the cooling of high pressure gas flow they react very nearly the same as two interrupters in series. Interrupter configurations were available that permitted the incorporation of double flow into a single compact arrangement as shown in Figures 2-3 and 2-16. This is the only interrupter configuration that was considered during this project.

## 2.1 LIQUID $SF_6$ INTERRUPTER

### a. Test Model

The overall interrupter layout is shown in Figure 2-2. It consists of the interrupter assembly mounted on a sub-frame assembly. The overall height is 143.1 inches and the width at the base is 42.5 inches. The liquid $SF_6$ and interrupter are contained in a glass reinforced epoxy tube. The tube is 17 inches inside diameter and 64 inches long. The sub-frame supports the interrupter assembly, the air reservoir, and the liquid $SF_6$ pump operators. The contact operators attach to the sub frame. The frame is made of standard structural steel angle members and steel plate.

A section of one half of the interrupter is shown in Figure 2-3. The interrupter is a double flow nozzle type with liquid $SF_6$ being fed into the nozzle from two sides. Each side is fed from a separate pump. The lower nozzle serves two functions. In addition to being a flow nozzle, it is also the stationary contact. The upper nozzle is made of virgin Teflon. The moving contact has a vent hole to help center the arc on the contact. The contact travel is 8.25 inches. The metal nozzle diameter is 1.25 inches and the insulating nozzle diameter is 1.45 inches. The initial liquid $SF_6$ level will cover up to and including the throat of the upper nozzle.

Figure 2-4 shows one liquid $SF_6$ pump. Its function is to force liquid $SF_6$ through the interrupter nozzles at high pressure. The pump in this layout has a 2 inch diameter and a 10 inch stroke. The cooling coils on the pump cylinders were not used on the test model however, any commercial application of this interrupter would require a cooling system to maintain liquid in the cylinders under high ambient temperature conditions. Since the liquid level in the complete breaker would vary as a function of the breaker temperature the most economical method to maintain liquid in the interrupter chamber and pump cylinders would be to provide local cooling on those parts.

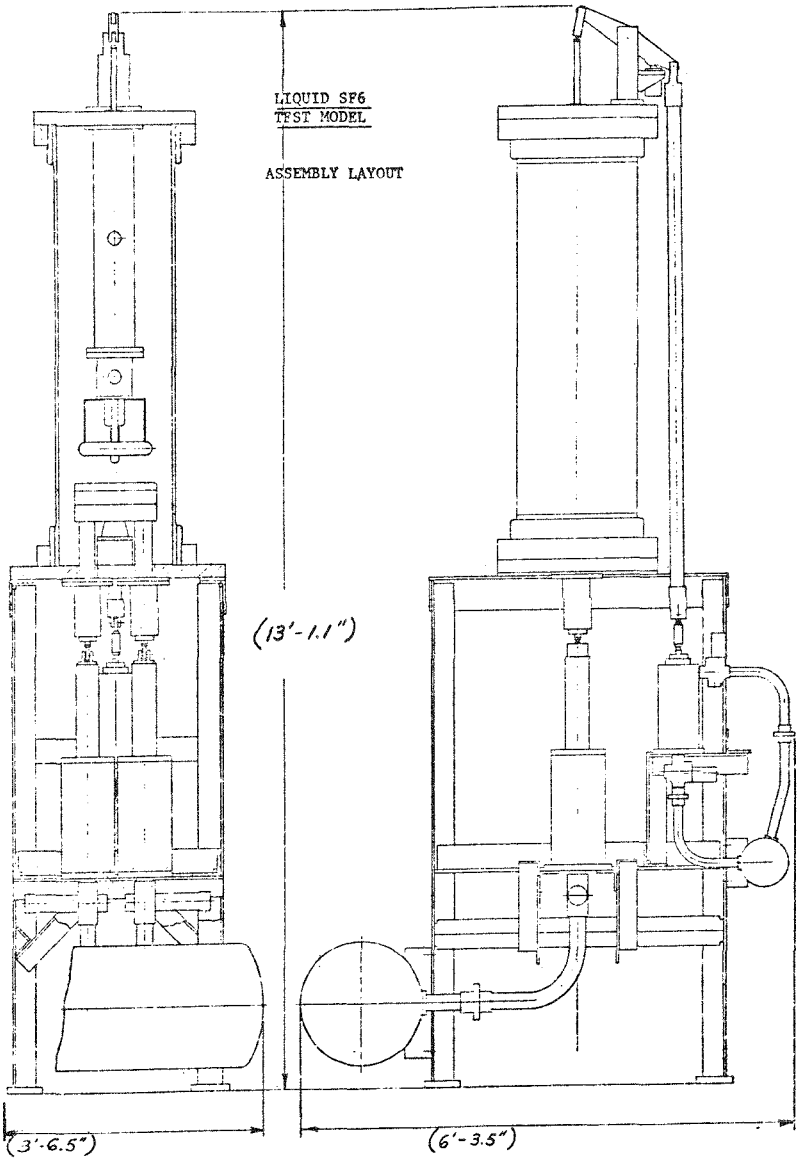


Figure 2-2 Liquid SF6 Test Model

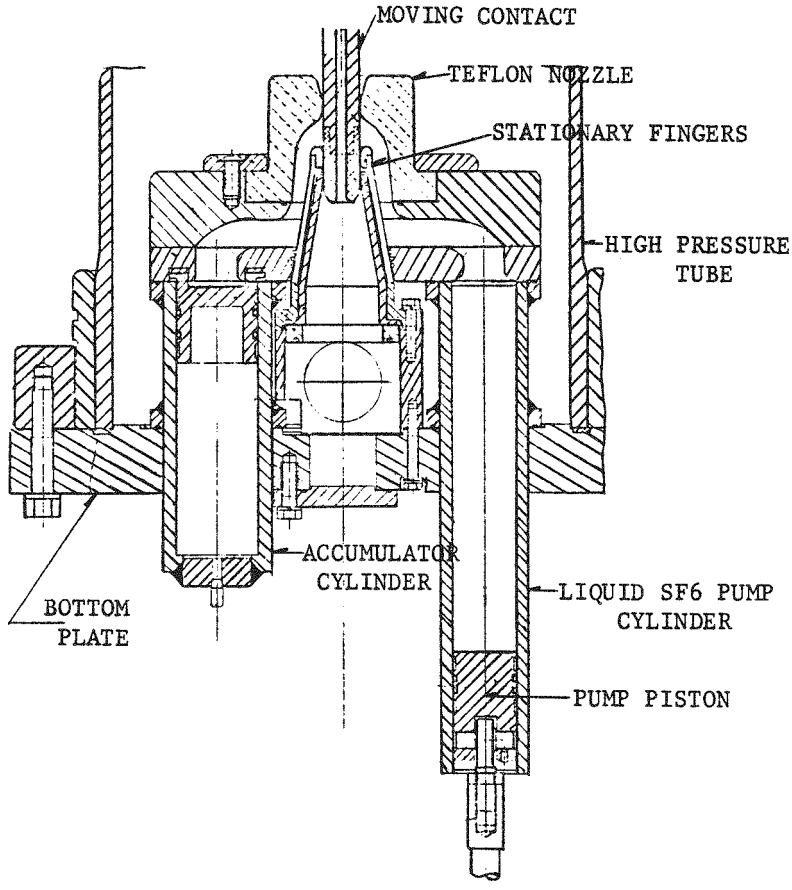


Figure 2-3 Liquid Interrupter Assembly One Pump and One Accumulator Shown for Simplicity

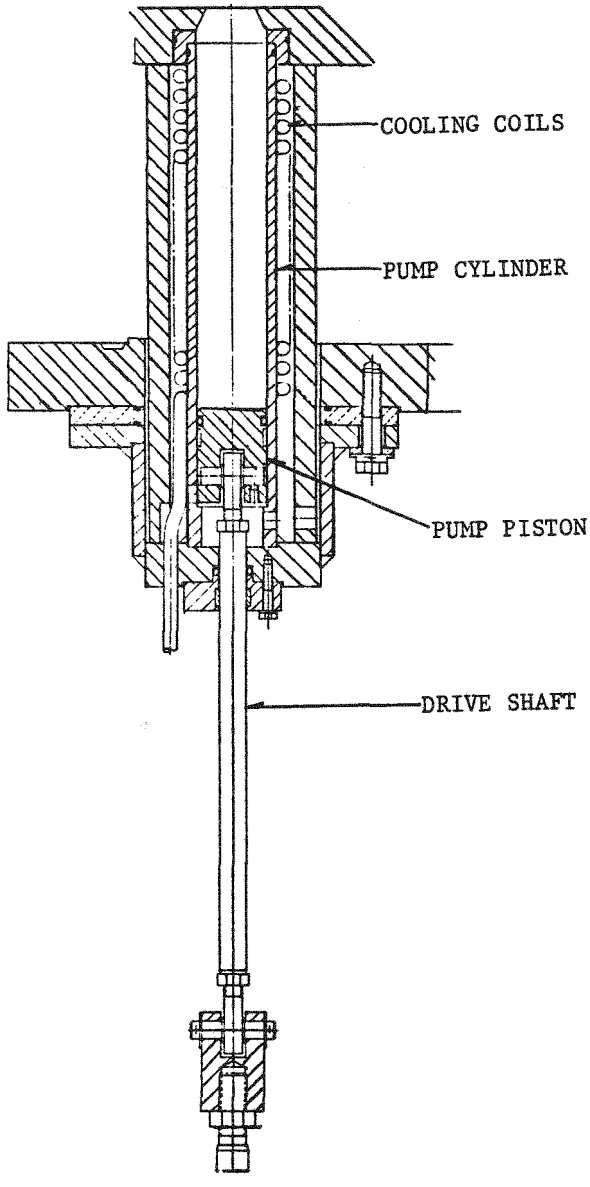


Figure 2-4 Liquid Interrupter $SF_6$ Pump Cooling Coils Assembly

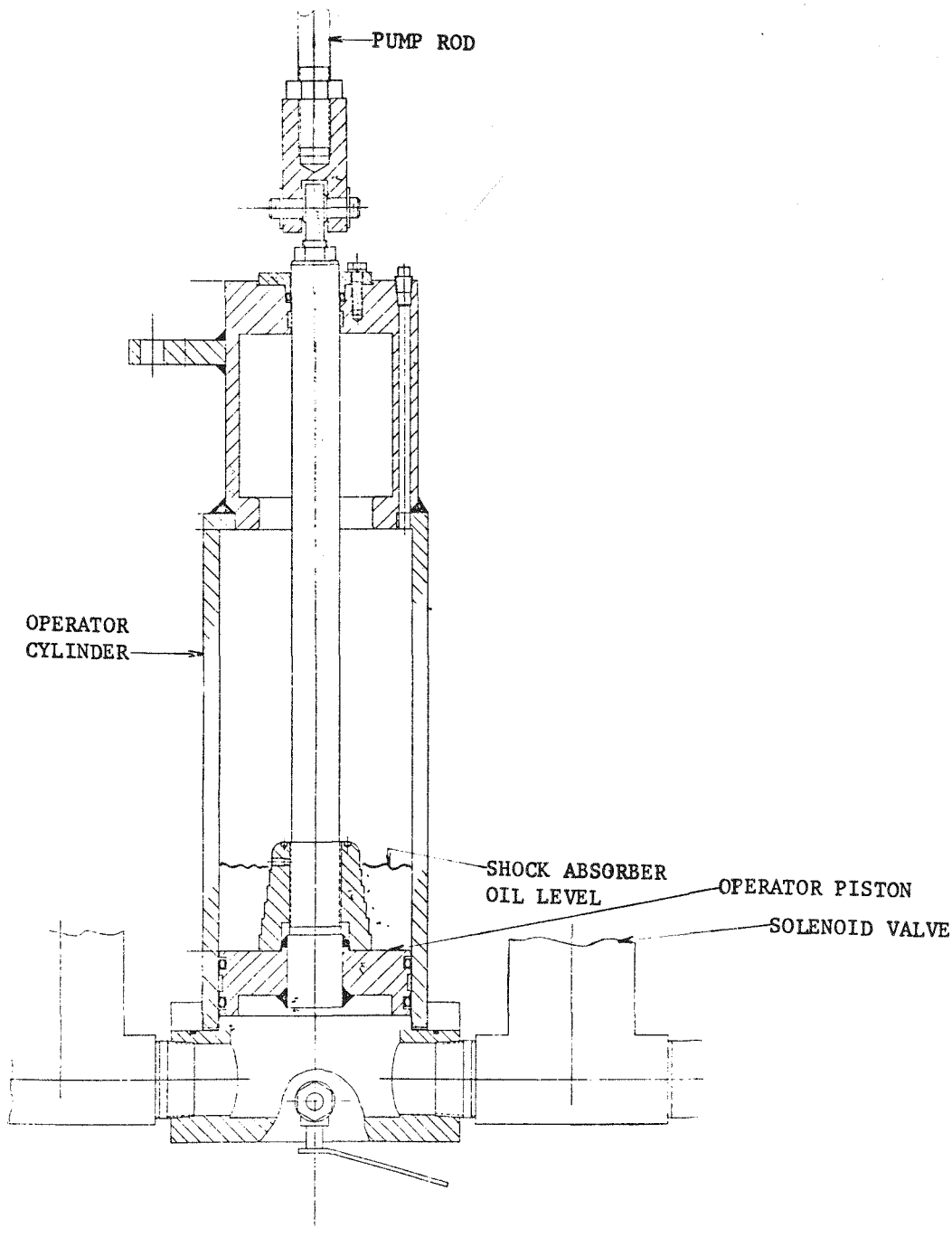


Figure 2-5 Liquid Interrupter Pump Operator

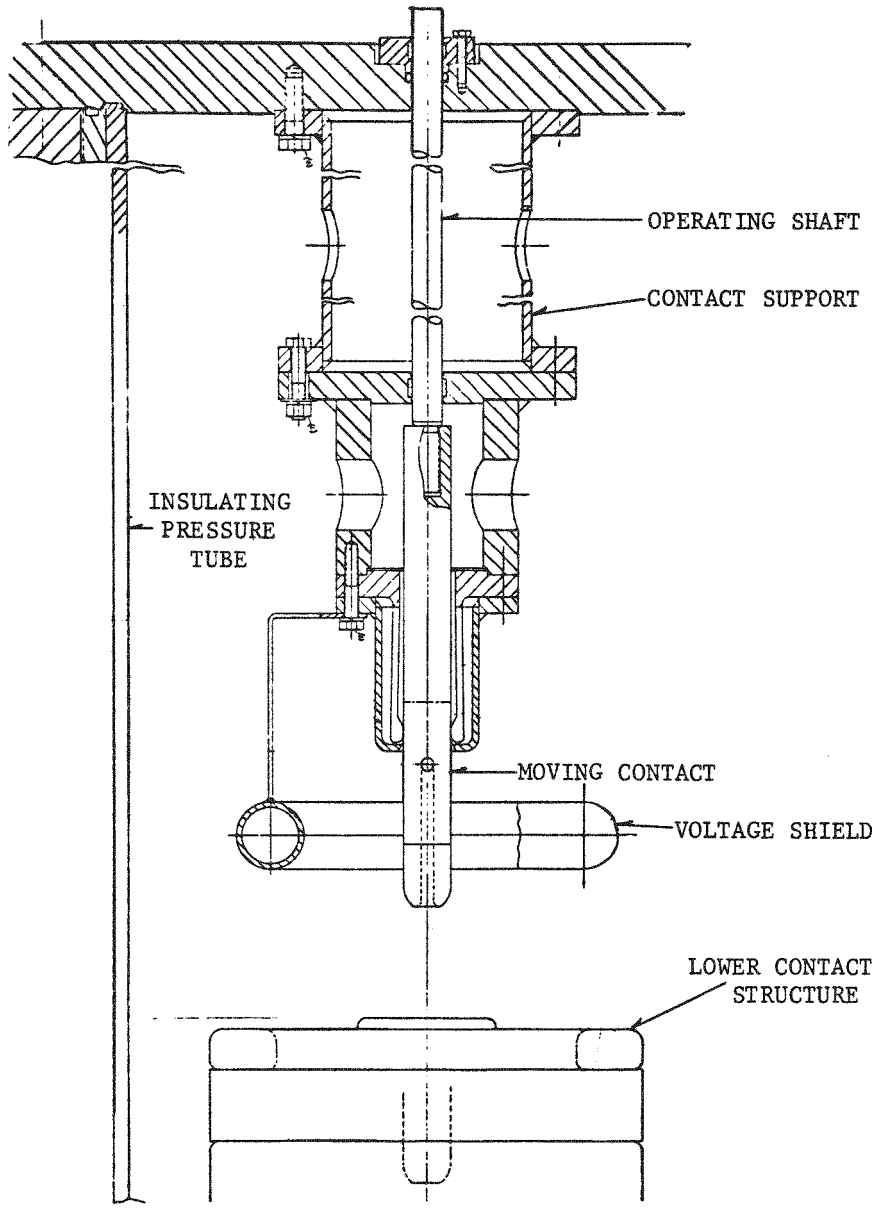


Figure 2-6 Liquid Interrupter Top Contact Assembly

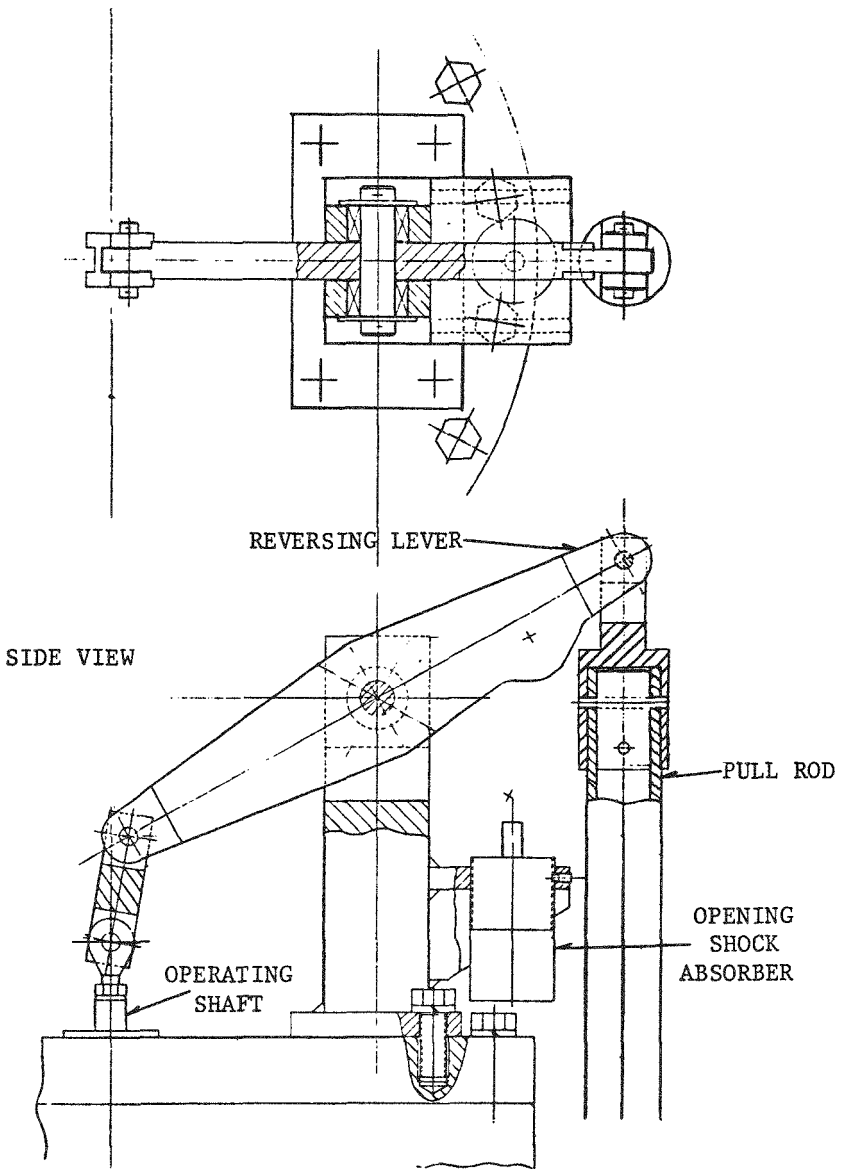


Figure 2-7 Moving Contact Drive Linkage

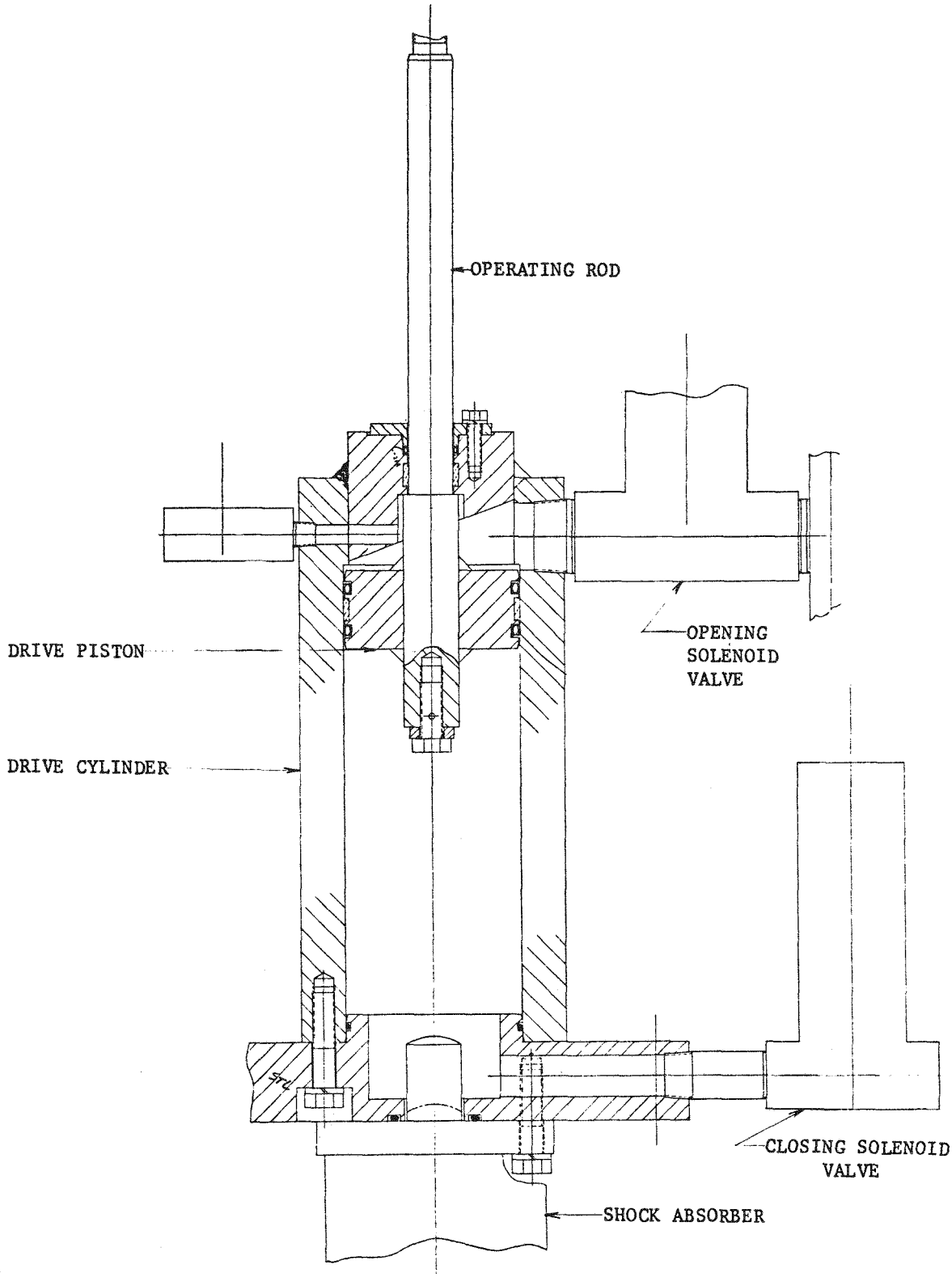


Figure 2-8 Liquid Interrupter Moving Contact Drive

The pump operator layout is shown in Figure 2-5. It consists of a single acting piston and cylinder, a hydraulic shock absorber, and a high pressure high flow rate air valve. The piston diameter is 6 inches.

Figure 2-6 shows the moving contact assembly. In order to keep the moving weight to a minimum, only the lower end of the contact assembly is made of cupaloy. The upper portion is made from a high strength steel rod. The current path is into the cupaloy contact, the sliding fingers, the concentric aluminum tube and into the upper end plate. A shield ring is located near the end of the contact to improve the voltage gradient in the open contact condition.

Figure 2-7 shows the moving contact linkage which is located on the top of the upper end plate. The hydraulic shock absorber absorbs opening stroke energy and acts as the full open stop. The glass epoxy pull rod extends down the side of the interrupter assembly to the contact drive.

Figure 2-8 shows the contact drive. It is a double acting air cylinder with solenoid valves used to actuate it to either the open or closed position.

b. Analysis of the Liquid SF6 Pump

The analysis of the liquid $SF_6$ pressure for arc interruption was done by computer utilizing a numerical analysis technique. The combined effects of arcing, pump inertia, and air valve characteristics are considered in the analysis.

The pump piston's travel characteristics are found by a sequential calculation of the pump piston's acceleration, velocity, displacement, and liquid $SF_6$ pressure for each time increment. The acceleration of the pump piston for each time interval is derived from the net force acting upon the pump piston. This analysis technique makes the assumption that the net force during each time increment is constant. This assumption approaches theoretical accuracy as the time increments approach zero.

The air pressure in the air cylinder which drives the pump piston is calculated for each time increment. The mass of air in the air cylinder and the volume of the air cylinder are used to calculate the pressure. The volume of the air cylinder is a function of the displacement of the piston pump. The mass of air gained by the air cylinder for a particular time interval is found by utilizing compressible flow theory. The effective flow area of the valve from the high pressure tank to the air cylinder is calculated from the air valve's flow area for

each time interval and estimates of flow coefficients. The air cylinder pressure can be calculated knowing the mass, volume, and temperature of the air for each time increment.

The quantity of liquid $SF_6$ that flows through the nozzles is calculated from the nozzle area and velocity of the pump piston. The contact displacement determines the actual nozzle area and the arc area is subtracted from the nozzle area resulting in a net flow area.

The arc area is calculated from the instantaneous current and pressure of the interrupter. The liquid $SF_6$ is modeled as an incompressible fluid. Bernoulli's equation therefore is used to calculate the liquid $SF_6$ pressure. The velocity of the liquid is proportional to the pump area divided by the net flow area times the pump velocity.

The assumption that liquid $SF_6$ is an incompressible fluid is valid within the operating range of two to four thousand psig. Compressibility is not negligable at pressures below 700 psig. The treatment of liquid $SF_6$ as an incompressible fluid should produce an error of less than 10%.

The computer model for the liquid interrupter was a simple one dimensional flow model shown schematically in Figure 2-9. The results obtained with this model showed that the initial air driven liquid pump design was not adequate. Figure 2-10 shows that at a current of 100 kA the arcing effect on pressure is so large that large transients occur in the interrupter chamber pressure and in fact the minimums occur near current zero when the highest pressure is needed for interruption. No calculations were done for assymetric currents because the response of the pressure to current was so fast that a very low pressure would still have occurred at current zero and that would have made the interrupter ineffective.

To solve this problem an accumulator was added to the liquid flow system near the interrupter with the minimum achievable moving mass and consequently the most rapid response time. This accumulator used a high pressure permanent gas as the spring and a light weight piston and seal to separate the liquid $SF_6$ from the gas. The charge pressure of the accumulator would determine the threshold pressure at which it would start to intereact with the liquid pumping system. By limiting the peak pressures reached by the liquid in the interrupter chamber it would effectively store energy and feed liquid into the system when the arc diameter decreases as the current approaches zero.

c. Accumulator Analysis

The computer model was modified from its original form to incorporate an accumulator into the analytical model as shown in Figure 2-11.

The results of the analysis, with the addition of the Liquid $SF_6$ Accumulator, can be seen on Figure 2-12. This shows the comparison of the pump system with and without the accumulator for the condition with arcing. The accumulator suppresses the severe liquid $SF_6$ pressure oscillation that was developed by the Pump System without an accumulator piston. The accumulator-pump system only allows a 300 psig oscillation whereas there is almost 3000 psig oscillation for the pump system without an accumulator. The accumulator-pump system must be optimized for each interruption current rating by varying the nitrogen pressure behind the accumulator. Variations from the optimum accumulator pressure will cause the accumulator piston to respond too quickly or too slowly.

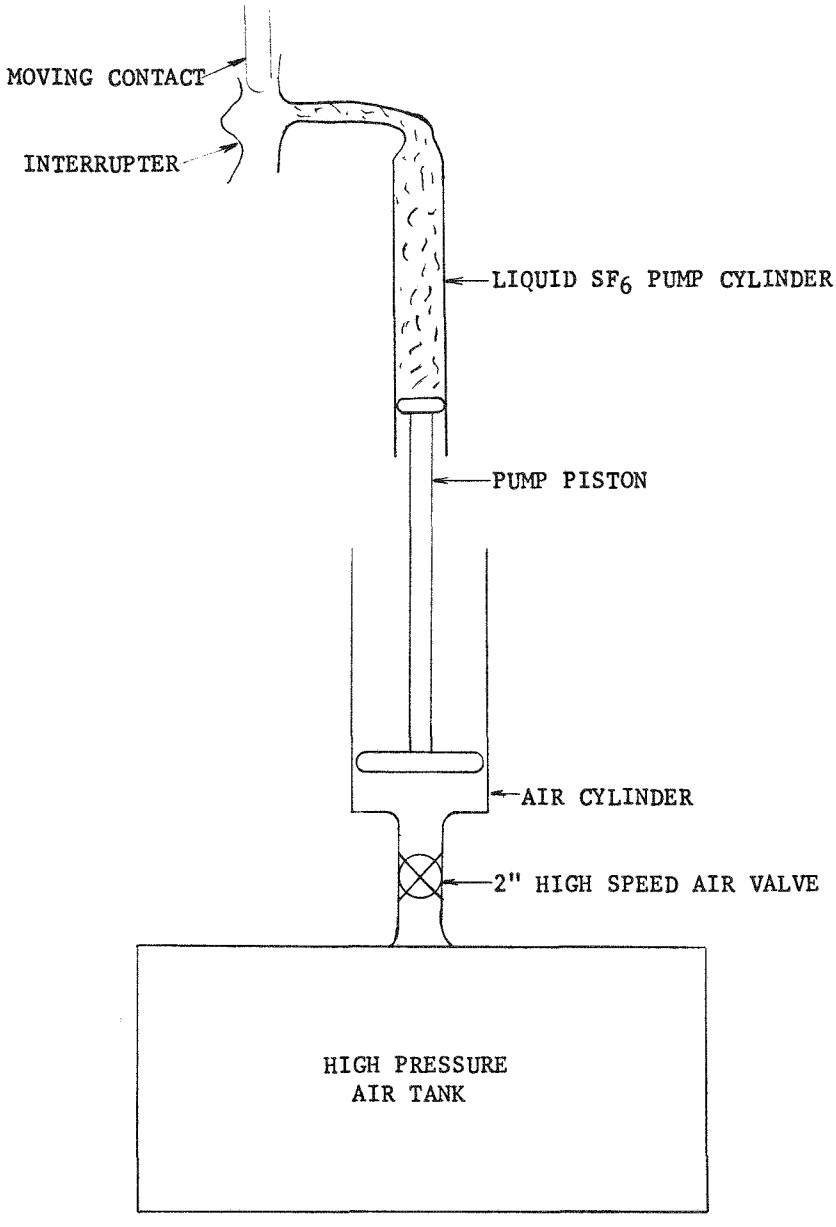


Figure 2-9 Liquid SF6 Pump Computer Model

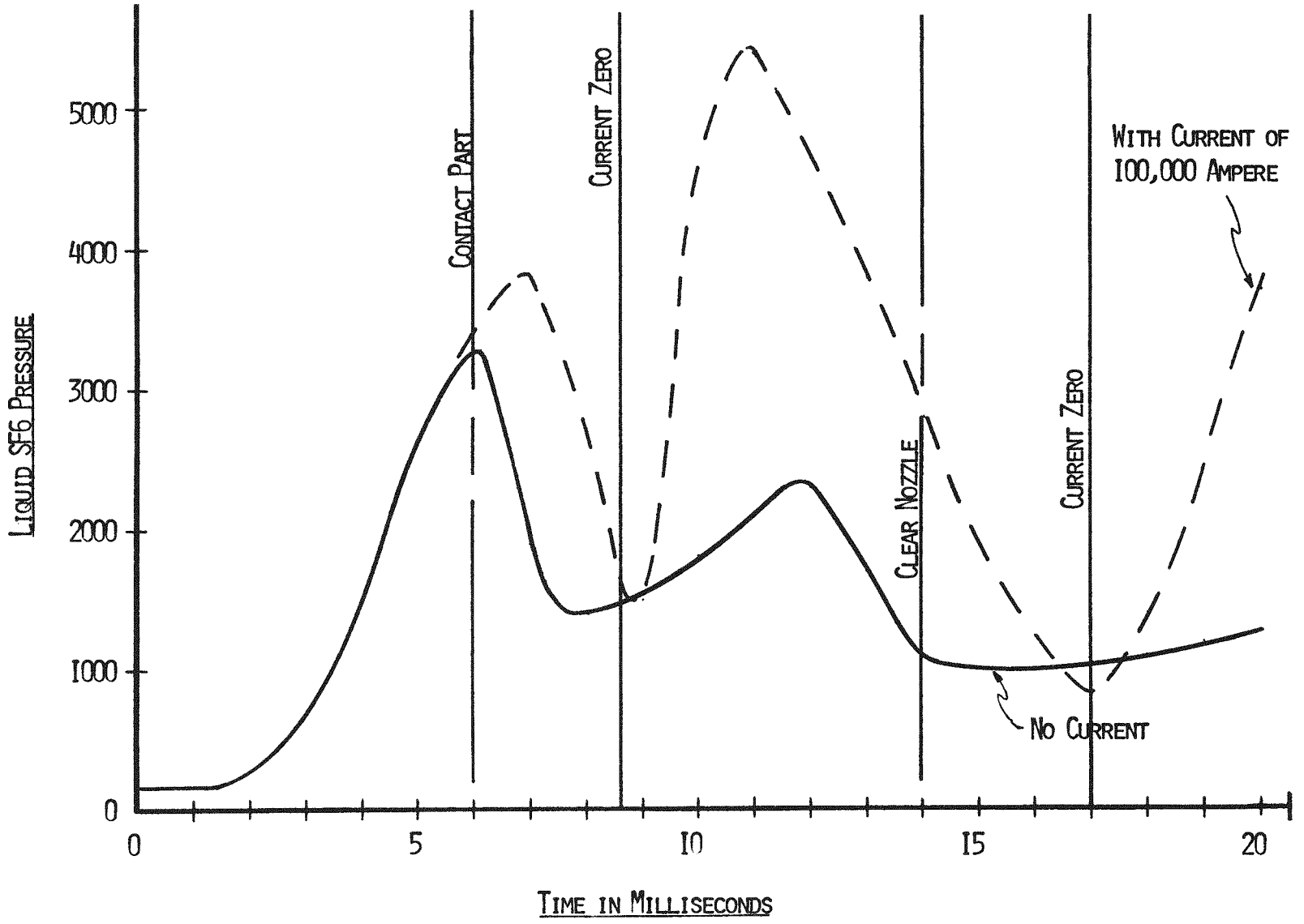


Figure 2-10 Computer Analysis of Liquid SF6 Pressure

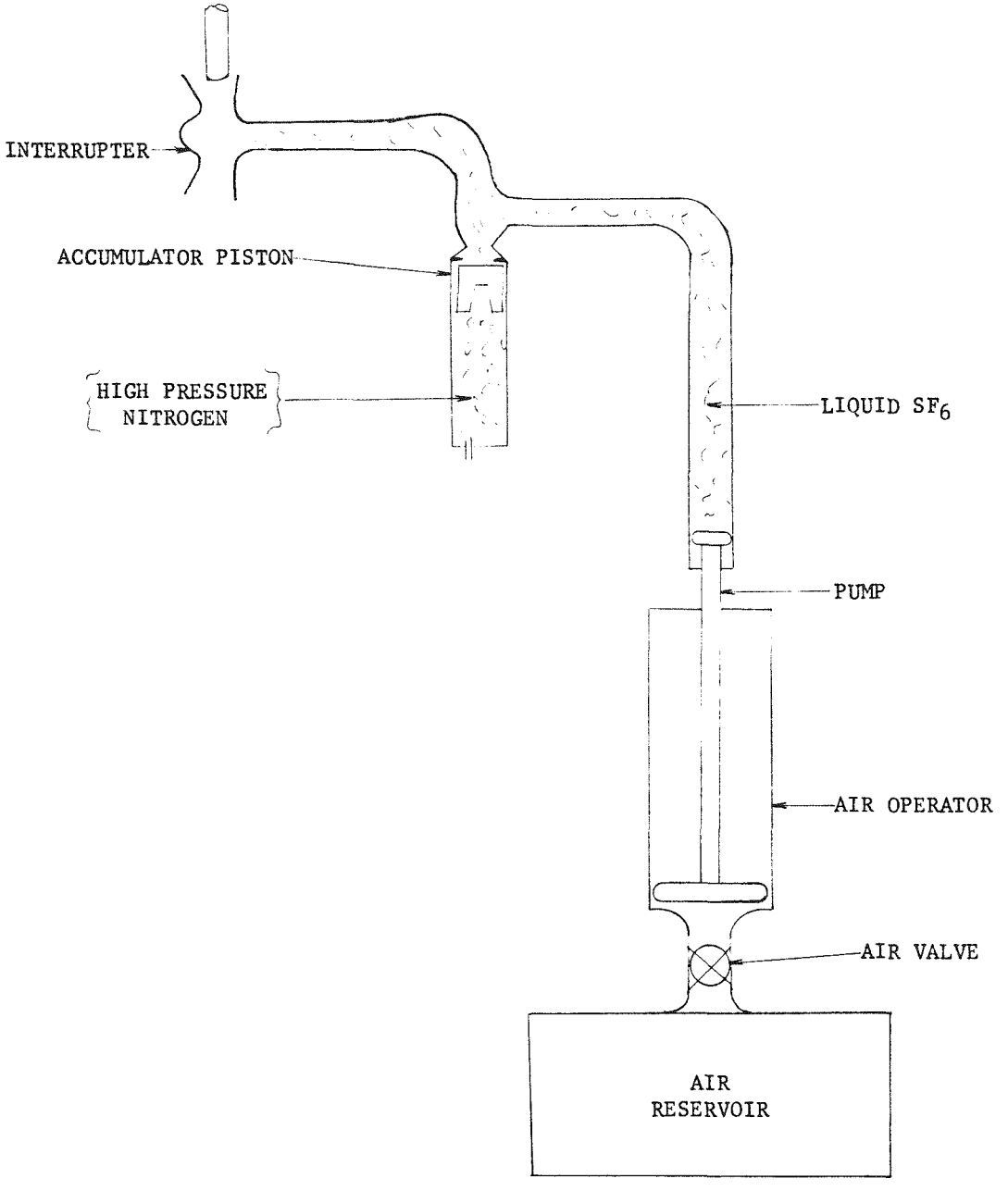


Figure 2-11 Liquid SF6 Pump-Accumulator Computer Model

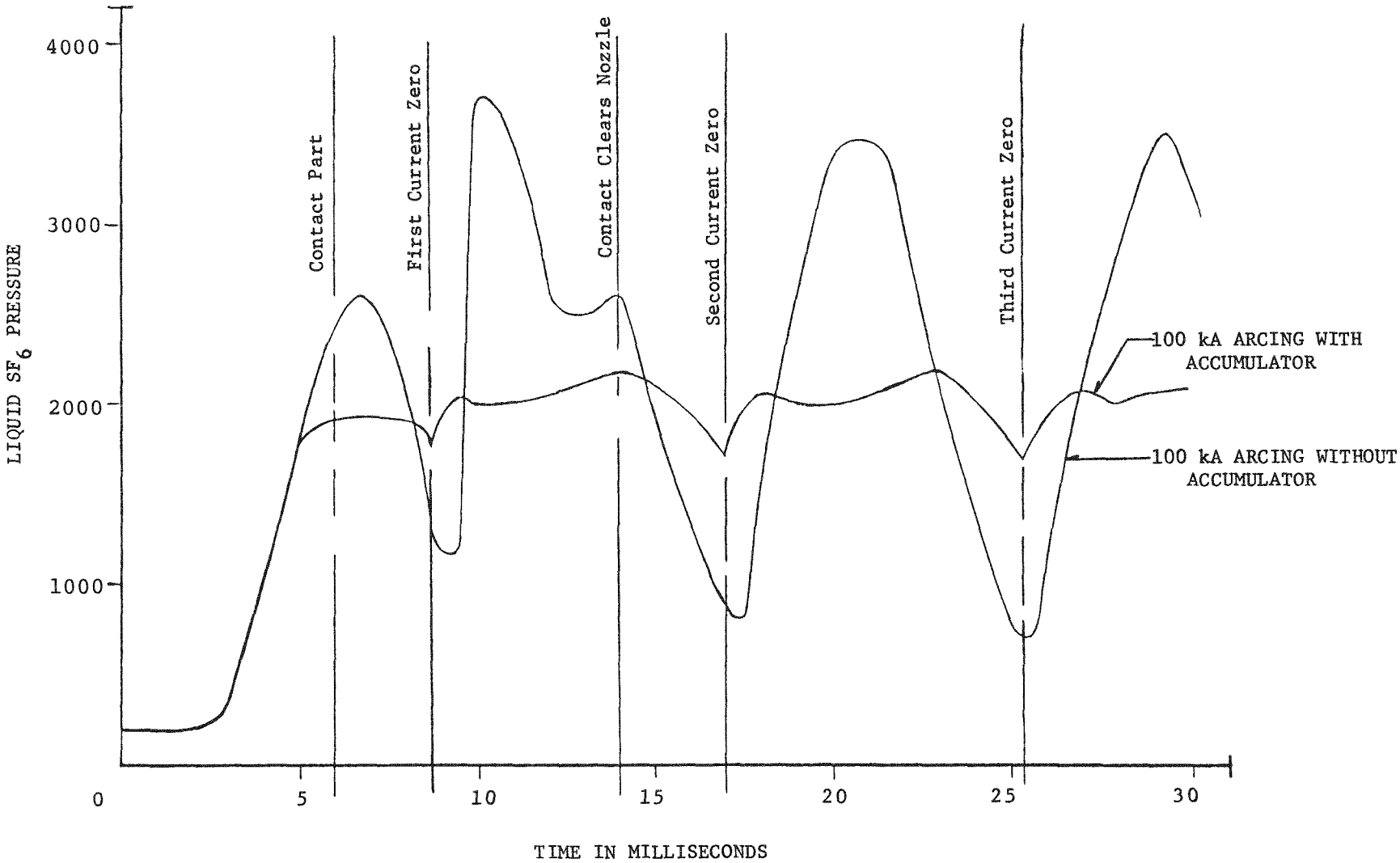


Figure 2-12 Computer Analysis of Liquid $SF_6$ Pressure Showing the Effects of an Accumulator

Either of the situations can allow the liquid $SF_6$ pressure to drop below the maximum at current zero. The various current ratings have optimum nitrogen fill pressures given below:

| Interrupting Current | Accumulator Charge Pressure |
|---|---|
| 120 kA | 2000 psig |
| 100 kA | 1900 psig |
| 80 kA | 1800 psig |
| 63 kA | 1700 psig |

The computer model showed that pressure at current zero for various arcing times was insensitive to arcing time. Since the model was not sensitive to arcing time it also should not be sensitive to current assymmetry.

Figure 2-13 shows the calculated capability of the model interrupter to generate pressure at current zero and compares it with the calculated requirements for interruption. The comparison is made for 80% short line fault conditions from 63 kA to 120 kA ratings. The design chosen should be satisfactory for obtaining successful interruptions at the 100 kA interrupting rating.

d. Operators

The stroke of the pump operator is variable from 10 to 13 inches. This stroke, was adjusted to provide an adequate supply of liquid $SF_6$. The shock absorbing capacity of the pump operator assembly was increased by incorporating the shock absorber function directly into the drive piston and cylinder assembly. Several inches of hydraulic oil was located on the upper face of the drive piston. At the end of the open stroke the oil was forced through a controlled annular area and results in a back pressure on the drive piston to give a constant deceleration for stopping the pump. This was required because pump velocities approach 70 ft/sec for no load mechanical operations.

The contact operator is shown in Figure 2-8. It is capable of operating at air pressures up to 500 psig. An opening shock absorber is attached to the bottom of the cylinder. The stroke of the operator is adjustable from 6 to 8 inches. A high speed solenoid valve feeds high pressure air into the top of the piston to drive the contacts open. The volume of the air reservoir feeding the valve is adjustable so that the pressure decay with time can be controlled to give the required travel characteristics. A computer analysis was made of the dynamic operation of moving contact assembly and operator system. A curve of the characteristics are shown in Figure 2-14.

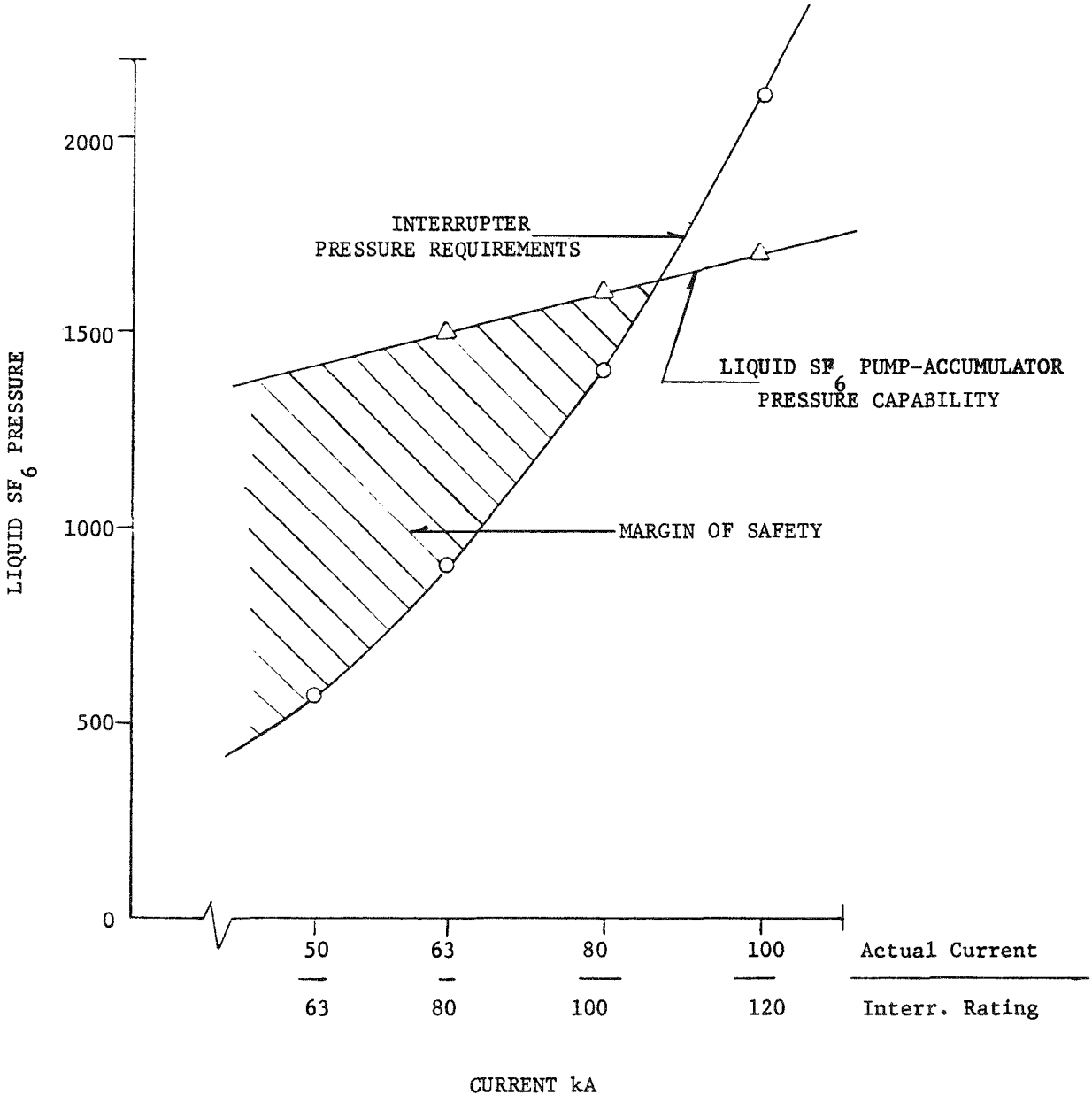


Figure 2-13 Short Line Fault Interrupting Pressure Requirements vs. Pump-Accumulator Capability

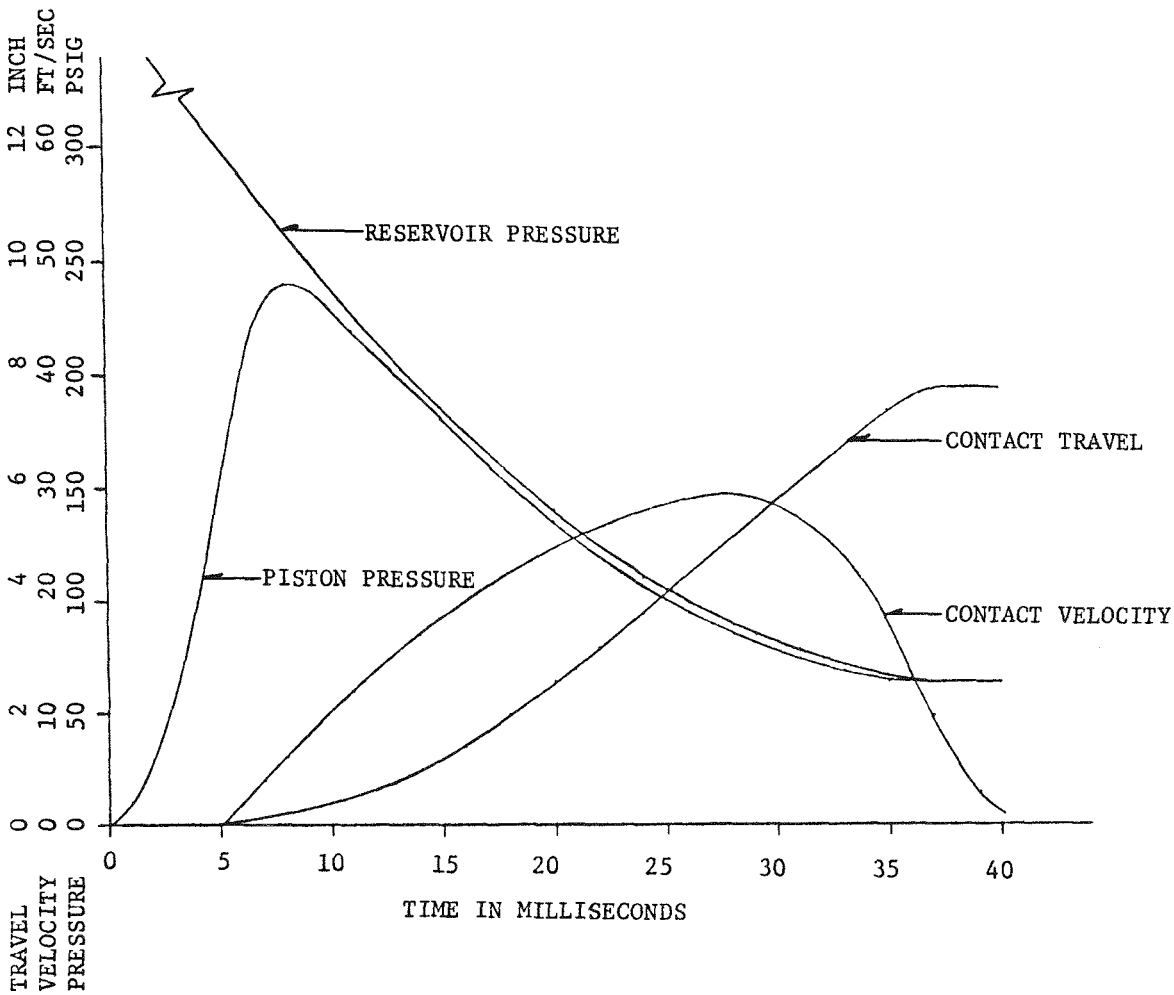


Figure 2-14 Liquid Interrupter Contact Travel vs. Time

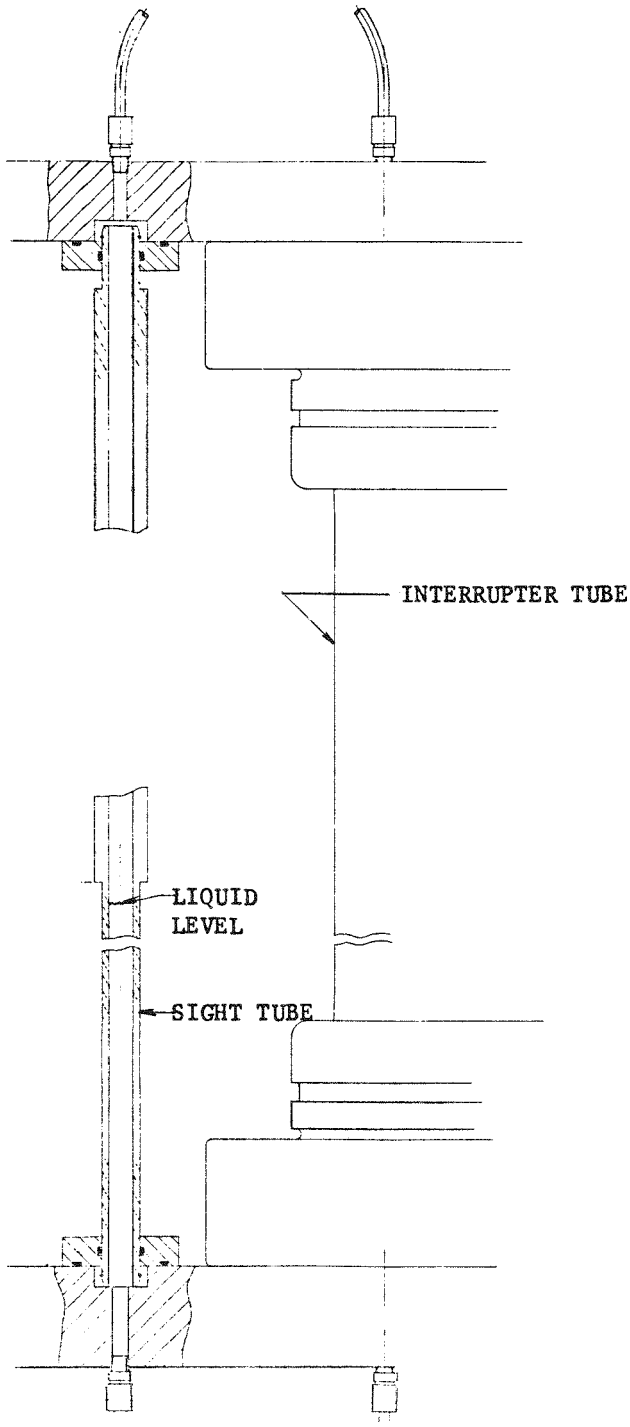


Figure 2-15 Liquid Interrupter Liquid $SF_6$ Level Indicator

e. Liquid Level Monitor

It was essential to have a accurate indication of the liquid $SF_6$ level in the interrupter for voltage and power testing. Various types of commercially available indicators were investigated. None were found to meet the requirements. It was decided to make one that met the needs of the test unit. The indicator is shown on Figure 2-15. It consists of a small diameter glass epoxy tube which runs the full length of the high pressure tube and is located external to it. Liquid level is determined by placing a light behind the tube and visually observing the liquid level.

## 2.2 HIGH PRESSURE $SF_6$ PUFFER INTERRUPTER

a. Test Model

The high pressure $SF_6$ puffer interrupter test model was designed and built to obtain actual data on the differential pressures required to interrupt currents up to 100 kA. This data would then be used to design an interrupter for the program objective of 120 kA.

The interrupter configuration selected was a 63 kA puffer that had been demonstrated to interrupt 63 kA in a two break 242 kV circuit breaker. The primary interrupter dimensions were retained with a puffer cylinder of 6.75 inch diameter with a 8 inch stroke as shown in Figure 2-16.

The internal diameter of 1.44 inches of the teflon interrupter nozzle was retained. The nozzle strength was increased by using a much heavier wall and increasing the strength of the nozzle mounting in order to withstand the much higher expected differential pressures. The copper alloy interrupter moving contacts were reinforced with additional arc resistant material to withstand the 100 kA arc currents and the higher differential pressures however the moving contact nozzle diameter of 1.4 inches was retained. Since the original interrupter had no provision to transfer the interrupter current from the copper alloy operating tube to the stationary piston a system of current collector fingers was designed to mount inside the piston and transfer current from the copper alloy operating tube to the piston. The collector fingers, designed to withstand the 100 kA fault current, used four rows of folded ribbon finger contacts that had been developed by the N.V. Coq Company for GIS applications.* Each row of the 3 inch diameter contacts provides 150 individually spring loaded

* N.V. Cog, Kanalweg 75, Utrecht, Netherlands

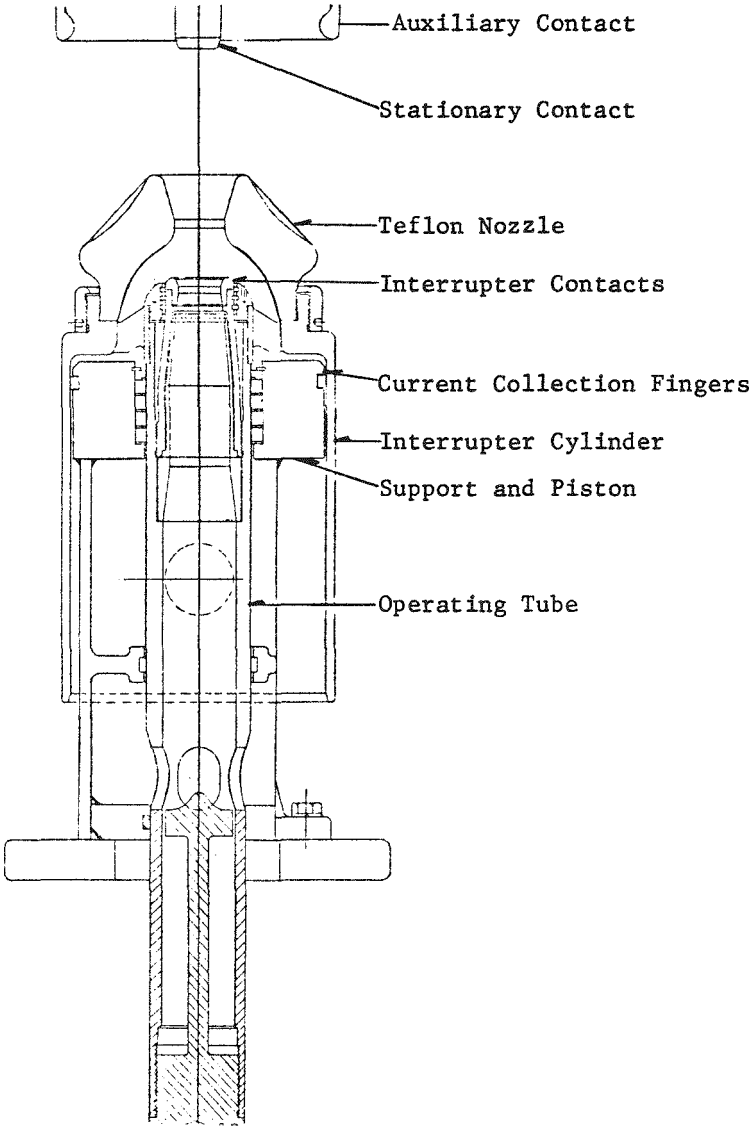


Figure 2-16 High Pressure Interrupter

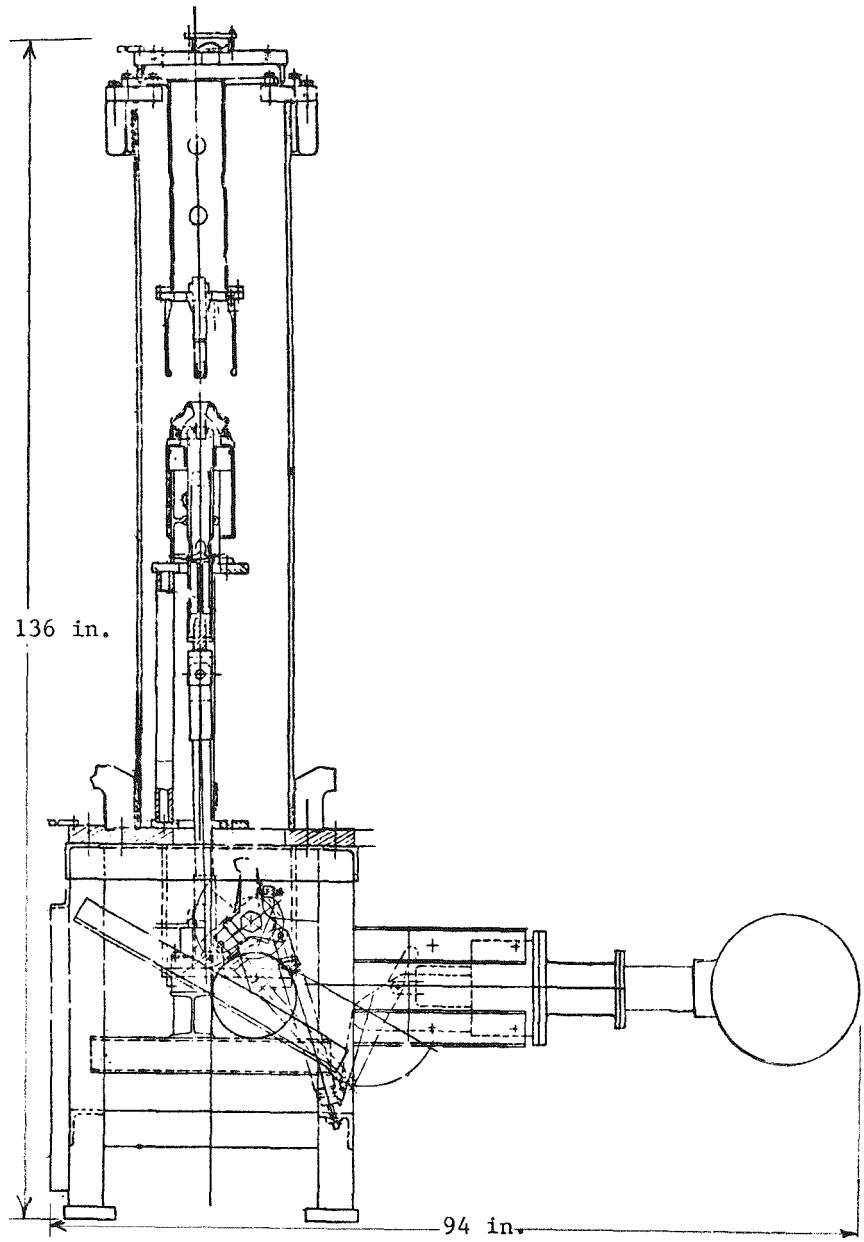


Figure 2-17 High Pressure Interrupter Test Model

finger contacts each of which has a fault current capability of 150A. and a continuous current capability of 15A. The aluminum piston and its support were also redesigned to withstand the higher interrupter pressures.

With the particular interrupter selected and an operating speed of about 30 ft. per second and a $SF_6$ fill pressure of 300 psig the total interrupter pressure at current zero was expected to be 900 psig. A glass reinforced epoxy tube about 60 inches long and 17 inches inside diameter was selected as the enclosure for the interrupter. This tube had been designed for a high pressure two pressure $SF_6$ circuit breaker and it was capable of withstanding the full recovery voltage in air and was pressure tested to 565 psig for mechanical strength.

The complete model interrupter assembly that was designed is shown in Figure 2-17. An existing support frame was adapted to mount the interrupter and enclosure with provisions for mounting the required mechanism. The interrupter stationary piston was mounted on support pedestal to approximately center the interrupter in the enclosure tube and the stationary contacts were mounted on a similar support pedestal from the top cover flange of the enclosure. A sealed lever box was used to couple the driving mechanism to the interrupter. The rotating operating shaft for the interrupter was brought out through a teflon chevron seal and bearing assembly similar to those used in commercial circuit breakers.

The interrupter is a double flow single pressure type which is shown in Figure 2-16.

b. Dynamic Analysis

A refined analysis was necessary to verify that test device would operate as required. The design parameters from this configuration were analyzed by an existing computer program. This program analyzes mechanisms of the type that will be used by this test model. The results indicate that two pneumatic mechanisms with 10 inch pistons type are adequate to operate the interrupter. The results of this analysis are plotted in Figures 2-18 and 2-19. The effects of varying the weights and pressures are illustrated with graphical plots. The results of this analysis show that reduced interrupter weight speeds up the time to contact part (1.5 in. of travel). This reduced weight system travels about the same speed as the reference calculation (the actual design of the model) but slows down more rapidly at the end of the travel. The calculations for the higher mechanism

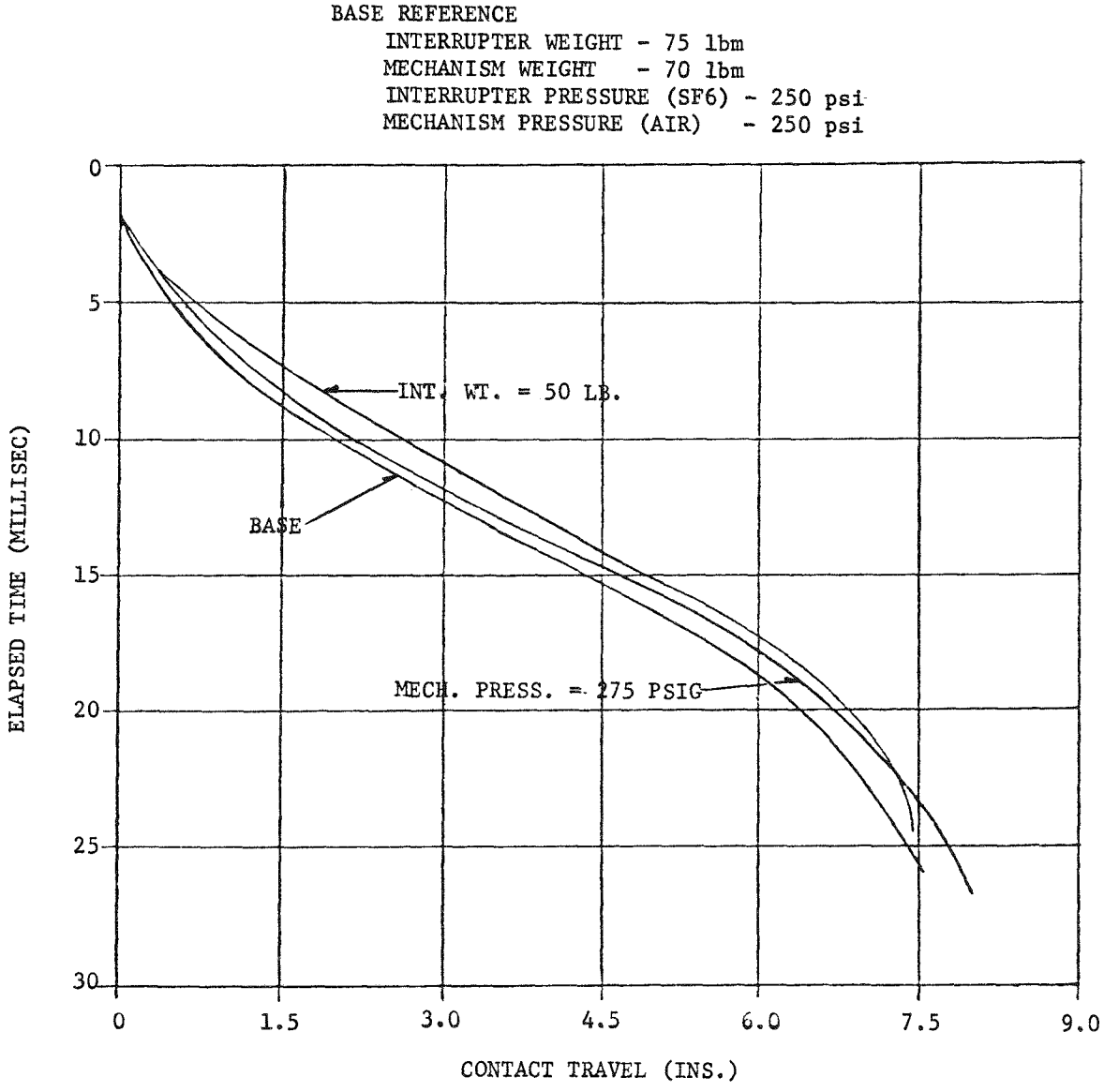


Figure 2-18 Contact Travel vs. Time for H.P. Interrupter

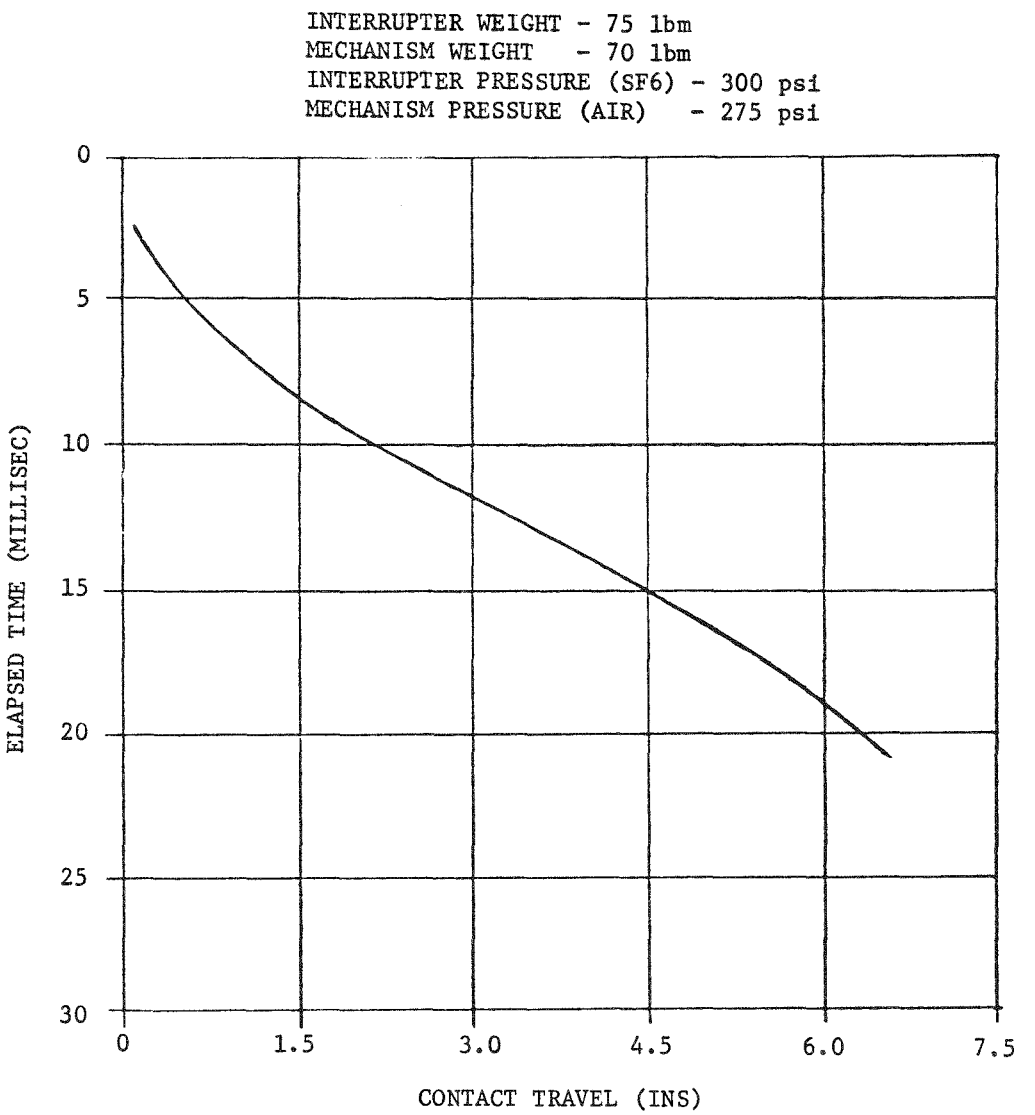


Figure 2-19 Contact Travel vs. Time for H.P. Interrupter

pressure show a generally higher speed and faster time to the end of the travel than the reference conditions. The higher interrupter pressure (Figure 2-19) slows the travel down more than the higher mechanism pressure speeds up the mechanism.

All of these calculations have speeds near 30 feet per second. This speed should be suitable for model testing purposes to determine the pressure requirements to interrupt 100 kA currents.

This analysis showed another problem. The increased weight of an additional mechanism and the increased speed of the interrupter increase the shock absorber requirements during mechanical tests. This potential problem was alleviated by providing for two shock absorbers mounted on a rigid support structure.

## 2.3 INSTRUMENTATION

In order to obtain data for the analysis of the performance of the two competing interrupter principles it was necessary to provide improved methods for accuractely recording the pressures and positions within the interrupters during tests at full test current and voltage. Existing methods for measuring pressures and position were not adequate for measurements in the severe electromagnetic fields, pressures and temperatures that would exist in these 100 kA interrupters.

The expected pressure transients range from 1000 psi in the high pressure interrupter to possible peaks of 4000 or 5000 psi in the liquid interrupter. Since these pressures respond to arc power variations as well as mechanical motion the frequency response of the pressure measurements would need to extend from a few Hertz to above 1 Kilohertz. Since the transducer and their leads must be located within a few inches of the main high current path, they could be exposed to magnetic fields of approximately 1 Tesla at 60 Hertz and frequencies up to many Megahertz.

The expected travel of the interrupters require accurate response to travel of approximately 12 inches with frequency components of travel from a few Hertz up to approximately 1 Kilohertz. The travel transducer for the liquid interrupter pumps could be located some distance from the high current path because the drive system is very rigid. The travel transducer for the high pressure interrupter must be located very near the interrupter in order to eleminate the effect of flexibility in the insulating drive rods. The travel transducer for the liquid interrupter

moving contact must be located at high potential end of the interrupter and near the high current leads.

In order to solve these problems, considerable effort was devoted first to the selection of suitable transducers and second to the transmission of the transducer output signals to the recording device which was generally a magnetic oscillograph.

a. Pressure Transducers

Since it is necessary to monitor the pressure near the arc during interruption it is important to shield the pressure transducer or to obtain one that is unaffected by high fields. Several types of transducers were examined and tested. The Omega Electric Model 1000 pressure transducer with a full scale pressure rating of 1000 psi and a sensitivity of 0.012 mv/psi which uses a semiconductor strain gauge with a built in amplifier to provide a maximum of $\pm$ 5 vdc output was rejected because it produced 10% of full scale output when subjected to a 60 Hz magnetic field of one Tesla.

The Entran model pressure transducer with a full scale pressure rating of 1000 psi and a sensitivity of 0.05 mv/psi uses a semiconductor strain gauge with a built in amplifier to provide a maximum of 5 vdc output was acceptable because it produced negligable output on a 100 psi/cm scale when subjected to a one Tesla 60 Hz magnetic field. This unit was used for the tests of the prototype interrupter and provided satisfactory measurement of the interrupter pressure under most conditions.

The Eaton Devices Model EPS-1032 series pressure transducer with a full scale pressure rating of 500 psi and a sensitivity of 0.25 mv/psi which uses a strain gauge type sensor with a built in amplifier to provide a maximum of 125 mV dc was used to measure the ambient pressure for both the liquid and high pressure models. This device provided satisfactory pressure measurements under no load conditions but was subject to severe interference for interrupter currents over 80 kA.

The Eaton Devices Model EPS-1032 series pressure transducer with a full scale pressure rating of 2500 psi and a sensitivity of 0.05 mv/psi was used to measure the interrupter pressure in the liquid model. This device provided satisfactory pressure measurements under no load conditions but was subject to severe interference for interrupter currents over 80 kA.

b. Travel Transducers

The travel transducer presented more of a problem since it is desirable to measure travel directly off the moving contact. Travel transducers are generally large and highly susceptable to magnetic fields. The environment in which these devices must funtion is subject to high magnetic fields caused by the interrupter currents of up to 100,000 amps. This current would produce a 1.3 Tesla field at 15 cm. This would induce 2.5 mv. into a conductor loop of only 0.5 $cm^2$.

It was desirable to look for devices that were small and therefore reasonable to shield or locate in a low field region.

The modern LVDT is relatively small, has no moving contacts to produce erratic outputs and is capable of operation at high velocities and high accelerations. In the high pressure interrupter the LVDT could be located inside the current carrying support tube. Since the LVDT was actually in the tube, the current through the tube would produce no net flux in the transducer. The LVDT for the liquid test model was also shielded and located to insure maximum isolation from the magnetic fields.

The Pickering Model 7311T5A LVDT was selected for this application. This device has a built in 2.6 kHz semiconductor oscillator and discriminator circuit that provides a linear dc output of -5 to +5 vdc for the 8 inch linear travel of the LVDT core which weighs only a few ounces and can be directly driven. The LVDT as supplied was equipped with a filter which limited the frequency response to 20 Hz. This filter was replaced with an external 2.6 kHz filter which provided an accurate response to the motion of the interrupters. The residual 2% 2.6 kHz ripple of the output introduced an error of less than 1/8 inch for the 8 inch stroke of the high pressure interrupter.

The same 8 inch travel device was used in the liquid test model. It was connected to the moving contact inside the $SF_6$ for travel measurement. Two more of the LVDT's were mounted externally to measure the liquid $SF_6$ pump travel.

c. Electrical Isolation Techniques

During model interrupter testing, it is desirable to gather as much data as possible from various areas of interest in the device being tested. One of the

major problems in design testing circuit breaker prototypes has been the interference that occurs during high power testing. This interference includes high magnetic fields and ground shifts during high current interruptions. The magnetic field can induce voltages in measuring devices and their leads. The ground shifts can cause large potential differences between points in the measuring circuit. Both types of interference make it difficult to interpret the output information. A new approach centers around the use of optical wave guides as a communication channel between the test device and the recording device. As described in the section above, pressure and travel transducers were used to make measurements during the high power tests. The block diagram shown in Figure 2-20 outlines the method used to transmit the output of the transducer to a Siemens oscillograph. The transducer outputs were connected to a voltage amplifier. The amplifier output was connected to a voltage-to-frequency converter that produced variable frequency light pulses from a light emitting diode. The light pulses were carried

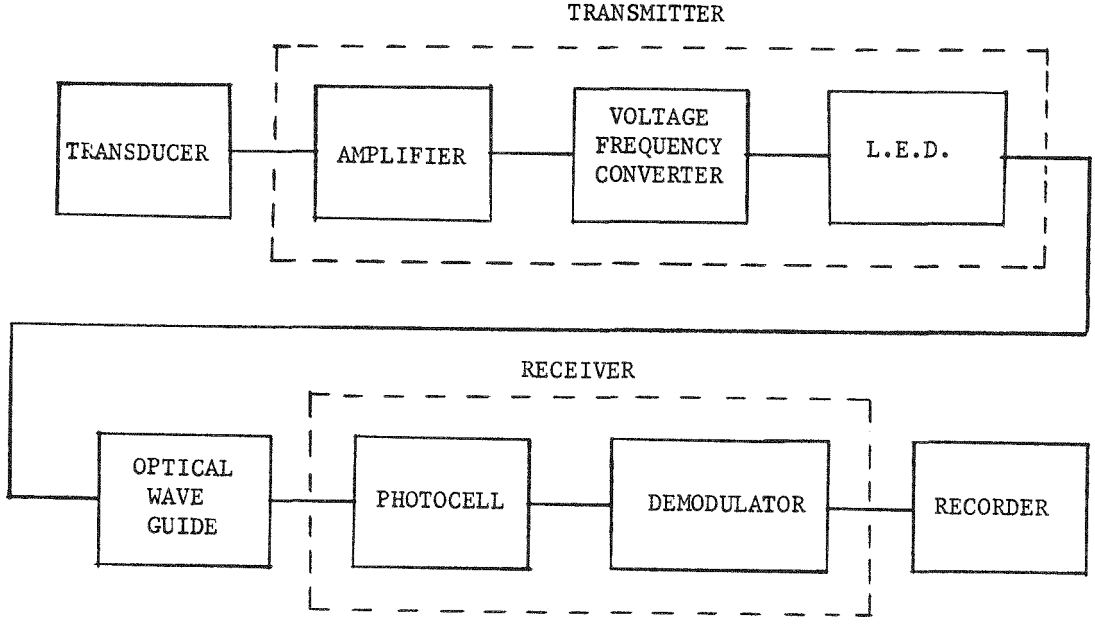


Figure 2-20 Block Diagram of Transducer System

by optical fibers to a photodiode receiver. The amplified output of the photodiode was transmitted by coaxial cable to a demodulator and amplifier that supplied the recording instruments. The electronics for the transmitter section (amplifier, VFO, LED) were battery powered and housed in a 1/4 inch thick steel container for shielding. The container was located on the outside of the model's pressure container. The fiber optics provided isolation between the transmitter and ground. High magnetic and electric fields cannot induce errors into the fiber optics. The receiver section (photodiode and demodulator) were also battery supplied to avoid interaction with the AC supply voltage that might also introduces interference.

A total of six instrumentation channels were built. The transmitters were able to take the output of either the pressure or the travel transducer. Both the transmitter and receiver were designed to operate a minimum of four hours without changing batteries. With this type of isolation, the transducer leads can be brought out of the high voltage terminal of the test model and the transmitter can be located at this exit point. The signal can be carried to the recorder at ground potential by way of the insulating optical wave guide.

The use of optical wave guides for this purpose was a state of the art method. This type of system was expected to provide reliable data that could be used to refine the design of circuit breaker interrupters. This system allowed taking data from interrupters at high potential. This had been very difficult, if not impossible, to do with conventional techniques. This capability was valuable for obtaining data in this project.

Details of this instrumentation is given in Appendix B.

d. Transducer Locations

Liquid Interrupter

The interrupter pressure transducer is located in the interrupter near the main flow path of the liquid $SF_6$ into the interrupter nozzles. Figure 2-21 shows the pressure transducer location. The leads for the transducer are bought out of the interrupter assembly through a steel tube. The aluminum plate that the transducer is located in and the steel tube shield the transducer and leads from the magnetic field produced by the high fault currents. Another pressure transducer is located in the bottom plate of the interrupter assembly. It records pressures that occur inside the high pressure tube of the test model.

LVDT transducers are used to record the interrupter contact and liquid $SF_6$ pump travels. The transducer for the interrupter contact is mounted inside the contact support tube as shown in Figure 2-22. Since the contact support tube also carries the fault current, mounting the transducer inside this tube keeps it in a magnetic field free region. The leads for the transducer extend up inside of the support tube to a high pressure connector in the top plate.

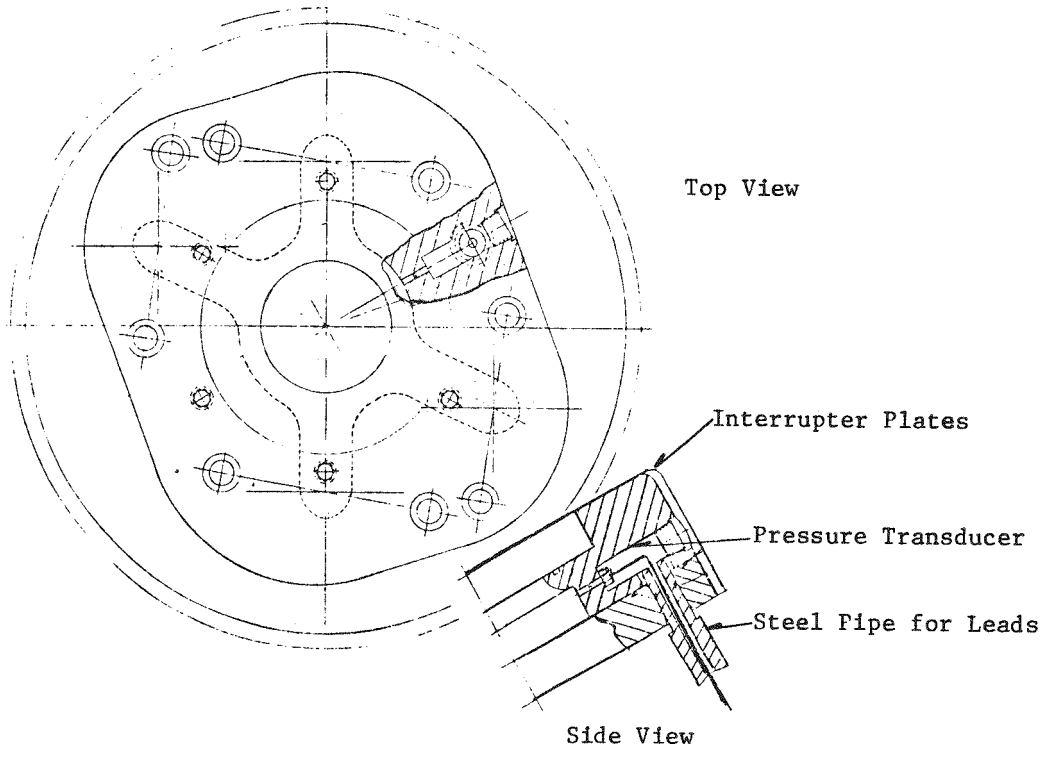


Figure 2-21 Liquid Interrupter Pressure Transducer-Location

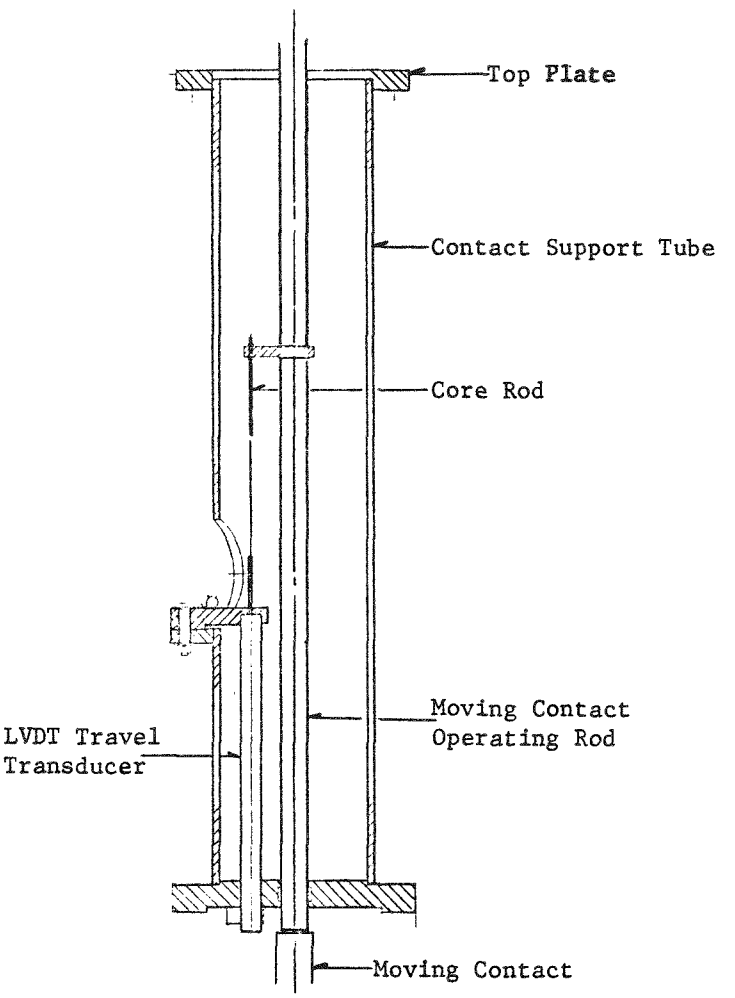


Figure 2-22 Liquid Interrupter Contact Travel Transducer-Location

## High Pressure Interrupter

The locations of the pressure transducers and the travel indicator for the high pressure interrupter can be seen in Figure 2-23 and 24. This pressure transducer, rated 2500 psi, measures the high pressure compressed within the single pressure interrupter and records pressure data in the compression chamber for both mechanical and power testing.

The transducer is mounted in a grooved disc. The goove mounting creates a symmetric current path that forces the current outside the transducer thus eliminates the magnetic field from the transducer. This reduces inaccuracies resulting from magnetic pick-up in the pressure transducer.

A LVDT is used to monitor the travel of the interrupter. The movable core is connected to the interrupter cylinder as is shown in Figure 2-24. The connecting rod and guide bearing are designed to allow the interrupter to rotate or shift a small amount during operation without impairing the measurement accuracy or reliability.

The leads of the pressure transducer extend through the interrupter and into the aluminum support tube. The LVDT is located in a steel tube within the aluminum support tube. The steel tube serves as a shield from magnetic fields produced by the high current. The function of the aluminum tube is to support the interrupter and carry the current to the interrupter.

Both leads extend into the lever box which is relatively free of magnetic fields. Normal cable shielding is used on the leads which are connected through a steel pipe to the steel amplifier box, both of which act as magnetic shields. The fiber optics transmitter is contained within the steel box. The transducers and their leads are shielded to give high accuracy pressure and travel records during high current tests.

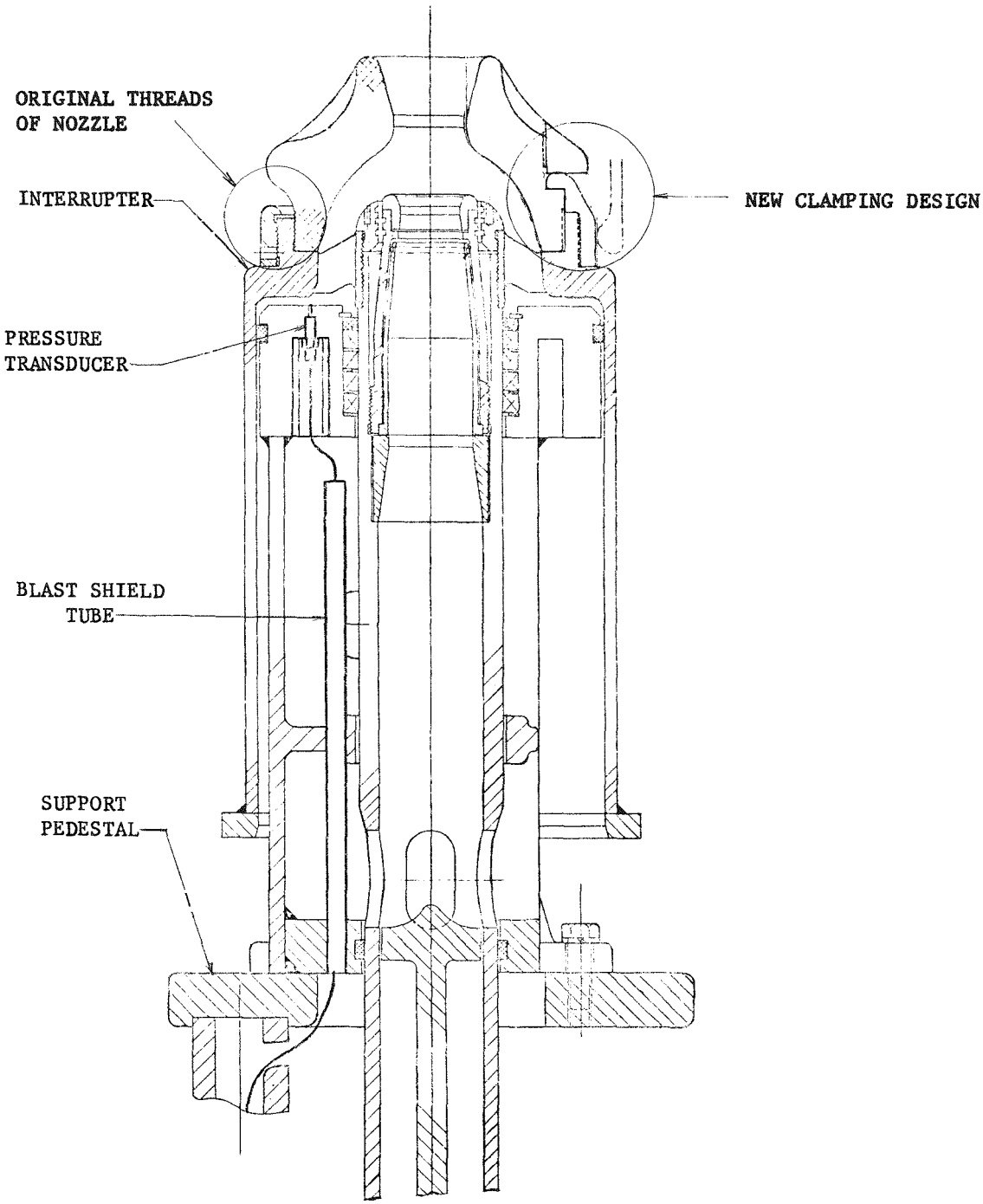


Figure 2-23 Interrupter Assembly

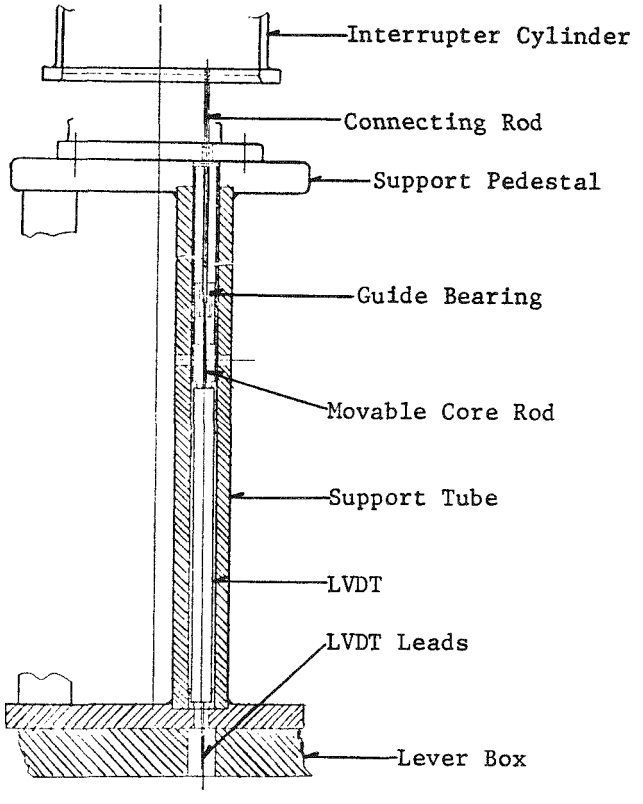


Figure 2-24 Interrupter Travel Indicator Assembly

Section 3

# MODEL INTERRUPTER TEST PROGRAM

## 3.1 LIQUID SF6 INTERRUPTER

Mechanical tests, dielectric tests and interruption tests were made with the liquid $SF_6$ model interrupter. Mechanical tests and interruption tests were made with the completed model; dielectric tests were made with sphere to plane and rod to plane electrodes to obtain data on withstand capability of the combination of liquid and gas $SF_6$.

### a. Mechanical Tests

The completed liquid $SF_6$ interrupter model was mechanically tested to verify its operating characteristics. Travel was recorded for the moving contacts (top travel) and the two liquid $SF_6$ pumps (right pump travel & left pump travel). Pressures within the test unit (chamber pressure) and interrupter (interrupter pressure) were measured. Contact indication, interrupter trip coil current and pump operating current were recorded. A typical oscillogram is shown in Figure 3-1.

After the interrupter was filled with liquid $SF_6$ at 300 psig at 20°C a contact opening velocity of 31 feet per second (Ft/s) was obtained with 300 psi air pressure. The liquid $SF_6$ pumps attained 70 ft/s with lower than predicted air pressure. A mechanism air pressure of 500 psig was estimated to be necessary for the pumps. However, only 300 psi was required. The operating valves apparently had greater than the calculated flow capacity. This may account for the improved performance. The pressure rise of the liquid pumped into the interrupter was 500 to 700 psi which corresponds to the estimated requirement for interrupting 100 kA.

### b. Dielectric Tests

Dielectric tests were performed with electrodes that simulate the liquid $SF_6$ interrupter gap to obtain preliminary information on the dielectric capability of liquid and gas $SF_6$. These tests were conducted using the liquid interrupter high pressure glass-filament tube and aluminum end plates.

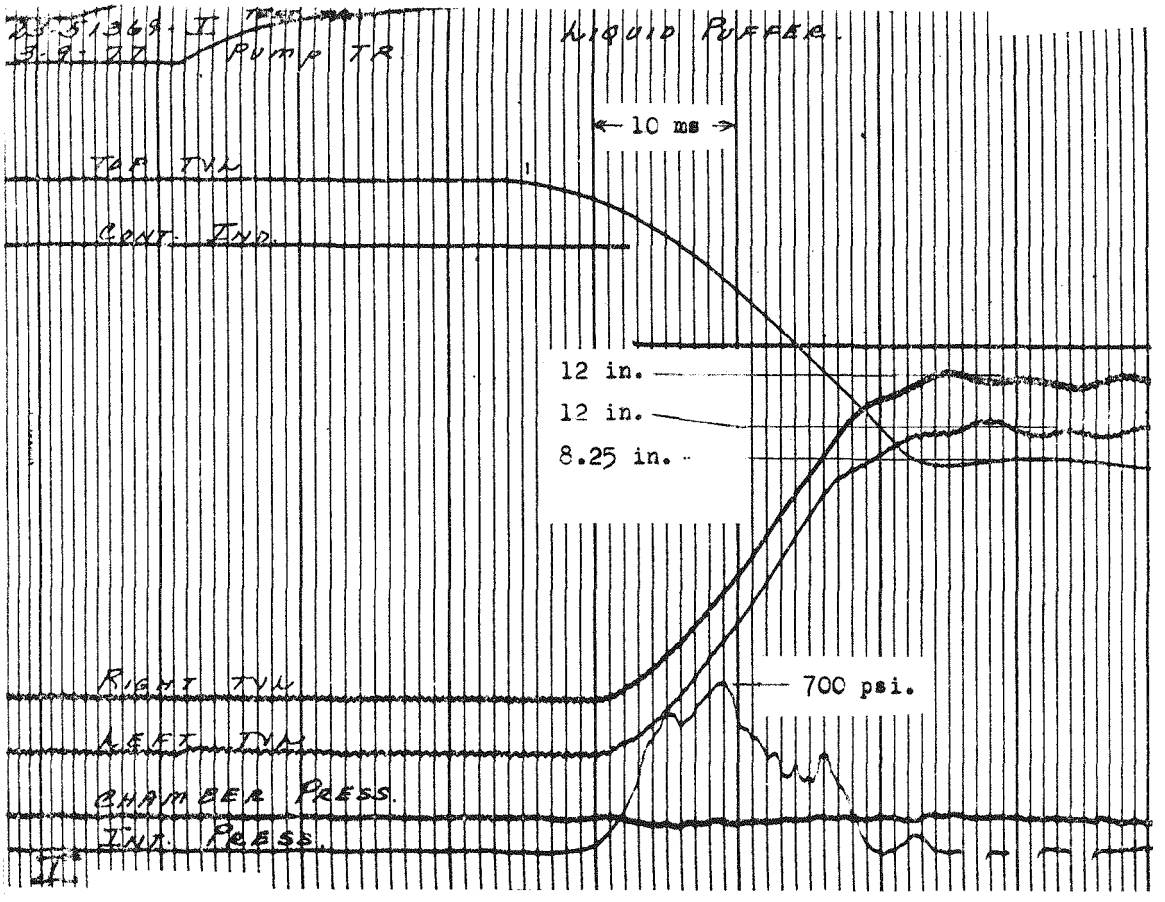


Figure 3-1 Mechanical Test of Liquid Model Interrupter

Two electrode configurations were tested. The first was a 5" diameter brass sphere to a 8" diameter steel plate and the second was a 0.5" diameter steel rod with a hemispherical tip to an 8" diameter steel plate. An outline of the sphere to plane electrode configuration in the test assembly is shown in Figure 3-2. For the rod to plane test, the sphere was removed and replaced by the 0.5 diameter rod. These configurations were selected because they provided calculable fields that can be used for later comparisons. Each configuration was tested at different gap lengths in high pressure SF6 and liquid SF6. A combination of gaseous and liquid SF6 between the electrodes was tested for the rod plane configuration only. The high pressure SF6 tests were made at about 250 psig with approximately 5" of liquid SF6 at the base of the test model. Due to the external withstand capability of the high pressure tube, voltage test levels were limited to less than 650 kV BIL and 300 kV 60 Hz. An impulse voltage wave of 1.2 x 46 us was used in these tests. The interval between the successive voltage applications was at least 30 seconds, the time required for charging the impulse generator.

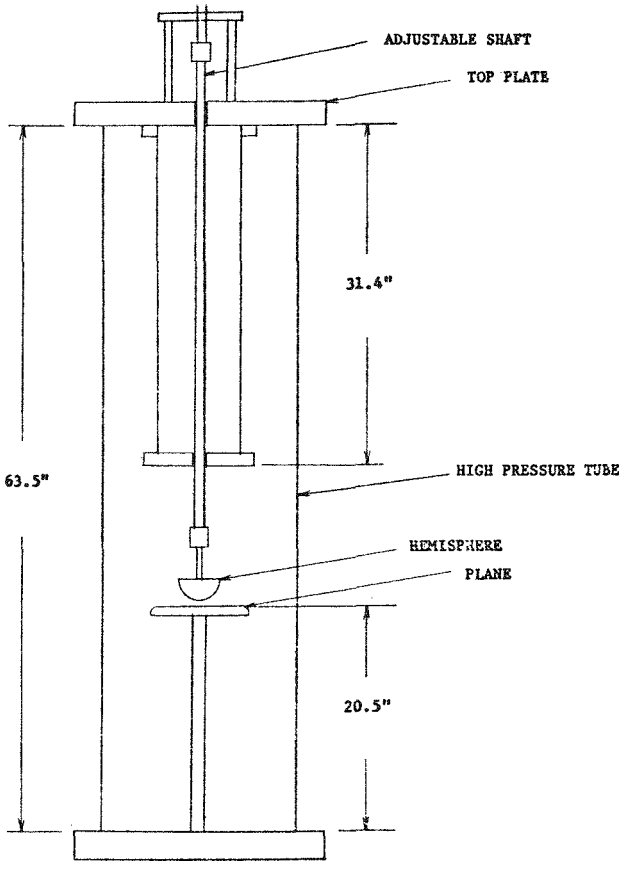


Figure 3-2 Test Chamber for Liquid Dielectric Tests

Table 3-1 shows the voltage breakdown levels for the various test conditions. Impulse breakdown values in this table were determined by the "Up and Down" method. Using this method, a starting value is assumed for each condition.

The test starts at this assumed value and the voltage level is increased by one step each time there is a withstand. The step size is the assumed standard deviation for the test series. At the first breakdown the series of 20 tests is begun. Each time there is a withstand, the test level is increased by one step. After each flashover the level is decreased by one step. After 20 tests, the critical flashover and standard deviation can be calculated with 90% confidence. The 60 Hz levels were obtained by applying a 12 kV per second ramp up to breakdown five times and an average was taken of these values.

The sphere to plane gap spacings were relatively small and did not permit introduction of a combination of liquid and gaseous SF6 in the gap.

TABLE 3-1

DIELECTRIC STRENGTH IN KILOVOLTS OF LIQUID AND GAS GAPS IN $SF_6$ AT 240 PSI

| Electrode Configuration | | Sphere - Plane | | Rod - Plane | | | |
|---|---|---|---|---|---|---|---|
| GAP (in) | | 0.125 | 0.25 | 0.5 | 0.75 | 1.25 | 1.5 |
| All Gas | | | | | | | |
| Impulse | + | 310 | - | 429 (465) | 486 (511) | 512 (542) | 526 (558) |
| | - | 385 | - | 434 (427) | 485 (470) | 580 (498) | - |
| 60 Hz rms | | 167 | - | - | - | - | - |
| + Impulse Ratio | | 1.3 | - | - | - | - | - |
| Gap 0.62" Liquid | | | | | | | |
| Impulse | + | - | - | - | - | 534 | - |
| | - | - | - | - | - | 575 | - |
| 60 Hz rms | | - | - | - | - | - | - |
| Gap 0.8" Liquid | | | | | | | |
| Impulse | + | - | - | - | - | 551 | - |
| | - | - | - | - | - | 519 | - |
| 60 Hz rms | | - | - | - | - | - | - |
| All Liquid | | | | | | | |
| Impulse | + | 154 | 252 | 235 | - | 297 | - |
| | - | 123 | 245 | 304 | - | 441 | - |
| 60 Hz rms | | 110 | 180 | 128 | - | 193 | - |
| + Impulse ratio | | 0.99 | 0.99 | 1.2 | - | 1.08 | - |

( ) numbers in parentheses are calculated values

The 0.125 gap impulse breakdown level decreased by almost 50% when filled with liquid SF6 as compared to the all gas condition. Increasing the gap to 0.25" in liquid SF6 predictably increased the impulse breakdown to approximately twice that of the 0.125" gap breakdown level in liquid. Based on these sphere to plane impulse breakdown values, calculations were made for rod to plane breakdown values. Table 3-1 shows the calculated value for positive and negative impulse "All Gas" conditions. The positive polarity calculated values are within 10% of the critical flashover test values. The 1.25 and 1.5 gap lengths show calculated values considerably lower than the test results for negative impulse. This polarity affect is normal for unsymmetrical electrode systems. Typically for sphere to plane electrode systems, this characteristic has been observed when the ratio of gap distance to sphere radius was greater than one.

Introduction of liquid $SF_6$ across part of the gap caused relatively little change in the impulse breakdown levels (Figure 3-3). This is probably because the liquid level above the plane changes the overall field only slightly. With the gap totally in liquid, the breakdown for the 0.5 and 1.25" gaps were reduced between 30 to 40% from the all gas condition. A reduction in dielectric strength of the liquid is caused in part by the presence of gas bubbles between the electrodes. This introduces two different dielectric constants in the gap and would increase the gradient in the lower dielectric constant gas and thus cause lower breakdown levels. This would not explain the large reduction in dielectric.

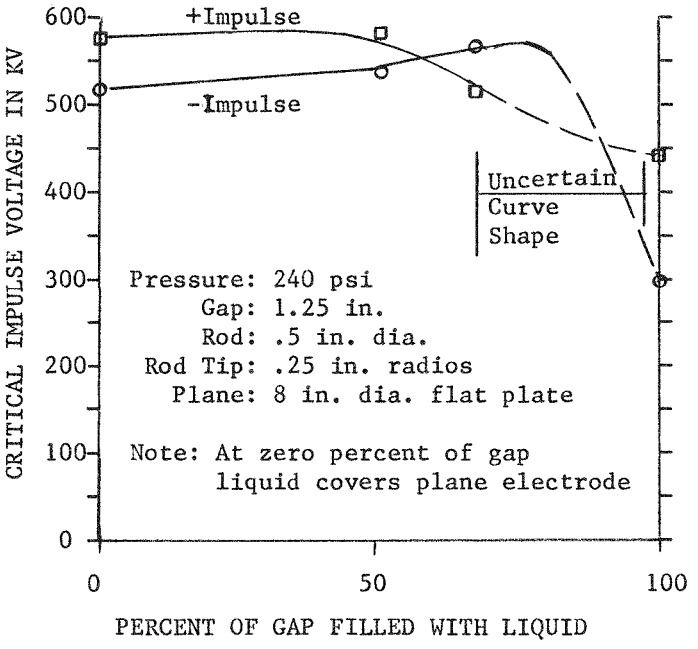


Figure 3-3 Dielectric Strength of Liquid-Gas Gap

strength observed. There are other possible causes such as free conducting particles or bubbles on the surface of the electrodes each of which reduce the dielectric strength of the liquid $SF_6$.

Regardless of the cause, the resultant dielectric strength of the liquid filled electrode gap had a moderate standard deviation (11%). This compares with the 5% standard deviation found with all gas. The 60 Hz breakdown values did not decrease as much due to liquid in the gap for the sphere to plane configuration as for the rod to plane configuration. Table 3-1 shows the ratio of positive impulse voltage crests to the 60 Hz average breakdown peak voltages. These values range from 0.99 to 1.3.

The liquid $SF_6$ used in these tests was taken directly from new bottles of gas. No filtering or cleaning to liquid was done initially or during these tests. This could also contribute to the lower dielectric withstand of the liquid since particles would possibly be suspended in the dense liquid which would normally settle in the gas. Liquid levels were determined by shining a high intensity light on the transulcent high pressure tank and observing the liquid levels on the opposite side of the tank from the light.

Figure 3-4 shows the values from Table 3-1 plotted for the rod to plane and sphere to plane conditions. The all gas and all liguid test conditions are compared. The data shown in Figure 3-4 shows that the liquid interrupter needs a gas space in the gap to withstand required interrupting and dielectric tests. The interrupter design incorporates a gas gap between the stationary and moving contacts.

c. Interruption Tests

Synthethic bus fault tests and short line fault tests were made for the 145 kV, 100 kA rating using the Weil-Dobke parallel current injection synthetic test circuit(1,2). Nominal currents were 100 kA for bus fault tests and 80 kA for short line fault tests.

The test facility had a symmetrical fault capability of 80 kA. The tests were performed in a slightly assymetric mode to make the last half-cycle have a RMS current of approximately 100 kA. The synthetic circuit produces the current slope and the recovery voltage characteristics of a 100 kA bus fault at 145 kV. Tests were made with different mechanism air pressures and accumulator pressures.

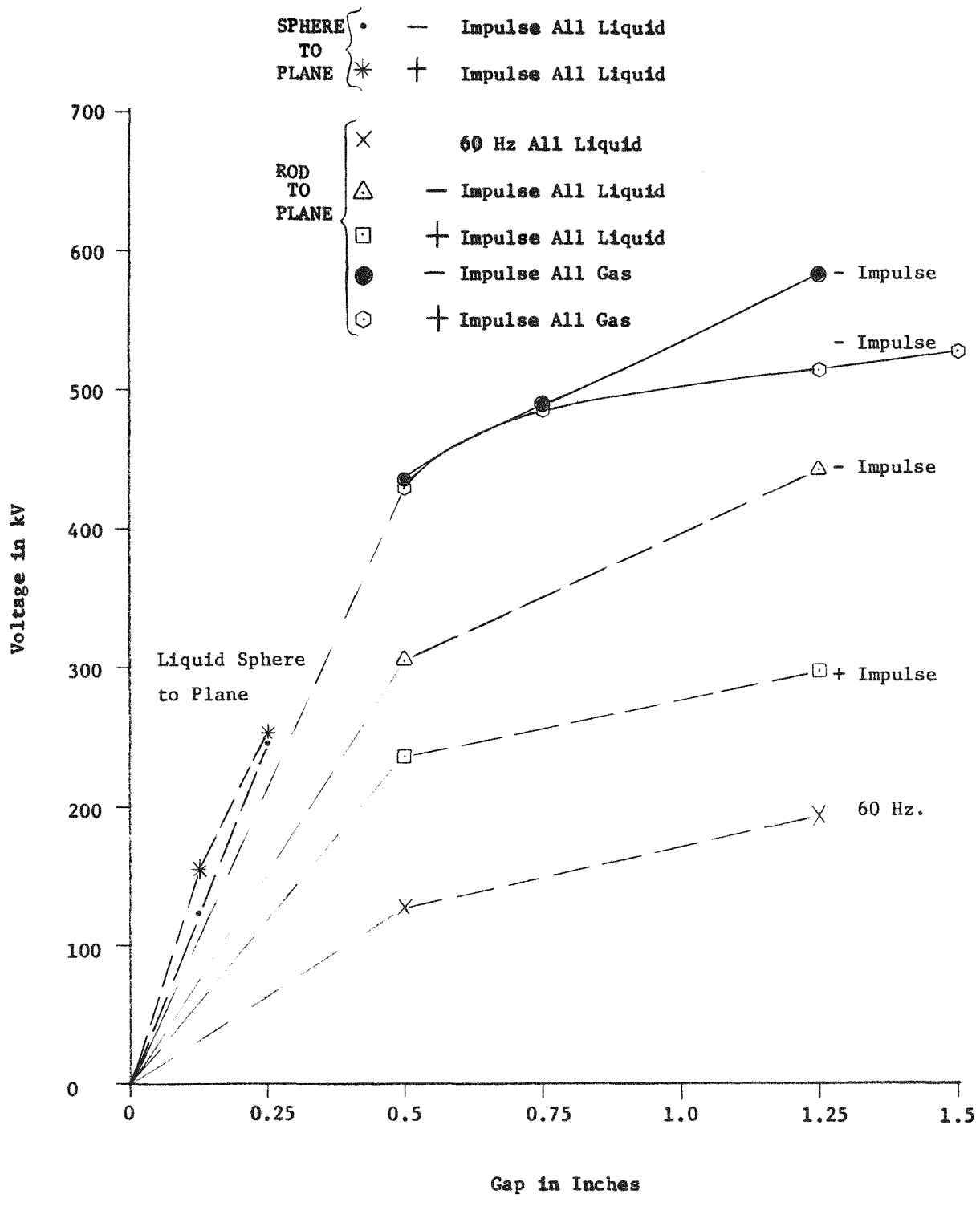


Figure 3-4 Critical Flashover of Gas and Liquid Filled Gaps for Impulse and 60 Hz Voltages

A differential pressure of less than 400 psi at current zero was required for bus fault interruption during power tests although the interrupter produced peak differential pressure up to 1800 psi. The tests were made with a fill pressure equal to the vapor pressure of liquid $SF_6$ at the ambient temperature of the time the tests were made since the interrupter test chamber was partially filled with liquid. The differential pressure in the interrupter at the instant of the final current zero is shown in Table 3-2, Column 2.

The result of the tests are tabulated in Table 3-2. The first four tests letters L, M, AB and AC were to demonstrate bus fault capability. Tests L and AB were successful and tests M and AC were failures. These tests show that the accumulator charge pressure must be at least 1000 psig since test M was a failure when the accumulator fill pressure was reduced to 500 psig and that the minimum arcing time is greater than 10.6 milliseconds since test AC was a failure. The required range of arcing times for a two cycle breaker is 10 milliseconds. These tests only show a range of less than 4 milliseconds however, the liquid $SF_6$ pumps can maintain these pressures for more than 10 milliseconds and it would be expected that the interrupter could operate over the entire required arcing range. This is considerably less than the calculated requirement of 1200 psi differential pressure. Two factors that help to account for the difference between calculations and actual measured values are:

First, with synthetic test, actual current zero occurs nearly one half millisecond later than for full power tests (3,4). Therefore, it is also one half millisecond later with respect to the point in time where the nozzle would become unclogged in a direct power test. This time delay is significant since interrupter pressure falls at a rate of approximately 500 psi per millisecond at current zero. This high rate of change of pressure is due to a very high mass flow rate out of the nozzle. This provides rapid cooling of the arc and improves bus fault interrupting ability. This very rapid fall in differential pressure may actually reduce the interrupting capability for short line faults where the rate of rise of voltage capability of the interrupter depends critically on the differential pressure at the instant of current zero.

Second, the pressure available at current zero is lower than calculated because the diameter of the arc is smaller than was calculated. This was confirmed by similar results from arc model calculations for high pressure puffer interrupter in this project. Typical oscillograms for bus fault are shown on Figure 3-5 and 3-6.

TABLE 3-2

DATA ON 145 kV - 100 kA LIQUID MODEL

| Test Letter | Diff. Press at I=0 (psig) | $SF_6$ Fill Press (psig) | Air Press Mech (psig) | Accum Charg Press (psig) | MEASURED CURRENT: Last Cycle (kA) (rms) | MEASURED CURRENT: Last 1/2 Cycle (kA) (rms) | Arcing Time (msec) | Ext.Arc Voltage (kV) (Peak) | RECOVERY VOLTAGE: LINE SIDE: 1st Peak (kV) | LINE SIDE: Time to 1st (Peak) (usec) | LINE SIDE: TRV kV/ (usec) | BUS SIDE: 1ST Peak (kV) | BUS SIDE: TIME to 1st | BUS SIDE: TRV (kV/ usec) Peak (usec) | Work/ Fail |
|---|---|---|---|---|---|---|---|---|---|---|---|---|---|---|---|
| 100 % BUS FAULT | | | | | | | | | | | | | | | |
| L | 295 | 290 | 300 | 1500 | 73.5 | 100.0 | 12.0 | NA | -- | -- | -- | 271 | 225 | 1.6 | W |
| M | 200 | 310 | 250 | 500 | 72.5 | 87.0 | 11.3 | NA | -- | -- | -- | -- | -- | -- | F |
| AB | 380 | ND | ND | 1000 | 73.5 | 85.0 | 14.5 | 2.3 | -- | -- | -- | 258 | 235 | 1.6 | W |
| AC | 70 | ND | ND | 1000 | 73.0 | 98.0 | 10.6 | NA | -- | -- | -- | -- | -- | -- | F |
| 80% SHORT LINE FAULT | | | | | | | | | | | | | | | |
| P | 780 | 205 | 350 | 1000 | 71.5 | 75.5 | 14.5 | 5.6 | 38.9 | 3.0 | 17 | 131 | 220 | | W |
| Q | 840 | 250 | 350 | 950 | 63.0 | 66.0 | 9.0 | 3.1 | (7) | -- | -- | -- | -- | | F |
| R | 960 | 180 | 350 | 950 | 73.5 | 73.5 | 11.6 | 4.4 | (12) | -- | -- | -- | -- | | F |
| S | 1014 | 200 | 350 | 1500 | 72.0 | 70.0 | 11.0 | 5.6 | NA | -- | | | | | F |
| T | 1050 | 200 | 350 | 1500 | 67.5 | 70.0 | 12.0 | 5.7 | 32.4 | NA | -- | 130 | 220 | | W |
| U | 1014 | 200 | 350 | 1500 | 66.0 | 65.0 | 12.1 | 5.7 | (16) | -- | -- | | | | F |
| V | 720 | 200 | 350 | 1500 | 66.0 | 64.0 | 15.0 | NA | NA | -- | -- | -- | -- | | F |
| W | 920 | 200 | 350 | 1500 | 74.0 | 70.0 | 14.6 | 5.2 | 40.0 | 3.2 | 16.5 | 132 | 220 | | W |
| X | ND | 200 | 350 | 1500 | 75.0 | 79.0 | 12.0 | NA | NA | -- | -- | -- | -- | | F |
| Y | 250 | 200 | 350 | 1500 | 73.5 | 72.5 | 18.5 | 2.5 | (5) | -- | -- | -- | -- | | F |
| Z | 150 | 200 | 350 | 1500 | 73.0 | 67.0 | 18.4 | 2.5 | (5) | -- | -- | -- | -- | | F |
| AA | 750 | 200 | 350 | 1000 | 52.5 | 45.0 | 17.7 | 5.2 | 10 | NA | NA | 93 | 220 | | W |

ND Data not available ( ) Indicates breakdown

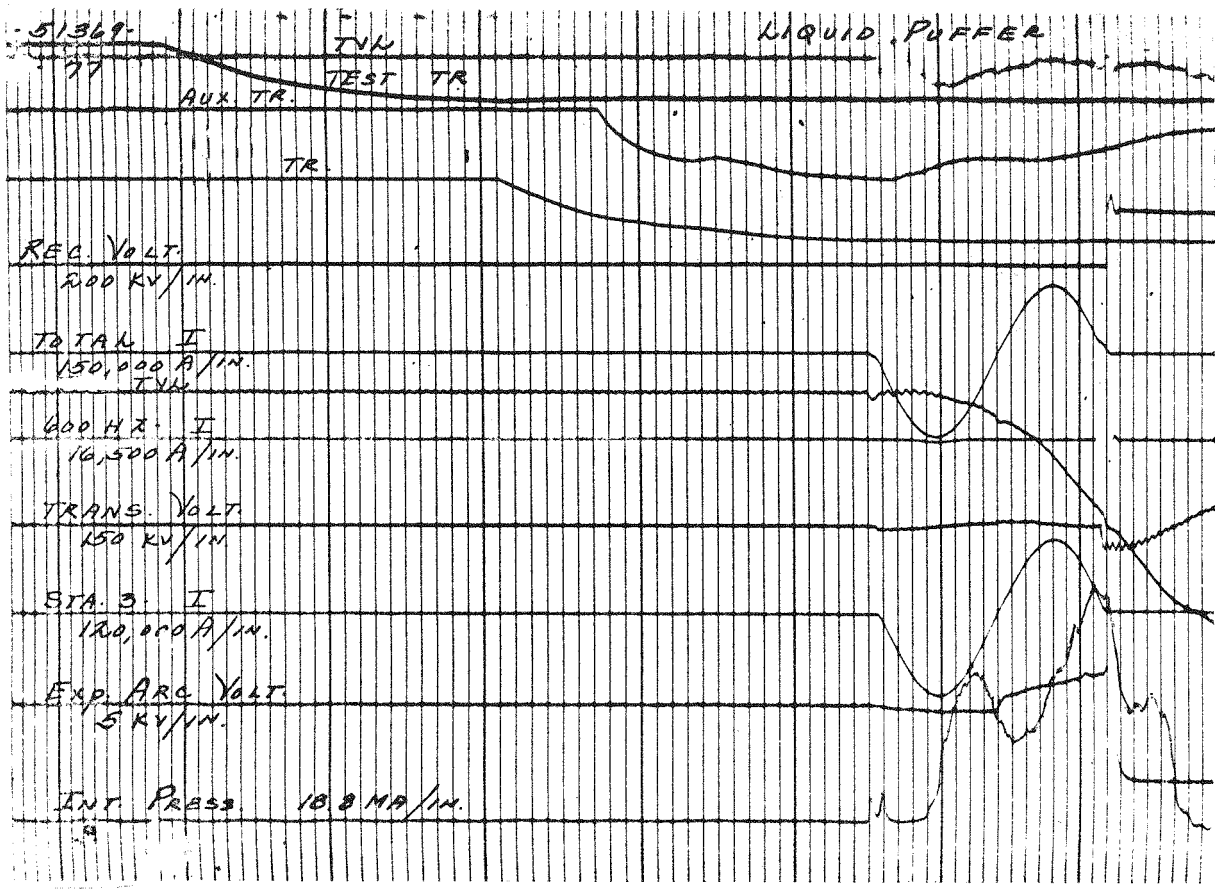


Figure 3-5 Bus Fault Test of Liquid Model Interrupter

Twelve short line fault tests were made with the liquid SF6 interrupter. Tests were made at the 80% level for the 100 kA, 145 kV rating.

Short line fault test results for the liquid interrupter are given in Table 3-2.

In this series of tests test letters P, T, W and AA were successful and the rest were failures. Tests R and U showed significant recovery during the first part of the short line fault transient but subsequently broke down. This indicated that these tests were very near critical for the interrupter. Tests T and U illustrate the variability of the liquid interrupter performance that was found. Although the timing and pressures are almost identical test T worked in spite of a slightly higher rms current during the last half cycle.

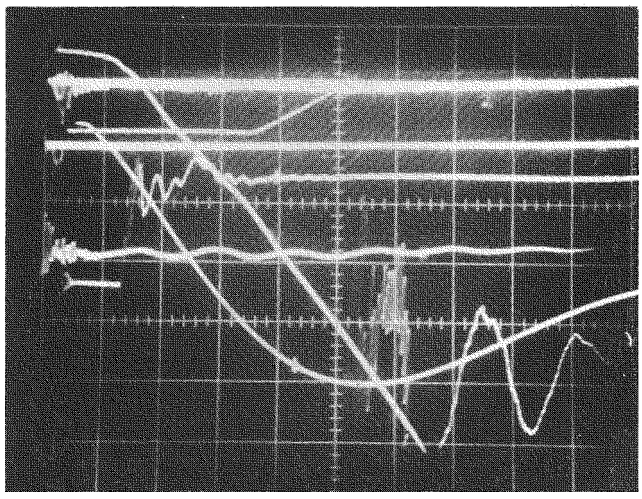

CALIBRATION: 12.9 kV/cm
SWEEP: 10 μs/cm

CALIBRATION: 64.5 kV/cm
SWEEP: 50 μs/cm

Figure 3-6 High Speed Oscillogram of Bus Fault Test

The required differential pressure at current zero for interruption was lower than the calculated value. The calculated differential pressure to interrupt the short line fault was 1200 psi at current zero. The short line fault tests showed variable performance. Short arcing times required 900 psi for differential pressure interruption, and these results were not consistent. At longer arcing times, differential pressures as low as 750 psi provided successful interruption.

To summarize although the liquid interrupter was inconsistant it always interrupted with lower differential pressures than were predicted. The same calculated differential pressure of 1200 psig was predicted by the computer model for both bus and short line faults (with 1000 pF capacitance). The test showed that bus faults were interrupted with a measured differential pressure of 295-380 psi. Tests for short line faults showed successful interruptions at differential pressures from 750-1050 psig.

## 3.2 HIGH PRESSURE $SF_6$ PUFFER INTERRUPTER

Mechanical tests, bus fault and short line fault tests were made on the complete model high pressure SF6 puffer interrupter.

a. Mechanical Tests

The mechanical tests were completed without any difficulties. The special instrumentation performed as desired. The time elapsed from 1.5 inches to 5 inches

travel was 10.5 milliseconds for 250 psi mechanism air pressure. This is the same as the calculated value. A time of 9.5 milliseconds was obtained by operating the dual mechanism system with 300 psi air pressure. This corresponds to an average velocity of 30.7 feet per second. Maximum interrupter differential pressure for this test was 456 psi. 250 psi mechanism pressure produced a 306 psi interrupter differential pressure rise. All of these tests were made with 240 psig SF6 fill pressure.

A fiber optic data acquisition system monitored the 2500 psig transducer in the interrupter piston, 500 psig transducer for the tank pressure, and the travel transducer located in the interrupter moving contact support pedestal. The receivers and decoders were used for mechanical tests of the puffer prototype, The oscillograph travel records were free of spikes and discontinuities observed on outputs of mechanical contact travel devices previously used. A complete description of the signal transmission system and its design is included in Appendix B of this report.

b. Interruption Tests

The interrupter was tested for 145 kV, 100 kA bus faults. The synthetic circuit test setup was the same as used for the liquid interrupter tests. The complete test data is given in Table 3-3.

The synthetic circuit was set for a the current slope at current zero equal to that of a 100 kA fault and the recovery voltage characteristics were set for a single break 145 kV interrupter. While adjustments were made to the circuit, the actual di/dt was 5% high whereas the initial dv/dt was 10% low. The crest voltage was a few percent high and the crest occurred more rapidly than desired (230 usec vs. 296 usec). All of these variations test the interrupter more severely than required by standards and, therefore, give pessimistic test results.

The first power test was made with the fill pressure of $SF_6$ at 300 psig and an arcing time of 13 ms. This first test was successful with 80 kA RMS for the last half cycle prior to interruption. The differential pressure in the interrupter was 515 pis at current zero. Design calculations for 100 kA bus faults give 600 psi as the minimum differential pressure for interruption. 80 kA would require 300 psi differential pressure on the same basis.

The next test was also successful with 10 ms arcing time. The differential pressure at current zero was 350 psi. Tests were continued at successively lower fill

pressures and with higher current on the last half cycle. The last of the six tests was done with 75 psi fill pressure at 10 ms arcing time with 95 kA on the last half cycle. All of the six tests were successful interruptions. The differential pressure at current zero in this last test was 300 psi. The test sequence of reducing pressure to find a minimum was directed towards finding the minimum fill pressure that allowed the interrupter to work.

The pressure required to obtain successful interruption was significantly lower than calculated for bus faults. The difference resulted in conservative rather than marginal design. Possible reasons for this improved performance were that the arc diameter did not increase as rapidly as calculated with these higher currents or that the model interrupter did not have flow stagnation regions between and around the electrodes present in previous interrupters used to develop interrupter theory. The majority of data used to develop the arc model was taken from single flow interrupters. These are some of the effects that can significantly change the calculated interrupter performance.

The contacts were in good condition after test considering the high current acing they were subject to during the testing. The nozzle had no unusual pitting or erosion as a result of the testing.

A series of short line fault tests was also completed. A total of 12 power tests were made during this test series at 80 to 90 kA which is the required current for 80% short line faults at the 100 kA, 145 kV rating. The complete test data is shown in Table 3-5. The interrupter worked significantly better than expected and critical test conditions were obtained for three values of shunt capacitance. It required 350-520 psi differential pressure for capacitance values over 2200 pFd. The interrupter contacts were in very good condition after the test series.

Test results with this interrupter show that interruption for both 100 kA bus faults and 80% short line faults are achieved with lower than predicted pressures. Bus fault interruption was achieved with a minimum of 280 psi differential pressure. Short line fault interruption was achieved with 380-520 psi differential pressure. The predicted differential pressure requirement for these two conditions was 600 psi.

TABLE 3-3

DATA ON 145 kV - 100 kA PUFFER MODEL

| Test Letter | Diff. Press at I=0 (psig) | $SF_6$ Fill Press (psig) | Air Press Mech (psig) | Shunt Capac $C_S$° (pF) | MEASURED CURRENT: Last Cycle (kVA) (rms) | MEASURED CURRENT: Last 1/2 Cycle (kA) (rms) | Arcing Time (msec) | Contact TVL at I = 0 (in.) | Ext.Arc Voltage (kV) (Peak) | RECOVERY VOLTAGE: LINE SIDE: 1st Peak (kV) | LINE SIDE: Time to 1st Peak (usec) | LINE SIDE: TRV kV/ (usec) | BUS SIDE: 1ST Peak (kV) | BUS SIDE: TIME to 1st Peak (usec) | BUS SIDE: TRV (kV/ usec) | Work/ Fail |
|---|---|---|---|---|---|---|---|---|---|---|---|---|---|---|---|---|
| 100% BUS FAULT | | | | | | | | | | | | | | | | |
| Z | 515 | 300 | 280 | 6000 | 73.5 | 79.5 | 14.0 | - | 4.6 | | | | 245 | 245 | 1.5 | W |
| AA | 350 | 300 | 280 | 6000 | 71.0 | 71.5 | 10.7 | - | 3.6 | | | | 245 | 245 | 1.6 | W |
| AB | 345 | 300 | 280 | 6000 | 73.5 | 83.0 | 10.7 | - | 3.2 | | | | 262 | 235 | 1.6 | W |
| AC | 355 | 200 | 280 | 6000 | 73.5 | 89.0 | 10.9 | 4.5 | 3.1 | | | | 259 | 235 | 1.6 | W |
| AD | 280 | 125 | 280 | 6000 | 73.5 | 99.0 | 11.4 | 4.9 | 3.6 | | | | 264 | 228 | 1.7 | W |
| AE | 300 | 75 | 280 | 6000 | 73.5 | 98.0 | 11.7 | 5.2 | 3.6 | | | | 263 | 230 | 1.6 | W |
| 80% SHORT LINE FAULT | | | | | | | | | | | | | | | | |
| AH* | 441 | 300 | 300 | 4800 | 76.0 | 77.5 | 16.8 | 6.6 | 6.7 | 42.0 | NA | NA | 135.0 | 215 | | W |
| AI* | 411 | 300 | 300 | 4800 | 73.5 | 72.0 | 12.3 | 4.7 | 5.0 | 42.0 | 5.4 | - | -- | - | | F |
| AJ* | 185 | 300 | 300 | 4700 | 73.5 | 68.0 | 10.0 | 3.6 | - | NA | NA | - | -- | - | | F |
| AK | 445 | 310 | 300 | 4800 | 73.5 | 90.0 | 11.0 | 3.7 | 3.6 | 42.6 | 5.4 | 8.7 | 135.0 | 215 | | W |
| AL | 380 | 300 | 300 | 2200 | 73.0 | 87.0 | 10.7 | 3.9 | 4.2 | 41.1 | 4.6 | 12.9 | 135.5 | 215 | | W |
| AM | 370 | 300 | 300 | 0 | 73.0 | 88.0 | 10.9 | 4.0 | 4.4 | 42.5 | 2.8 | 18.4 | 135.5 | 215 | | W |
| AN | 330 | 200 | 300 | 0 | 73.5 | 88.0 | 10.8 | 4.0 | 4.1 | (14.0) | NA | 12.3 | -- | - | | F |
| AO | 510 | 200 | 300 | 0 | 72.0 | 88.0 | 14.9 | 5.7 | 6.9 | 40.0 | 2.7 | 17.4 | 135.0 | 215 | | W |
| AP | 440 | 200 | 300 | 0 | 74.0 | 89.0 | 13.2 | 5.0 | 6.4 | (19.9) | (1.6) | 14.4 | -- | - | | F |
| AQ | 400 | 125 | 300 | 2600 | 74.0 | 87.0 | 12.9 | - | 4.1 | (21.9) | (1.6) | 10.1 | -- | - | | F |
| AR | 520 | 125 | 300 | 2600 | 72.0 | 72.5 | 15.7 | - | 4.9 | 43.0 | 4.0 | 13.2 | 131 | 220 | | W |
| AS | 430 | 125 | 300 | 2600 | 72.0 | 74.0 | 13.9 | - | 5.2 | 41.3 | 4.4 | 12.9 | 132 | 220 | | W |

ND Data not available ( ) Indicates Breakdown * Pressure Calibration Questionable

REFERENCES


1. J. Biermanns, "The Weil Circuit for Testing High Voltage Circuit Breakers with Very High Rupturing Capacities", Report 102, CIGRE, 1954.

2. ANSI/IEEE, "Guide for Synthetic Fault Testing of AC High Voltage Circuit Breakers Rated on a Symmetrical Current Basis", C37.081-1981.

3. E. Slameka, W. Rieder and W. T. Lugton, "Synthetic Testing - The Present State", Proceedings IEE, Vol. 125, No. 12, Dec. 1978.

4. IEC, "Reporting on Synthetic Testing of High Voltage AC Circuit Breakers", Report 427 (1973).

Section 4

# MATERIALS STUDY

Westinghouse pioneered the development of $SF_6$ gas circuit breakers. In this process, the $SF_6$ gas subjected to arcing was found to seriously effect many common insulating materials. The presence of moisture increased the effect. Methods were developed to test the capability of insulating materials to withstand the circuit breaker environment. Methods were also developed to test the yield strength of metals. Most of the insulating materials and metals currently being used in $SF_6$ circuit breakers were selected by these tests.

Insulating materials were evaluated at a temperature of 125°C or below, and the present hot spot temperature limit of metals is set at 105°C. These temperature limits are generally considered to be adequate for the state of the art $SF_6$ circuit breakers. Interrupting and continuous current requirements, on the other hand, are increasing and the demand of increased temperature capabilities of insulation metals is becoming more and more critical. The interrupter developed in this project will subject materials to higher stresses both thermal and electrical than commercial interrupters.

For this reason, an evaluation of insulation and metal parts at higher temperatures and stresses was included as one of the essential tasks in this project.

## 4.1 Scope of Work

The scope of this task was to determine whether thermal or electrical limits affect interrupter design. Existing test systems were adapted for testing the materials under controlled temperature, mechanical and electrical stresses. Tests of the performance of insulating materials, metal parts and current carrying contacts in $SF_6$, and arced $SF_6$, at high temperatures and high electrical stresses were carried out. The decomposition of $SF_6$ gas and effects of the decomposition products on materials at temperatures up to 150°C were evaluated. A complete list and description of the materials tested is given in Appendix A Table 1.

Insulating materials were studied at temperatures up to 135°C and superior materials were reviewed to determine the possibility of increasing this temperature limit.

Based on this scope of work this task was carried out in the following manner.

a. Insulating and metallic materials to be evaluated were selected from those known to be of superior quality considering the needs of single pressure $SF_6$ circuit interrupters.

b. Detailed test procedures were established.

c. A high pressure test chamber used in previous material tests was rebuilt and hydrostatically tested to above 1000 psig. The test chamber which is shown in Figure 4-1 was designed to perform screening tests of insulating materials for use in $SF_6$ circuit breakers. It has 16 high pressure bushings that are used to mount 16 samples in the chamber. Figure 4-2 shows one bushing with the insulating sample mounted for test. THe usual procedure for evaluating an insulating sample consisted of mounting the samples in the test chamber, measuring the leakage current of the sample in $SF_6$, then generating about 80 kW-sec of arc energy in the small gas volume inside the steel tube to shield the samples from the arc radiation and then measuring the leakage current of the samples at 1 kV as a function of time. In some tests the effect of injecting water into the chamber after arcing was studied. This test simulates the effect of opening a circuit interrupter for maintenance and then returning it to service without cleaning. The past experience has shown that satisfactory insulating materials do not develop measurable leakage under these conditions while unsatisfactory materials do develop measurable leakage. The bushings also permit dielectric test of the samples up to 15 kV rms. Experience with this test indicate that acceptable materials easily withstand this test voltage on a surface gap of 0.1 inch.

d. The test chamber, $SF_6$ system, and instrumentation were assembled, and thoroughly checked out for test conditions.

e. Insulating materials were evaluated at 135°C with 500 psig arced $SF_6$. The effect of water vapor was tested. Leakage current and a.c. dielectric strength were measured at intervals.

f. The effects of arced $SF_6$ on surface conditions of metals were investigated in at 150°C with 50 psig $SF_6$. The effect of water vapor was also investigated.

g. Variations of contact resistance of silver coated cupaloy contacts and of silver coated aluminum contacts were measured in 150°C and 520 psig $SF_6$ environments with and without the presence of water vapor.

h. Metals and glass fiber reinforced rods were exposed to 135°C and 500 psig arced $SF_6$ environments. Changes in the yield and tensile strengths were investigated. Springs of three different materials were also evaluated.

i. Five insulating materials, including one control material, and four metals were selected and exposed to a 135°C and 500 psig arced $SF_6$ gas environment for 300 hours. Changes in leakage current and dielectric strength of the insulating materials during and after the 300 hour exposure were measured. For the metals, hardness measurements were taken before and after the test.

j. $SF_6$ gas samples and deposits obtained after certain exposure tests were analyzed.

## 4.2 SUMMARY OF RESULTS

Most of the insulating materials tested showed low leakage currents of 1 uA or less at 1 kV and at a temperature of 135°C. Two materials, cloth micarta and cast epoxy, showed between 15 and 60 uA. Nylon showed a high leakage current and, after an electric breakdown, the leakage current increased drastically. Porcelain showed excellent electrical characteristics, but the specimens cracked because of thermal stress.

Five insulating materials showed excellent electric characteristics during and

after a 300 hour exposure to arced $SF_6$ at 135°C and 500 psig. These materials are: Virgin Teflon, Pultruded Glass Epoxy resin, Glass Polyester, Glass Epoxy, and Cast Epoxy Resin.

The effects of exposure of metal parts to arced $SF_6$ gas at 135°C and 500 psig, or 150°C and 520 psig were negligible. The effect of added water vapor was also negligible.

The contact resistance of silver coated cupaloy butt contacts remained low in an $SF_6$ environment of 150°C and 520 psig with or without added water vapor. However, the resistance of silver coated aluminum contacts which are acceptable at 125°C increased and varied widely in a random manner after exposure to these conditions.

Mass spectrometric analyses of $SF_6$ gas samples withdrawn at various stages of test indicated that the $SF_6$ gas is unaffected when exposed for 2 hours to a 135°C or a 150°C temperature in the presence of the selected materials.

Analyses by emission spectroscopy of dusts collected after exposure tests indicated that the two primary components of the material were copper and iron, derived from the electrodes and the arc confining tube, respectively.

Appendix A is a detailed report of this material study.

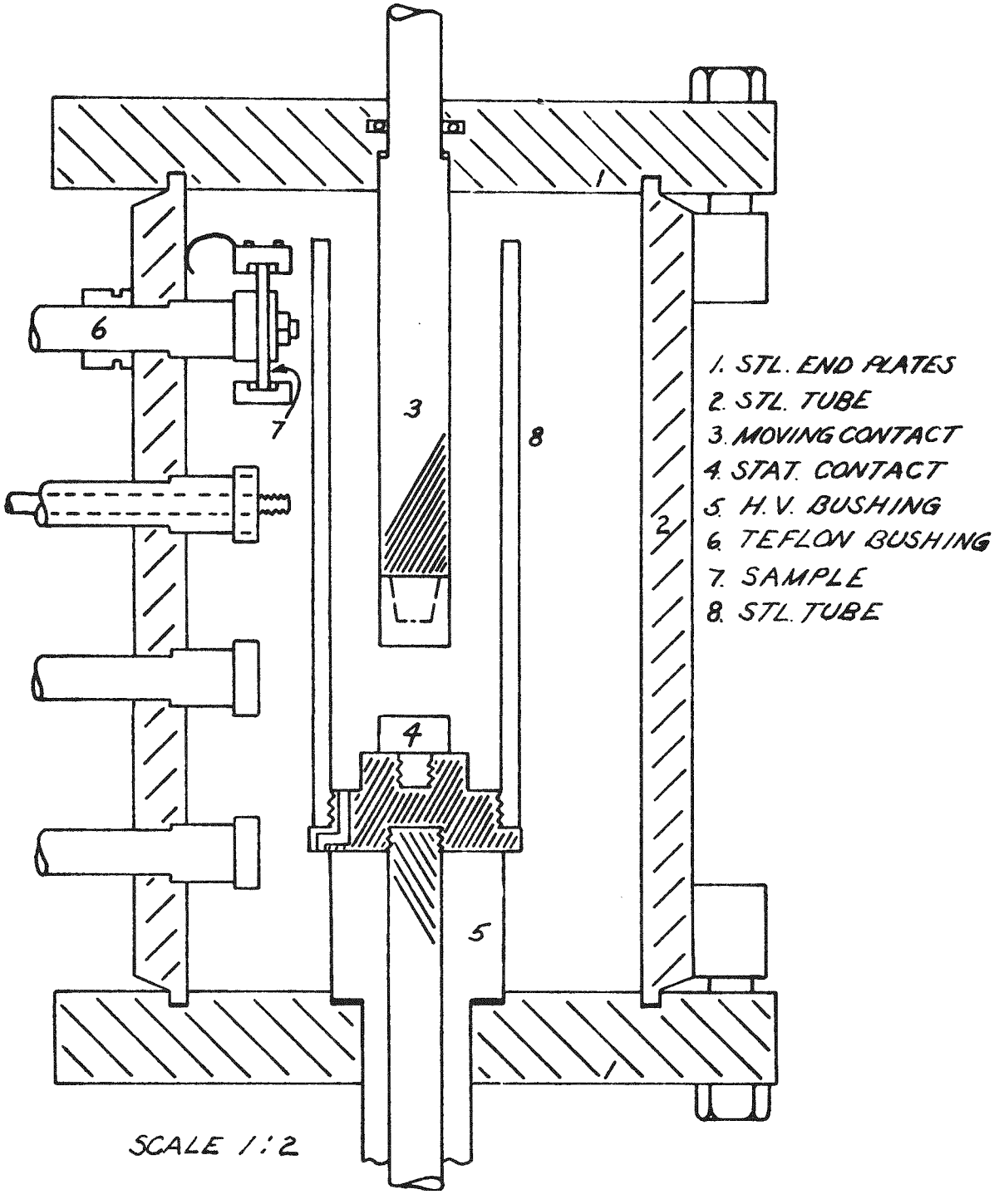


Figure 4-1 Arcing Chamber for Insulation Samples

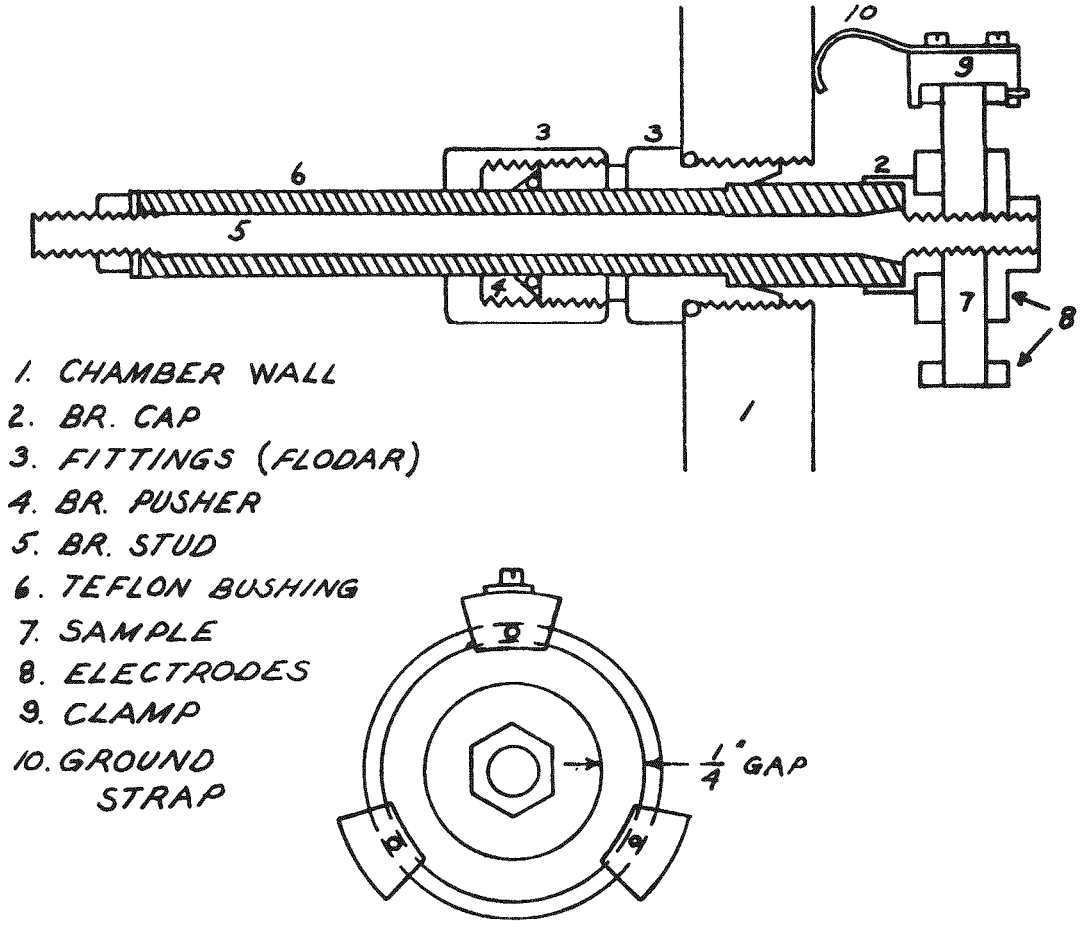


Figure 4-2 Mounting for Insulation Test Samples

Section 5

# PROTOTYPE DESIGN

## 5.1 INTRODUCTION

The objective of this task was to design the optimum interrupter for the required interrupting ratings i.e. 100 kA 242 kV and 120 kA 145 kV. The required application of the interrupter would be for a single break dead tank breaker with gas to air bushings and bushing type CT's. The assumptions made was that since they are common to all versions of the interrupter, the bushings and CT's do not affect the optimization. However the rest of the circuit breaker is considered in the optimization process and the specific key components evaluated were:

a. Interrupter
b. Gas fill pressure and heaters when required to prevent liquification
c. Line to ground shunt capacitance to control TRV on SLF
d. Mechanism
e. Tank

The basis for the optimization would be for the minimum manufactured cost of the complete circuit breaker of suitable reliability.

After reviewing the results of the model interrupter tests it was decided that the high pressure $SF_6$ puffer was superior to the liquid $SF_6$ interrupter for this application. The liquid interrupter showed inconsistant performance during short line fault tests. Even when the differential pressure exceeded 1000 psi and the 60 Hz current was only 80 kA the interrupter worked on one test and failed on the next test under the same conditions. The erosion and damage to the liquid interrupter was excessive after a series of 14 tests at currents near 70 kA.

Under the same kind of test conditions the high pressure $SF_6$ puffer suffered little damage during a series of 12 tests at currents from 73-90 kA. The puffer also was very consistant in the condition that would produce successful interruptions and did not produce widely varying interrupter pressures.

Given these characteristics of the two model interrupters, the conclusion was reached that the high pressure $SF_6$ puffer should be selected for the prototype

interrupter. In order to determine the optimum puffer interrupter design, three different interrupter concepts were developed and analyzed with respect to each other. These were the floating piston puffer, the driven piston puffer and the simple puffer shown in Figures 5-1, 2 and 3. Concepts for three types of single pressure interrupters were developed to the point that they could be evaluated along with their effect on other circuit breaker requirements.

The cost of the mechanism was derived from the interrupter driving requirements assuming a pneumatic mechanism would be used. The cost estimates were based on the contractors years of experience with the manufacture of a wide variety of pneumatic mechanisms.

The tank cost estimates are based on the labor and material content of the required tank as a function of operating pressure and required clearance for insulation which are also a function of pressure.

## 5.2 INTERRUPTER REQUIREMENTS

The basis for comparison of the three interrupters was to require that the three different puffer configurations should produce the same current zero pressure rise as the model interrupter when equipped with the same interrupting chamber. Where the interrupting chamber is made up of the stationary and moving contacts and the flow directing nozzle. The three different puffers considered then are just three different ways of producing the same $SF_6$ compression to produce the same pressure rise at current zero. In general we can characterize the various parameters for interrupter design in Table 5-1.

Characterizing a single pressure interrupter is difficult because of the complex relationships that exist between the parameters cited above. First, any given interrupting chamber the interrupting capability is measured by its ability to stop the current at or near a natural current zero, which is primarily a function of the interrupting chamber design and the interrupting chamber pressure at the instant of current zero. However the pressure at current zero is a function of the arcing history where heating of the gas and ablation of the insulating nozzle add to the pressure that would be developed by the compression function alone.

TABLE 5-1

CHARACTERIZATION OF A SINGLE PRESSURE INTERRUPTER FOR AN $SF_6$ CIRCUIT BREAKER

| INPUTS | INTERRUPTER CHARACTERISTICS | OUTPUTS |
|---|---|---|
| Mechanism Driving Force = F (t) | Interrupting chamber | Interrupter pressure = P (I, t, S) |
| Circuit Voltage = V (t) | Gas fill pressure | Dielectric capability = D (I, t, S) |
| Circuit Current = I (t) | Shunt Capacitance | Voltage across interrupter = Vi (I, t, S) |
| Inherent Circuit Parameters | Effective mass = M (S) | Hot gas = HG (I, t, S) |
| | Position = S (t) | |
| | Friction = f (S, V); V = dS/dt | |
| | Compression function = CG (S) | |

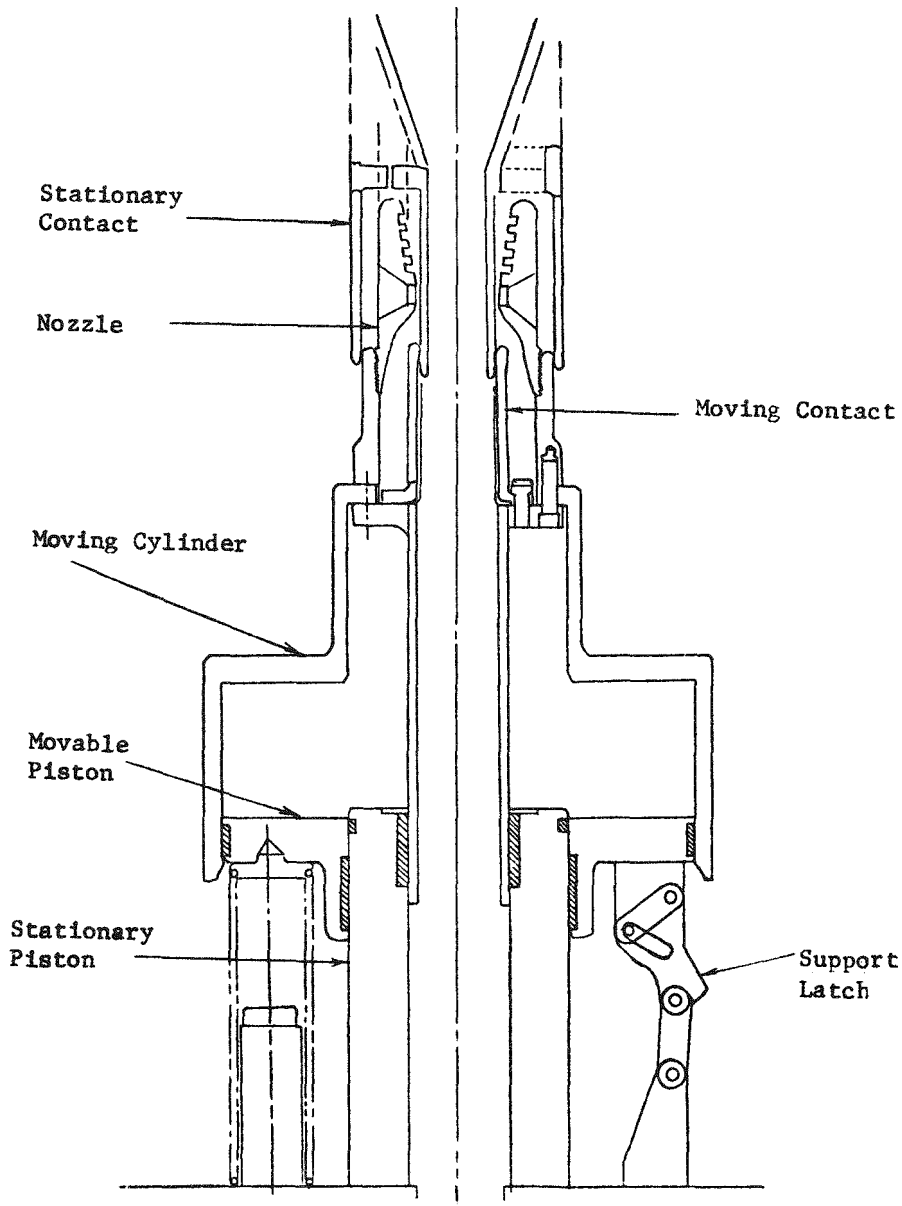


Figure 5-1 Floating Piston Puffer

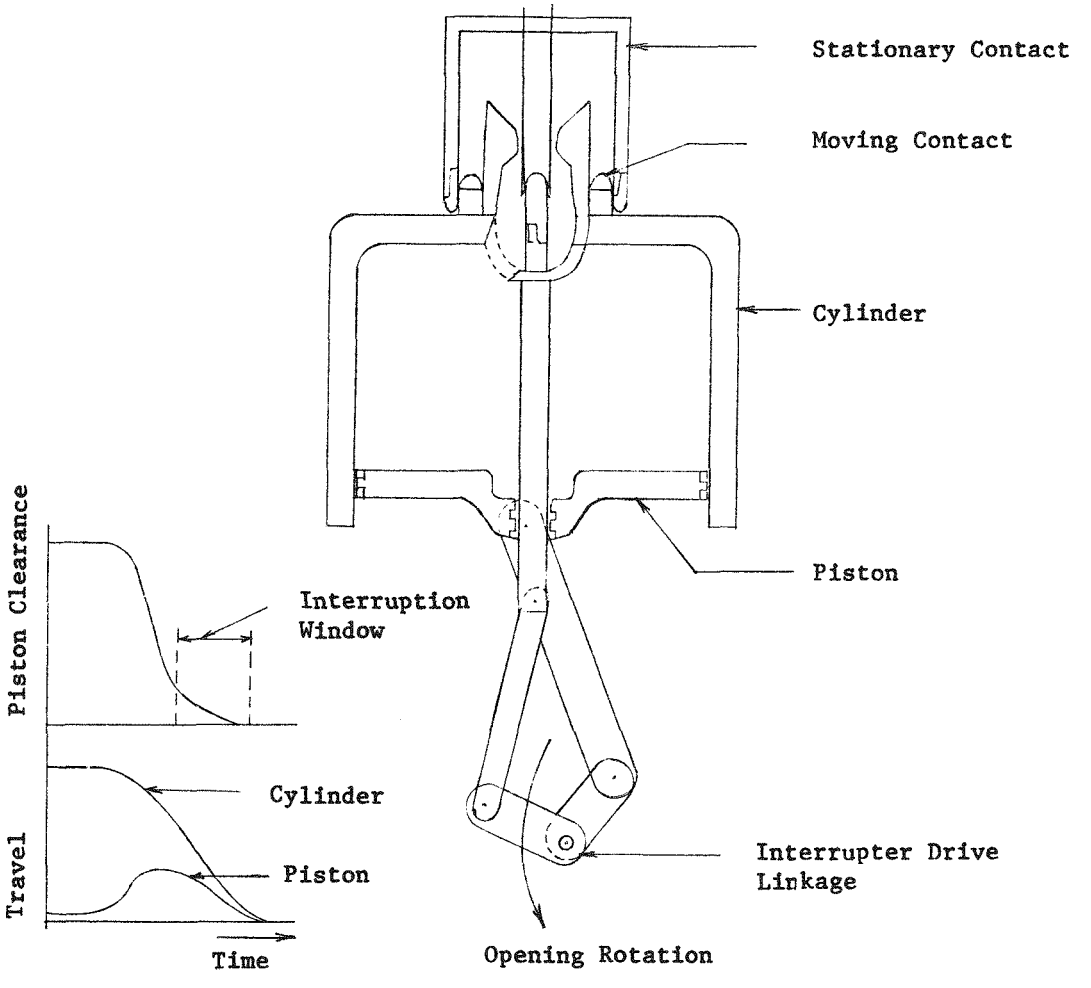


Figure 5-2 Driven Piston Puffer

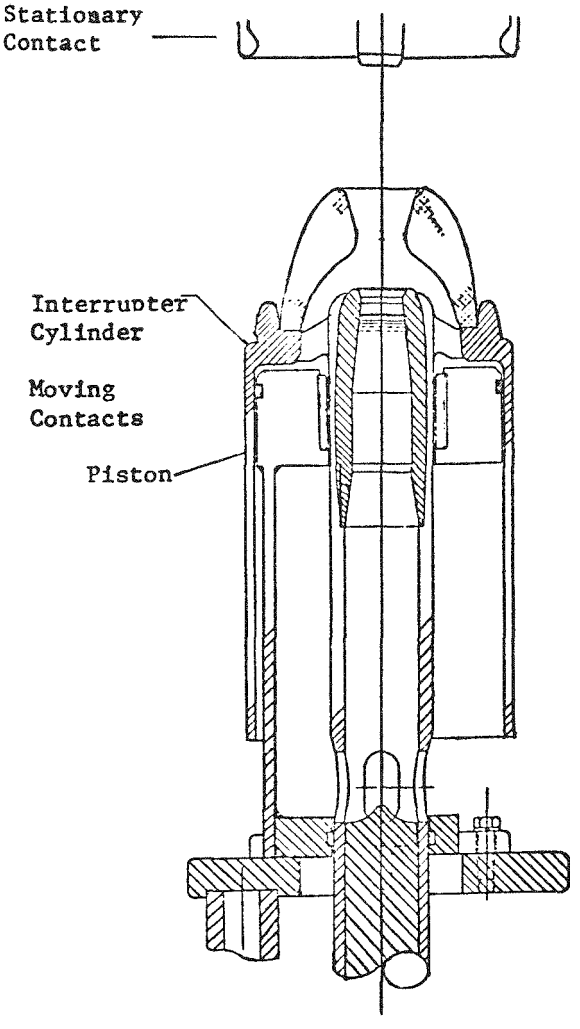


Figure 5-3 Simple Puffer

Second, the interrupting capability is measured by the ability of the interrupter to withstand recovery voltages that occur across it due to the response of the connected circuit. In this case the utilization factor of the electrodes and their separation determines the dielectric strength subject to the effect of accumulated and flowing hot gases that are produced by the arc.

Based upon these two primary characteristics of interrupters there are three prime types of normal switching duty that control the design of the interrupter. These are capacitor switching (or line dropping), bus faults and short line faults.

b. Capacitor Switching

For capacitor switching the current to be interrupted is low and the TRV rate is very low so that the interruption can occur at almost zero contact gap and thus the contacts must open fast enough so that the interrupter can withstand the full applied voltage which is more than two per unit at 8.3 msec after current zero. Under this condition since there is little or no arcing there is no hot gas to deal with and only the cold gas, plus the effects of flow, control the dielectric strength of the gas space.

c. Bus Faults

For bus faults the interrupter must interrupt the maximum currents but the peak TRV applied is limited to approximately 1.8 per unit and the rate of rise of recovery voltage is fairly low. In this case the accumulation and flow of hot gases is at its maximum and the consequent reduction of dielectric strength of the gas in the electrode gap is also maximum.

d. Short Line Fault

For short line faults the currents are reduced to 90% or less of the maximum bus fault by the impedance of a short section of transmission line between the breaker and the fault. In this case the rate of rise of recovery voltage is very high and the primary requirement for the interrupter is to develop dielectric strength through the previously conducting arc column. This is primarily achieved by the high differential pressure developed by the interrupter and the consequent cooling of the arc channel. Since the overall TRV is lower than that for bus faults and the current is also lower this type of interruption is less sensitive to the accumulation and flow of the hot gases. This type of interruption is strongly affected

by the amount of shunt capacitance that appears across the short transmission line, and this can be used to improve the performance.

e. Range of Arcing Time

We expect that the circuit breaker will be called upon to interrupt all of the required faults and load currents with random tripping. The start of motion of the interrupter is therefore completely random with respect to the power frequency current and voltage. Then consideration of all of the interrupting conditions will require the consideration of the full range of possible times at which a current zero can occur. For capacitor switching the most severe case occurs when the current zero occurs immediately after contact part. In this case the interrupter has only 8.3 msec to develop a dielectric capability of greater than two per unit i.e. 2 times the peak value of the nominal line to ground voltage rating of the interrupter. For the bus fault case the results from the model interrupter tests show that a minimum of 5 inch gap is required to develop sufficient interrupting chamber pressure and sufficient dielectric capability to successfully interrupt the circuit.

One very important characteristic of single pressure interrupters is their self synchronizing character. That is they conserve gas in the interrupting chamber by clogging of the exit nozzles until near current zero where the high speed flow of gas is required for interruption. Also the peak pressure increases as the arcing time increases to provide an even higher pressure that is required to cool the larger quantity of gases produced by the longer arcing time.

For the short line fault condition the same kind of conditions apply with the added requirement that the arc voltage achieved just prior to current zero $E_o$ is critical to the interrupting capability as shown in Equation 1 of Appendix C.

## 5.3 INTERRUPTER SELECTION

a. Interrupter Configuration

Having established these criteria for the interrupter then we can consider the three interrupter concepts that were analyzed. First the floating piston puffer shown in Figure 5-1 was considered to be a promising candidate for obtaining the high interrupter pressures thus reducing the value of shunt capacitance necessary to interrupt 120 kA. This design was capable of reaching this goal. The

principle of operation is as follows: during the first part of the interrupter travel the gas in the puffer cylinder is compressed by the large movable piston which is supported by latches. When the moving cylinder reaches the latch the moveable piston is released and it is driven directly by the moving cylinder. At this point in the travel the stationary piston enters the smaller diameter section of the moving cylinder and compresses the gas to very high pressures during the last half of the interrupter travel.

This puffer action can achieve very high interrupter chamber pressures and could reduce the amount of shunt capacitors required for 120 kA short line fault interruptions. This type of design is capable of reaching this goal, but after analysis of the driving force and system inertia it became apparent that the mechanism would have to have a high moving effective mass to prevent stalling in midstroke particularly at the critical point when the large piston is released and a large quantity of gas must be driven into the smaller high pressure chamber. This higher mass for the mechanical system requires a larger mechanism with a higher cost to achieve the required speed for the interrupter and this higher cost offsets any possible savings in the shunt capacitor cost.

The driven piston puffer as shown in Figure 5-2 allows tailoring the compression of the gas to achieve the optimum combination of puffer pressure vs main contact stroke. Where the initial compression rate can be varied by changing the lever arms and initial angles for the drive for the moving piston and cylinder. Figure 5-4 shows the variation in compression function that can be achieved with all three puffer concepts. The driven piston puffer curves are based on the variation in compression function that can be achieved with a 7.5 in diameter moving piston in a moving cylinder with a total travel of the cylinder of 12 inches.

Analysis based on these curves and the comparable curve for the simple puffer shows that the best curve for the puffer compression function is the simple puffer which gives the longest time at lower pressure in the cylinder. With this condition the size of the arc is larger through most of the stroke and the consequent gas heating and ablation are more effective in increasing the pressure available at current zero for the final interruption. This condition enhances the self synchronizing action of the puffer by compressing the gas more slowly and providing more time for the self synchronizing effect of puffer pressure to occur.

Figure 5-5 shows that for low initial compression of 1, which is equal to that for a simple puffer, the total cost is minimum. This is primarily because of the

lower cost of the interrupter and shunt capacitance. The cost of the mechanism is high but only by about 30% over the minimum value which is the case for the initial compression rate of 3 which corresponds to curve 3 of Figure 5-4. More capacitance is required for this case because the gas is compressed more quickly to a higher pressure and thus the gas heating upstream is reduced and the ablation is also reduced. Both of these factors reduce the differential pressure that is available at current zero.

Comparing the driven piston puffer and the simple puffer it is obvious that the added cost and complication of driving both the piston and the cylinder is not justifiable when compared to the cost of the simple puffer. Therefore, a simple puffer was selected as the best interrupter configuration for application.

1. Driven piston puffer low initial compression rate (1)
2. Driven piston puffer medium initial compression rate (2)
3. Driven piston puffer high initial compression rate (3)

Std.-fixed piston constant diameter puffer, FP-floating piston puffer with D1/D2 = 2

All assumed to have 10:1 compression ratio

(1) an initial compression rate equal to that of the standard puffer

(2) an initial compression rate equal to 2X

(3) an initial compression rate equal to 3X

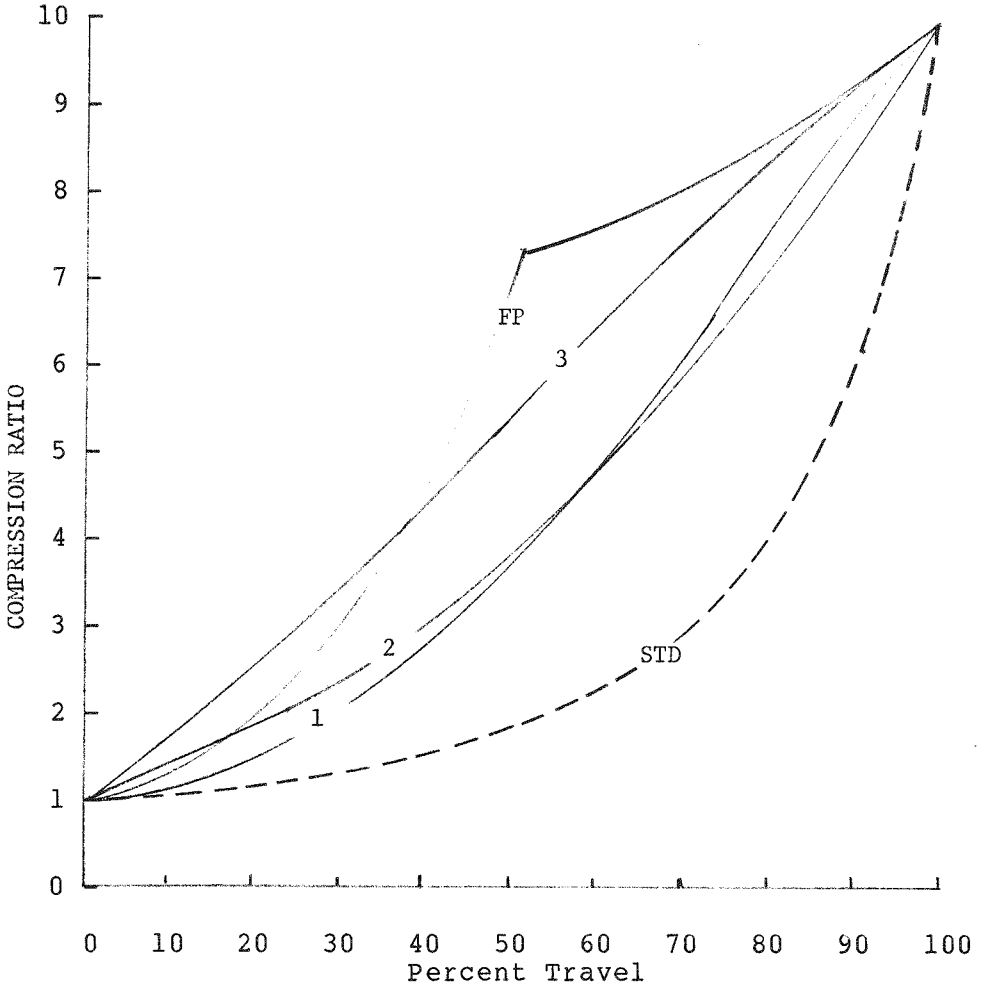


Figure 5-4 No Load Compression Function of Alternate Puffer

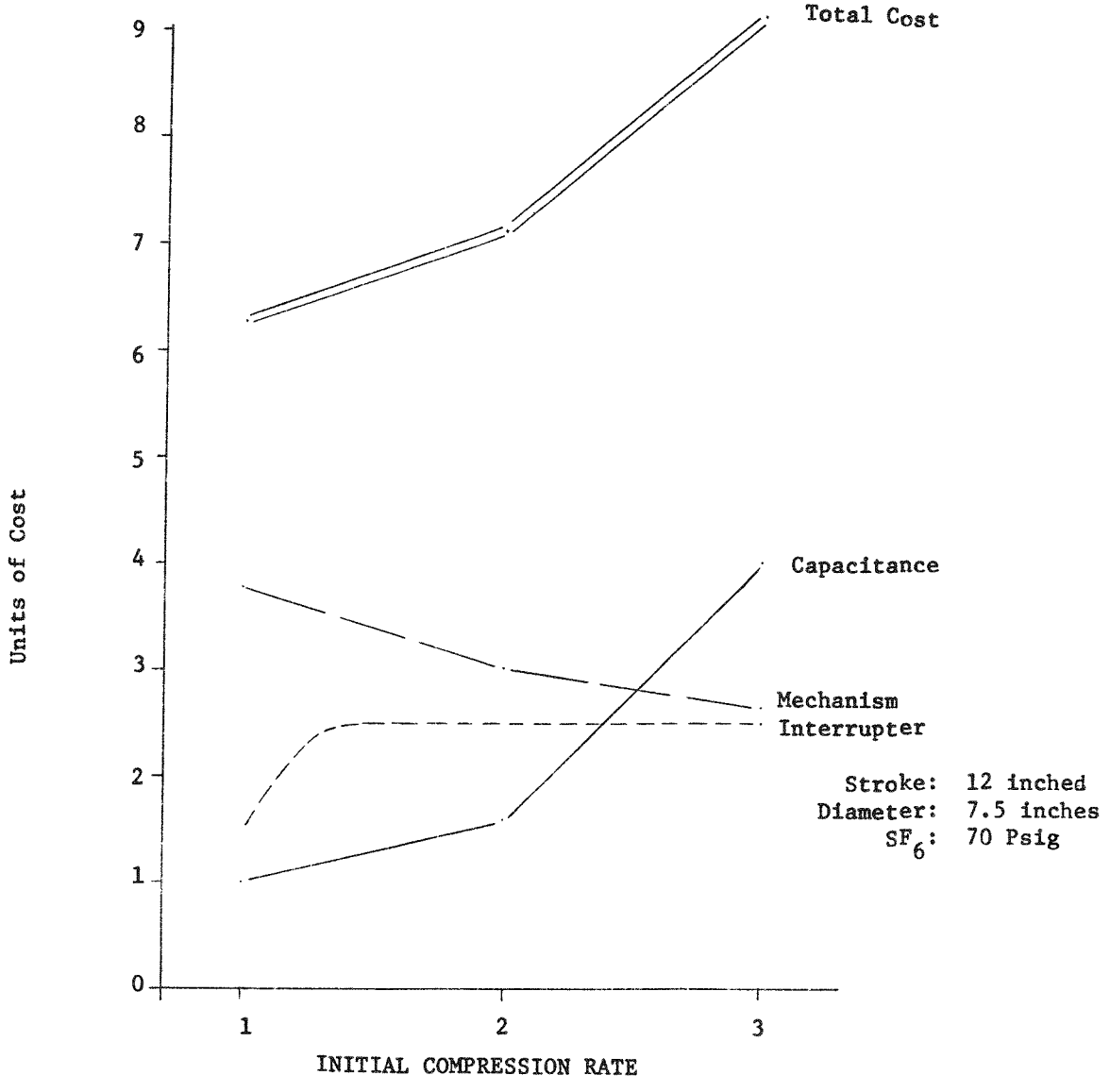


Figure 5-5 Cost Comparison of Initial Compression Rate by Modification of an Interrupter Design

b. Design Pressure

The first design constraint that must be approached is to determine the design pressure of $SF_6$. The technique used to determine this pressure was to compare the variable costs in a circuit breaker that vary as a function of fill pressure for a given calculated performance level. The cost components that significantly vary with design fill pressure are the cost of the tank, the heaters, the mechanism and shunt capacitors used in the eventual circuit breaker.

c. Heater Requirements

Heaters are required in $SF_6$ circuit breakers that operate at gas densities above 2.5 pounds per cubic foot (75 psig at 20°C) because the gas liquifies at the low end of the temperature range (-30 to +40°C). This liquification reduces the density of the gas in the circuit breaker and therefore reduces its performance. For the evaluation in this study we assumed that the circuit breaker would be operating in the Minneapolis, Minn. average monthly temperatures and that the fixed cost of providing auxiliary power was $500/kw. Figure 5-6 shows the comparison of the heater cost with the other variable costs on an arbitrary scale where 10 units is the total cost for the variable components for a 75 psig fill pressure at 20°C. The cost of heaters increases approximately as the square of the fill pressure because required minimum tank temperature is proportional to pressure and the heat loss are also proportional to tank temperature rise.

d. Tank Cost

The cost of the tank is approximately proportional to the square root of the operating pressure. The material thickness and weight of the tank increase proportional to operating pressure however the size of the tank can be reduced at a rate less than proportional to pressure because of the higher dielectric strength of the gas. The net result is a cost that increases less than proportionally with pressure.

e. Mechanism and Shunt Capacitor Cost

These two parameters are considered together because as is shown in Figure 5-5 they are closely interrelated. The size of the shunt capacitor can be reduced at the expense of increasing mechanism operating energy. Similarly the mechanism cost can be reduced by increasing the fill pressure of the circuit breaker. Based upon

pneumatic mechanism cost and the offsetting cost of internally mounted shunt capacitors, the curve of Figure 5-6 shows a declining cost of the mechanism/capacitor combination with increasing fill pressure. However the total of these costs only drops from about 5 units at 75 psig to 2.5 units at 300 psig. Since the mechanism must both accelerate the moving parts of the circuit breaker and compress the gas for interruption the mechanism energy can only be reduced to about half by increasing fill pressure. The mechanism cost is assumed to be proportional to the square root of the total mechanism energy. The cost of internal shunt capacitors was assumed to be proportional to capacitance. The value of capacitance that could be used was limited by size. The capacitor package was limited to the same volume as the interrupter. With this criteron the capacitor would be limited to about 12,000 pF at 145 kV and 9000 pF at 242 kV.

A second and less easily defined limitation on the shunt capacitor is the potential harmful effects of large shunt capacitors on the substation circuit. The limitation of 12,000 pF at 145 kV and 9,000 pF at 242 kV correspond to the values of potential device capacitors that are used in general practice. With this limitation the shunt capacitance values selected should be acceptable.

f. Conclusions with Regard to Variable Costs

The total curve of Figure 5-6 shows a monotonic increase of total circuit breaker variable cost with fill pressure. Even though all of the factors have not been included the general effect of increased working pressure would be to increase the cost of all of the other circuit breaker components except the interrupter itself. Since the interrupter constitutes a small part of the total cost it cannot significantly affect the conclusion that the best fill pressure that can be selected is 75 psig which is also the maximum pressure that can be used without heaters.

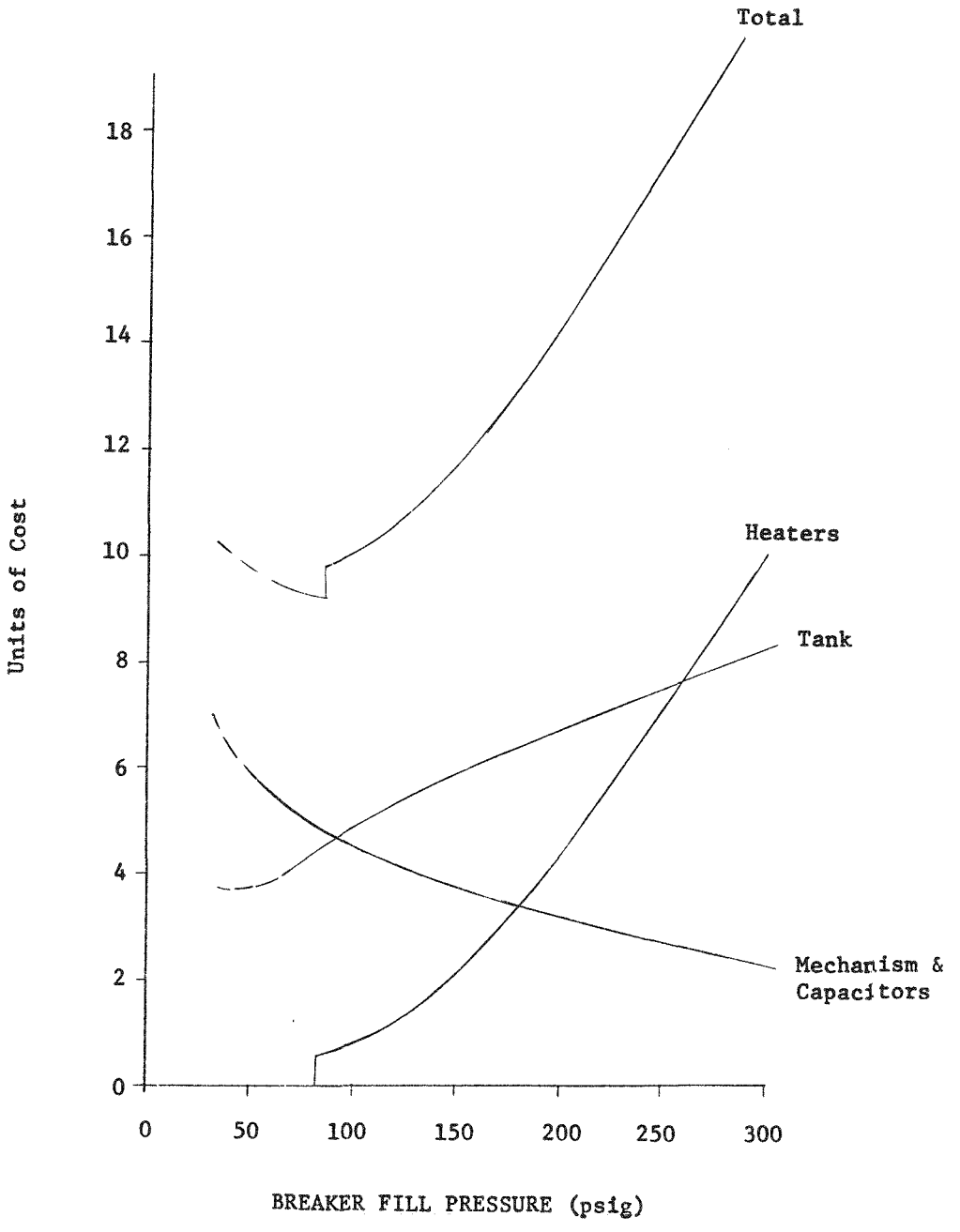


Figure 5-6 Comparison of Variable Costs vs. Breaker Fill Pressure at 70°F

## 5.4 INTERRUPTER ANALYSIS AND DESIGN

The previous section has dealt with the selection of certain interrupter parameters that permit optimization of the circuit breaker. This section deals with the design of the simple puffer and its mechanical drive system to provide interrupting differential pressures. The model puffer interrupter that was tested during the first part of this project has shown the inherent capability of interrupting all of the fault requirements for the 242 kV 100 kA rating. As will be shown later in this section the critical short line fault for this rating is 90% or 90 kA and the test data for the puffer model clearly shows the ability to interrupt this rating. The bus fault requirement for the 242 kV rating was demonstrated with tests at 98 and 99 kA with the required rate of rise of transient recovery voltage however the maximum voltages required for 242 kV were not reached during the model tests. The successful interruption of up to 90 kA under short-line-fault conditions clearly shows that the interrupting chamber is superior to any that has been previously reported. Therefore, this model interrupting chamber is also the best interrupting chamber available for upgrading to the 120 kA rating required. The components that are considered parts of the interrupting chamber are the moving and stationary contacts and the teflon flow director nozzle. The task then for this design is to determine how to obtain the required interrupter differential pressure and dielectric withstand. In terms of the parameters given in Table 5-1 the following parameters must be derived:

- Puffer piston diameter and travel as a function of time
- Dielectric withstand capability of the interrupter as a function of position and of arcing history.

In order to derive these two critical parameters for a realistic circuit breaker conditon it is necessary to consider all of the interractions that occur during the complete operation of a circuit breaker including this interrupter.

### a. Computer Model

The approach used for this design was to use a computer model of the total response of the interrupter in a test breaker including all of the test breaker characteristics. This computer model of a puffer circuit breaker has been developed throughout this project from an early proprietary program developed by Messers. Frost and Swanson of the Westinghouse R&D Center. The program has

gradually grown to include the dynamics of the Model interrupter, mechanism, and linkage and the effects of teflon nozzle ablation based upon results obtained by Noeske (1).

b. Differential Pressure

In order to derive the required interrupter dimensions it was first necessary to determine the required differential pressure to interrupt the critical short line faults and bus faults. Appendix C shows the derivation of interrupter pressures at current zero required to interrupt the short line faults as a function of shunt capacitance and fault fraction. Figure 5-7 shows that the maximum current zero pressure is required for fault fractions of about 85%. By extrapolating from this curve it was determined that a current zero pressure of 540 psia would be required for the 120 kA 145 kV rating when a shunt capacitance of 12,000 pF is used. With an $SF_6$ fill pressure 90 psia the differential pressure of 450 psi would be required. Similarly Figure 5-8 shows the required current zero pressure for interrupting 242 kV is a maximum for a fault fraction of about 90%. By extrapolating from these curves it was determined that a current zero pressure of 510 psia would be required for the 100 kA 242 kV rating when a shunt capacitance of 9000 pF is used. With an $SF_6$ fill pressure of 90 psia a differential pressure of 420 psi would be required.

c. Factors Affecting Puffer Interrupter Pressure

Three factors in addition to simple mechanical compression affect the actual interrupting pressure achieved by a puffer. These are the ratio of specific heats, blocking of the nozzle by the arc and ablation of teflon upstream from the vena contracta.

The ratio of specific heats for $SF_6$ increases sharply as the pressure approaches the critical pressure for the gas. This factor is included in the computer puffer model and accounts for a pressure increase 50% higher than simple adiabatic compression would produce.

Blocking of the nozzle by the large high temperature arc leads to additional pressure rise during puffer operation. Analysis of model puffer tests lead to the development of the following arc area equation.

$$A = Ka\ I\ P^{-1.5}$$

Similarly an expression for the effect of ablation was derived to fit the model puffer tests. The equation takes the form

$$\frac{dm}{dt} = km \quad I^{1.5} \quad p^{-2}$$

Where $\frac{dm}{dt}$ is the rate of ablation of the Teflon nozzle in kilograms per second.

The combination of these factors leads to significantly higher interrupter pressures than could be achieved by simple mechanical compression. These factors are incorporated into the puffer computer model in order to provide the best fit of calculated pressure with experimentally measured pressures.

d. Piston Diameter

The required puffer piston diameter was determined by using the computer model to calculate the piston diameter that would provide the interrupting pressures over the arcing range and still provide adequate dielectric strength for the capacitor switching requirement. A diameter of 9.75 inches was selected. A larger piston could provide the interrupting pressures but would have too short a gap to withstand the full capacitor switching recovery voltage. A smaller piston could provide the required pressures over the arcing range but it would have more than the required recovery capability and would also require higher velocities than the optimum and therefore higher mechanism energy. A second and closely related requirement is the dielectric strength of the interrupter gap in the fully open position. Although this is obviously not independent it is treated separately in the this section.

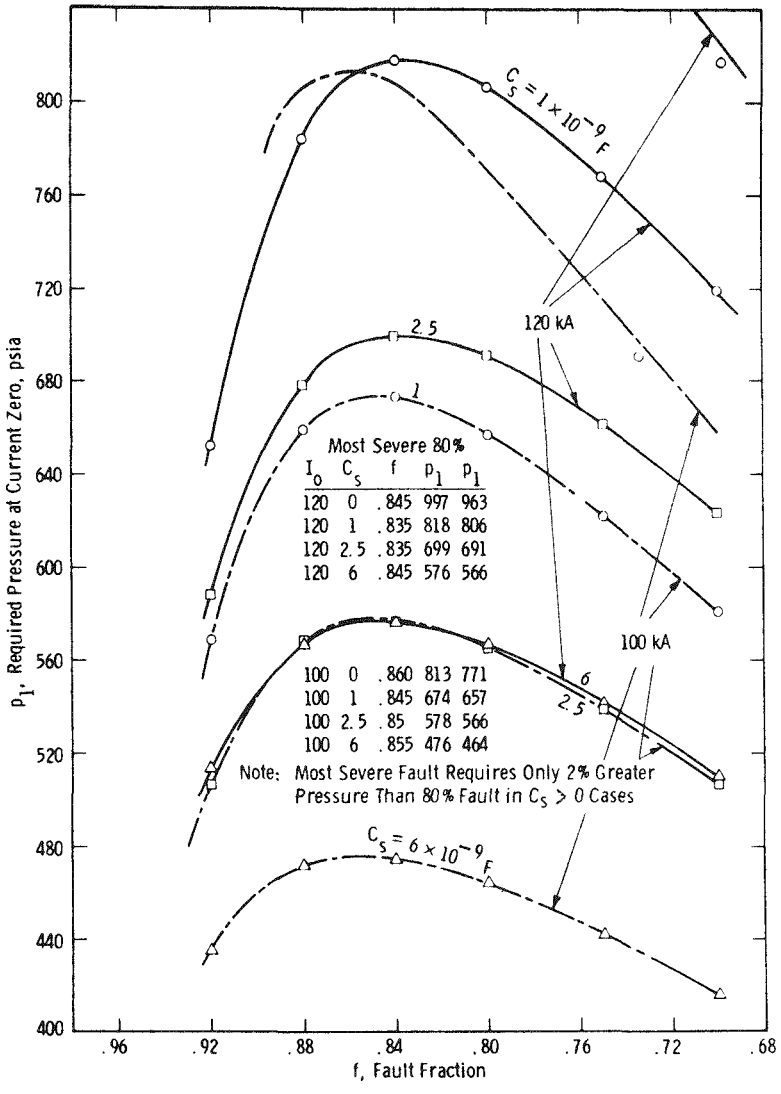


Figure 5-7 - Required i = 0 pressure for 145 kV, 1 bk., 120 & 100 kA, 450 ohm line

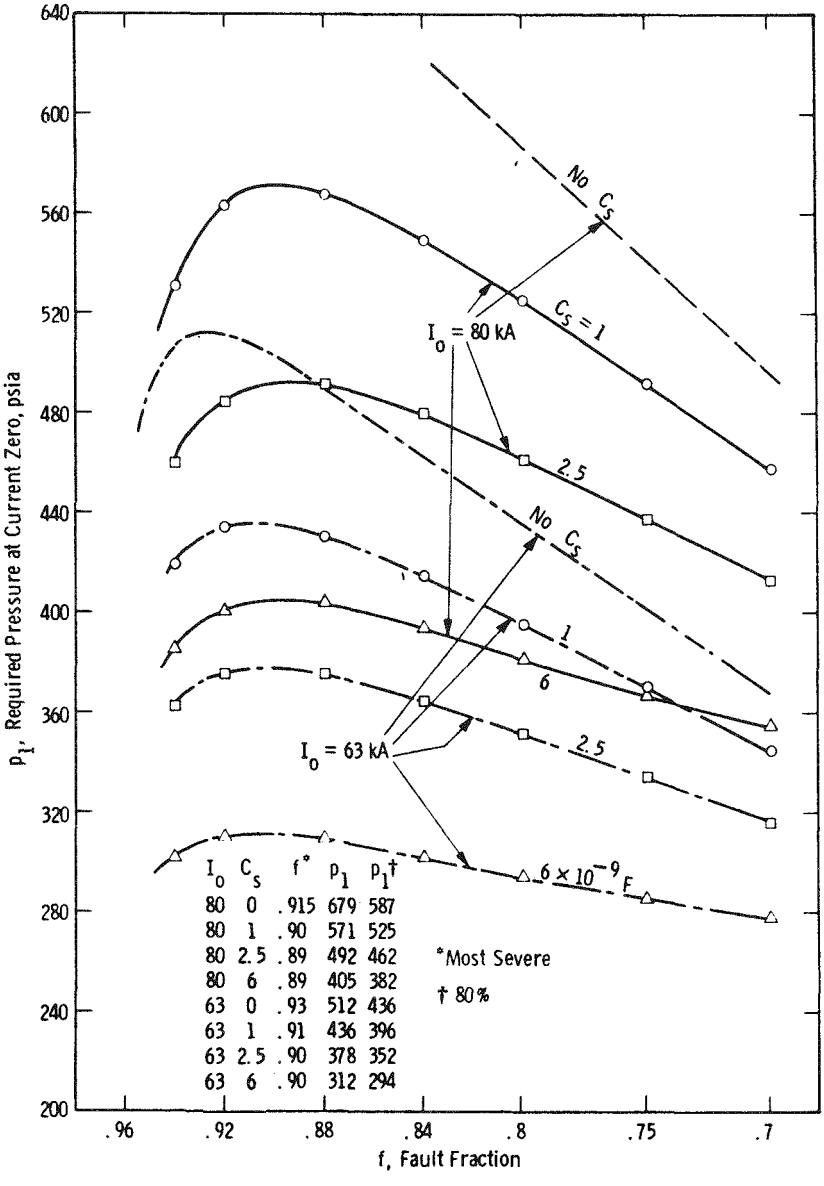


Figure 5-8 Required i = 0 pressure for a 450 ohm line at 242 kV 1 break, 80 and 63 kA

e. Sample No Load Calculation

Figure 5-9 shows the calculated interrupter parameters as a function of time for the no load condition. This establishes the ability of the interrupter to provide adequate dielectric strength for capacitor switching and the curves show the response of the primary functions calculted for the interrupter. The curves show the response of the self braking provided by the pneumatic mechanism that was obtained by putting an orifice in the driving piston that allows some of the driving air to pass through. Then when the mechanism nears full stoke this air is trapped and provides some of the energy absorption necessary to safely stop the mechanism and the interrupter. It also shows the effect of an externally mounted hydraulic shock absorber that shares the stopping duties.

The travel curve of the interrupter shows that at 8.3 milliseconds after contact part, 21.5 ms, it has achieved a contact gap of more than 2 inches which is adequate to withstand the capacitor switching recovery voltage. Since the puffer circuit breaker has to reach maximum arcing position in less than two cycles of power frequency it is quite close to resonant with the power frequency. In fact this record shows a natural frequency of the mass and spring system created by the interrupter, linkage and mechanism at about 100 Hz.

A complete tabulation of Input Data for the no load calculation is included in Appendix D along with a complete listing of the program.

f. Sample SLF Calculation

The second computer plot shown in Figure 5-10 shows the interrupter response to a 100 kA current interrupted at 28 milliseconds which is 5 ms before the maximum interrupting time established for the 2 cycle breaker. In this case the 120 Hz pressures developed by the current drive the nearly resonant mechanism and linkage system through an even wider range. The effect of this is shown in a small 120 Hz response in the travel record. The damping of the puffer pressure on this oscillation is sufficient to prevent any reversals of the travel before the current is interrupted. However after that interruption there is a small but measurable oscillation of the interrupter before it continues to full stroke position. The high $SF_6$ pressure developed by the puffer absorbs so much of the mechanism energy that it is still traveling slowly toward the full open position at the end of the 54 millisecond period of calculation. This calculation shows that the differential pressure achieved by the interrupter reaches a peak of 492 psi just before current zero and this is adequate for this early interruption. For longer arcing times

the differential pressure achieved increases until at 33 ms interruption time the maximum pressure reaches 675 psi which is more than adequate for interruption.

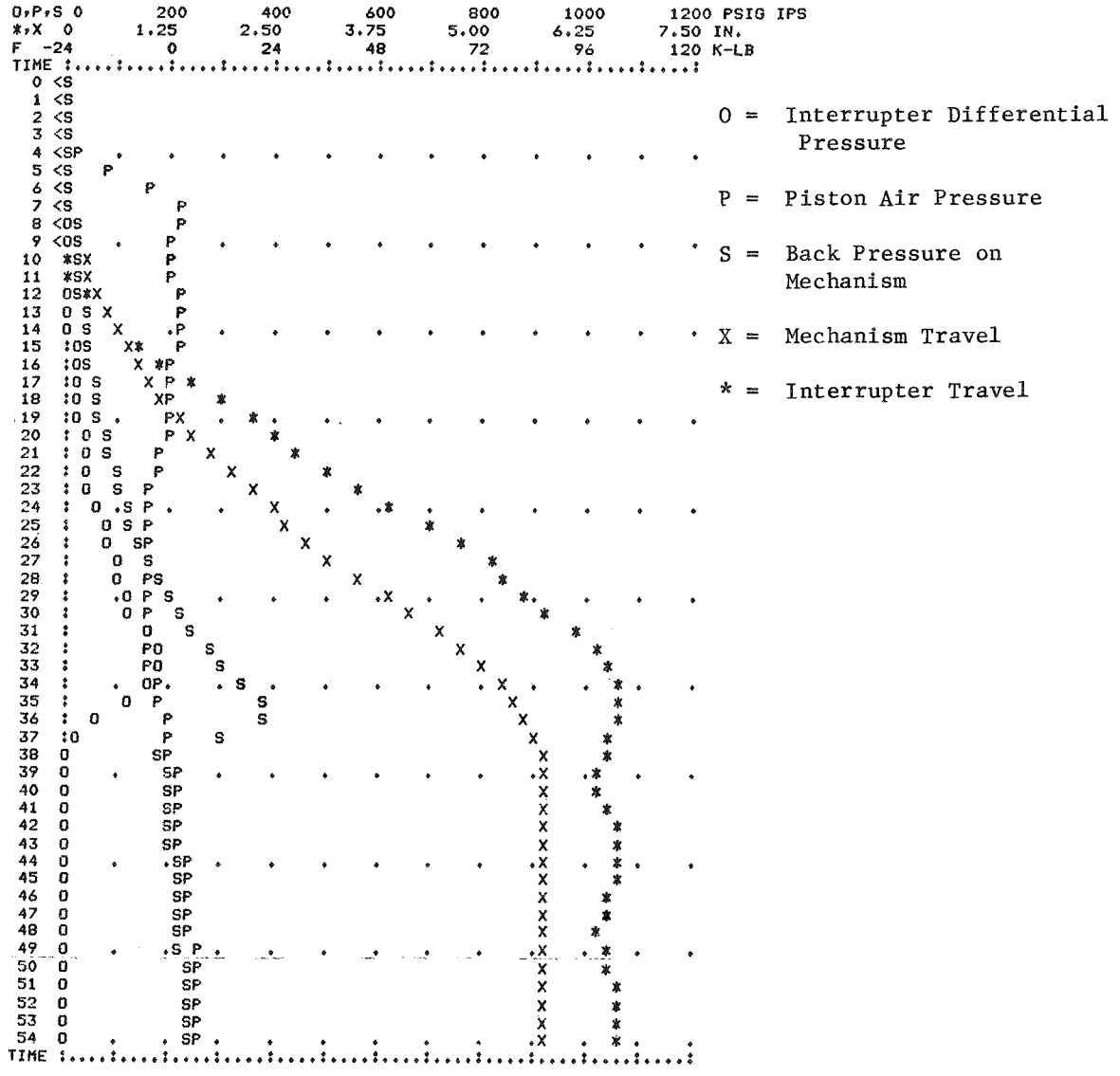


Figure 5-9 Calculated Interrupter Performance with No Current

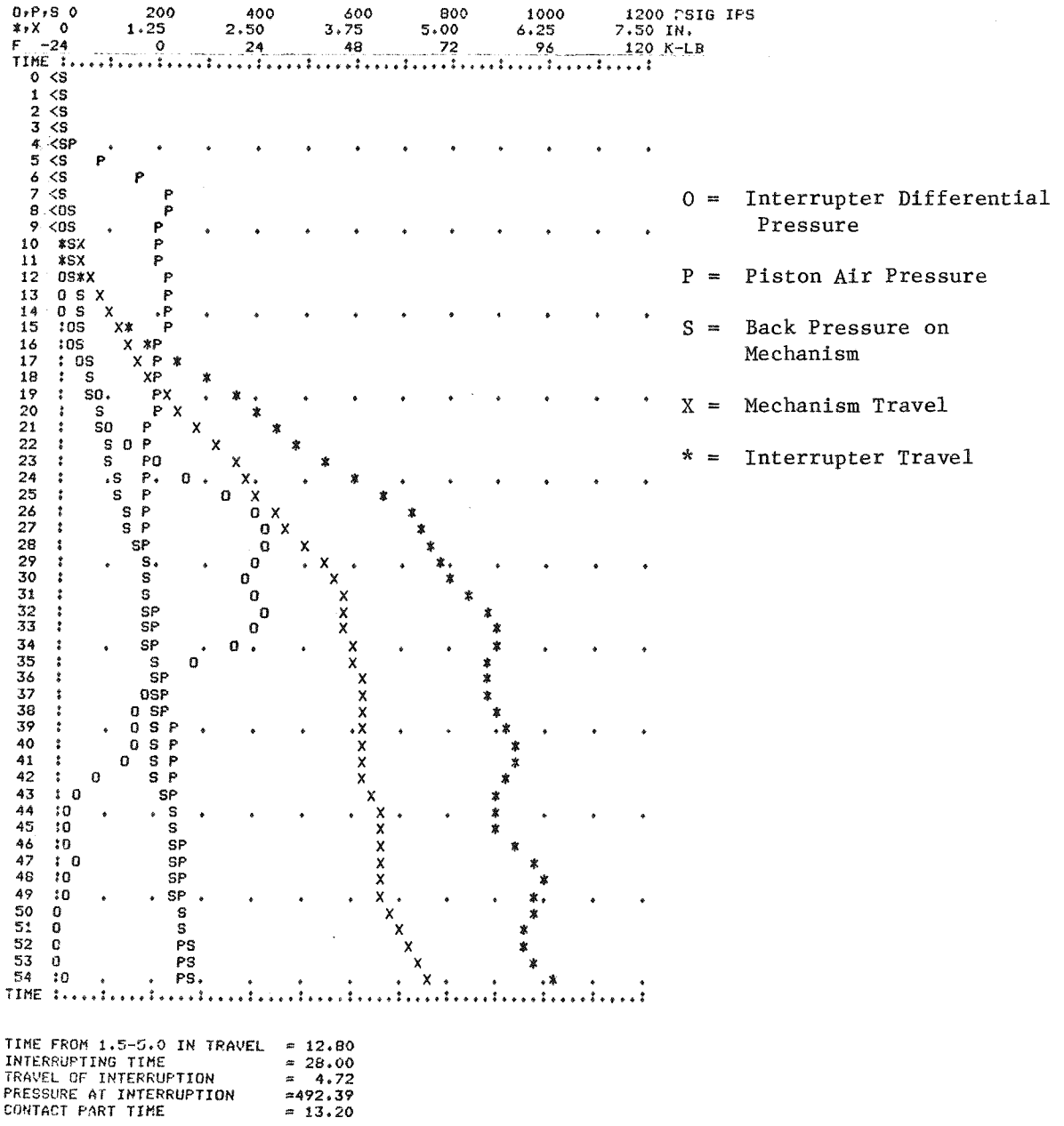


TIME FROM 1.5-5.0 IN TRAVEL = 12.80
INTERRUPTING TIME = 28.00
TRAVEL OF INTERRUPTION = 4.72
PRESSURE AT INTERRUPTION =492.39
CONTACT PART TIME = 13.20

Figure 5-10 Calculated Interrupter Performance at 100 kA

g. Dielectric Capability

The dielectric capabiliy of the interrupter is really determined from 7 different conditions and those are not independent of the other interrupter parameters. Specifically the various requirements are:

- 425 kV rating capacitor switching (8.3 milliseconds after contact part)
- 475 kV bus fault recovery voltage (approximately 8 msec before full stroke)
- 316 kV short line fault voltage (less than the bus fault requirement at lower currents)
- 900 kV basic insulation level (1.2 x 50 usec impulse) at full open
- 1040 kV 3 usec chopped wave at full open
- 1160 kV 2 usec chopped wave at full open
- 425 kV rms 60 Hz 1 minute withstand at full open

We would expect the limiting conditon would be the 2 usec chopped wave or 1160 kV which would determine the dielectric requirement in the full open position. The dielectric strength of metal to metal gaps of interrupters in $SF_6$ is approximately 25% higher for chopped wave impulse than for the crest of 60 Hz voltages. The chopped wave withstand requirement of is almost 2 times the crest 60 Hz withstand requirement of 600 kV. Therefore the limiting condition will be for chopped waves.

For metal to metal electrodes in $SF_6$ at 75 psig the practical limit for dielectric stress on the electrodes has been found to be about 600 kV per inch. Based on these criteria, electrostatic flux maps made with a water table analog field plotter were used to determine the required shielding for the moving and stationary contacts to withstand the 1160 kV when mounted in a tank that would support the required voltage to ground. Figure 5-11 shows one sample plot that was used in this determination. Figure 5-12 shows that the assumed tank diameter has only a very slight effect on the breakdown between the two contacts and thus the assumed tank diameter of 18 inches is satisfactory with regard to the dielectric strength between contacts.

Figure 5-13 shows that for the assumption that the contacts can be approximated by two toroids there is only a small effect on the dielectric strength for increasing

the gap beyond 5 inches. (contact gap = travel less 1 inch overlap of the arcing contacts.) Therefore a 6 in travel was selected.

## 5.5 CONCLUSIONS

Based upon all of the calculations the complete interrupter assembly shown in Figure 5-14 was designed. It incorporates the 9.75 inch piston with a 6 inch travel into an assembly that is capable of providing all of the required interrupter characteristic.

Figure 5-15 shows how this interrupter was mounted in the same insulating tube test chamber as the Model interrupter. The mechanism and linkage system was modified to provide the required driving energy.

References:

1. Noeske, IEEE Summer Power Meeting 1976, PES F76-443-2 July, 1976.

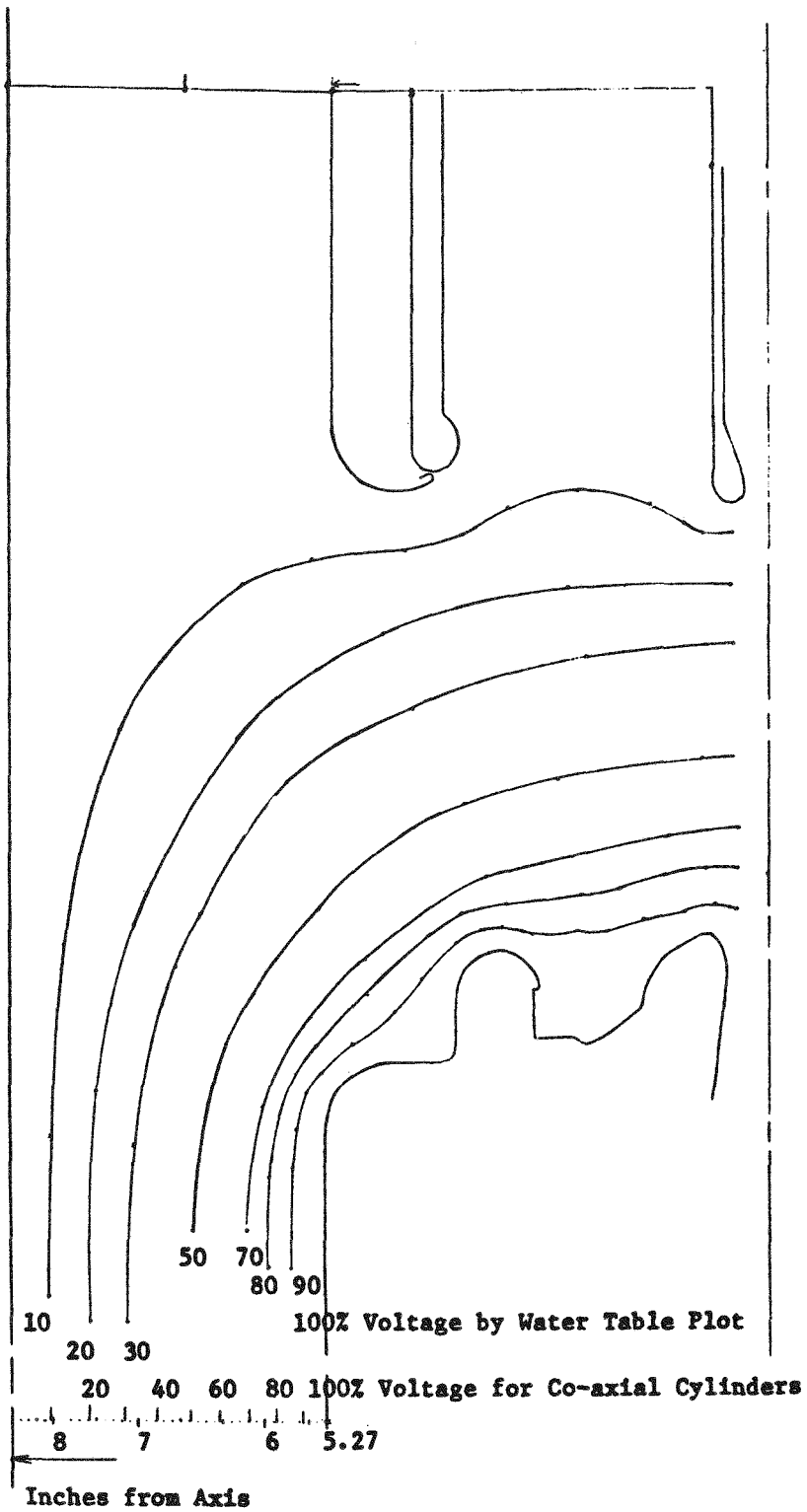


Figure 5-11 Field Plots for Interrupter in 18 inch Diameter Tank with the Stationary Contact Grounded

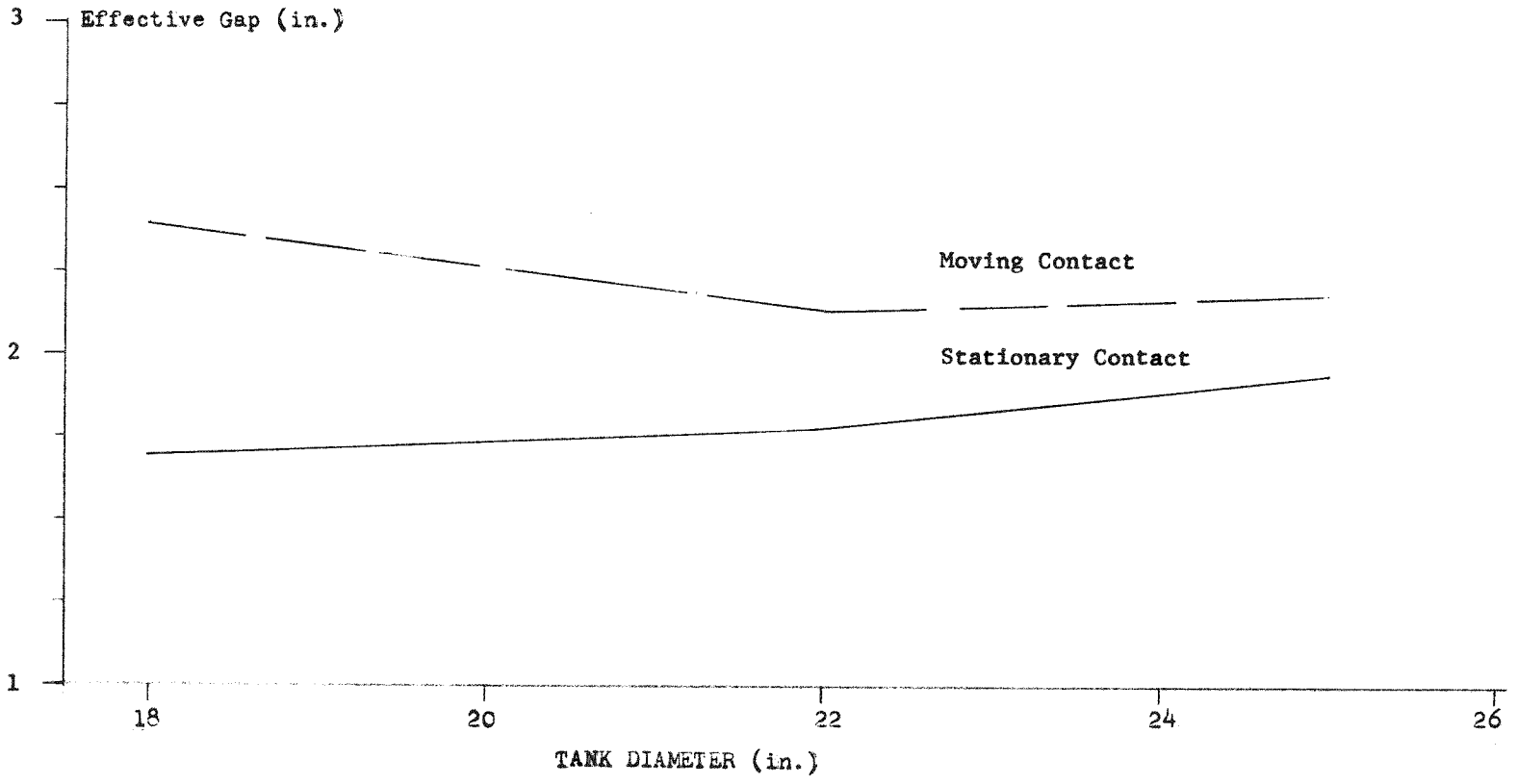


Figure 5-12 Effective Interrupter Gap vs. Tank Diameter

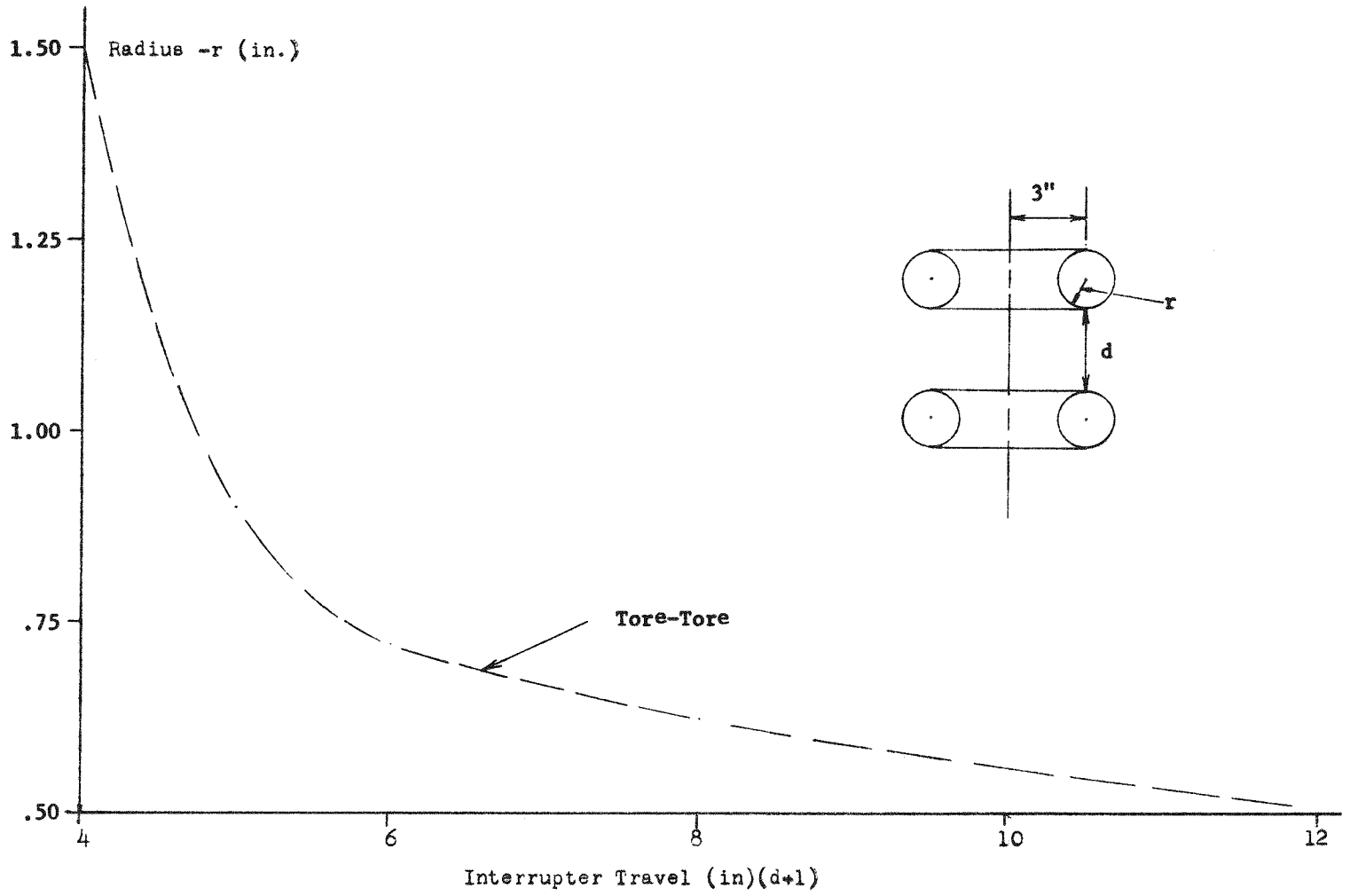


Figure 5-13 Approximation for Interrupter Radius Required for 242 kV on 1 Break

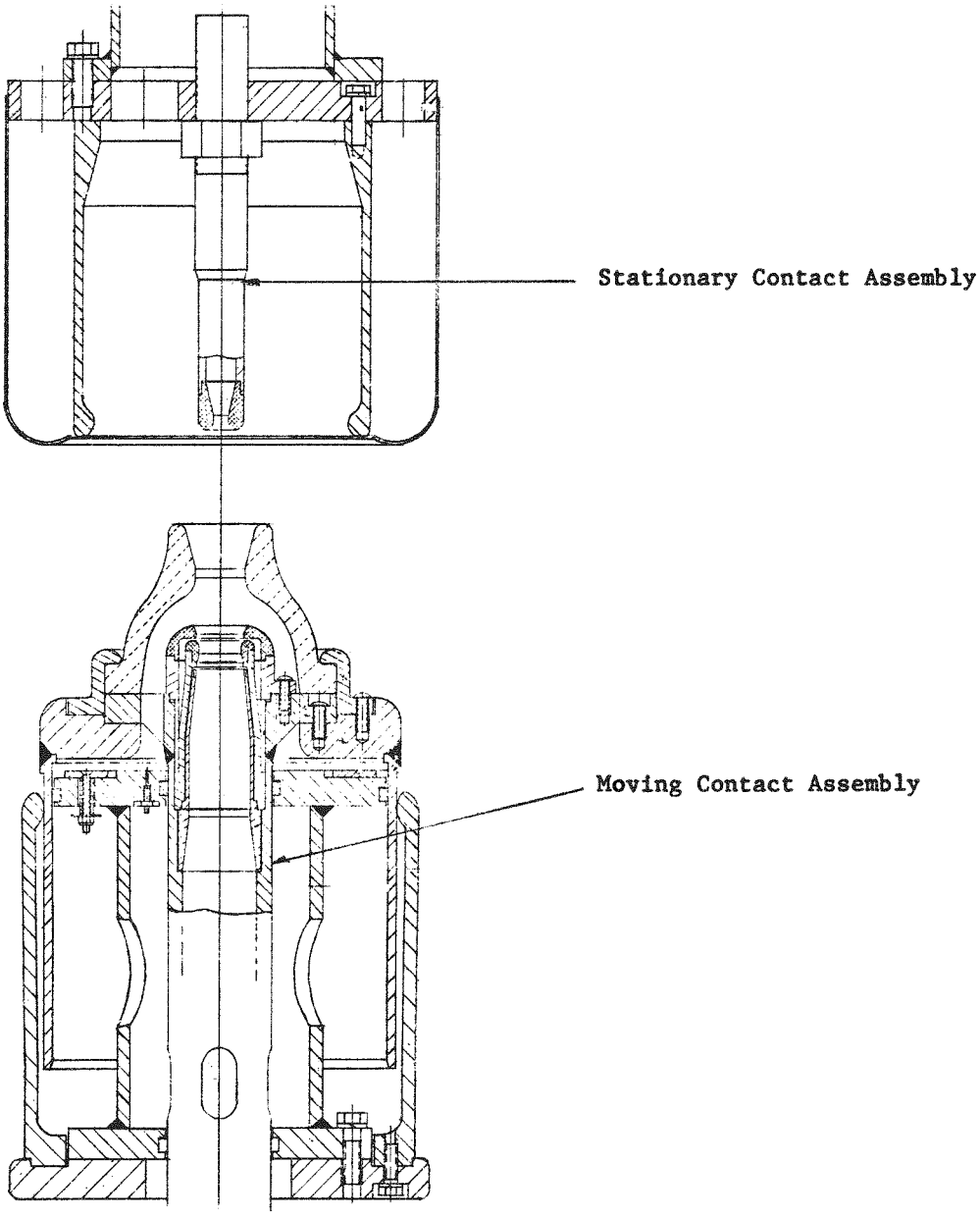


Figure 5-14 Prototype Interrupter

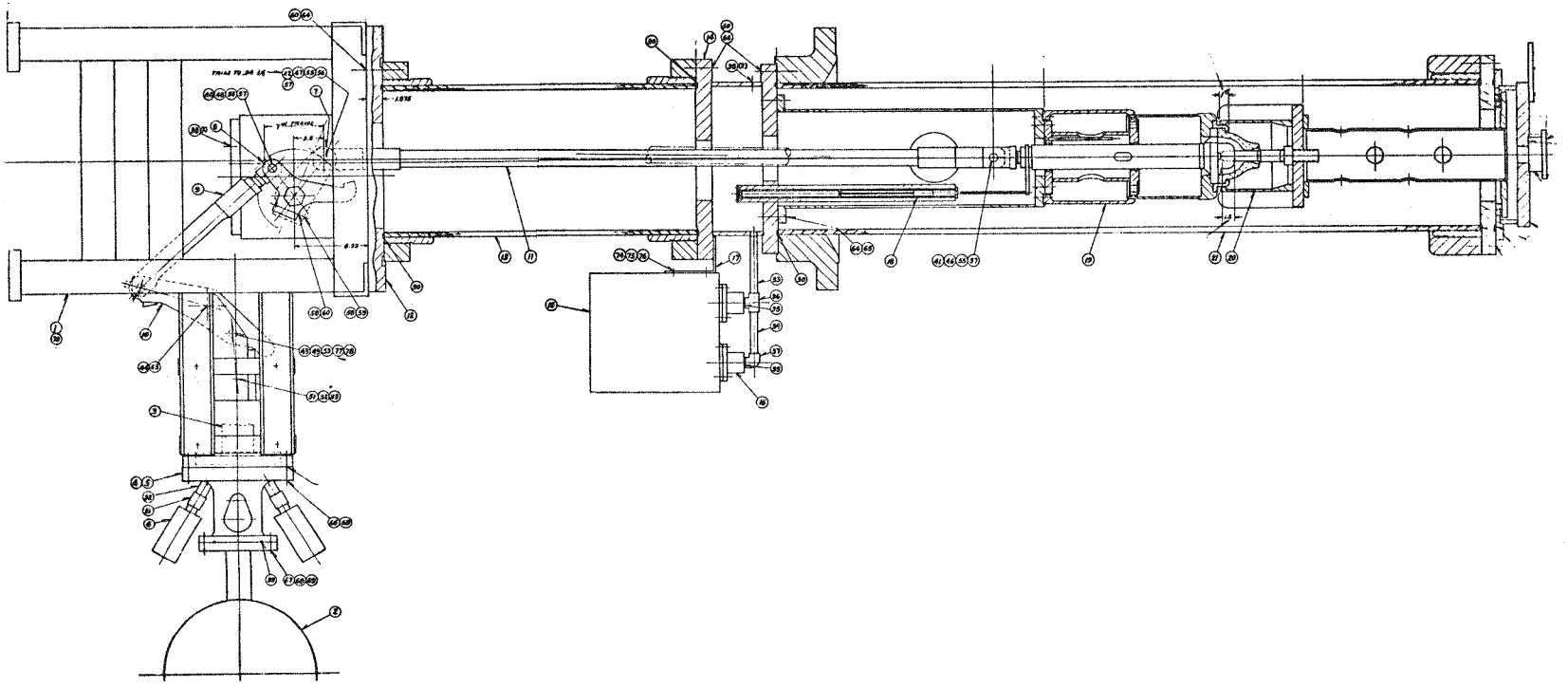

Figure 5-15 Super Pressure Interrupter Test Model

Section 6

# DESCRIPTION OF TEST PROGRAM FOR PROTOTYPE INTERRUPTER

## 6.1 PLANNED INTERRUPTING TESTS

Five kinds of tests were planned for the verification of the prototype interrupter design. These were:

a. 242 kV Line Dropping
b. 145 kV - 120 kA - 85% Short Line Fault
c. 242 kV - 100 kA - 90% Short Line Fault
d. 145 kV - 120 kA Bus Fault
e. 242 kV - 100 kA Bus Fault

These particular tests were shown to be the critical tests for these ratings based upon the analysis of interrupter characteristics given in Section 5 "Prototype Design".

Since these tests are not within the published capabilities of any high power laboratory the principle testing laboratories worldwide were contacted directly to obtain their estimates of the cost and difficulty of performing adequate tests for these ratings. After reviewing the response the contractor and EPRI concluded that the best laboratory for the tests in terms of cost, schedule and capability was the Westinghouse High Power Laboratory.

The electrical test requirements are given in Table 1.

## 6.2 TEST LABORATORY LIMITATIONS

### a. Assymmetric Test Currents

The Westinghouse High Power Laboratory is limited to 95 kA symmetrical tests current for high voltage synthetic tests. By providing controlled assymetry of the test current it is possible to perform tests with the last loop of test current equivalent to 100, 108 or 120 kA rms required for these tests.

TABLE 6-1

TEST REQUIREMENTS FOR 100 kA 242 kV and 120 kA 145 kV RATINGS

| Test Current kA rms | RRRV kV/usec | Line Side TRV Crest kV | Line Side TRV Time to Crest | Bus Side TRV Crest kV | Bus Side TRV Time to Crest | Test Condition |
|---|---|---|---|---|---|---|
| 100 | 1.8 | NA | NA | 425 | 500 | 100kA 242kV Bus Fault |
| 90 | 21.6 | 35.7 | 1.65 | 255 | 500 | 100kA 242kV 90% SLF |
| 120 kA | 1.8 | NA | NA | 260 | 300 | 120kA 145kV Bus Fault |
| 102 kA | 24.6 | 32 | 1.3 | 145 | 294 | 120kA 145kV 85% Fault |
| 200 Amps | NA | NA | NA | 475 | 8333 | 200kA 242kV Line Dropping |

The use of assymmetric power frequency test current in synthetic tests do not significantly effect the rate of change of current at zero or the initial or final TRV because these are determined exclusively by the synthetic test circuit.

There is some effect of the assymmetric test current on the performance of a puffer interrupter because the pressure differential developed by the puffer is a function of the arcing history prior to current zero. Calculation of the arc energy developed by the interrupter for arcing times up to 12 milliseconds shows that the assymetric test produces 88% of the arc energy produced by a symmetrical test. The arc current and consequently the arc energy for both symmetrical and assymmetrical test match very closely for the last 4 milleseconds before the last current zero. This is the most critical period for bus fault interruption because the hot gases generated during this time are the hot gases that will be in the arc space downstream during the transient recovery voltage.

b. Capacitance Limitations

The laboratory is limited by the amount of capacitance available in the synthetic test circuit. The complete synthetic test circuit requires a large bank charged to high voltage as the voltage recovery source as well as a large capacitance to simulate the bus capacitance and control the recovery voltage. By selecting the best combination of capacitance for the required bus and SLF test circuits the laboratory was able to provide test capability approximating the interrupter requirements. In most cases the test circuit creates a test duty for the interrupter that is more severe than required. Table 6-2 shows the comparison of the actual test capability with the test requirements.

TABLE 6-2

Required and Actual
TEST REQUIREMENTS FOR 100 kA 242 kV and 120 kA 145 kV RATINGS

| Test Duty | dI/dT at I = 0 A/usec | | Line Side TRV Crest kV | | Line Side TRV Time to Crest | | Bus Side TRV Crest kV | | Bus Side TRV Time to Crest | |
|---|---|---|---|---|---|---|---|---|---|---|
| | R | A | R | A | R | A | R | A | R | A |
| 145 kV 120 kA 85% SLF | 54 | 50 | 32 | 30 | 1.3 | 1.5 | 145 | 170 | 274 | 225 |
| 242 kV 100 kA 90% SLF | 48 | 48 | 35.7 | 33 | 1.65 | 1.7 | 255 | 280 | 500 | 293 |
| 145 kV 120 kA Bus Fault | 64 | 6 | NA | NA | NA | NA | 255 | 260 | 240 | 300 |
| 242 kV 100 kA Bus Fault | 53 | 5.8 | NA | NA | NA | NA | 425 | 425 | 500 | 420 |

In order to approach the 500 usec to crest required by standards the synthetic test circuit was adjusted to give a 285 Hz injection current. This setting produced a transient recovery voltage of 425 kV with 420 usec to crest. This was achieved by reducing the slope of the current approaching zero and the initial rate of rise of voltage was correspondingly reduced from values required by standards. However for this particular interrupter it was felt that the initial transient recovery capability would be established by bus fault tests for the 120 kA 145 kV rating. Whereas the prime limitation for the 100 kA 242 kV rating was the maximum voltage produced across the gap. Since this is a dielectric strength problem the history of the voltage up to crest is not a factor.

c. Maximum Test Voltage

Prior to this project the laboratory was limited to less than 400 kV, maximum recovery voltage by the insulation of the synthetic test circuit. During the preparation for these tests the insulation level of the synthetic test components was increased to permit recovery voltage crest up to 425 kV. This required the installation of a high voltage bushing between the synthetic test components and the test circuit breakers as well as the elemination of some of the components normally used for synthetic tests. A number of tests of the synthetic test circuit capability were performed before the prototype interrupter was subjected to test.

d. Auxiliary Circuit Breaker

A new auxiliary circuit breaker used to isolate the high current circuit from the

tests. The original auxiliary circuit breaker used a two break 63 kA Type SFA two-pressure circuit breaker. For these tests a four break 80 kA Type SFA two-pressure breaker was used. The only problem encountered with this circuit breaker was accelerated erosion of the interrupter contacts. Ordinarily for tests up to 64 kA the breaker contacts can be used for 50 or more tests. During tests of this interrupter the contacts were replaced after each test series of 12 to 20 tests.

## 6.3. PRELIMINARY MECHANICAL TESTS

During preliminary mechanical tests of the prototype interrupter two primary problems were encountered. First the air pressure required to drive the interrupter at the design speed was only 77% of the calculated value. Second the mechanical loads on the test unit caused by stopping the interrupter at the end of the stroke were much higher than expected and resulted in mechanical damage to the mechanism and frame.

The computer model for the prototype interrupter mechanical operation was used to calculate the predicted air pressure that would be required to achieve the observed opening speed of 37 ft/sec. The predicted value of 450 psi was 28% higher than the actual value found experimentally. A review of the computer model showed that the source of this error was the assumed flow coefficient of 0.8 for the air valve. When the flow coefficient was changed to 1.0 the calculated result agreed very well with the actual.

Excessive forces were produced in the mechanism and frame due to stopping to quickly. These forces bent stops, extruded polyurethane bumpers and broke pins in the linkage system. Two alternate solutions were considered. The first was to use a hydraulic dashpot on the linkage system. This solution was rejected because of cost and time to implement. The second alternative was to use the main drive cylinders as dashpots by trapping air in the end of the cylinder to produce a braking force as the piston approached the end of the cylinder. The amount of air trapped in the closed-end cylinder was adjusted by the size of bleed control ports in the main drive piston which allowed opening stroke.

This solution proved very effective, it reduced the maximum acceleration at the end of the stroke from more than 1000 G's to less than 500 G's. This prevented damage to the mechanism and linkage system. However it was found that the required air pressure to achieve the design velocity of 30 ft/sec was approximately 500 psi instead of the 350 psi that was required with the original solid piston in the pneumatic mechanism.

## 6.4. INITIAL POWER TESTS

### a. 242 kV Line Dropping

The prototype interrupter was tested for line dropping for the 242 kV rating at 200 amps. Initially a problem was encountered with flashovers external on the test rig. Flashovers were eliminated by placing a plastic bag filled with $SF_6$ around the insulating tube.

Table 6-3 lists the line dropping tests. Tests Q through U were made at the design speed of 30 ft./sec. and there were no restrikes or reignitions. Tests A through P were made at 25% below design speed and one reignition occurred on Test O. This would have produced a surge of less than one per unit on a transmission line.

### b. 242 kV Bus Fault

242 kV Bus Faults were made for the 100 kA fault current rating. Table 6-4 lists these test.

TABLE 6-3

242 kV - LINE DROPPING

| Test Letter | Test Voltage kV(rms) | Test Current Amp(rms) | Interrupter Time (ms) | Arc Time (ms) | Contact Separation Inches(EST) | Flashover or Reignition | | | Recovery Voltage kV(Peak) | Test Pressure $SF_6$/Air Psig |
|---|---|---|---|---|---|---|---|---|---|---|
| | | | | | | Time (ms) | Voltage kV | Contact Separation Inches | | |
| A | 51 | 103 | 19 | 1 | .25 | | | | 142 | 71/350 |
| B | 216 | 220 | 19 | 1 | .25 | 5 | 370* | 1.5 | | " |
| C | 51 | 131 | 19 | 1 | .25 | | | | 152 | " |
| D | 162 | 210 | 19 | 1 | .25 | | | | 472 | " |
| E | 160 | 207 | 23 | 5 | 1.25 | | | | 466 | " |
| F | 160 | 200 | 24 | 6 | 1.5 | | | | 478 | " |
| G | | | 20.5 | 2.5 | .7 | | | | 475 | " |
| H | 159 | 207 | 18 | 0 | 0 | | | | 468 | " |
| I | 163 | 204 | 19.5 | 1.5 | .35 | 4.5 | 296* | 1.5 | 478 | 70/350 |
| J | 163 | 204 | 21.7 | 3.7 | .9 | | | | 474 | " |
| K | 66 | 102 | 22.5 | 4.5 | 1.1 | | | | 232 | " |
| L | 159 | 204 | 23.0 | 5 | 1.25 | | | | 468 | " |
| M | 159 | 201 | 25 | 7 | 1.75 | | | | 468 | " |
| N | 164 | 200 | 25.5 | 7.5 | 1.87 | | | | 478 | " |
| O | 159 | 200 | 18.5 | 0.5 | .12 | 3 | 228 | .85 | 480 | " |
| P | 159 | 216 | 21.5 | 3.5 | .85 | | | | 468 | " |
| Q | 160 | 201 | 17.5 | 1.5 | .6 | | | | 474 | 72/500 |
| R | 159 | 198 | 16.8 | .8 | .3 | | | | 468 | " |
| S | 159 | 201 | 24.0 | 8.0 | 3.0 | | | | 474 | " |
| T | 159 | 198 | 17.0 | 1 | .4 | | | | 472 | " |
| U | 159 | 201 | 23.8 | 7.8 | 2.9 | | | | 478 | " |

*External Flashover

TABLE 6-4

242 kV - 100 kA - BUS FAULT

| Test Letter | Test Results | Test Voltage kV | Test Current kA (rms) | Inj. Current kA (rms) 285 Hz | Measured Current Last 1/2 Cycle kA(rms) | Interrupting Time (ms) | Arcing Time (ms) | Est. Int. Travel kV | Ext. Arc Voltage kV(Peak) | Bus Recovery Voltage 1st. Peak kV | Bus Recovery Voltage Crest Time (us) | Test Pressure $SF_6$/Air Psig |
|---|---|---|---|---|---|---|---|---|---|---|---|---|
| V | F* | 22 | 20.1 | 2.3 | 27.5 | 28.2 | 12.2 | 5.7 | 7.1 | 374* | 320 | 70-$SF_6$ |
| X | F* | 22 | 19.5 | 2.3 | 26.8 | 28.3 | 12.3 | 5.7 | 6.3 | 342* | 270 | 500-Air |
| Y | F* | 22 | 19.8 | 2.3 | 26.4 | 28.0 | 12.0 | 5.6 | 7.0 | 335* | 260 | |
| Z | F* | 22 | 19.7 | 1.9 | 26 | 28.2 | 12.2 | 5.7 | 7.0 | 328* | 410 | |
| AA | F* | 22 | 19.7 | 2.3 | 26 | 28.2 | 12.2 | 5.7 | 5.9 | 425* | 320 | |
| AB | F* | 22 | 19.7 | 2.3 | 26 | 28.2 | 12.2 | 5.7 | 6.9 | 415* | 330 | |
| AC | W | 22 | 19.5 | 2.3 | 26.2 | 28.4 | 12.4 | 5.7 | 6.8 | 439 | 420 | |
| AD | W | 22 | 86.5 | 2.3 | 97.8 | 25 | 9.0 | 4.4 | | 440 | 450 | |
| AE | W | 22 | 90.8 | 2.3 | 110 | 23.5 | 7.5 | 3.8 | | 440 | 450 | |
| AF | F | 22 | 90.7 | 2.3 | 111 | 32.8 | 16.8 | 6.2 | | 100 | 70 | |
| AG | F | 22 | 88.0 | 2.3 | 109 | 29.5 | 13.5 | 6.0 | | 150 | 100 | |
| AH | F | 22 | 90.0 | 2.3 | 110 | 27.5 | 11.5 | 5.3 | | 150 | 100 | |
| AI | F | 22 | 90.8 | 2.3 | 113 | 22 | 6.0 | 3.3 | Aux.Bkr.Failed 40-100? | | | Affected |
| AJ | F | 22 | 79.4 | 2.3 | 82.2 | 27.2 | 11.2 | 5.2 | 5.9 | 206 | 150 | probability by shield off |

* Breakdown in test circuit  Voltage shield blown off - H.P. tube blackened inside -- discovered on disassembly.

The first series of tests V through AC were made to work out problems with the laboratory synthetic test circuit and achieve the full expected recovery voltage.

c. First Prototype Power Tests

Power tests AD throug AI were made in the 100 kA range with various arcing times as shown in Table 6-4. The breakdown voltages were so low at long arcing times that it was felt that there was something wrong or broken in the interrupter. Test AJ was made with 80 kA as a further check on this. The test rig was then disassembled to determine the cause of the observed poor performance. The voltage shield outside the stationary contact fingers had blown off and the side of the high pressure tube had charred and blackened much more than expected. There was no arcing on the back of shield where the material had been torn when the shield blew off and there was a large pitted surface area on the front of the shield. This showed that the shield was blown off by pressure and the failures were due to breakdown across the interrupter gap.

d. Repair of the Prototype Interrupter

The test rig was rebuilt with a new voltage shield fastened down with four times the number of bolts. The arcing contacts and nozzle were replaced. The cupaloy clamping ring for the nozzle was sanded to remove arc terminals and smooth the eroded surfaces. The high pressure tube was sanded to remove the carbonized areas.

Since the demonstrated recovery voltage from tests AD through AI was less than required for any of the other tests that were planned, the decision was made to repeat the 242 Bus Fault Tests to determine what effect the shield had on the recovery voltage capability.

e. Second Prototype Power Tests

Test AK was done at relatively long arcing time to determine if the shield had an effect on the previously observed low recovery voltage breakdowns. Test AK broke down at a very low voltage. The test current was reduced to 60 kA and the breakdown for this test was 100 kV which is still very low. The test current was reduced to 20 kA to repeat test AC. Full recovery voltage was achieved on this test. However, 1.5 milliseconds after interruption a flashover occurred in the test rig and badly carbonized the high pressure tube. This showed that the high pressure tube carbonization probably did not cause the low voltage breakdowns in

the two previous tests and the breakdown was to the shield across the interrupter gap. Detailed data for this test series is shown in Table 6-5.

After this test series the auxiliary fingers and the outside of the interrupter cylinder were eroded. The current per contact finger (6 kA) was apparently high enough so that local magnetic forces at the contact of the finger to the cylinder wall were sufficient to lift the fingers, break contact and start arcing. The worst pitting occurredc in the closed position before the interrupter cylinder moved. It was observed during the testing that little spots of light were falling to the bottom of the upper high pressure tube. These bright spots seemed to start from the elevation corresponding to these auxiliary fingers. In commercial circuit breakers monentary currents up to 15 kA per contact finger are commonly used for copper to silver plated copper contacts. In this case the silver plated aluminum puffer cylinder and the contact geometry apparently reduced the momentary current capability.

f. Instrumentation Problems at 100 kA

During these tests at 100 kA all of the instruments recording pressure, travel, synthetic test current and transient recovery voltage on a fast time scale produced useless records or no records at all. In rearranging the test circuit with the new auxiliary breaker and the higher insulation level the size of the current loop carrying the full 100 kA was increased by 3 or 4 times. This larger loop caused saturation of steel shielding for the high speed cathode ray oscillographs and induced excessive error voltages into the travel and pressure transducer systems.

Although all of the more sophisticated records were lost, the simple direct magnetic oscillograph records showed clearly the inability of the interrupter to withstand high voltages after long arcing times.

TABLE 6-5

242 - 100 kA - BUS FAULT

| Test Letter | Test Results | Test Voltage kV | Nominal Current kA (rms) | Inj. Current kA (rms) 285 Hz | Measured Current: Last 1/2 Cycle kA(rms) | Interrupting Time (ms) | Arcing Time (ms) | Est. Int. Travel kV | Ext. Arc Voltage kV(Peak) | Bus Recovery Voltage: 1st. Peak kV | Bus Recovery Voltage: Crest Time (us) |
|---|---|---|---|---|---|---|---|---|---|---|---|
| AK | F | 22 | 89.3 | 2.3 | 102 | 30.5 | 14.5 | 6.1 | | | |
| AL | F | 22 | 60.3 | 2.3 | 71 | 30.4 | 14.4 | 6.1 | 7.2 | 110 | 100 |
| AM | W** | 22 | 18.6 | 2.3 | 24.1 | 29.5 | 13.5 | 5.9 | 8.2 | 440 | 450 |

** F.O. at 250 kV, 1500 us external

## 6.5. ANALYSIS OF INITIAL TESTS

### a. Line Dropping Tests

The calculated capability of the prototype interrupter corresponds well with the test results for line dropping. With the interrupter opening at 22 ft/sec there is a region from 2.5 to 4 milliseconds where reignitions are likely. Breakdowns are unlikely after 4 milliseconds. When the interrupter is opened at 30 ft/sec, restrikes or reignitions were not likely from calculations and were not found during the testing.

### b. 242 kV 100 kA Bus Fault Tests

Tests AD and AE showed that the interrupter has the fundamental capability of interrupting the 242 kV bus fault of 98 and 110 kA for short arcing times. However it is apparent that the withstand capability falls off with long arcing times much faster than other puffer interrupters. The 145 kV model interrupter tests showed higher capability than the prototype interrupter for 13.5 ms arcing time. There is not a significant difference between the model and prototype results since the prototype interrupter probably would have withstood the 145 kV recovery voltage with only 1 ms less arcing time.

The rapid reduction in recovery capability is thought to be due to hot gasses generated during the high current arcing period stagnating and recirculating across the interrupter gap. The dielectric capability of unionized hot gas is direcly proportional to the gas density. Breakdowns at less than 100 kV indicates that the gas temperature is over 3000°K and is partly ionized. Table 6-3 shows a comparison of critical design parameters the Model and the Prototype interrupters.

This table shows that the changes in the test chamber between the Model and the Prototype interrupters led to two factors which tend to enhance clogging and stagnation of hot gas flow through the interrupter. First the effective flow area through the stationary contact was reduced from 45 to 20 square inches. This causes the cold flow capability of the stationary contact to be reduced from 170 to 180 cubic inches per millisecond at a fixed pressure drop and more importantly the volume of hot gas pumped through the puffer nozzle is 220 cubic inches per millisecond for the Prototype as compared to 150 cubic inches per millisecond for the Model interrupter. Although the stationary contact shield volume of the prototype was increased from 350 cubic inches for the Model to 950 cubic inches this volume would be filled with hot gas in 4.3 milliseconds while the minimum

arcing time is more than 7 milliseconds and the maximum arcing time is about 16 milliseconds.

Second the clearance between the interrupter and the enclosure wall was decreased from 4.5 to 2.24 inches. This would increase burning of the enclosure as well as inhibit flow. In fact the flow area is reduced from 175 square inches to 105 square inches. Based upon these conclusions it was decided to propose a drastically different configuration for the prototype interrupter that would have improved design parameters and at the same time be a more realistic arrangement for the eventual circuit breaker design.

## 6.5 PROPOSED DEAD TANK PROTOTYPE

By taking advantage of an existing dead tank circuit breaker tank and an available cast epoxy 242 kV bushing a test arrangement was possible for the Prototype interrupter that overcame most of the disadvantages of the close fitting fiber-glass enclosure. The third column of Table 6-6 shows the corresponding parameters for the Prototype interrupter mounted in a 32 inch tank as shown in Figure 6-1. The flow area for the stationary contact was increased by 4:1 which permits all of the hot gas to flow through the stationary contact with a lower pressure drop than the Model interrupter. A large plenum was added to the outlet of the stationary contact and coolers were installed in the plenum to prevent filling it with hot gases, and to cool gases before they are released into the space between the plenum and the tank. Detailed calculations for the cooler are given on Appendix E. The stroke of the puffer was increased to 7 inches in order to provide higher pressure and high mass flow. When agreement was reached with EPRI that this design should be tested the dead tank prototype was built and prepared for test.

TABLE 6-6

DESIGN PARAMETERS COMPARISON

| Design Characteristics | 145 kV Model | 242 kV Prototype | Proposed Dead Tank Prototype |
|---|---|---|---|
| 1. Effective flow area through stationary contact | 45 $in^2$ | 20 $in^2$ | 80 $in^2$ |
| 2. Estimated cold gas flow through stationary contact at 15 psig | 170 $in^3/ms$ | 80 $in^3/ms$ | 320 $in^3/ms$ |
| 3. Estimated maximum flow of hot ionized gas from nozzle of interrupter | 150 $in^3in/ms$ | 220 $in^3/ms$ | 220 $in^3/ms$ |
| 4. Contact shield volume | 350 $in^3$ | 950 $in^3$ | 2400 $in^3$ |
| 5. Time to fill shield | 2.3 ms | 4.3 ms | 11 ms |
| 6. Clearance to stationary wall on magnetic loop side | 4.5 in. | 2.25 in. | 8 in. |
| 7. Container diameter | 17 in. | 17 in. | 32 in. |
| 8. Annular return flow area between shield and container | 175 $in^2$ | 105 $in^2$ | 500 $in^2$ |

TABLE 6-7

145 kV - 120 kA - BUS FAULT @ 75 PSI FILL PRESSURE $SF_6$

| Test Letter | Result | Test Current kA rms | Interrupting Time ms | Arcing Time ms | Line Side TRV kV | Line Side TRV usec | Bus Side TRV kV | Bus Side TRV usec | Shunt Capacitance NFd | Mechanism Air Pressure | Speed ft/sec |
|---|---|---|---|---|---|---|---|---|---|---|---|
| A | Timing | | | | | | | | | 350 | 19.2 |
| B | Timing | | | | | | | | | 450 | 23.6 |
| C | F | 123 | 27.6 | 9.6 | | | | | | 450 | 23.4 |
| D | F | 123 | 30 | 12 | | | | | | 500 | 25 |
| E | F | | 33.8 | 15.8 | | | | | | 500 | NA |
| F | Timing | | | | | | | | | | |



TABLE 6-8
145 kV 120 kA 85% SLF

| Test Letter | Result | Test Current kA rms | Interrupting Time ms | Arcing Time ms | Line Side TRV kV | Line Side TRV usec | Bus Side TRV kV | Bus Side TRV usec | Shunt Capacitance NFd | Mechanism Air Pressure | Speed ft/sec |
|---|---|---|---|---|---|---|---|---|---|---|---|
| S | F | 105.5 | 28.8 | 14.3 | -- | -- | -- | -- | 0 | 350 | 30.6 |
| T | F | 103.9 | 27 | 12.5 | -- | -- | -- | -- | 5.2 | " | NA |
| U | F | 105 | 26.6 | 12.1 | -- | -- | -- | -- | 9.8 | " | NA |
| V | F | 102.5 | 29.9 | 15.4 | -- | -- | -- | -- | 9.8 | " | 28.5 |
| W | F | 102.5 | 29.8 | 15.3 | -- | -- | -- | -- | 15 | " | 29.3 |
| X | F | 87.6 | 29.8 | 15.3 | -- | -- | -- | -- | 15 | " | 29.3 |
| Y | W | 72 | 29.8 | 15.3 | 24.6 | 8 | 112 | 216 | 15 | " | NA |
| Z | Timing | | | | | | | | | | |

NA - Data not available

Inspection of the interrupter showed that the cooler structure had been bent by the pressure drop in the flow of hot gases. Otherwise the interrupter was in good condition.

It was decided to make another series of tests at reduced current with the coolers completely removed in order to determine the limiting interrupting ability of the prototype. These tests were made at the 242 kV 100 kA 90% SLF rating. The test results shown in Table 6-9 show that the interrupter is indeed able to interrupt the 90 kA current level with the full transient recovery voltage of the 242 kV circuit but only for a very narrow range of arcing times. At the design speed of 30 ft/sec the interrupter worked at an arcing time of 14.5 ms but failed as all shorter and longer times. When the speed was increased to 32-35 ft/sec the interrupter was able to withstand the high rate of rise of the line side transient but was unable to withstand the full recovery voltage of the bus side transient. Inspection of the interrupter after the tests showed that there had been breakdown between the top of the plenum and the tank due to hot gases flowing out of the plenum without being adequately cooled.

Section 7

# DESIGN AND DEVELOPMENT EXPERIENCE

In recounting the experience gained from a long and diverse project such as this one it is desirable to first classify problems as to their significance. Of course the most important problems are those dealing with the interrupter itself becuase it is the primary object of the project. Problems that involve the interraction of the interrupter with its surroundings are also important but they may be a unique result of the configuration studied and not representative of problems that would be expected when the interrupter is finally applied to a complete circuit breaker. It is also instructive to review problems that affected the associated equipment and methods and significantly affected the cost and performance of the project.

This report section will deal with the problems that affected the three interrupters studied, the interraction of the interrupters with their surroundings and finally problems that occurred in associated equipment and methods that were applied.

## 7.1 LIQUID INTERRUPTER

The model liquid interrupter shown in Figure 7-1 developed problems in five specific areas during the evaluation tests. These areas shown by the identifying circles numbered 1 to 5 are: 1) Shield rings for the moving contact 2) The arc resistant tip on the moving contact 3) Arc resistant tips on the stationary contact fingers 4) Teflon flow directing nozzle surrounding the stationary fingers and 5) Flanges between the interrupter support tubes and the bottom on the interrupter.

1. The shield rings were broken off and were lying on top of the interrupter after the power tests. These rings were probably broken off of their support brackets by the high velocity liquid pushed upward in the chamber by the large bubble of hot gases formed during the interrupter process.

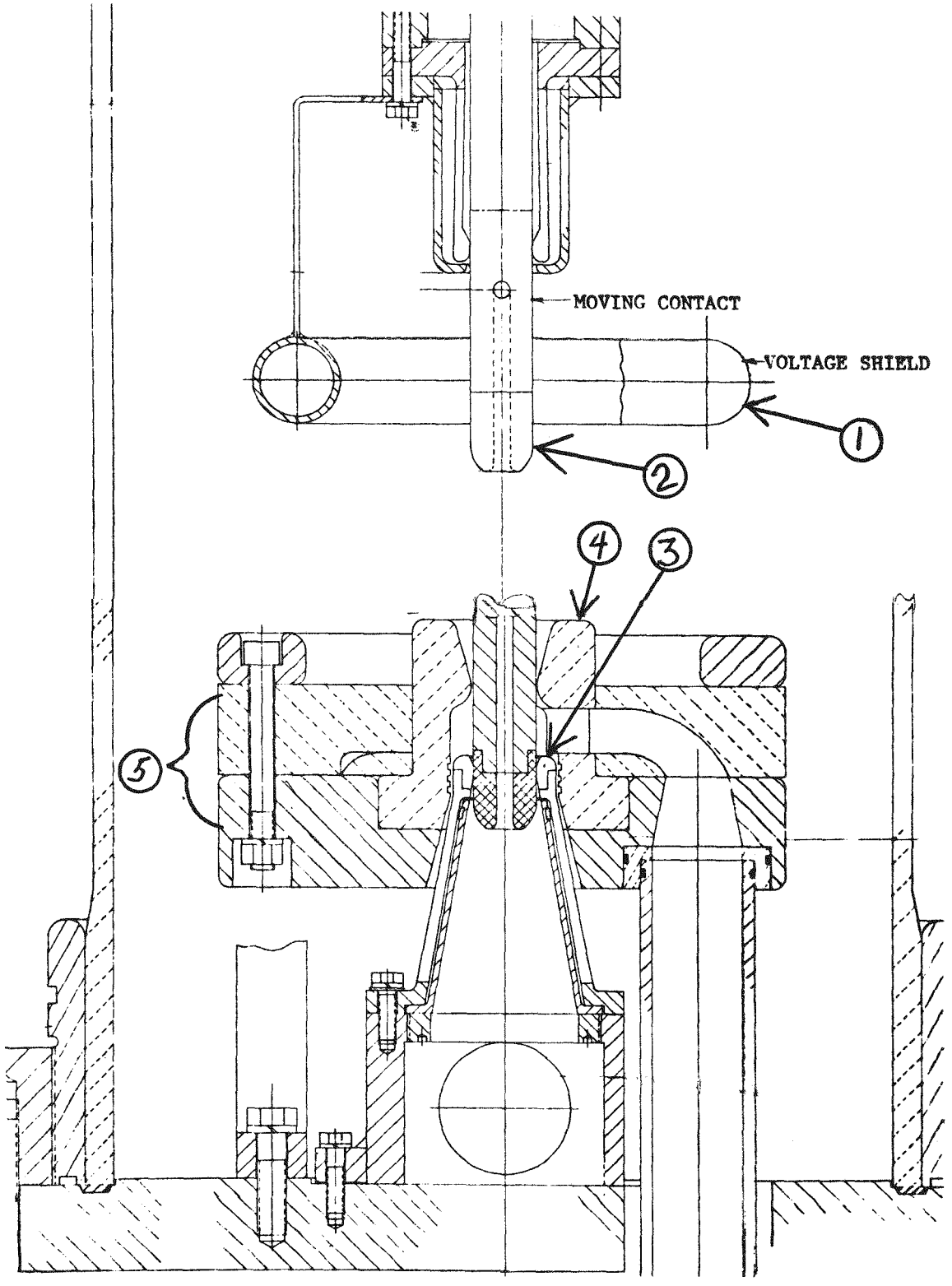


Figure 7-1 Liquid Interrupter

2. The arc resistant tip of the moving contact came off late in the testing program and this was probably due to very high degree of concentration of heating and arcing as well as the fact that this small diameter contact carried the full current during these tests. In a practical application of this interrupter it would require main contacts in parallel with the interrupting contact to carry the rated continuous current. These main contacts would carry the current during the first 10 milliseconds or so after the breaker is tripped and this alone would reduce the heating and wear of the moving contact. Finally this interrupter was subjected to 15 interrupting tests at currents from 70 kA up to 100 kA and the requirement for a power circuit breaker is only four full power interruptions for a set of contacts.

3. The stationary contact fingers sustained similar damage in burning off of arc resistant tips due to the large number of operations at high currents. Some of the fingers were also bent by the high pressure developed by the liquid pumping system and the pressure increase that occurred under arcing conditions. A steel liner could be included in an improved version of this interrupter to provide secure support for the fingers and prevent mechanical failure of the fingers.

4. The teflon interrupter nozzle was slightly expanded by the high differential pressures developed by the interrupter. This structure was designed to operate at the yield strength of the teflon with the expectation that the very short time of application of the pressure load would not result in any permanent deflection. These tests show that any future nozzle that will be subjected to pressures of over 1000 psi will require reinforcement. This can be provided either by a high strength insulating support tube around the nozzle or by using a highly filled teflon. Both of these possibilities were considered during the design of the nozzle but they were not used because they would have introduced additonal possible failure modes that would have required extensive investigation before they could have been used.

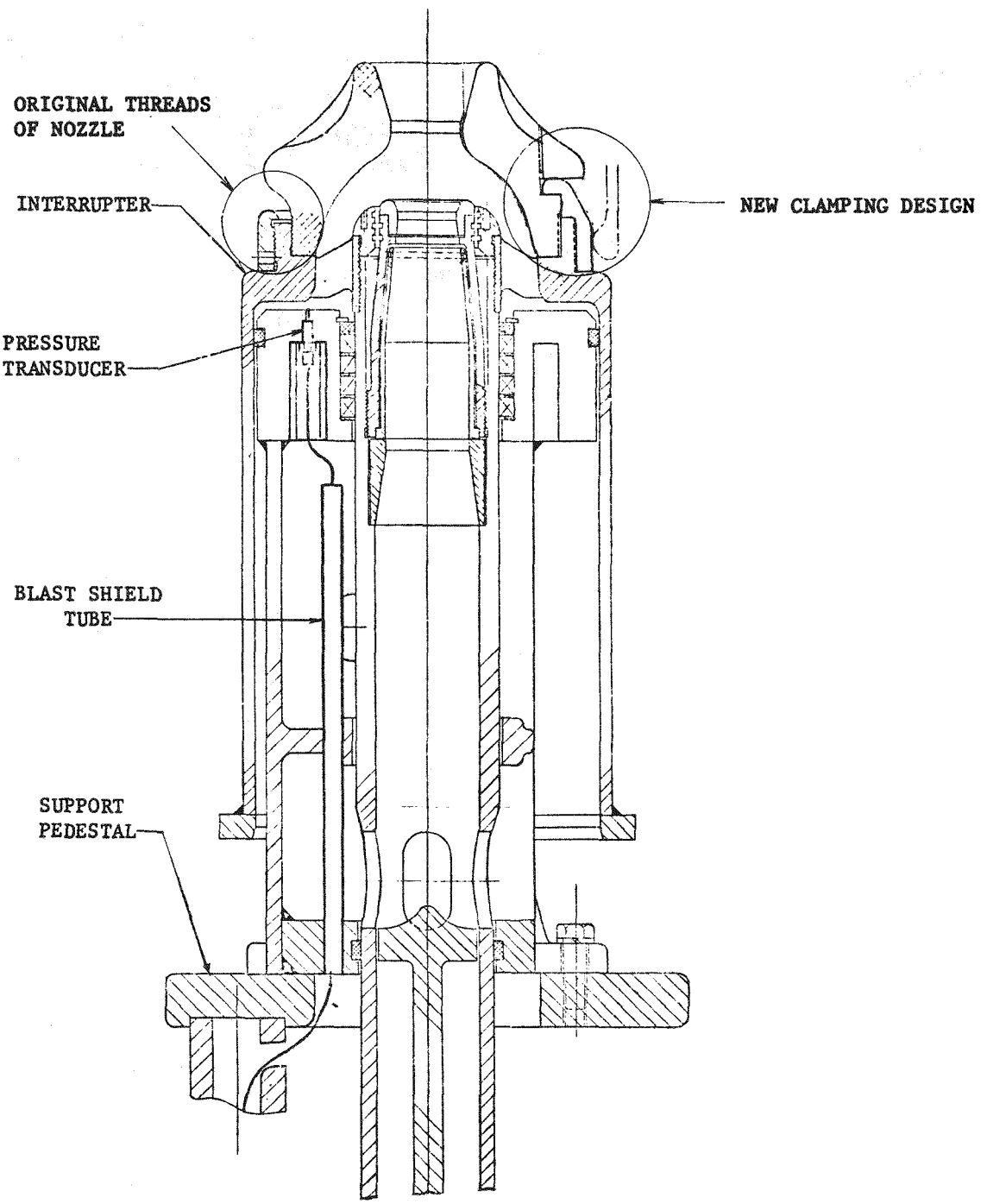


Figure 7-2 Model Puffer Interrupter

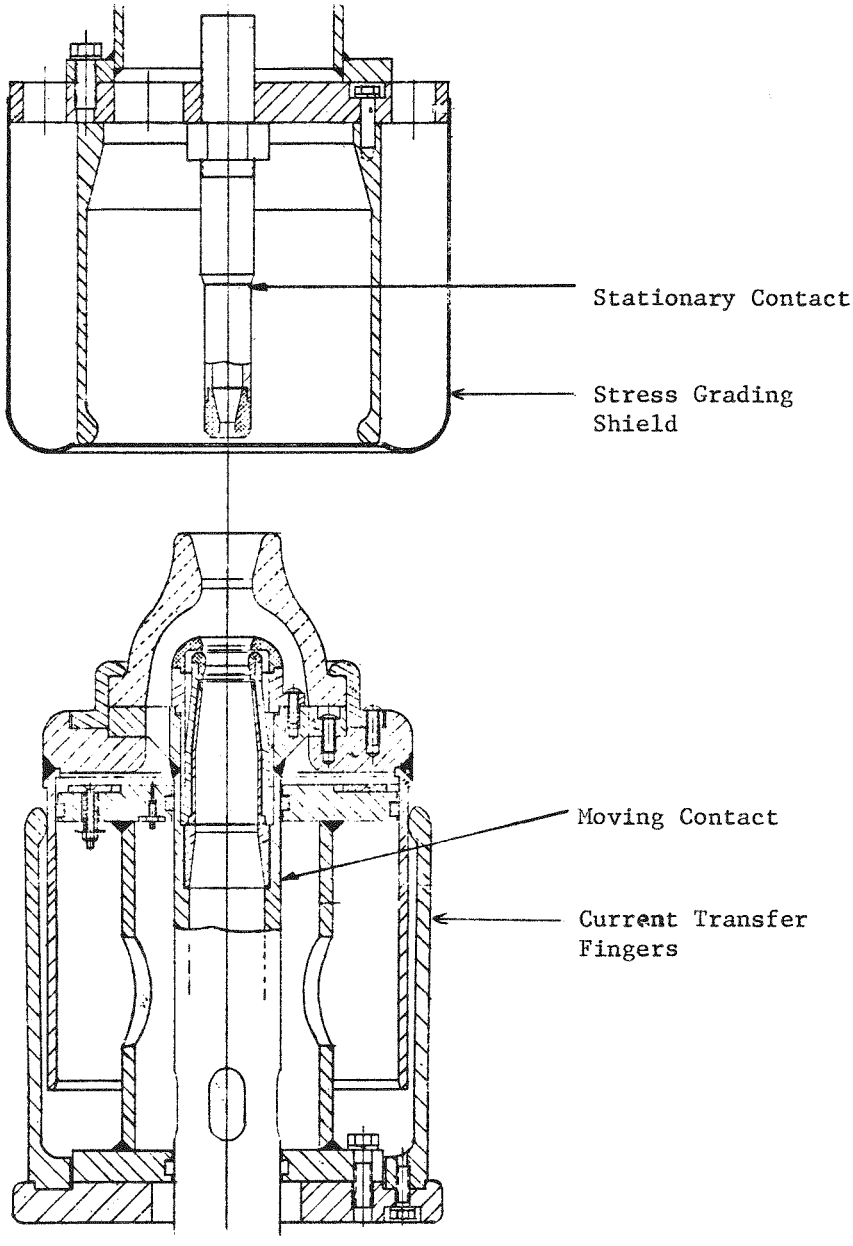


Figure 7-3 Prototype Interrupter

5. The flanges which connect the interrupter assembly to the support tubes were bent by the high internal pressure. Review of the design showed that the stresses generated were well above the material stress limits. This problem was easily solved by adding external tie bolts that reduced the stress on the flanges.

## 7.2 MODEL PUFFER INTERRUPTER

The model puffer interrupter shown in Figure 7-2 developed problems in only one area during the evaluation tests. The teflon nozzle first sheared off threads that secured it to the interrupter cylinder during mechanical tests. The nozzle mounting was redesigned to use a clamping ring capable of withstanding 1000 psi. There were no further problems with the nozzle mounting. During the high current tests with this interrupter differential pressures up to 900 psi were developed without affecting the nozzle mounting system.

## 7.3 PROTOTYPE PUFFER INTERRUPTER

The prototype puffer interrupter was actually tested and evaluated in two different configurations. Those two configurations were first in an insulating pressure chamber that was used for the model puffer and the second in a larger diameter grounded metal tank. Some of the problems that appeared during testing in the insulating pressure chamber were overcome by using the larger metal tank.

### a. Prototype Puffer in an Insulating Pressure Chamber

During the evaluation tests of this interrupter problems appeared on two distinct areas shown in Figure 7-3. First the external current transfer fingers between the puffer cylinder and the stationary piston, second in the stress grading shield around the stationary contact.

1. The current transfer fingers on the outside of the puffer cylinder were not able to carry the 12 kA per finger used in the initial design. In past applications of transfer fingers making contact to high velocity plated copper surfaces currents up to 15 kA per finger have been successfully used. In this application to a silver plated aluminum cylinder the contacts showed burning even in the fully closed position. There was also considerable burning of the contacts all along the 6.5 inch travel of the cylinder. Although the number of fingers was later doubled to reduce the

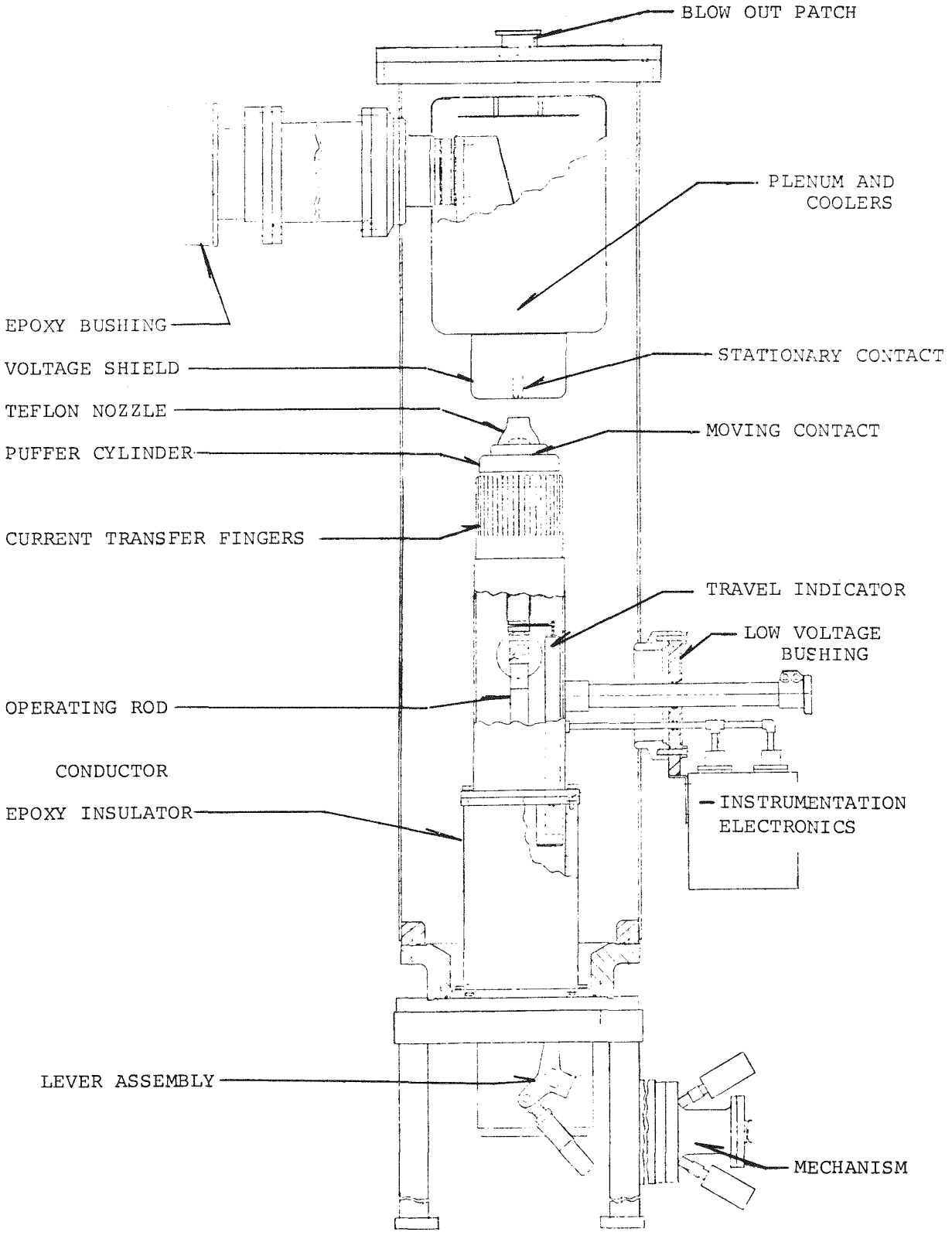


Figure 7-4 Dead Tank Test Model

current per finger to 6 kA there was still considerable burning of these contact surfaces. Clearly there is a need for additional development of this type of contact for high current puffers.

2. The stress grading shield around the stationary contact was blown off during early power tests. This was due to a much higher than expected pressure rise in this shield. Review of the flow passages and predicted pressures lead to the redesign of the flow passages through the stationary contact and the reinforcing of the mounting for the shield. When the mounting was reinforced the shield mounting problem was solved.

   Even though the reinforced mounting of the shield kept it in place the pressure rise due to the flow passages lead to delayed breakdown of the interrupter open gap after interruption. This was the probable cause of the greatly reduce dielectric strength of this interrupter during the transient recovery voltage period and it lead to a severe reduction in the bus fault recovery capability of the interrupter.

b. Prototype Puffer in a Larger Diameter Grounded Metal Tank

The intitial problems with seriously reduced recovery capability of the interrupter gap was caused by hot gases filling the space between the contacts. The approach taken to this problem was to add a large plenum downstream from the stationary contact and insert coolers in the flow path to reduce the volume of the hot gases as well as to cool them. This would prevent accumulation of hot gas in the gap. This arrangement is shown in Figure 7-4. The power tests of this configuration showed that the coolers were obstructing the flow of hot gases and in fact did not improve the performance.

The final approach that was taken to the resolution of these problems was to remove the coolers and permit the hot gases to flow freely into the large volume of the plenum. This approach did improve the interrupting performance but the pressures in the plenum after a 100 kA interruption rose high enough to break the top cover loose from the plenum and cause breakdown to the tank. Finally when the top cover was strengthened and vented to reduce the pressure rise the hot gases flowed through the pleunum and lead to breakdown to the top of the grounded metal tank.

The conclusion from this array of problems is that considerable more study is needed of the flow, cooling and control of the hot gases exhausted from a puffer interrupter for currents of the order of 100 kA. Although the basic interrupter gap was able to recover dielectric strength the surrounding insulating gaps were subject to dielectric failure because the exhaust gases were not adequately controlled.

## 7.4 PROBLEMS WITH PERIPHERAL INTERRUPTER TEST DEVICES

Since this project was directed to the development of an interrupter only the minimum amount of effort was devoted to the design and development of the mechanical driving systems. Commercial pneumatic drive cylinders were used with available valves and controls. The shock absorber systems were made as simply as possible to provide the required driving characteristics and the insulating support structures were adpated from available high pressure tubes. There were numerous mechanical problems with the stopping of the interrupters in a relatively short distance at the end of the interrupting stroke. In both the liquid and the prototype interrupters the use of conventional shock absorbers was not adequate to provide control of the decelleration loads. Unconventional shock absorbing actions were incorporated into the driving cylinders to obtain the required characteristics. In the case of the liquid interrupter the addition of an integral oil shock absorbing action in the end of the drive cylinder provided the necessary control. In the case of the prototype interrupter a set of ports directly in the driving piston permitted the driving air to flow through and build up a back pressure in the driving cylinder. Both of these methods solved the immediate problem of testing an interrupter but neither approach could be used directly in a commercial circuit breaker because of the high speed reclosing action required.

Problems with mechancial linkages caused by high decellerating forces were solved by straightforward mechanical design methods. However these problems did lead to program delays and additional costs. They also highlighted the fact that in the development of an interrupter with a high degree of interaction between the interrupter and the mechanism the development of the mechanism should properly be included in the project work.

Problems with the high pressure insulating tubes used as interrupter test chambers centered around the tubes inability to withstand large numbers of high current tests in which it was subjected to high levels of radiation and to exposure to hot arced gases. The liquid interrupter tube suffered little damage during the tests

probably because a small number of tests were made and the liquid $SF_6$ provided a degree of protection for the tube. On the other hand the insulating tube used for the prototype and model puffer interrupters was subjected to many high current tests and it was carbonized by the hot gases and radiation.

Although it was partially restored by cleaning it was not suitable for withstanding the high dielectric stresses that were imposed by capacitor switching tests. These tests have shown that an insulating structural tube must either be located farther away from a high current arc or it must be provided with a much better form of protection. These tubes were coated with a thin (0.06 in) coating of arc resistant material. A more satisfactory protection could be provided by a thicker layer of teflon which would absorb radiation and cool the exposed surfaces by ablation.

## 7.5 TEST PROBLEMS

Problems in performing tests at these high currents and voltages centered around three principal areas. These were high voltages, efficiency of synthetic testing and instrumentation.

### a. High Voltages

The maximum crest TRV required for the 100 kA 242 kV tests exceed the original capability of the laboratory. Initially a solid dielectric cable was used to carry the high TRV from the synthetic test circuit to the test interrupter. The cable termination proved to be unable to withstand the maximum recovery voltage. The final solution to this problem was to install a gas insulated bushing between the two areas.

### b. Test Efficiency

The difficulties encountered in carrying out synthetic tests at the absolute maximum capability of the test laboratory proved to be primarily in efficiency. That is the number of power tests made was much larger than the number of complete synthetic tests of the interrupter. First it is difficult to synchronize the many components required to make one successful test. Second in order to minimize risk to the laboratory large numbers of trial tests were made and this resulted in undesireable wear of the test device. Both of these factors reduce the efficiency and increase the cost of testing.

c. Instrumentation

The special fiber optic isolated system built for this test program was less than satisfactory for a number of reasons. First the power supply batteries were not capable of supplying the instruments under the low ambient temperatures that were encountered in the laboratory. This problem was overcome with heaters. The fiber optic transmission system was short and the electronic components for both transmitting and receiving were subjected to the high magnetic fields produced by the test currents. As a result of these problems there were not satisfactory measurements of pressure and travel of the interrupters during high current tests.

The standard laboratory instrumentation for recording currents, voltages and transient recovery voltages performed satisfactorily at currents up to 80 kA. However for higher test currents there was serious interference with high frequency measurements of current and voltage. During the tests of the two model interrupters adequate current and voltage measurements were made.

When the prototype interrupter was tested the higher voltage rating required that the size of the high current circuit be increased and this generated higher magnetic fields in the area where high speed oscilloscopes recorded the test current and voltage. These higher magnetic fields penetrated the shielded oscilloscopes and prevented the accurate recording of current and voltage on a fast time scale.

These experiences show that it would be desireable to completely check out the operation of a testing laboratory before a new and severe type of test is made on a test device. However this is not a new conclusion and probably the economic and schedule pressure on testing laboratories will always present this approach from being properly implemented.

# APPENDIX A

# A STUDY OF SELECTED CONSTRUCTION MATERIALS FOR $SF_6$ CIRCUIT BREAKERS UNDER HIGH STRESS CONDITIONS

## A.1 SELECTION OF MATERIALS

Materials selected for evaluation were those already known to be of superior quality and of the types required for the high current $SF_6$ interrupter to be built during this project.

The insulating materials selected are listed in Table A-1A. Kel-F was used as control sample. The bushings for sample mounts are made of Kel-F because of its excellent insulating and sealing performance.

For investigation of surface conditions of metals, samples were selected from those commonly used as electrical conductors, contacts and structural members. These are given in Table A-1B.

Since silver coated cupaloy and silver coated aluminum are most commonly used as current carrying contacts in $SF_6$ circuit breakers, these two materials were selected for investigating variations of contact resistance. These are listed in Table A-1C.

For stress bearing metallic and insulating materials, the materials listed in Table A-1D were selected. Variations in tensile strength were investigated. Springs made of three different materials were also included.

TABLE A-1A

MATERIALS SELECTED FOR EVALUATION AS INSULATING MATERIALS

| TEST MATERIAL | MATERIAL DESIGNATION | GENERIC DESCRIPTION | USE |
|---|---|---|---|
| A1 | Cloth Micarta (NEMA LE) | Laminated cotton - Pheonlic sheet | Shims, Washers & Spacers |
| A2 | Nylon (6/6) | | Spacers |
| A3 | Virgin Teflon | Polytetrafluoroethylene | Nozzles |
| A4 | *Glass Epoxy (NEMA G-11) (HY-180-1) | Laminated glass-epoxy sheet (NEMA G-11) | Feed Tubes |
| A5 | Cast Epoxy Resin | Cycloaliphatic epoxy resin filled with silica | Insulators |
| A6 | Cast Epoxy Resin | Cycloaliphatic epoxy resin filled with Alumina Trihydrate | Resistor Plates |
| A7 | Glass Epoxy Resin | Pultruded fiber glass filled epoxy resin | Pull Rods, Studs |
| A8 | Porcelain | Electric Porcelain | Bushings & Insulators |
| A9 | Polyimide Film (Kapton HF) | Kapton Tape | Resistor Insulation |
| A10 | Glass Epoxy | Filament wound fiber glass and epoxy resin | Feed Tubes |
| A11 | Glass Epoxy (NEMA G-10) | Laminated glass-epoxy sheet (NEMA G-10) | Insulating Supports |
| A12 | Glass Polyester | Filament wound fiber glass and polyester resin | Insulating Supports |
| A13 | Improved Coating #53533FE | A Westinghouse Proprietary coating for insulators exposed to arced $SF_6$ | |
| A14 | Epoxy Castings | Bisphenol A epoxy filled with silica | Spacers |

TABLE A-1B

MATERIALS SELECTED FOR EVALUATION - EFFECT OF ARCED $SF_6$ ON SURFACE CONDITION OF METALS

| TEST MATERIAL (I.D.) | MATERIAL DESIGNATION | USE |
|---|---|---|
| B1 | Carbon Steel | Enclosures, Supports, Levers, Shafts, etc. |
| B2 | Alloy Steel (#11 Tool Steel) | Levers, Shafts, etc. |
| B3 | Stainless Steel (301) | Enclosures, Supports, Levers, Shafts, etc. |
| B4 | Aluminum Alloy (6061T6) | Enclosures, Structural Members, Conductors |
| B5 | Cast Aluminum Alloy (356) | Supports, Structural Members |
| B6 | Copper | Contacts, Conductors |
| B7 | Cupaloy (chrome copper) | Contacts, Support Structures |
| B8 | Anodized aluminum alloy (6061T6) | Aluminum blast valve parts |

TABLE A-1C

MATERIALS SELECTED FOR EVALUATION - VARIATION OF CONTACT RESISTANCE

| TEST MATERIAL (I.D.) | MATERIAL DESIGNATION | USE |
|---|---|---|
| C1 | Cupaloy (chrome copper) | Contacts, Support Structures |
| | Coated with Silver | Cupaloy contact surface |
| C2 | Aluminum Alloy (6061T6) | Enclosures, Structural Members Conductors |
| | Coated with Silver | Brush plating on aluminum flanges and contact surfaced |

TABLE A-1D

MATERIALS SELECTED FOR EVALUATION OF METALLIC MATERIALS
GLASS FIBER REINFORCED STRAIN RODS AND FITTINGS

| TEST MATERIAL (I.D.) | MATERIAL DESIGNATION | USE |
|---|---|---|
| D1 | Carbon Steel | Enclosures, Supports, Levers, Shafts, etc. |
| D2 | Alloy Steel (#11 tool steel) | Levers, Shafts, etc. |
| D3 | Stainless Steel (301) | Enclosures, Supports, Levers, Shafts, etc. |
| D4 | Aluminum Alloy (6061T6) | Enclosures, Structural Members, Conductors. |
| D5 | Cast Aluminum Alloy (356) | Supports, Structural Members |
| D6 | Music Wire Spring | |
| D7 | Oil Temper Wire Spring | |
| D8 | Chrome Vanadium Wire Spring | |
| D9 | Glass Epoxy (NEMA G-10) | Insulating Supports |
| D10 | Filament wound fiberglass and epoxy resin | Pull Rods, Studs |
| D11 | Filament would fiberglass and polyester resin | Insulating Support |
| D12 | Glass Epoxy Resin (D10) Cemented to metal rod ends | Pull Rods, Studs |

## A.2 TEST APPARATUS

### Test Chamber

The test chamber used consisted of a 6.25 inch ID, 12 inch long steel tube mounted between two end plates as shown in Figure A-1. It has a volume of approximately 300 $in.^3$, and has a pressure withstand capability in excess of 1000 psig. There are sixteen sample mounts, arcing contacts, and a cylinder to shield the test specimen from direct exposure to the arc.

### Arcing Contacts

The stationary contact is a 1 inch diameter copper-tungsten tip brazed to a cupaloy piece of the same diameter, which, in turn, is threaded into a larger brass piece to which a 0.75 inch brass rod is attached. This assembly is supported and insulated from the chamber by an epoxy bushing. A 2.5 inch diameter steel tube surrounds the contact to shield the test sample from direct radiation of the arc.

The moving contact is designated as Item 3 in Figure A-1. Because of sealing difficulties with an O-ring, however, it was redesigned making use of 2-ply stainless steel bellows. The contact tip is 1 inch diameter copper tungsten brazed to a cupaloy rod which is threaded onto an operating rod.

### Sample Mount and Test Specimen

The sample mount used for insulating material test is shown in Figure A-2. Four vertical rows of four sample mounts each were mounted equally spaced circumferentially around the test chamber wall. Each sample mount consists of a 0.25 inch diameter brass stud inserted through the wall of the test chamber and insulated from it by a Kel-F (polychlorotrifluoroethylene) bushing. The sample mount is held to the chamber wall by fittings and gas sealing is accomplished by means of Viton O-rings.

The test specimens for insulating material tests were 1.875 inch diameter disks 0.25 inch thick with a 0.25 inch diameter center mounting hole. Samples were held by 1 inch diameter brass disks on either side which acted as inner electrodes. The outer electrodes were 1.875 inch OD x 1.5 inch ID brass rings clamped to the test specimen. A 0.25 inch radial gap is maintained on both sides of the test samples for leakage current and dielectric strength measurements. The outer

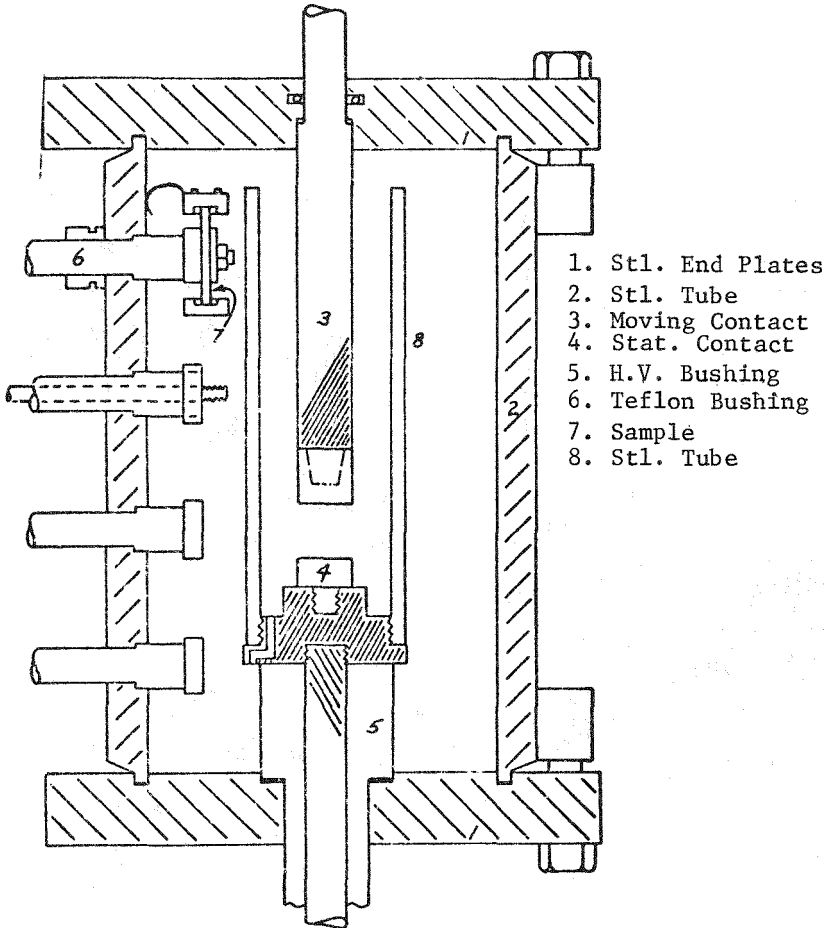


Figure A-1 High Stress Materials Test Chamber

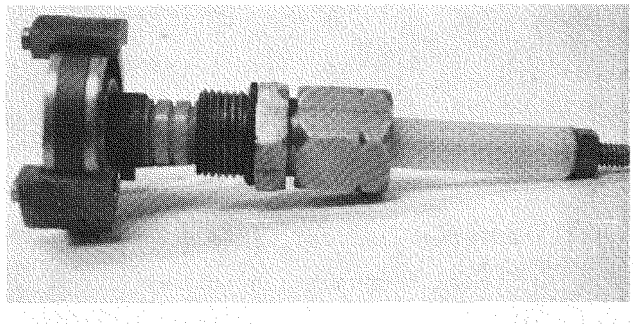

Figure A-2 Insulating Sample Mount

electrode is connected to the chamber wall by means of ground straps, and the inner electrode is connected to the center stud of the sample mount, which is insulated from the chamber wall by Kel-F bushing.

Chamber Filling Technique

Prior to introducing $SF_6$ gas into test chamber the apparatus was evacuated to 0.1 mm Hg while the chamber was heated to 10°C above ambient. The chamber contained 0.2 lbs. of 13X molecular sieves. After 1 hour minimum of pumping, heating was discontinued while the vacuum was maintained. When the chamber temperature reached room temperature, the chamber was filled with $SF_6$ gas from commercially supplied $SF_6$ cylinders to the density corresponding to 300 psig at 20°C. The chamber was then heated to 135°C (or 150°C) and maintained to within $\pm$ 1°C. At this temperature, $SF_6$ gas pressure was theoretically 570 psig (or 600 psig). However, actual pressure was approximately 500 psig, (or 520 psig for the 150°C initial case).

Instrumentation for Measurement and Control

For heating, eight 150 watt strip heaters were placed around the test chamber wall, and temperature was controlled to $\pm$ 1°C accuracy at 135°C or 150°C depending on test categories, by using a LFE Model 232 0-300°C temperature controller and a relay. Other items used for temperature and pressure sensing and measuring were:

a. Omega Quick Disconnect Thermocouple Assemblies with Iron-Constantan - 6 inch (2)

b. Robinson Halpern Static Pressure Transducer Model P40-260D-2505, 0-600 psig (1)

c. OMNI-AMPIIB-J Thermocouple Amplifier (1)

d. Digital Voltmeters for Temperature and Pressure Readouts, respectively. (2)

For evacuating the test chamber a CENCO Hypervac 23 vacuum pump, 240 liters/min at atm., was used and vacuum was measured by a McLeod gage.

Electric arcs were drawn from the a.c. transformer banks at the Westinghouse Electric Corporation LRMD Laboratory. Arc current was set at 2000A at 2500 V. Arc currents and voltages were recorded on Visiscoder Oscillograms, and arc energy was calculated by graphically integrating the product of arc voltage and current.

As a precaution, a pressure relief valve, Republic Cat. No. 665-8-3/8" D1 (Buna N), was added to the test chamber. The relief pressure was set at 800 psig.

Preliminary Test

Prior to actual tests, the test chamber was pressurized following the procedure given above and the temperature control, gas seals, high pressure withstand capability of the test chamber and gas systems thoroughly checked out.

For this test, all the openings for sample mounts were plugged except for four sample mounts, two with Kel-F bushings and two with Vespel (DuPont tradename for polyimide resin).

The $SF_6$ test was heated to 135°C at a pressure of 500 psig, and this temperature was maintained for two hours. Then heaters were then turned off and the gas was allowed to cool to room temperature. A $SF_6$ gas sample was withdrawn for mass spectrometric analysis.

The gas was replaced with fresh $SF_6$ gas and the test was repeated at a temperature of 150°C instead of 135°C. Another gas sample was withdrawn.

These preliminary tests confirmed the following:

a. The temperature control was accurate to within $\pm$ 1°C.

b. The Vespel bushings were bettern mechanically than the Kel-F ones. (However, it was later discovered that the Vespel bushings were electrically unsatisfactory, with lower dielectric strength along the surface and surface tracks after flashovers.)

c. The entire system was satisfactory for high temperature and high pressure. After these tests, the system was left over a weekend at full pressure. The leak rate was only 7 psi in 64 hours.

## A.3 TEST FOR INSULATING MATERIALS

### Scope

Insulating materials listed in Table A-1A were subjected to $SF_6$ gas at 135°C and 500 psig, with and without arcing. Some exposure tests were conducted after 1.6 cc of water was injected into the test chamber. Variations in leakage current, dielectric strength, and sample weight were investigated. Measured and recorded parameters were: gas temperature, gas pressure, arc current, arc voltage, arc energy, leakage current, dielectric strength, ambient temperature and time of measurement.

### Test Procedures

The leakage resistance of each sample was measured with a 1000 volt d.c. power supply and a microammeter in the closed vented chamber at 1 atm air. The chamber was then evacuated to 0.1 mm Hg while the chamber was heated to approximately 10°C above ambient with 0.2 lb. of 13X molecular sieve in the chamber. After at least 1 hour of pumping, the heaters were turned off. When chamber temperature fell to room temperature it was filled with $SF_6$ gas to 300 psig. The chamber was then heated to 135°C, and maintained at 135°C $\pm$ 1°C for 2 hours.

Leak resistance of each specimen was measured at 135°C and 500 psig. Gas temperature and pressure were also recorded.

At the same temperature and pressure, a.c. dielectric strength of one set of the duplicate samples was measured. The maximum voltage of the a.c. high voltage tester was set at 15 kV rms because the air gap dielectric strength along the Kel-F bushing was approximately 17 kV rms.

The chamber was allowed to cool to room temperature. An $SF_6$ gas sample was withdrawn for analysis.

After the above tests were completed, arc energy of approximately 84 kW-s was applied. This value was selected as a simulation of four 1.2 cycle arcing periods at 120 kA rms with an arc voltage of 2000 volts in a breaker pole unit with a volume of 40 $ft.^3$. This arc energy was obtained by four arcing periods of approximately 8 half cycles each at a current of 2000 amperes.

Immediately after arcing, heaters were turned on, and when the temperature reached 135°C leakage resistance of each specimen was measured. Gas temperature and pressure were also recorded.

The chamber was allowed to cool to room temperature and leakage resistance of each sample was measured. The chamber was then reheated for one hour at 135°C. Leakage resistance of each specimen was measured.

Dielectric strength tests were performed on all speciments at 135°C psig with voltage at 15 kV rms in the first tests and then at 20 kV rms in subsequent tests. The chamber was then allowed to cool, and a gas sample was withdrawn. Test specimens were removed and weighted to nearest milligram.

After two series of tests were completed, a new set of speciments, one each from the materials list given in Table A-1A, were weighed and mounted in the test chamber, 1.6 cc of water was injected into the test chamber. The test chamber was then filled with $SF_6$ gas to 300 psig at room temperature. A $SF_6$ gas sample was withdrawn for mass spectrometric analysis. Residues collected on the surface of a few representative samples were collected for chemical analysis. Test specimens were removed and weighed to nearest milligram.

Test Results

The test results obtained without injection of water are summarized in Tables 2 and 3. When the test chamber was heated up to 135°C, some materials such as laminated cotton phenolic sheet, nylon and cast epoxy resin (filled cychloaliphatic epoxy resin), showed high leakage currents, but most of the remaining samples showed less than 1 micro ampere leakage. All the samples except nylon and polyimide film withstood a 15 kV rms voltage.

One of the nylon samples broke down at 7.5 kV rms, and the polyimide film broke down at 11 kV. In case of the latter breakdown, examination revealed that it occurred through the sample which consisted of two layers placed between the ground strap and the chamber wall. Since the published dielectric strength of this film is 725 volts per mill,[5] the breakdown voltage of 11 kV rms is actually higher than expected.

TABLE A-2

INSULATING MATERIALS TEST RESULTS

Leakage Current and Dielectric Strength of Samples
before and after 0, 2 & 4 hrs exposure to arcing in $SF_6$

| | | Leakage uA at 1000 VDC | | | | Dielectric Strength kV RMS | |
|---|---|---|---|---|---|---|---|
| | | Before | After | | | Before | After |
| | | (1) | 0 | 2 Hrs. | 4 Hrs. | | 4 Hrs. |
| Gas Temperature °C | | 135 | 135 | 29 | 135 | 135 | 135 |
| Gas Pressure PSIG | | 490 | 475 | 295 | 468 | 490 | 468 |
| Material | Sample No. | | | | | | |
| A1 Cloth Micarta | 1 | 35 | 37 | 0 | 30 | 15 | 15 |
| | 2 | 37 | 42 | 0 | 33 | -- | 15 |
| A2 Nylon | 1 | 238 | 3000 | 0 | -- | 7.5 | 3 |
| | 2 | 192 | 1250 | 0 | 1120 | -- | 4.5 |
| A3 Teflon | 1 | 0 | 0 | 0 | 0 | 15 | 15 |
| | 2 | 0 | 0 | 0 | 0 | -- | 15 |
| A4 G11 Glass Epoxy | 1 | .3 | .3 | 0 | .4 | 15 | 15 |
| | 2 | .2 | .2 | 0 | .3 | -- | 15 |
| A5 Cast Epoxy | 1 | .5 | .9 | 0 | 1.1 | 15 | 15 |
| | 2 | .5 | .5 | 0 | .9 | -- | 15 |
| A6 Cast Epoxy | 1 | 25 | 53 | 0 | 62 | 15 | 15 |
| | 2 | 28 | 56 | 0 | 65 | 15 | 15 |
| A7 Pultruded Glass Epoxy (2) | 1 | .2 | .4 | 0 | .3 | 15 | 15 |
| | 2 | .3 | .4 | 0 | .4 | -- | 15 |
| Kel-F | 1 | 0 | 0 | 0 | 0 | 15 | 15 |
| | 2 | 0 | 0 | 0 | 0 | -- | 15 |

Note (1) - All samples had no measureable leakage at room temperature before or after exposure to arcing tests.

Note (2) - The pultruded glass epoxy rod was coated with protective coating.

TABLE A-3

INSULATING MATERIALS TEST RESULTS

Leakage Current and Dielectric Strength of Samples
before and after 0, 2 & 4 hrs exposure to arcing in $SF_6$

| | Leakage uA at 1000 VDC | | | | Dielectric Strength kV RMS | |
|---|---|---|---|---|---|---|
| | Before | After | | | Before | After |
| | (1) | 0 | 2 Hrs. | 4 Hrs. | | 4 Hrs. |
| Gas Temperature °C | 135 | 135 | 32 | 32 | 135 | 135 |
| Gas Pressure PSIG | 525 | 480 | 305 | 305 | 480 | 468 |
| Material / Sample No. | | | | | | |
| A8 Porcelain | 1 | .4 | 15 | .5 | 0 | .2 | 15 |
| | 2 | .5 | | .6 | 0 | .1 | 15 |
| A9 Polyimide Film | 1 | 0 | 11 | 0 | 0 | 0 | 2.5 |
| | 2 | 0 | | .1 | 0 | 0 | 12 |
| A10 *Glass Epoxy | 1 | .1 | 15 | .1 | 0 | 0 | 15 |
| | 2 | .2 | | .2 | 0 | 0 | 15 |
| A11 *Glass Epoxy G10 | 1 | .3 | 15 | .3 | 0 | .1 | 15 |
| | 2 | .2 | | .2 | 0 | .1 | 15 |
| A12 *Glass Polyester | 1 | .2 | 15 | .3 | 0 | .1 | 15 |
| | 2 | .2 | 15 | .2 | 0 | .1 | 15 |
| A13 Improved Coat. | 1 | .4 | 15 | .5 | 0 | .2 | 15 |
| | 2 | .45 | | .4 | 0 | .2 | 15 |
| A14 Cast Epoxy | 1 | 0 | 15 | 0 | 0 | 0 | 15 |
| | 2 | 0 | | 0 | 0 | 0 | 15 |
| Kel-F | 1 | 0 | 15 | 0 | 0 | 0 | 15 |
| | 2 | .1 | | 0 | 0 | 0 | 15 |

NOTE (1) All samples had no measureable leakage at room temperature before or after exposure to arcing tests.

* Coated with Arc Resistant Coating A13

TABLE A-4

INSULATING MATERIALS TEST RESULTS WITH WATER

Leakage Current and Dielectric Strength of Samples before and after 0, 2 & 4 hrs exposure to arcing in $SF_6$ with 1.6 cc. $H_2O$

| | Leakage uA at 1000 VDC | | | | Dielectric Strength kV RMS |
|---|---|---|---|---|---|
| | Before | After | | | After |
| | (1) | 0 | 2 Hrs | 4 Hrs | 4 Hrs |
| Gas Temperature °C | 135 | 135 | 41 | 135 | 135 |
| Gas Pressure PSIG | 490 | 505 | 335 | 515 | 515 |
| Material | | | | | |
| A1 Lam. Cotton Phenolic Res. | | 31 | .15 | 21 | 15 |
| A2 Nylon 101 (6/6) | | 653 | .10 | 505 | 4.5 |
| A3 Teflon | | 0 | 0 | 0 | 15 |
| A4 *Glass Epoxy G11 | | 0 | 0 | 0 | 12 |
| A5 Cast Epoxy Resin | | .3 | 0 | .3 | 15 |
| A6 Cast Epoxy Resin | | 15.5 | 0 | 16.1 | 15 |
| A7 *Pultruded Glass Epoxy Resin | | .2 | 0 | .2 | 15 |
| A9 Polyimide Film | | 0 | 0 | 0 | 12 |
| A10 *Glass Epoxy | | .2 | 0 | .1 | 15 |
| A11 *Glass Epoxy G10 | | .3 | 0 | .15 | 15 |
| A12 *Glass Polyester | | .2 | 0 | .15 | 15 |
| A13 Impr. Coating | | .2 | 0 | .2 | 15 |
| Epoxy Casting | | 0 | 0 | 0 | 20 |
| Kel-F | | 0 | 0 | 0 | 15 |
| Kel-F Bushing Only | | 0 | 0 | 0 | 15 |

NOTE (1) All samples had no measureable leakage at room temperature before or after exposure to arcing tests.

* Coated with Arc Resistant Epoxy

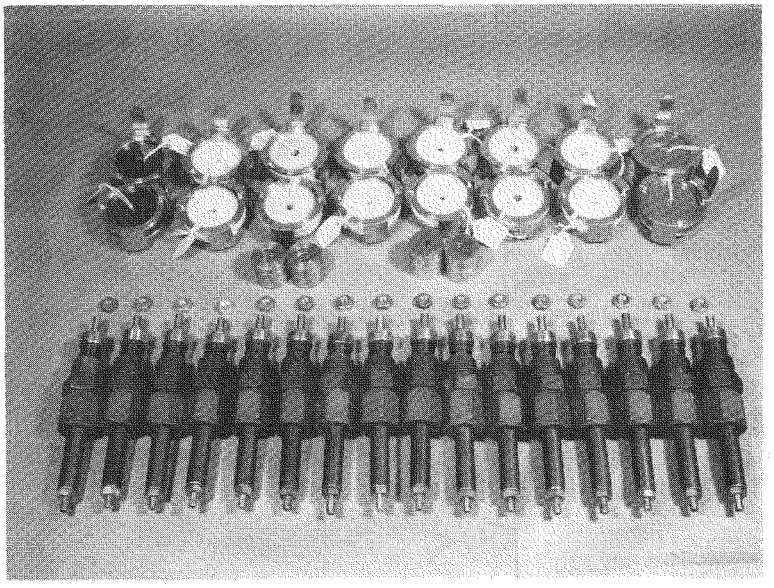

(a) Representative Insulating Materials Samples and Bushings

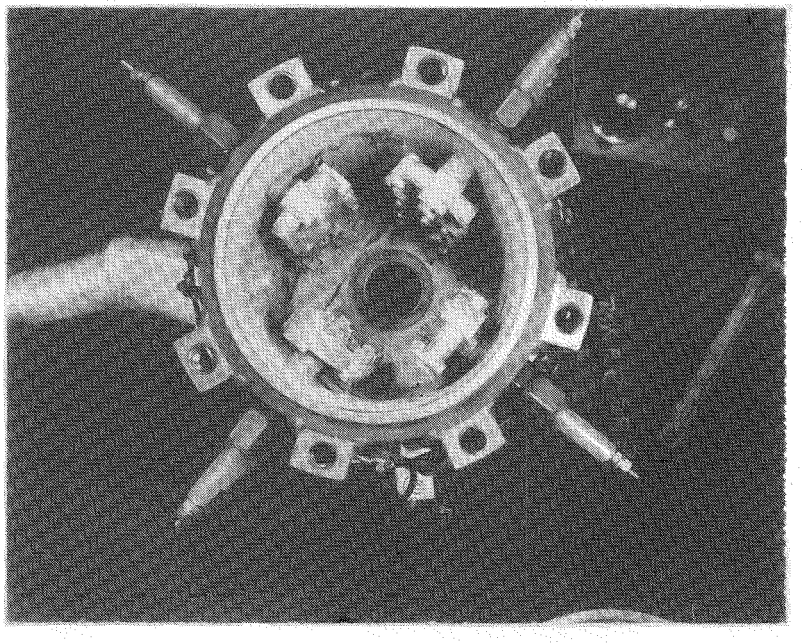

(b) After tests

Figure A-3 Insulating Material Samples in the Test Chamber

After the nylon sample broke down at 7.5 kV and was exposed to arced $SF_6$, the leakage current increased to 3000A. Subsequently, it increased drastically and broke down at 3 kV on the dielectric test. The other of the pair of nylon samples broke down at 4.5 kV at the last stage of the same test series.

The rapid increase in leakage current after one dielectric breakdown followed by a lower voltage dielectric failure indicates the necessity of simultaneous testing of duplicate samples. We reserved one of a pair of same material samples until the end of a test series to determine the effect of exposure to arced $SF_6$ on the dielectric strength of the material.

The porcelain samples performed well electrically, but one sample cracked through the center, probably due to thermal stress.

Test in the presence of water showed the same results. Nylon showed extremely high leakage currents at 135°C. The porcelain sample cracked again through the center. The laminated cotton phenolic sheet and cast epoxy resin (filled cycloaliphatic epoxy resin) showed relatively high leakage currents as before.

Some representative material samples before and after these tests are shown in Figure A-3. Nylon and porcelain samples are designed as (a) and (b) respectively. Others are samples of laminated cotton phenolic sheet (b), filled epoxy, (c) and cast epoxy resin (e).

Weights of each sample obtained before and after exposure tests showed no significant change.

Gas samples were withdrawn for mass spectrographic analysis. Also, dust was collected from some samples for chemical analysis. Results of these analyses will be discussed in Section A-8.

## A.4 EFFECT OF ARCED $SF_6$ ON SURFACE CONDITION OF METALS

The metallic materials listed in Table A-1B were subjected to $SF_6$ gas at a temperature of 150°C and a pressure of 250 psig, before and after arcing. Some exposure test was repeated with 1.6 cc of water injected into the chamber. Weights and hardness of test samples were measured before and after exposure to these environments. Surface changes such as pitting and roughness, $SF_6$ decomposition, and exposure byproducts were also investigated.

Test Setup

The test setup is the same as that used for the insulating material tests.

Test speciments wer 0.75 or 1 inch diameter disks machined to 0.25 inch thickness with 0.25 - 20 threads at the center for mounting on the brass stud of the sample mount. The surface was smoothed and buffed after machining.

Test Procedure

The same test procedure as for insulating samples was applied to the metal samples with a maximum temperature of 150°C. An $SF_6$ gas sample was withdrawn for mass spectrometric analysis. Dusts were collected for chemical analysis. Each speciment was removed, visually examined, and cleaned. Each specimen was then weighed to closest milligram. Hardness tests were performed on each specimen.

Test Results

Results of hardness measurements obtained before and after exposure tests are tabulated in Table A-5, which shows no significant variations before and after the exposure.

TABLE A-5

TEST RESULTS OF EFFECT OF ARCED $SF_6$
ON SURFACE CONDITON OF METALS

Effect of Exposure to Dry Arced $SF_6$ after 4 Hours

| Material Sample Samples | Rockwell Hardness Number | Before $R_g$ | Before $R_e$ | After $R_g$ | After $R_e$ |
|---|---|---|---|---|---|
| B1 Carbon Steel | 1 | 61 | | 62 | |
| | 2 | 61 | | 62 | |
| | 3 | 62 | | 62 | |
| | 4 | 62 | | 62 | |
| B2 Alloy Steel | 1 | 87 | | 87 | |
| | 2 | 87 | | 87 | |
| | 3 | 87 | | 87 | |
| | 4 | 87 | | 87 | |
| B4 Alum. Alloy | 1 | 59 | | 58 | |
| | 2 | 61 | | 60 | |
| | 3 | 60 | | 60 | |
| | 4 | 60 | | 59 | |
| B3 Stainless Steel | 1 | 93 | | 95 | |
| | 2 | 94 | | 95 | |
| | 3 | 94 | | 95 | |
| | 4 | 92 | | 95 | |
| B5 Cast Al. Alloy | 1 | | 84 | | 87 |
| | 2 | | 84 | | 87 |
| | 3 | | 84 | | 87 |
| | 4 | | 84 | | 86 |
| B6 Copper | 1 | | 85 | | 86 |
| | 2 | | 83 | | 86 |
| | 3 | | 83 | | 86 |
| | 4 | | 84 | | 86 |
| B7 Cupaloy | 1 | 79 | | 79 | |
| | 2 | 78 | | 80 | |
| | 3 | 78 | | 80 | |
| | 4 | 78 | | 80 | |
| B8 Anodized Alum Alloy | 1 | 61 | | 61 | |
| | 2 | 61 | | 61 | |
| | 3 | 61 | | 61 | |
| | 4 | 62 | | 61 | |

## A.5 VARIATION OF CONTACT RESISTANCE

Silver coated cupaloy and silver coated aluminum butt contacts listed in Table 1C, were subjected to 150°C and 520 psig $SF_6$ gas environment for 100 hours during which variation of contact resistance was investigated at a contact force of 20 lbs. Same tests were made with 1.6 cc of water injected.

A $SF_6$ gas sample was withdrawn after each series of tests for mass spectrometric analysis.

### Test Procedure

In the test chamber, the arcing contacts were replaced by a pair of test contacts two of which are shown in Figure 4A. The voltage measuring terminals were threaded into the electrodes from the side.

Instrumentation for control and measurement of temperature and pressure was the same as described for earlier tests. For the contact resistance measurement, an Alber Engineering, Inc. Model RT-2 digital microohmmeter was used. This instrument has a 100 ampere d.c. current source.

The contact resistance was measured at room temperature and $SF_6$ gas pressure of 300 psig with a contact force of 20 lbs.

### Test Results

Test results are summarized in Tables A-6 and A-7 for the silver coated cupaloy contacts, and in Table A-8 and A-9 for the silver coated aluminum ones. For the silver coated cupaloy contacts, the measured contact resistances were 3 uohm, except for one at 4 uohm, throughout the test series. However, for the silver coated aluminum contacts, resistances varied in a wide range, for 24 uohm to 632 uohm.

In each setting, three resistance measurements were made. There were practically no variations with the silver coated cupaloy contacts, as shown in Tables 6 and 7. However, because of the wide variation with the aluminum contact, the average readings were recorded in Tables 8 and 9.

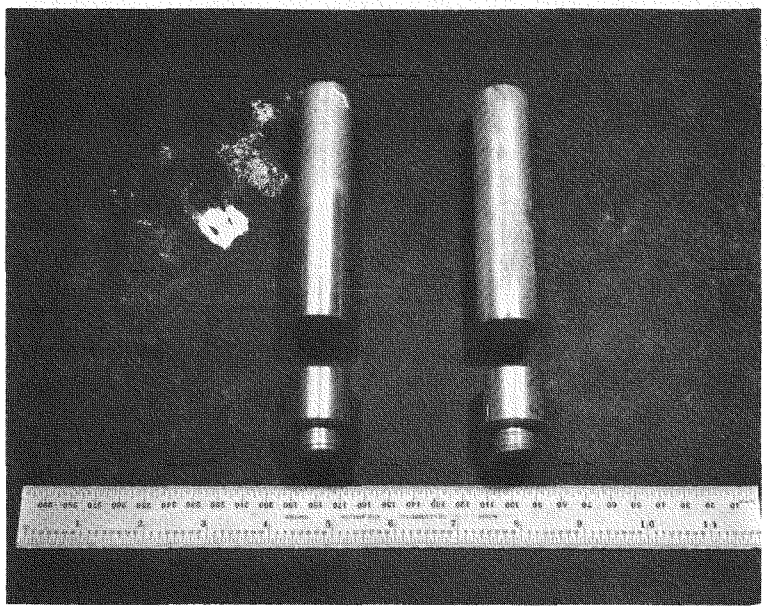

(a) Moving and Stationary (bottom) Contacts

Left - Silver-coated Cupaloy
Right - Silver-coated Aluminum

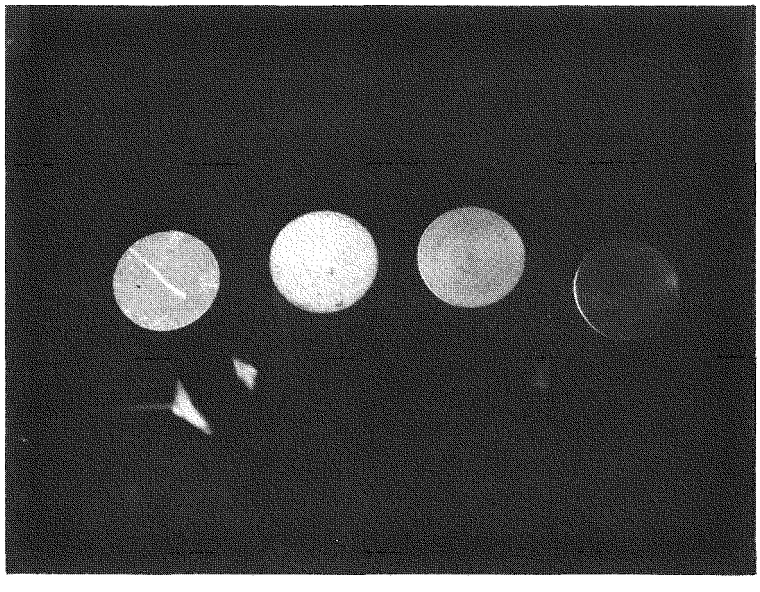

(b) Contact Surfaces

2 on left - Aluminum, 2 on right - Cupaloy

Figure A-4 Contacts Used in Test Sequence

The variations with the aluminum contacts appear to be random. However, the reason for these variations is not certain. $SF_6$ gas samples were withdrawn upon completion of each series of tests for mass spectrometric analyses. The result of these are given in Section A-8.

After the above tests, contacting surfaces did not appear to hve changed from the original condition. These are shown in Figure A-4b. No adverse effect is noticeable.

TABLE A-6

CONTACT RESISTANCE OF CUPALOY ELECTRODES COATED WITH SILVER

Dry Arced $SF_6$
Effect of Prolonged Exposure to Dry Arced $SF_6$

| Elapsed Hours | SF6 Pressure psig | Temp. °C | Contact Res. uohm |
|---|---|---|---|
| 0 | 300 | 25 | 3 |
| 21.5 | 515 | 152 | 3 |
| 24.0 | 510 | 152 | 3 |
| 28.75 | 503 | 152 | 3 |
| 45.50 | 462 | 152 | 3 |
| 48.25 | 455 | 152 | 3 |
| 52.75 | 450 | 152 | 3 |
| 76.75 | 515 | 152 | 3 |
| 94.25 | 510 | 152 | 4 |
| 96.00 | 508 | 152 | 3 |
| 100.75 | 505 | 152 | 3 |

1138A

TABLE A-7

CONTACT RESISTANCE OF CUPALOY ELECTRODES COATED WITH SILVER

Effect of Prolonged Exposure to Arced $SF_6$
with 1.6 gm Water in $SF_6$

| Elapsed Hours | SF6 Pressure psig | Temp. °C | Contact Res. uohm |
|---|---|---|---|
| 0 | 300 | 27 | 3 |
| 17.17 | 510 | 152 | 3 |
| 21.50 | 510 | 152 | 3 |
| 26.42 | 510 | 152 | 3 |
| 42.67 | 505 | 152 | 3 |
| 47.42 | 505 | 152 | 3 |
| 50.25 | 505 | 152 | 3 |
| 67.25 | 497 | 152 | 3 |
| 71.25 | 495 | 152 | 3 |
| 74.25 | 495 | 142 | 3 |
| 41.25 | 487 | 152 | 3 |
| 95.50 | 485 | 152 | 3 |
| 98.25 | 485 | 152 | 3 |

TABLE A-8

CONTACT RESISTANCE OF ALUMINUM ALLOY ELECTRODE COATED WITH SILVER

Effect of Prolonged Exposure to Dry Arced $SF_6$

| Elapsed Hours | SF6 Pressure psig | Temp. °C | Resistance uohm |
|---|---|---|---|
| 0 | 295 | 25 | 29 |
| 2.50 | 510 | 152 | 612 |
| 19.08 | 498 | 152 | 57.7 |
| 21.42 | 496 | 152 | 28.3 |
| 26.33 | 495 | 152 | 31.0 |
| 43.25 | 480 | 152 | 23.7 |
| 45.58 | 478 | 152 | 29.3 |
| 50.50 | 478 | 152 | 31.1 |
| 67.25 | 468 | 152 | 31.0 |
| 69.33 | 468 | 152 | 38.7 |
| 74.33 | 466 | 152 | 148.3 |
| 90.92 | 459 | 152 | 167.3 |
| 93.58 | 457 | 152 | 123.3 |
| 99.33 | 455 | 152 | 85.0 |

1138A/

TABLE A-9

CONTACT RESISTANCE OF ALUMINUM ALLOY ELECTRODES
COATED WITH SILVER

Effect of Prolonged Exposure to Arced $SF_6$ with 1.6 cc Water

| Elapsed Hours | SF6 Pressure psig | Temp. °C | Resistance uohm |
|---|---|---|---|
| 0 | 295 | 25 | 24.7 |
| 3.87 | 510 | 152 | 55.7 |
| 20.53 | 498 | 152 | 73.3 |
| 22.87 | 497 | 152 | 64.0 |
| 27.87 | 495 | 152 | 69.0 |
| 44.70 | 473 | 152 | 172.7 |
| 46.87 | 482 | 152 | 280.3 |
| 51.87 | 482 | 152 | 234.0 |
| 68.62 | 470 | 152 | 253.3 |
| 70.95 | 469 | 152 | 71.7 |
| 75.95 | 467 | 152 | 57.0 |
| 92.62 | 458 | 152 | 33.0 |
| 94.87 | 456 | 152 | 42.0 |
| 99.87 | 455 | 152 | 45.7 |

1138A/

## A.6 METALLIC MATERIALS AND GLASS FIBER REINFORCED STRAIN RODS

The materials listed in Table A-1D which are stress bearing metallic and fiber reinforced plastic materials were subjected to $SF_6$ gas at 135°C and 500 psig, before and after arcing and after 1.6 cc of water was injected into the test chamber. Variations in the stress of test samples during the exposure, and variations in the hardness and yield and breaker strengths before and after the exposure were investigated. Variations in spring characteristics of three candidate spring materials were also investigated.

### Test Procedure

Figure A-5a is a photograph of a test jig with a pair of test specimens loaded. The loading cells are visible on the tops of the strain bars, on which temperature compensated variable resistance strain gauges are mounted Note that the strain bars are screwed into respective loading cell blocks.

Only two of these test jigs fitted into the test chamber at one time because the remaining space in the chamber was needed to bring out the strain gauge terminals. Fouth insulating material samples mounts were used with each test jig to connect the strain gauge leads. Only the strain from one load cell in one test jig was measured because each cell needed four leads.

Figure A-5b is a photograph of the instruments used for the strain measurement, a Vishay P-350 a Atrain Indicator and a Vishay SB-1 10-Channel Switching and Balance Control.

Proper loading was accomplished by tightening or loosenin the nuts on the top of the loading jig.

### Test Procedure for Metallic Speciments

Tests of hardness, yield and ultimate strength, and other related tests were performed on one unused specimen of each material.

Two test jigs were placed in the test chamber and the strain gauge leads were connected to the brass studs of sample mounts. Test chamber was filled with $SF_6$ gas at 300 psig at 20°C. The $SF_6$ gas was heated for two hours at 135°C.

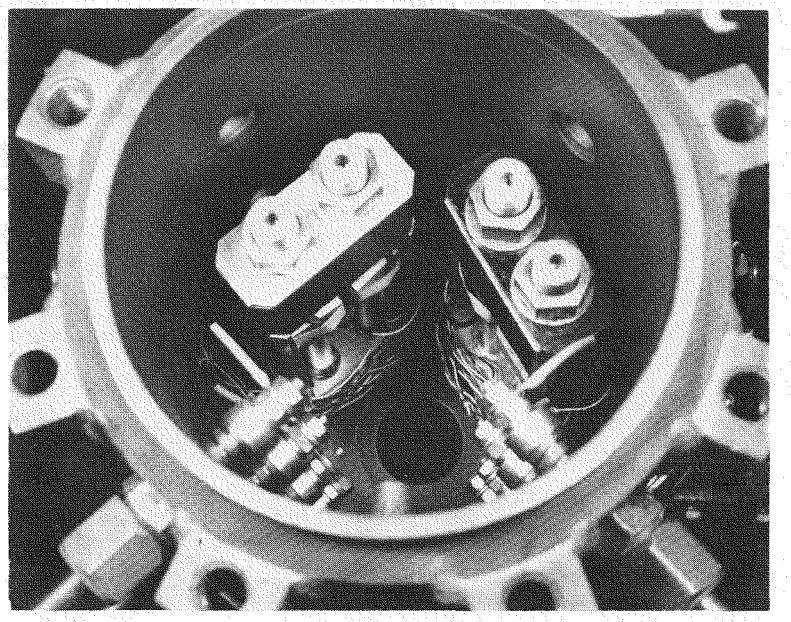

(a) Strain Bar Samples Mounted in Test Chamber

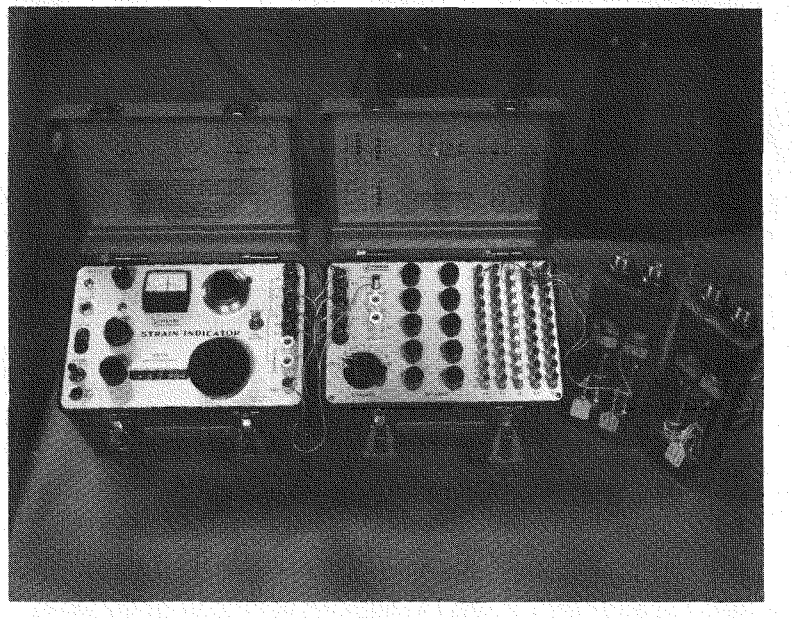


(b) Strain Measurement Setup

Figure A-5 Strain Measurement Test Setup

Arc energy of 84 KW-sec was applied, and then heaters were turned on. When the gas temperature reached 135°C (gas pressure approximately 500 psig the strains were measured. The temperature was cycled from room temperature to 135°C. The strains were measured and the sample hardness was measured after they were removed from the test chamber. The same test was repeated with a new set of specimens, but with 1.6 cc of water injected. The the test sequences were then repeated with another set of materials. The results of these tests are given in Tables A-10, A-11, A-12, A-13 and A-14. No significant variations were found.

TABLE A-10

STRAIN ROD TESTS CARBON STEEL AND CAST ALUMINUM RODS

Effect of Prolonged Exposure to Dry Arced $SF_6$

| Elapsed Hrs | SF6 psig | °C | CARBON STEEL LOAD CELLS 2 and 3 Average uE | Load lbs | Stress psi | CAST ALUMINUM ALLOY LOAD CELLS 6 & 7 Average uE | Load lbs | Stress psi |
|---|---|---|---|---|---|---|---|---|
| 0 | 300 | 28 | 3300 | 3911 | 2,368 | 2368 | 2870 | 14,330 |
| 66.17 | 300 | 23 | 3324 | 3940 | 19,671 | 2404 | 2914 | 14,548 |
| 69.18 | 475 | 136 | 3135 | 3716 | 18,553 | 1833 | 2222 | 11,093 |
| 71.92 | 283 | 25 | 3252 | 3854 | 19,242 | 2492 | 3021 | 15,081 |
| 88.42 | 240 | 22 | 3253 | 3855 | 19,247 | 2510 | 3042 | 15,190 |
| 91.80 | 482 | 135 | 3101 | 3675 | 18,348 | 1878 | 2276 | 11,365 |
| 93.67 | 295 | 26 | 3244 | 3845 | 19,197 | 2477 | 3002 | 14,990 |
| 96.08 | 475 | 137 | 3104 | 3679 | 18,368 | 1789 | 2169 | 10,826 |
| 112.75 | 266 | 23 | 3232 | 3831 | 19,127 | 2470 | 2994 | 14,948 |

1138A

TABLE A-11

STRAIN ROD TESTS

Carbon Steel and Cast Aluminum Rods
Effect of Prolonged Exposure to Arced $SF_6$ with 1.6 cc Water

| Elapsed Hrs | $SF_6$ | °C | CARBON STEEL LOAD CELLS 2 and 3 Average uE | Load lbs | Stress psi | CAST ALUMINUM ALLOY LOAD CELLS 6 & 7 Average uE | Load lbs | Stress psi |
|---|---|---|---|---|---|---|---|---|
| 0 | 292 | 24 | 3263 | 3867 | 19,306 | 2304 | 2793 | 13,943 |
| 3.12 | 489 | 136 | 3054 | 3620 | 18,073 | 1532 | 1857 | 9,271 |
| 93.69 | 240 | 20 | 3164 | 3750 | 18,722 | 2235 | 2709 | 13,525 |
| 97.5 | 496 | 136 | 3022 | 3582 | 17,884 | 1548 | 1876 | 9,368 |
| 99.0 | 305 | 28 | 3146 | 3729 | 18,617 | 2182 | 2645 | 13,205 |
| 100.97 | 488 | 136 | 3020 | 3579 | 17,869 | 1492 | 1809 | 9,029 |
| 117.5 | 262 | 22 | 3137 | 3718 | 18,563 | 2196 | 2662 | 13,289 |

1138A

TABLE A-12

STRAIN ROD TESTS IN ARCED $SF_6$ GAS WITH ALLOY STEEL AND STAINLESS STEEL RODS

Effect of Prolonged Exposure to Arced $SF_6$ with 1.6 cc Water

| Elapsed Hrs | SF6 psig | °C | CARBON STEEL LOAD CELLS 2 and 3 Average uE | Load lbs | Stress psi | CAST ALUMINUM ALLOY LOAD CELLS 6 & 7 Average uE | Load psi | Stress psi |
|---|---|---|---|---|---|---|---|---|
| 0 | 300 | 32 | 4330 | 5139 | 25,645 | 3266 | 3959 | 19,765 |
| 1.95 | 470 | 136 | 4029 | 4795 | 23,840 | 3294 | 3993 | 19,934 |
| 18.78 | 300 | 24 | 4144 | 4911 | 24,521 | 3202 | 3881 | 19,377 |
| 20.45 | 460 | 135 | 3997 | 4737 | 23,651 | 3264 | 3956 | 19,753 |
| 23.11 | 270 | 24 | 4130 | 4895 | 24,438 | 3194 | 3872 | 19,329 |
| 25.20 | 410 | 136 | 3985 | 4723 | 23,580 | 3278 | 3973 | 19,837 |
| 89.70 | 120 | 22 | 4116 | 4878 | 24,355 | 3188 | 3864 | 19,293 |

1138A/

TABLE A-13

STRAIN ROD TESTS - ALUMINUM ALLOY RODS

Effect of Prolonged Exposure to Arced $SF_6$ with 1.6 cc Water

| Elapsed Hrs | SF6 psig | °C | ALUMINUM ALLOY LOAD CELLS 2 & 3 uE | Load lbs | Average Stress psi |
|---|---|---|---|---|---|
| 0 | 300 | 30 | 3853 | 4567 | 22,799 |
| 2.98 | 460 | 136 | 2843 | 3370 | 16,823 |
| 20.73 | 465 | 136 | 2924 | 3466 | 17,302 |
| 22.57 | 285 | 29.4 | 3790 | 4492 | 22,426 |
| 24.57 | 415 | 136 | 2830 | 3354 | 16,746 |
| 40.23 | 200 | 23 | 3840 | 4551 | 22,722s |

1138A

TABLE A-14

EFFECT OF EXPOSURE TO HIGH TEMPERATURE $SF_6$ GAS
ON MECHANICAL PROPERTIES OF METALS

Exposure Conditions: 135°C - 300 psig $SF_6$
Arc Energy: 84 kW-sec with 1.6 cc $H_2O$

| | Yield Strength 0.2% Offset-lb/in$^2$ | | Ultimate Strength lb/in$^2$ | | % Elongation in 2.0 in. | | % Area Reduction | | Rockwell Hardness | |
|---|---|---|---|---|---|---|---|---|---|---|
| | Before | After | Before | After | Before | After | Before | After | Before | After |
| Carbon Steel(1) | 38540 | 38920 | 56510 | 58645 | 42 | 37 | 70.5 | 68.3 | $63R_B$ | $64R_B$ |
| Carbon Steel | NA | 40770 | NA | 57025 | NA | 40 | NA | 68.9 | NA | $59R_B$ |
| #11 Tool Steel | 103100 | 102850 | 129400 | 128810 | 21 | 23 | 63.3 | 67.5 | $24R_C$ | $26R_C$ |
| Stainless Steel | 79200 | 79880 | 99450 | 98975 | 21 | 22 | 58.8 | 58.9 | $45R_B$ | $95R_B$ |
| Cast Al Alloy | 28570 | 31390 | 36390 | 37040 | 3.6 | 2.5 | 3.2 | 2.6 | $89R_e$ | $92R_e$ |
| Sample No. 2 | | 30330 | | 36715 | | 2.9 | | 3.0 | | $90R_e$ |
| Aluminum Alloy | 45610 | 46240 | 49070 | 49995 | 16 | 16 | 46 | 44 | $102R_e$ | $102R_2$ |

NOTE: (1) One carbon steel sample was exposed to dry arced $SF_6$.

Test Procedure for Glass Reinforced Strain Rods

Strain rods of the glass reinforced plastic materials listed in Table A-1D were machined to the same dimensions as those of the metallic rods. However, because of much weaker shear strength of the loading threads, loading of the specimens had to be drastically reduced. Tests were carried out as stated for metallic samples. Furthermore, instead of testing yield and tensile strength, compressive shear strengths were measured. These results are given in Table A-15. No significant change occurred.

Test Procedure for Springs

Three candidate spring materials were selected and springs were made to dimensions of circuit breaker components that also would fit into the test chamber. The spring characteristics, such as free length and load displacement characteristics, etc., were measured prior to exposure to 135°C and 500 psig arced $SF_6$ environment, with water present as described earlier. The quantities measured after the test are given in Table 16. No significant change occurred.

TABLE A-15

EFFECT OF EXPOSURE TO HIGH TEMPERATURE $SF_6$ GAS ON COMPRESSION SHEAR STRENGTH OF VARIOUS PLASTIC MATERIALS

Exposure Conditions: 135°C (275°F) - 300 psig $SF_6$ Gas
Arc Energy: 84 kW-sec - $H_2O$ Present

| Sample Identification | Compression Shear Strength - $lb/in^2$ | |
|---|---|---|
| | Before | After |
| Glass Polyester | 5620 | 5830 |
| Glass Epoxy | 8810 | 10085 |
| Epoxy Resin | 9055 | 10225 |

TABLE A-16

EFFECT OF EXPOSURE TO HIGH TEMPERATURE $SF_6$ GAS ON COMPRESSION SHEAR STRENGTH OF VARIOUS STEEL SPRINGS

Exposure Conditions: 135°C (275°F) - 300 psig $SF_6$ Gas
Arc Energy: * 84 kW-sec - $H_2O$ Present

| MATERIAL | MUSIC WIRE | OIL TEMPER WIRE | CHROME VANADIUM WIRE |
|---|---|---|---|
| Wire Diameter (in) | .1875 | .1875 | .1875 |
| Spring O.D. (in) | 1.188 | 1.188 | 1.188 |
| Total Turns | 12 | 12 | 12 |
| Active Turns | 10 | 10 | 10 |
| Free Length Before Exposure (in) | 3.94 | 3.94 | 3.94 |
| Free Length After Exposure (in) | 3.75 | 3.87 | 3.87 |
| Final Length (in) (Expected Loading) | 2.58 | 2.7 | 2.44 |
| Final Load Before Exposure (lbs) | 231 | 213 | 261 |
| Final Load After Exposure (lbs.) | 213 | 195 | 255 |
| Fiber Stress (psi) During Exposure | 120,000 | 110,000 | 133,000 |

1138A

## A.7 LONG TIME EXPOSURE TEST

### Scope

Five selected insulating materials plus the Kel-F control material and four metallic materials were exposed to an arced $SF_6$ environment of 135°C and 500 psig for 300 hours. The materials are listed in Table A-17.

For the insulating materials, the effect of long time exposure on leakage resistance and dielectric strength was investigated. For the metallic materials variations of surface conditions were investigated.

$SF_6$ gas samples and dusts collected after the exposure were analyzed.

### Test Procedure

Each sample was weighed to the nearest milligram. The chamber was filled with $SF_6$ to 300 psig at room temperature. An arc energy of 84 KW-sec was applied. $SF_6$ gas was heated to 135°C, at which $SF_6$ pressure was approximately 500 psig. Leakage currents were measured twice a day, once at 8 or 9 a.m. and once at 4 p.m. Immediately after leakage current measurements were made, dielectric strength was tested on one of the pair of each insulating material specimens, to a maximum voltage of 15 kV rms. At the end of the 300 hours exposure, dielectric strength tests were performed on each insulating material specimen with maximum test voltage set at 15 kV rms.

Two $SF_6$ gas samples were withdrawn, one midway, and one at the end of the exposure. At the end of the test series, dusts were collected for chemical analysis. Test specimens were weighed to the nearest milligrams. Hardness and surface conditions of the metallic specimens were investigated.

### Test Results

No measurable leakage current was detected for the insulating samples. Table A-18 shows weights measured before and after the exposures. There were no noticeable changes in the weights for the metal specimens before and after test. Where were some small changes for the insulating material specimens.

TABLE A-17

MATERIALS SELECTED FOR A 300 HOUR EXPOSURE
TEST IN ARCED $SF_6$ AT 136°C AND 500 psig

| Test Material I.D. | Material | Use |
|---|---|---|
| A3 | Virgin Teflon** | Nozzle |
| A7 | *Glass Epoxy Resin (Pultruded) | Pull Rods, Studs |
| A12 | *Glass Polyester | Insulating Support |
| A10 | *Glass Epoxy | Feed Tubes |
| A5 | Cast Epoxy Resin | Insulators |
| A15 | Kel-F*** (Control Sample) | Bushings |
| B4 | Aluminum Alloy | Enclosure, Str. Members, Cond. |
| B7 | Cupaloy | Contacts, Support, Structures |
| B6 | Copper | Contacts, Conductors |
| B3 | Stainless Steel | Enclosure, Supports, Levers, Shafts, etc. |

* Coated with arced $SF_6$ & track resistant epoxy

** Tetrafluoroethylene

*** Chlorotrifluoroethylene

TABLE A-18

WEIGHT OF TEST SPECIMEN BEFORE AND AFTER RESULTS OF TEST WITH 300 HOUR EXPOSURE TO ARCED $SF_6$ AT 135°C AND 500 psig

All samples showed no measurable leakage current during the 300 hour test. All samples withstood 15 kV rms tests during and after the 300 hour test.

| Test Material I.D. | Sample Number | Material Designation | Weight (Gram) Before | After |
|---|---|---|---|---|
| A3 | 1 | Virgin Teflon | 24.500 | 24.730 |
| | 2 | " " | 24.525 | 25.805 |
| A7 | 3 | *Glass Epoxy Resin | 24.935 | 24.895 |
| | 4 | " " " | 25.485 | 25.405 |
| A12 | 5 | *Glass Polyester | 26.680 | 26.615 |
| | 6 | " " | 26.980 | 26.910 |
| A10 | 7 | *Glass Epoxy | 24.385 | 24.325 |
| | 8 | " " | 24.280 | 24.215 |
| A5 | 9 | Cast Epoxy Resin | 19.371 | 19.320 |
| | 10 | " " " | 19.930 | 19.870 |
| A15 | 11 | Kel-F (Control Sample) | 23.900 | 23.965 |
| | 12 | " " " | 23.966 | 24.025 |
| B7 | 13 | Cupaloy | 26.980 | 26.980 |
| B6 | 14 | Copper | 27.040 | 27.045 |
| B3 | 15 | Stainless Steel | 22.010 | 22.010 |
| B4 | 16 | Aluminum Alloy | 8.075 | 8.075 |

* Coated with an arced $SF_6$ and track resistant Epoxy

1141A

## A.8 CHEMICAL ANALYSES

### Sulfur Hexafluoride Gas

$SF_6$ gas samples were withdrawn from the test chamber during and after various tests for mass spectrometric analyses. The purpose of these analyses was to investigate the effects of high temperatures, 135°C and 150°C, arcing, presence of water and presence of insulating and metallic materials on the decomposition of the $SF_6$ gas.

The results of the spectrometric analyses are given in Table A-19 for the principle impurities and continued in Table A-20 for the trace impurities. As can be seen from the first three Samples 1 to 3 the $SF_6$ gas is unaffected when exposed to a 135°C or a 150°C temperature environment over a two hour period.

The remaining analyses show that some interaction occurred between the $SF_6$ gas and the various materials exposed to it under high temperature and arcing conditions. In all cases except Sample 25 the purity of the $SF_6$ gas after arcing remained above 99.2 mole %.

The low level of impurities of the trace gases combined with the complex spectrum of $SF_6$ made a precise determination of the trace components shown in Table A-20 impossible. However, by examining the variations in the measurements at the seven selected mass numbers it was possible to estimate the composition and quantity of the trace gases. Table A-20 shows the best estimate of the quantity of these components based on the assumption the trace gases are Methanthiol, Sulfur Dioxide, Tetrafluoromethane, Dichlorofluoromethane, and Silicontetrafluoride. Due to the complex mass spectra and low concentration of these gases it was not possible to differentiate between Methanethiol and Sulfur Dioxide or between Tetrafluoromethane and Dichlorofluoromethane. Silicontetrafluoride was clearly identifiable.

### Deposit Analyses by Emission Spectroscopy

Upon completions of tests to investigate the effects of a 300 hour exposure dusts that had settled on test specimens were collected randomly in glass jars, which were sent to Westinghouse R&D Center for chemical analyses.

These were analyzed by emission spectroscopy for their metallic constituents and fluroide. The results of these analyses are summarized in Table A-21. It will be noted from the data that the two primary components of the material were copper and iron considered to have been derived primarily from the electrodes and the arc confining tube, respectively.

TABLE A-19

MASS SPECTROMETRIC ANALYSIS OF $SF_6$ GAS DRAWN FROM TEST CHAMBER DURING AND AFTER VARIOUS EXPOSURE TESTS

| | Sample | Mole % | | | |
|---|---|---|---|---|---|
| | | $CO/N_2$ | $O_2$* | $CO_2$ | $SF_6$ |
| 1 | Direct from gas cylinder | 0.10 | 0.03 | -- | 99.90 |
| 2 | $SF_6$ held @ 135°C - 2 h | 0.37 | 0.09 | -- | 99.54 |
| 3 | $SF_6$ held @ 150°C - 2 h | 0.11 | 0.03 | -- | 99.84 |
| 4 | PTFE Samples - Before Arc | 0.24 | 0.06 | -- | 99.70 |
| 5 | PTFE Samples - After Arc | 0.14 | 0.03 | -- | 99.60 |
| 6 | Epoxy Glass Samples - Before Arc | 0.32 | 0.08 | 0.06 | 99.62 |
| 7 | Epoxy Glass Samples - After Arc | 0.22 | 0.06 | 0.07 | 99.71 |
| 8 | Epoxy Glass Samples - After Arc+$H_2O$ | 0.30 | 0.08 | 0.13 | 99.57 |
| 9 | Metal Specimens - Before Arc | 0.31 | 0.08 | 0.06 | 99.62 |
| 10 | Metal Specimens - After Arc | 0.22 | 0.06 | 0.23 | 99.55 |
| 11 | Metal Specimens - After Arc +$H_2O$ | 0.16 | 0.03 | 0.08 | 99.76 |
| 12 | Ag Coated Cupaloy - Arced | 0.07 | 0.02 | 0.05 | 99.88 |
| 13 | Ag Coated Cupaloy - Arced +$H_2O$ | 0.06 | 0.01 | 0.02 | 99.92 |
| 14 | Ag Coated Aluminum - Arced | 0.06 | 0.01 | 0.03 | 99.90 |
| 15 | Ag Coated Aluminum - Arced +$H_2O$ | 0.05 | 0.01 | 0.01 | 99.93 |
| 16 | Carbon Steel/Cast Al - Before Arc | 0.14 | 0.04 | 0.07 | 99.75 |
| 17 | Carbon Steel/Cast Al - After Arc | 0.23 | 0.06 | 0.24 | 99.47 |
| 18 | Carbon Steel/Cast Al-Before Arc +$H_2O$ | 0.15 | 0.04 | 0.07 | 99.74 |
| 19 | Carbon Steel/Cast Al-After Arc +$H_2O$ | 0.18 | 0.04 | 0.57 | 99.21 |
| 20 | #11 Tool Steel/SS - After Arc +$H_2O$ | 0.17 | 0.03 | 0.28 | 99.52 |
| 21 | Al Alloy/Springs - After Arc +$H_2O$ | 0.08 | 0.02 | 0.26 | 99.64 |
| 22 | Glass Epoxy/Glass Polyester - After Arc +$H_2O$ | 0.08 | 0.02 | 0.65 | 99.25 |
| 23 | Glass Epoxy/#53320TF Cement - After Arc +$H_2O$ | 0.12 | 0.03 | 0.36 | 99.49 |
| 24 | Various Metals & Insulations (see Table VIB) After 150 h | 0.10 | 0.02 | 0.04 | 99.84 |
| 25 | Various Metals & Insulations (see Table VIB) After 300 h | 0.40 | 0.10 | 2.16 | 97.30 |

* Oxygen mole % based on nitrogen concentration.

TABLE A-20

ESTIMATED CONTENT OF TRACE GASES IN PARTS PER MILLION BY VOLUME

A = Methanethiol ($CH_3SH$) or Sulfur Dioxide ($SO_2$)

B = Tetrofluoromethane ($CF_4$) or Dichlorofluoromethane ($CHCl_2F$)

C = Silicontetroafluoride ($SiF_4$)

| | Sample | A | B | C |
|---|---|---|---|---|
| 1 | Direct from gas cylinder | 0 | 0 | 0 |
| 2 | $SF_6$ held @ 135°C - 2 h | 0 | 0 | 0 |
| 3 | $SF_6$ held @ 150°C - 2 h | 0 | 0 | 0 |
| 4 | PTFE Samples - Before Arc | 25 | 1800 | 150 |
| 5 | PTFE Samples - After Arc | 250 | 600 | 1600 |
| 6 | Epoxy Glass Samples - Before Arc | 100 | 2800 | 400 |
| 7 | Epoxy Glass Samples - Arced | 250 | 2500 | 1100 |
| 8 | Epoxy Glass Samples - Arc +$H_2O$ | 75 | 4600 | 450 |
| 9 | Metal Specimens - Before Arc | 500 | 2500 | 750 |
| 10 | Metal Specimens - Arced | 750 | 4100 | 850 |
| 11 | Metal Specimens - Arced +$H_2O$ | 650 | 2900 | 450 |
| 12 | Ag Coated Cupaloy - Arced w/o$H_2O$ | 450 | 1400 | 150 |
| 13 | Ag Coated Cupaloy - Arced w/$H_2O$ | 300 | 1000 | 100 |
| 14 | Ag Coated Aluminum - Arced w/o$H_2O$ | 75 | 1100 | 650 |
| 15 | Ag Coated Aluminum - Arced w/$H_2O$ | 250 | 1000 | 600 |
| 16 | Carbon Steel/Cast Al - Before Arc | 500 | 1500 | 900 |
| 17 | Carbon Steel/Cast Al - Arced | 850 | 3400 | 1500 |
| 18 | Carbon Steel/Cast Al-Before Arc w/$H_2O$ | 650 | 1900 | 1700 |
| 19 | Carbon Steel/Cast Al- Arced w/$H_2O$ | 600 | 3000 | 1400 |
| 20 | #11 Tool Steel/SS - Arced w/$H_2O$ | 400 | 1500 | 200 |
| 21 | Al Alloy/Springs - Arced w/$H_2O$ | 600 | 1300 | 400 |
| 22 | Glass Epoxy/Polyester - Arc w/$H_2O$ | 400 | 1100 | 180 |
| 23 | Glass Epoxy Arced w/$H_2O$ | 600 | 1500 | 100 |
| 24 | Various Metals & Insulations After 150 h w/o $H_2O$ | 150 | 300 | 75 |
| 25 | Various Metals & Insulations After 300 h w/o $H_2O$ | 400 | 2400 | 200 |

TABLE A-21

METALLIC CONSTITUENTS CONTAINED IN DEPOSITS REMOVED FROM TEST SPECIMENS AFTER EXPOSURES TO ARCED $SF_6$ at ELEVATED TEMPERATURE (Weight Percent)

| Element / Sample | Al | Ag | B | Bi | Ca | Cd | Co | Cr | Cu | Fe | K | Li | Mg | Ma |
|---|---|---|---|---|---|---|---|---|---|---|---|---|---|---|
| A | 0.1 | 0.4 | 0.1 | 0.1 | 0.4 | 0.3 | 0.2 | 0.2 | 20 | 7 | 0.1 | 0.1 | 0.1 | 0.1 |
| B | 0.1 | 0.4 | 0.1 | 0.1 | 0.2 | 0.3 | 0.2 | 0.2 | 20 | 7 | 0.1 | 0.1 | 0.1 | 0.1 |
| C | 0.1 | 0.1 | 0.01 | 0.03 | 0.05 | -- | 0.1 | 0.03 | 10 | 8 | ND | ND | 0.01 | 0.05 |
| D | 2.5 | 0.1 | 0.01 | 0.01 | 0.3 | 0.1 | 0.01 | 0.01 | 10 | 10 | 0.03 | 0.001 | 0.06 | 0.2 |

| Element / Sample | Mo | Na | Nb | Ni | Pb | Sb | Si | Sn | Ta | Ti | V | Zn | Zr | Ba |
|---|---|---|---|---|---|---|---|---|---|---|---|---|---|---|
| A | 0.1 | 0.1 | 0.3 | 0.1 | 0.2 | 0.3 | 0.1 | 0.3 | 0.1 | 0.1 | 0.1 | 0.2 | 0.2 | 0.1 |
| B | 0.1 | 0.1 | 0.3 | 0.1 | 0.2 | 0.3 | 0.1 | 0.3 | 0.1 | 0.1 | 0.1 | 0.2 | 0.2 | 0.1 |
| C | 0.05 | 0.1 | 0.1 | 0.02 | 0.05 | 0.05 | 0.1 | 0.05 | ND | 0.01 | 0.01 | 0.1 | 0.05 | ND |
| D | 0.01 | 0.4 | 0.1 | 0.1 | 0.1 | 0.1 | 1.0 | 0.1 | 0.001 | 0.08 | 0.01 | 0.1 | 0.02 | 0.01 |

Sample A = Residue taken from Teflon specimens -- 2 h exposure

B = Residue taken from Teflon specimens -- 2 h exposure

C = Residue taken from Teflon specimens -- 2 h exposure

D = Residue taken from metal specimens -- 300 h exposure

Remarks: Values reported in wt %. Accuracy of spectrochemical analysis is 1/3X to 3X estimates.

ND% Not Detected.

NOTE: Fluoride content of deposits varied from 13% to 18% (wt).

# APPENDIX B

## DATA ACQUISITION SYSTEM

### B-1. INTRODUCTION

This single pressure breaker development program had a need for a data acquisition system for pressure, contact travel, and drive system travel parameter monitoring. The primary objective of this system was to provide an accurate and reliable means of bringing the relatively low level pressure and travel transducer output information to a recording system loacted in the control room during high power breaker testing.

An instrumentation package, featuring precision, highly noise-immune electronic information processing circuitry and electro-optical data transmission, has been developed. A photograph showing an encoder unit (left), a photo-receiver unit (right), an optical cable (coiled), and the six channel decoder unit is presented in Figure B-1.

### B-2 SYSTEM DESCRIPTION

A block diagram of a single channel system is shown in Figure B-2. The information processing is performed by voltage-to-frequency (encoder unit) and frequency-to-voltage (decoder unit)techniques. This method was selected because it permits a relatively simple circuit implementation to achieve the required accuracy. More importantly, an FM type of system can minimize the effects of electrical noise and transients on the transmitted signal. Because of cost concerns the optical data link, which originally was to be implemented the full distance (about 500 ft) from the breaker test area to the control room, was only used to bring the FM signal out of the breaker housing where the noise is most intense. The photo-receiver, located in an intermediate area where the ambient noise is much lower, converts the modulated light back to an electrical FM signal. This signal is then transmitted by a conventional coaxial cable to the control room where the decoder unit performs the demodulation and provides the proper interface with the recording and monitoring equipment.

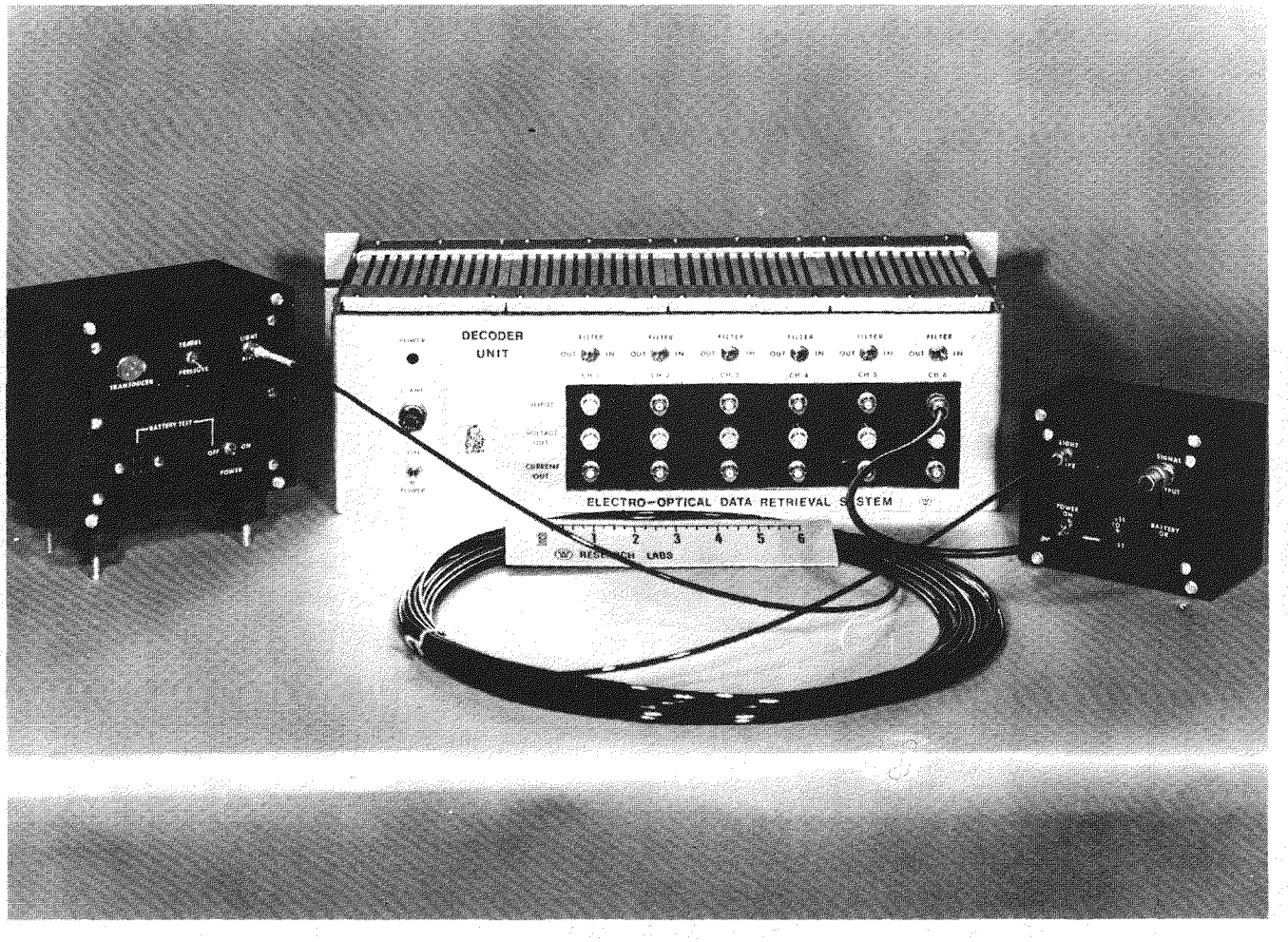


Figure B-1 Electro-Optical Data Acquisition System

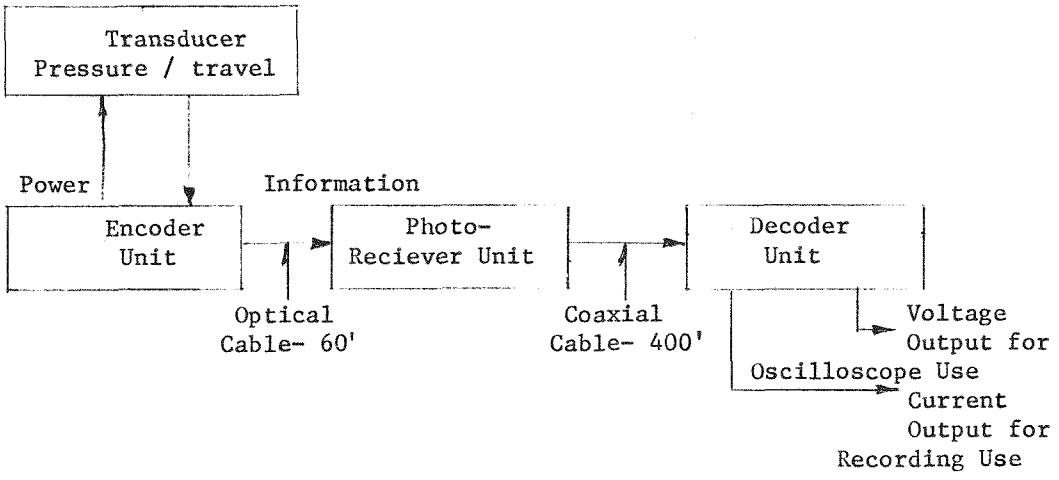


Figure B-2 System Block Diagram

Encoder Unit

A functional block diagram of the encoder circuit is shown in Figure B-3. This circuit is designed to accept the output from either the pressure or travel transducer. The pressure transducer has a full scale output of about 120 mV while the travel transducer has a full scale output of about 4.8 volts. The level difference between these two outputs is compensated by the front-end amplifier through a manually operated switch. The switch is a 3-pole, two-position type. The other two poles are used to control the frequency response and the dc voltage shifting embodies in the second amplifier circuit for pressure and travel operations. A completely balanced arrangement is implemented in the input circuitry of the front-end amplifier to yield maximum common-mode noise rejection. At the second amplifier output, the signal will yield an amplitude change of 6 volts corresponding to the full scale output of either transducer. With zero input signal the second amplifier output is 3 volts. The voltage-to-frequency (v/f) converter has a transfer gain of 10 kHz/volt. Thus, with zero volts transducer output the (v/f) converter output is 30 kHz and will reach 90 kHz when a full scale input is applied. The pulse width at the v/f converter output is about 5 us. The frequency output is then converted into pulsed infrared light throught the light-emitting-diode (LED) drive circuitry and the LED. The light output is coupled into the fiber cable via a BNC-like connector. The practical circuit of the encoder including a regulated power supply circuit is shown in

Figure B-4. The power supply circuit also supplies a well-regulated voltage to power the transducers. The power source for the encoder unit is dry mercury cells.

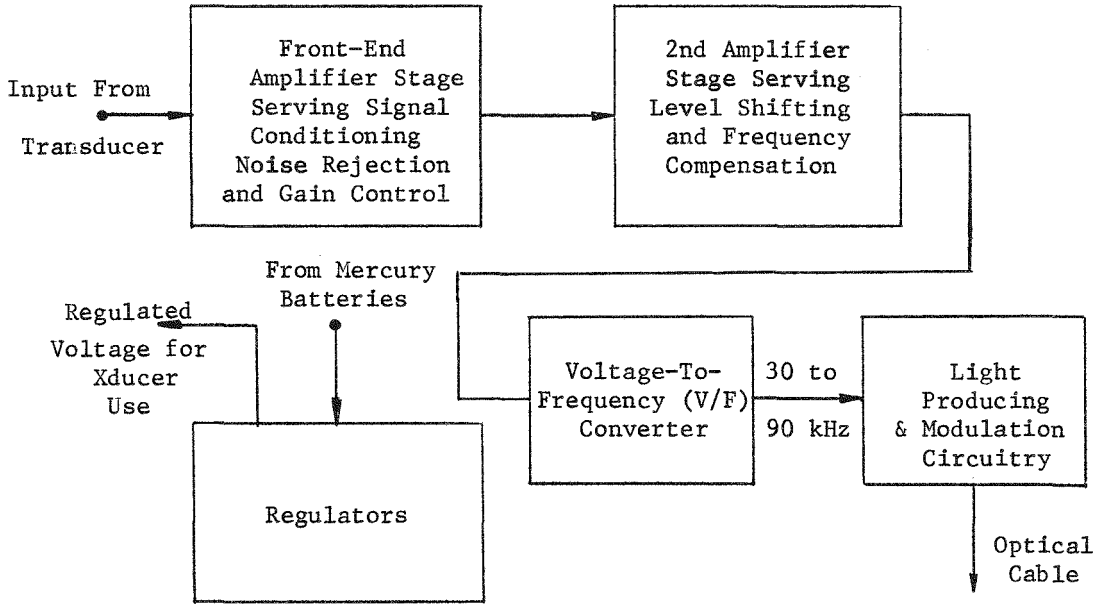


Figure B-3 Functional BLock Diagram of Encoder Unit

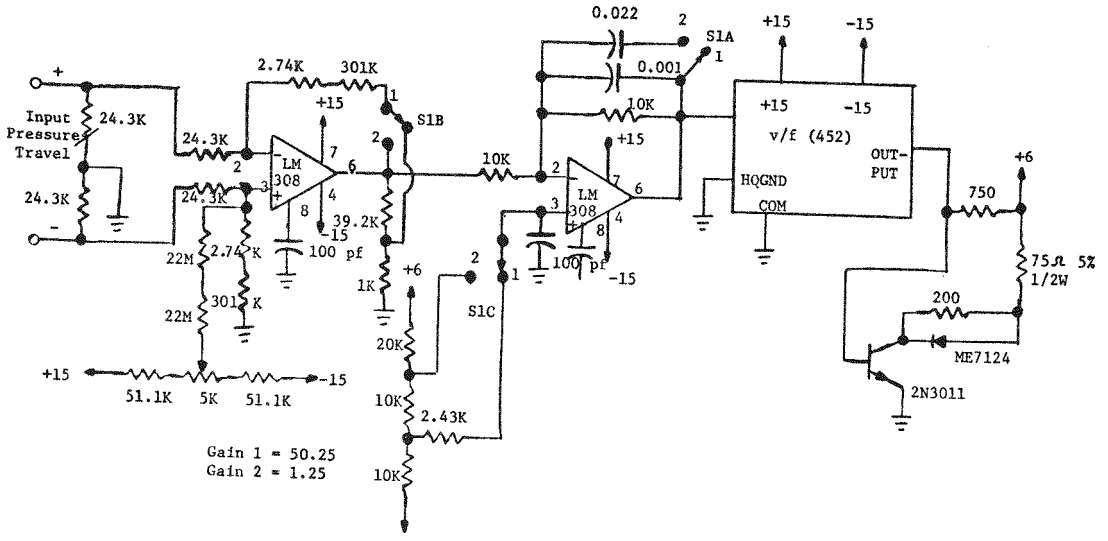


Figure B-4a Pressure/Travel Encoder Circuit

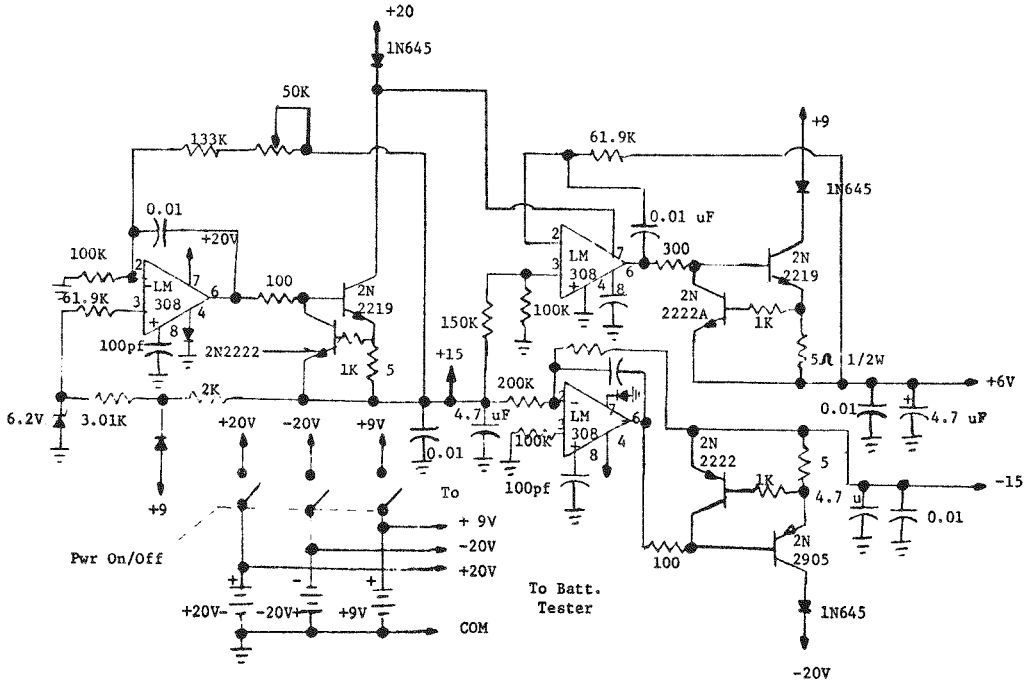


Figure B-4b Encoder Power Supply

## Photo-Receiver Unit

The practical design of the photo-receiver unit is shown in Figure B-5. The circuit employs a photo PIN diode (MD2) for light detection. The photo current generated is injected into the feedback path of an operational amplifier circuit. This circuit is designed to provide and extremely high ac gain while maintaining a unity dc gain for maximum stability. The second stage amplifier is similarly designed. The dc bias of this stage is accomplished by taking the average dc voltage of the first stage amplifier to ensure good dc stability for the entire circuit. The circuit is designed to drive a 50 ohm impedance cable. The slew rate of both amplifieres is about 35V/us. Like the encoder, this ciruit is also battery powered.

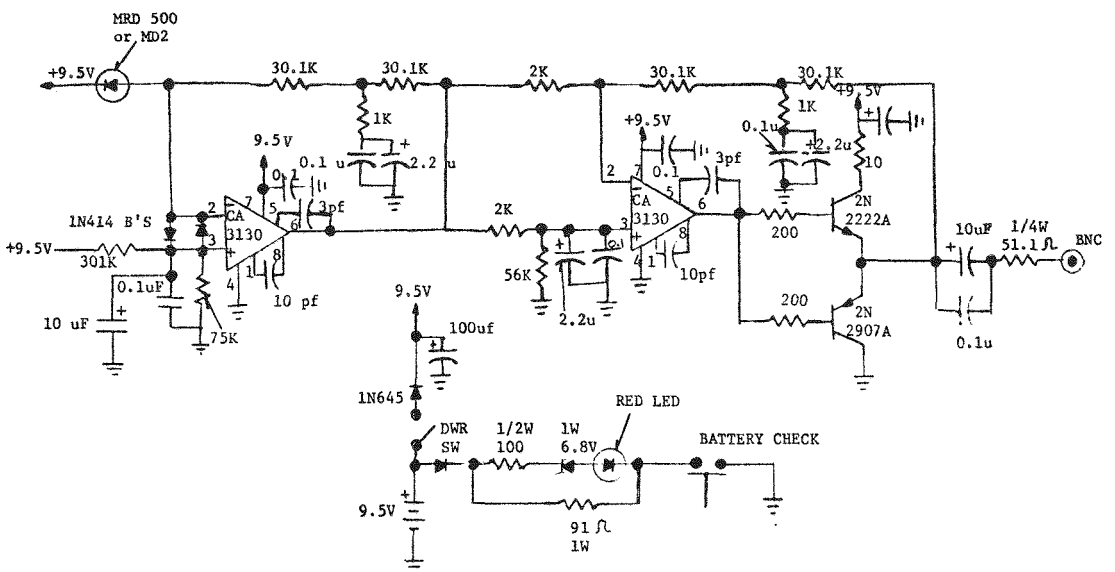


Figure B-5 Photo-Receiver Schematic

## Decoder Unit

The decoder circuit shown in Figure B-6 begins with a balanced differential amplifier followed by a comparator circuit. The first amplifier mainly provides a proper interface with optimized common-mode noise rejection features. The comparator circuit serves as a limiter stage to reject amplitude-modulated noise.

The one-shot multivibrator circuit (NE555) defines a proper pulse width of the treated FM signal required by the frequency-to-voltage (f/v) converter circuit.

The output of the f/v circuit is level-shifted and amplified to yield a zero to ten volts amplitude scale corresponding to the full range of inputs of either transducer (pressure or travel) operation. A filter circuit is also embodied in this amplifier stage to provide the required transient response performance for the entire.

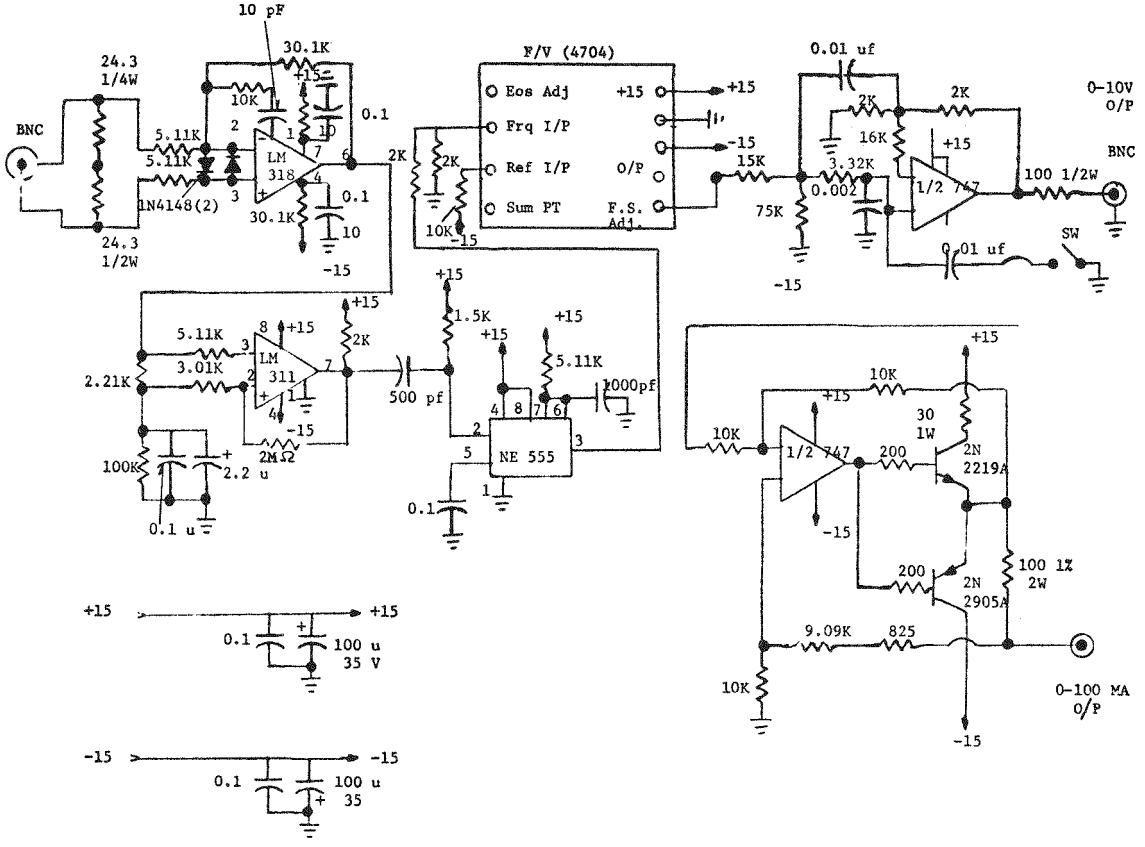


Figure B-6 Decoder Schematic

encoder-decoder system. The voltage output of this stage, which can be used directly for monitoring, is further converted into a current output for driving the recording equipment. The current output has a rate of 10 mA/volt with a maximum magnitude of 100 mA. The burden onthis current should be limited to not more than 100 ohms.

A power supply circuit (Figure B-7) is also included as part of the decoder unit. It supplies two well-regulated voltages, +15V and -15V, each with about one ampere

capability, enough to power eight encoder cards. The design is completed with a current fold back overload protection feature. The power supply utilizes 120V ac (50-60 Hz) as its power source.

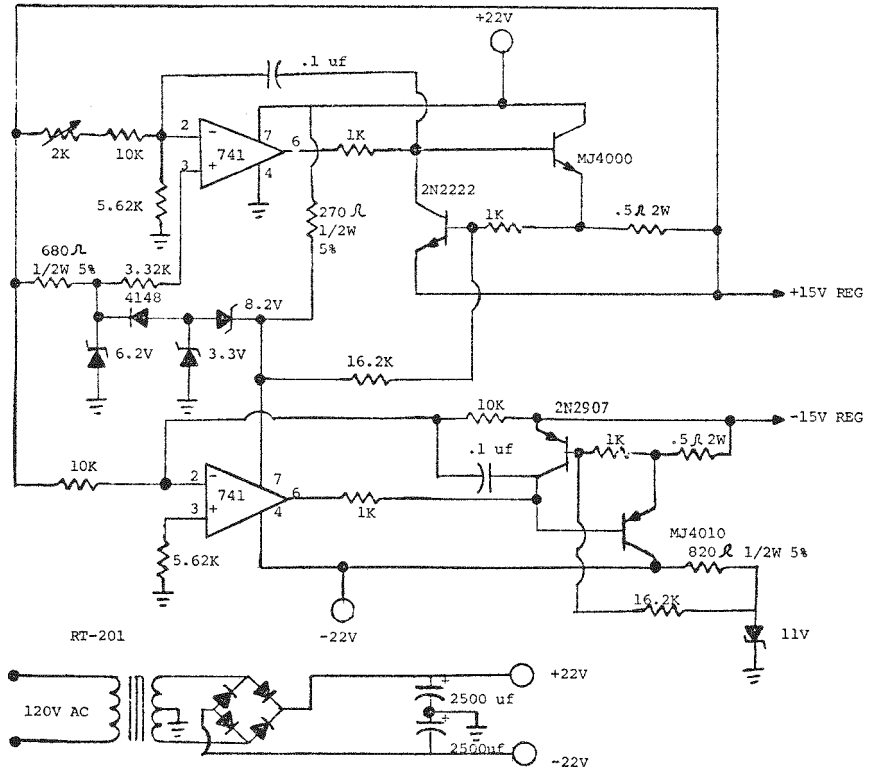


Figure B-7 Decoder Power Supply Schematic

## System Performance

The performance of all six channels was checked indivually with simulated inputs as well as with the actual transducers. Reading accuracies of better than 2% were obtained in all channels. The frequency response of the system is about 0 to 4.5 kHz for pressure operation and 0 to 2.5 kHz for travel operation. The system step response performance is illustrated in Figure B-8 and a triangular signal performance (linearity illustration) is given in Figure B-9.

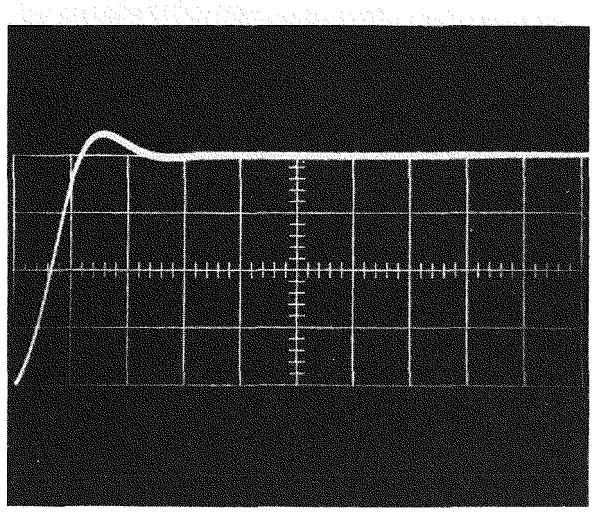

a. Pressure Operation

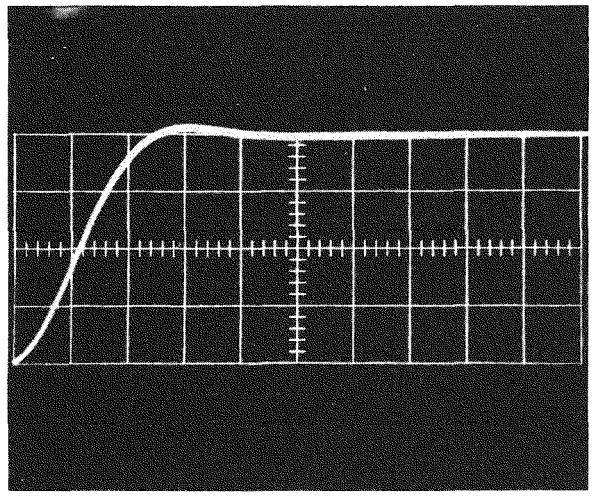

b. Travel Operation

Figure B-8 System Step Responses taken at Voltage Output of Decoder Circuit

Vertical -- 2V/div
Horizontal -- 0.1 ms/div.

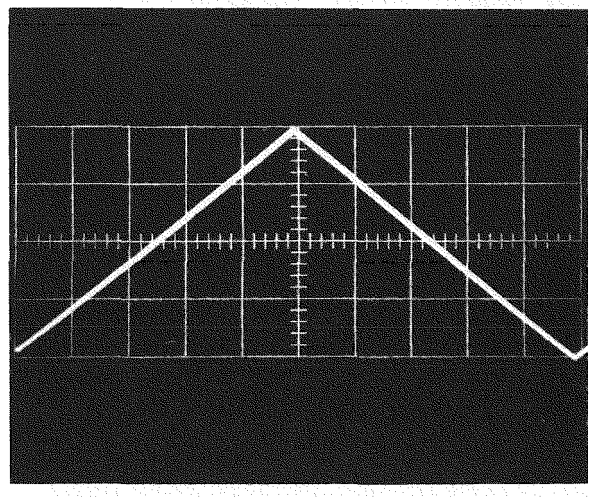

a. Pressure Operation

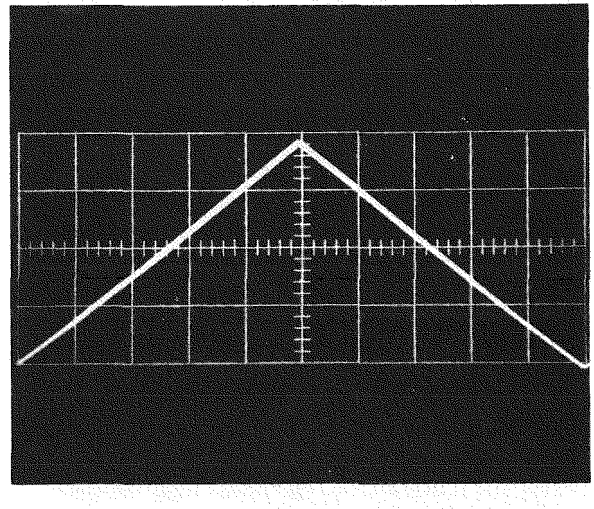

b. Travel Operation

Figure B-9 System Triangular Signal Respones (Linearity Illustration) taken at Voltage Output of Decoder

Vertical -- 2V/div
Horizontal -- 2 ms/div

## APPENDIX C

## PROTOTYPE INTERRUPTER REQUIREMENTS

Of the twelve 80% short-line fault (SLF) tests made on the model puffer interrupter, seven with data listed on Table C-1 were close to the critical line between successes and failures, and were analyzed by the dynamic arc model methods. A useful correlation with the pressure, $P_1$, at current-zero, is shown in the upper part of Figure C-1. There performance $E_o/0$ is found to vary as $p_1^2$.

Assuming dependence as $I^{3/2}$ (I equals fault current), as found for other interrupters, points are plotted on Figure C-1 on the quadratic curve for the half-cycle range performance values, of the other interrupters scaled to 80 kA. The curve predicts current-zero pressures of 210 and 303 psia for these interrupters; no data is available on actual pressure measurements at current-zero, but these values seem plausible, the first representing about 45 psi flow pressure drop in a two pressure interrupter from the 255 psia reservoir, and 303 psia being reasonable effort a configuration similar to the model puffer interrupter but at lower current and fill pressure. It is, therefore, estimated that the model puffer interrupter has a performance given by

$$E_o/0 = 3.2 \times 10^{-5} p_1^2 \, (80/I)^{3/2} \qquad \text{(C-1)}$$

a dependence shared by lower performance two pressure and puffer interrupters. Although less than a full half-cycle range was explored in the SLF tests, Table C-1, expressing $E_o/0$ in terms of current-zero pressure $P_1$ shows that for differing arcing times, this incompleteness in the data is less important.

The $E_o/0$ values for the four tests in Table C-1 without shunt capacitance are plotted in Figure C-1, the pair marked by an asterisk (in the Table) defining a point on the critical curve dividing successful interruptions from failures near 14.5 kV/us. Similarly, the tests with $2.6 \times 10^{-9}$F added shunt capacitance contain a critical pair and give $E_o/0$ proportional to $p_1^2$; powers between 1.5 and 2.5 also fit, though less well. The upper curve of Figure C-1 shows that performance varies as $P_1^2$.

Similarly, in the lower part of Figure C-1 the $E_o$ data from Table C-1 and for the other two interrupters is plotted. The equation found to best fit the data is

$$E_o = 8 \times 10^{-3} \; p_1 \; (80/I)^{1/2} \qquad (C\text{-}2)$$

TABLE C-1

DYNAMIC ARC ANALYSIS DETERMINATION OF LIMITING $E_o/e$ VALUES FOR 7 NEAR-CRITICAL SLF TESTS ON THE SUPER-PRESSURE PUFFER

| Test Letter | $P_1$, pressure at i = 0, psia | $SF_6$ fill pressure, psig | Fail/ Work | $C_s$, Shunt cap $10^{-9}$F | $t_a$, arcing time, ms | $E_o$ Extinction Voltage, kV | Performance $E_o/e$, kV/μs |
|---|---|---|---|---|---|---|---|
| AN | 545 | 200 | F | 0 | 10.8 | 5.0 | <14.36 |
| AO | 725 | 200 | W | 0 | 14.8 | 6.9 | >14.85 |
| AP | 655 | 200 | F | 0 | 13.1 | 6.4 | <14.56* |
| AM | 685 | 300 | W | 0 | 10.9 | 5.4 | >14.5* |
| AQ | 540 | 125 | F | 2.6 | 12.9 | 4.4 | < 9.74* |
| AS | 570 | 125 | W | 2.6 | 13.9 | 5.2 | > 9.98* |
| AR | 660 | 125 | W | 2.6 | 15.6 | 4.9 | > 9.89 |

*Critical Pairs

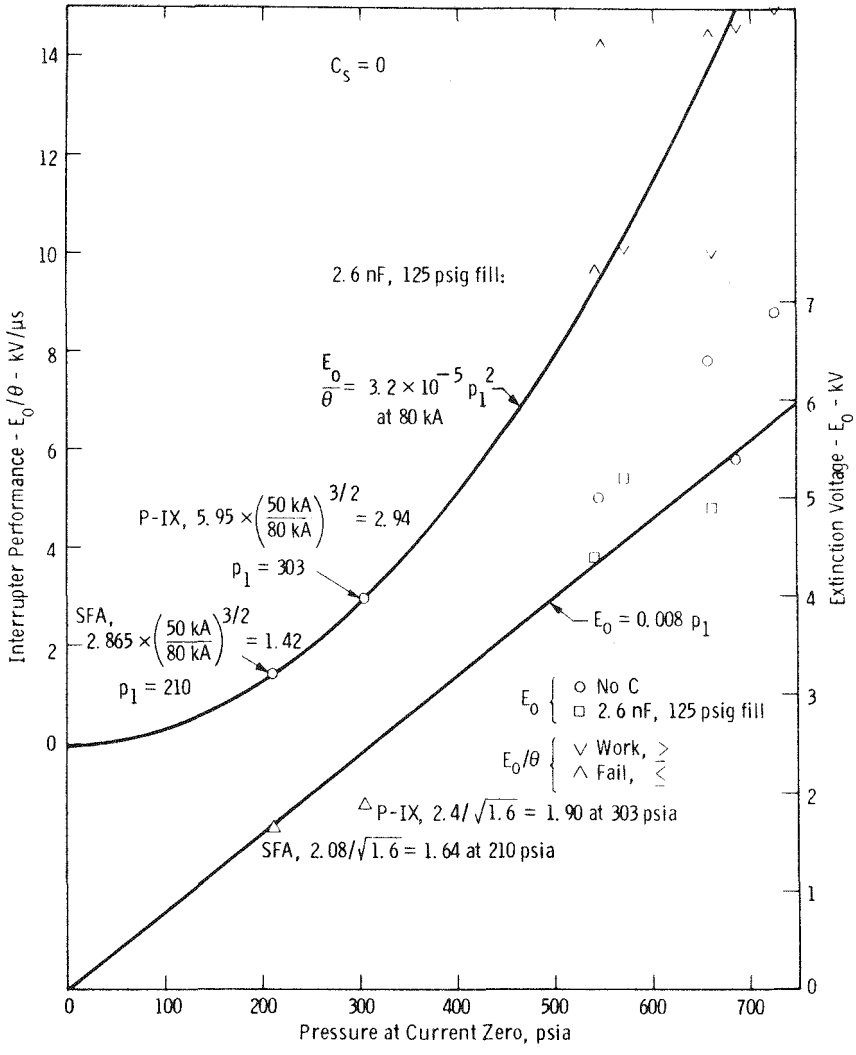


Figure C-1 Super Pressure Puffer Performance and Extinction Voltage vs. Pressure at i = 0

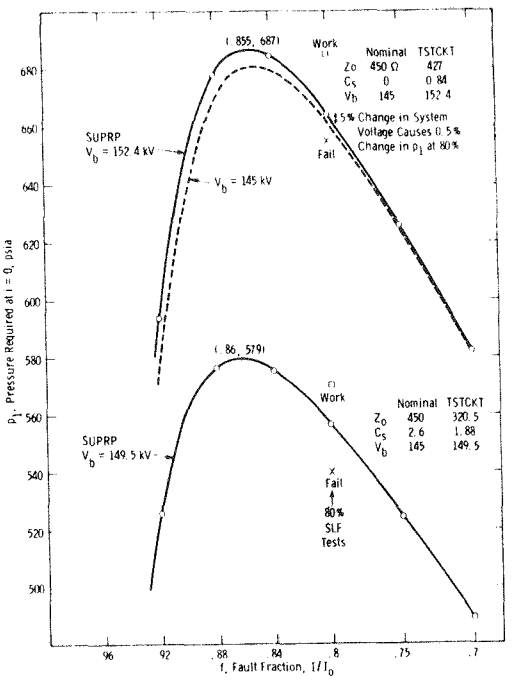


Figure C-2 100 kA 80% SLF Supper Puffer Tests and Predictions

With Eqs. C-1 and C-2 and the dynamic arc model it is possible to calculate the value of $P_1$ required to interrupte SLF's of arbitrary fault fractions in any desired system; calculations were made for several systems.

In Figure C-2 is plotted the required current-zero pressure, $P_1$, as calculated by the capacitance-shunt program for the test circuit parameters, listed in Figure C-2 as found from the $E_o/0$ values. The measured values of $P_1$ for the near-critical work and fail tests, from Table C-I, are plotted, and properly bracket the curve in both cases. Note the very small (0.5%) change in required $P_1$ for a 5% change in system voltages.

Design curves are given in Figure C-3 for one puffer break at 100 and 120 kA bus fault ratings. Note the large reduction in $P_1$ due to a shunt capacitance of 1 x $10^{-9}$F (1 nF), about the amount usually present as stray capacitance. Since the curves are coincident, the same activating mechanism would suffice on 100 kA with 2.5 nF and on 120 kA with 6 nF shunt capacitance.

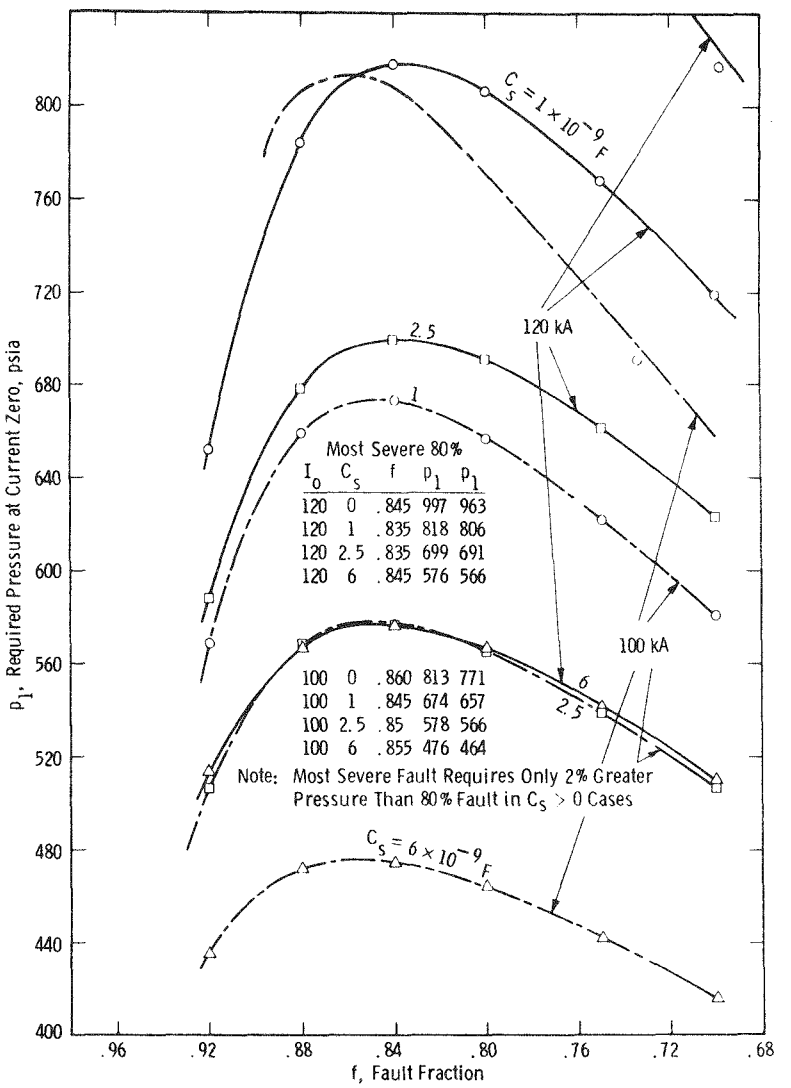


Figure C-3 Required i = 0 pressure for 145 kV, 1 bk., 120 & 100 kA, 450 ohm line

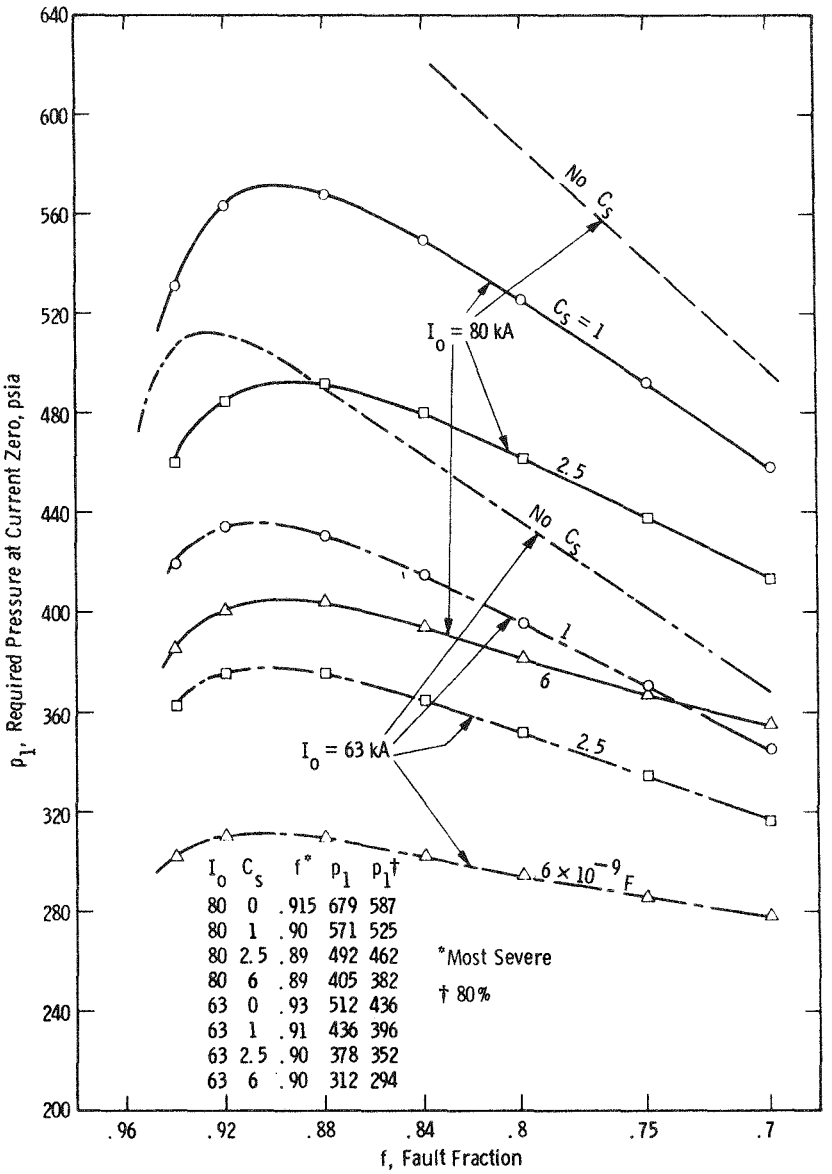


Figure C-4 Required i = 0 pressure for 450 ohm line, 242 kV, 1 break, 80 and 63 kA

Higher system voltage, lower bus fault current, one break high pressure puffer design curves are given in Figure C-4. The peaks have moved to the left, i.e., to higher fault fraction, as system voltage increases.

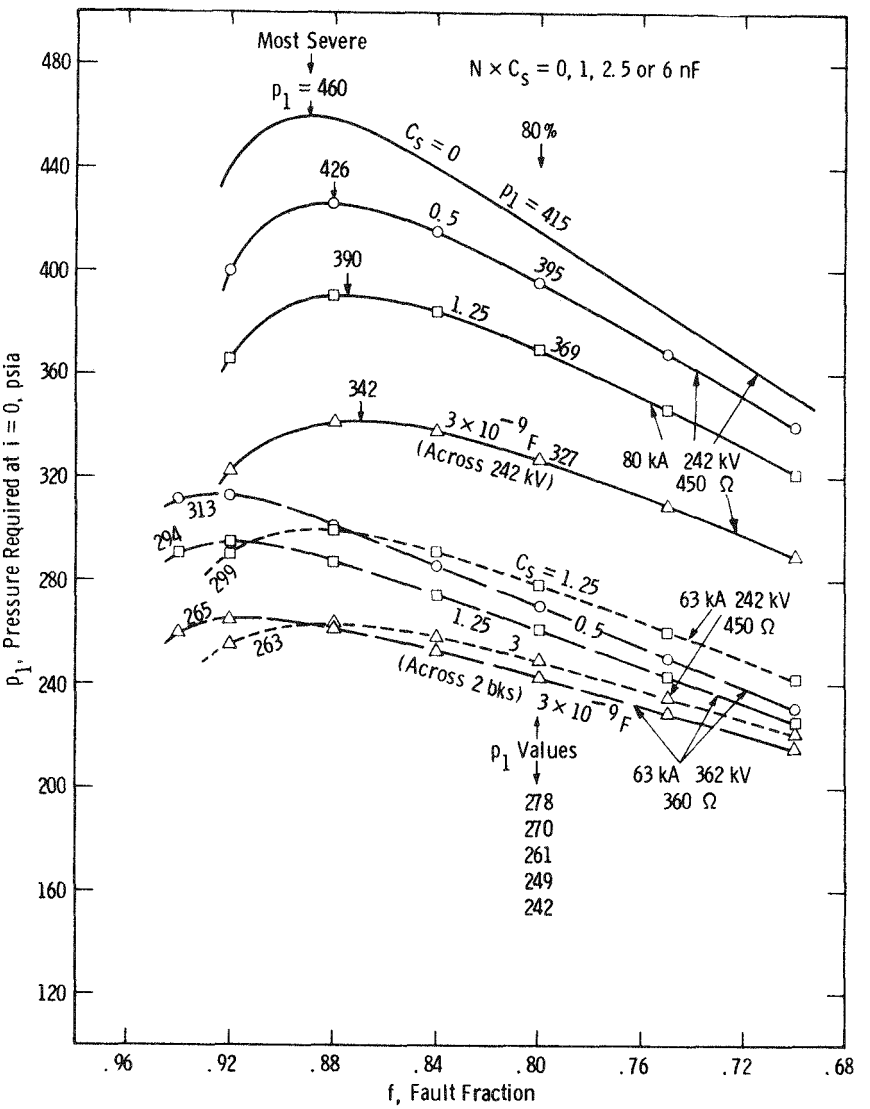


Figure C-5 2-Break systems at 63, 80 kA and 242, 362 kV

Figure C-5 gives 2-break super-pressure puffer design curves. In these and later multibreak systems, the previously chosen capacitance values of 0, 1, 2.5 or 6 nF, are chosen across one break, so that the capacitance across the entire breaker of N breaks is 0, 1/N, 2.5/N, or 6/N.

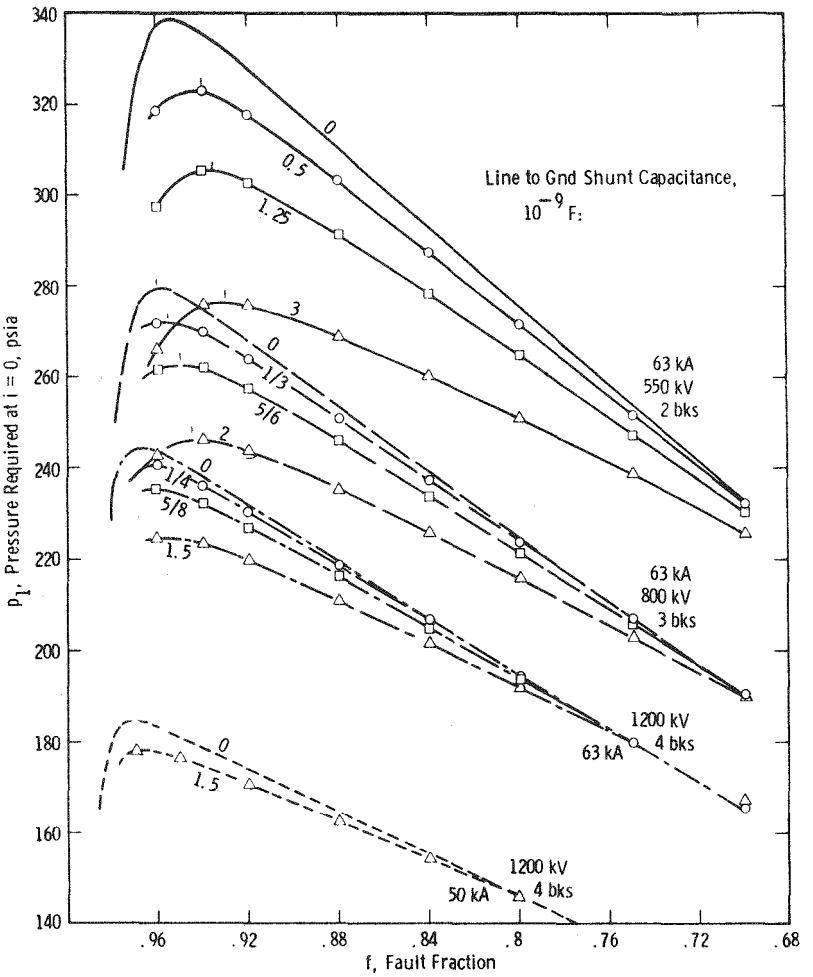


Figure C-6 High voltage systems, 360 ohm, 0, 1, 2.5 or 6 x $10^{-9}$ across each break

Note in Figure C-6 how easy the SLF requirement becomes, i.e. the required current-zero pressure $p_1$ falls, as the number of breaks increase; this is because the SLF is limited by the rate of rise of recovery voltage, which is equally shared by all breaks and thereby greatly reduced across each break as N increase. It is expected that the value of $p_1$ required to meet the bus fault standards will not fall as N increase, so that it will probably be higher than that required for SLF's for N = 2.

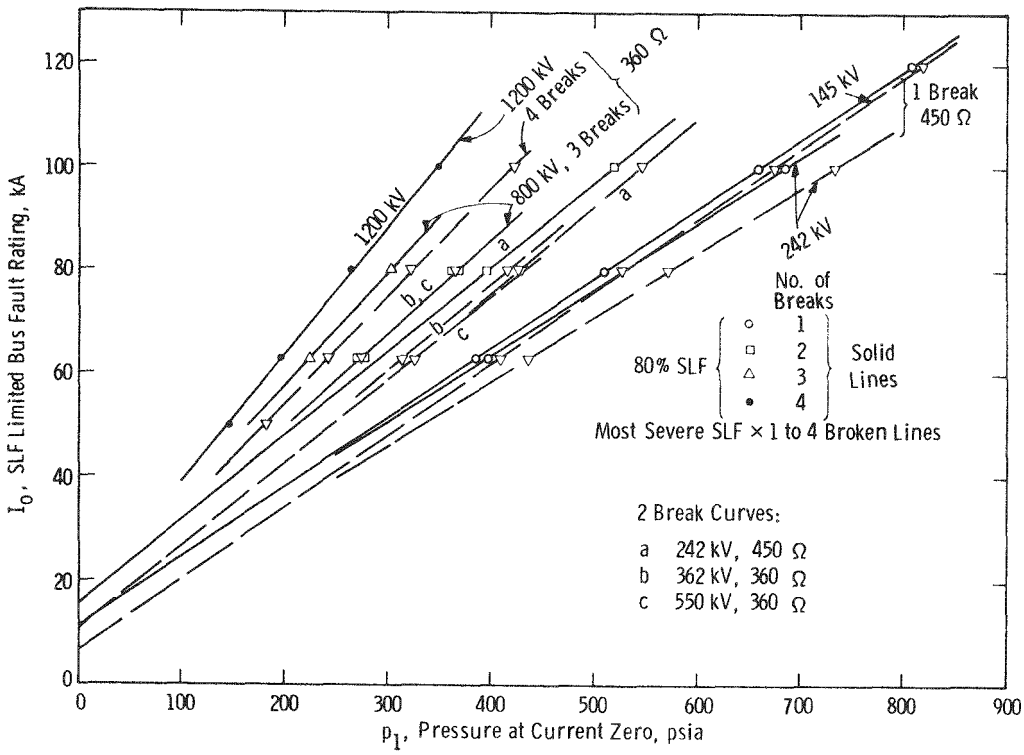


Figure C-7 SLF limited bus fault current rating vs. pressure in arc chamber at current zero for the super-pressure puffer in several systems

Figure C-7 summarizes the design data with 1 nF across each break by showing the SLF limited bus fault rating achieved by a given current-zero pressure $p_1$ for all systems, both at 80% and at the most severe SLF. In the range covered by the calculations, all curves are nearly linear, and extrapolate back to $I_o$ intercepts in the narrow ranges shown.

## CONCLUSIONS

In conclusion, the performance of the super-pressure puffer has been specified, and design calculations made to give the required upstream pressure occurring at current zero for successful interruption of the severe range of SLF's in a number of systems.

## RECOMMENDATIONS

The predicted values of current zero pressure derived here should be used as input data for actuator calculations. The precise specification of required pressure neatly eliminates the complexity of the arc interruption problem, greatly simplifying the mechanism design task.

APPENDIX D

# COMPUTER PROGRAM FOR CALCULATING PUFFER CIRCUIT BREAKER PERFORMANCE

The computer program used to describe the operation of a puffer circuit breaker and subsequently used to optimize the puffer interrupter in this project has grown over a number of years from original work that was done by Frost and Swanson. They initially developed this program to describe the operation of two pressure $SF_6$ circuit breakers. The program has since then expanded to include all of the mechanical components of $SF_6$ puffer circuit breakers. The interaction of the arc with the gas flow from the puffer which in turn produces mechanical reactions in the circuit breaker operation is a key part of the calculation.

Figure D-1 shows the overall structure of the computer program. The main program is a step by step solution of the many simultaneous relationships that occur during the the puffer operation. The time steps are usually 0.2 milliseconds. The program provides for varying the step size to obtain more accurate or more efficient solutions.

The main program calls on seven separate subroutines to perform the calculation and one more to plot the results after the calculations are completed.

Pages D-5 thru D-17, shows a complete flow chart for the main program and the seven subroutines. Pages D-5 thru D-8 show the main body of the program including a description of the factors and subroutines that are used at each step of the calculation. For each step this program calculates the amount of $SF_6$ in the puffer cylinder, the amount flowing out, the air in the mechanism, the amount of air flowing in, the loads due to the mechanism and puffer and the consequent motion of the puffer and mechanism.

So after one cycle of calculation with the change in $SF_6$ and air pressure in the two chambers we have the starting point for the next step calculations. Several parameters are calculated to determine the starting condition for the each step.

Table D-1 is the first part of the printout of the computer program for a no load operation of the circuit breaker. After listing the program introduction and

entry a complete table of the input parameters are presented to permit interpertation of the result. Since the input data is in computer file form this printout section provides feedback that the engineer can use to understand the result and compare with other solutions.

In this case the calculations are made at 0.2 ms steps and the results are plotted out for each 1 millisecond interval. The following values are the key mechanical and gas properties used and the last few lines show the $SF_6$ fill pressure as 70 psig (at 20°C) an interrupted current of 0 and an interrupting time of 28 milliseconds, of course in this case the interrupting time is not significant because the current is zero.

The results that are printed out for this case in Figure D-2 show the $SF_6$ pressure developed in the interrupter and the pressure that drives the mechanism piston. The travel of the mechanism and the puffer are plotted separately because there is a time displacement and a response displacement as well as the difference in total travel that is due to the lever arm ratio between the mechanism and the interrupter. The mechanical system is treated as two masses coupled by a spring which represents the linkage. Half of the linkage mass is assumed to be added to the mass of each end. This spring and mass system has a natural resonance which is near the power system frequency, because it is required to complete its function in two cycles of power frequency. This resonant effect is shown by the small oscillation in the mechanism and puffer travel. There are many approximations that are incorporated into the program. Page D-8 shows the details of subroutine SPEC which uses a polynomial curve fit to calculate $SF_6$ gas characteristics. The gas at the high pressures reached by this interrupter has specific heat characteristics that are very non linear, because these pressures are near the triple point for $SF_6$. The published curves for gas properties are used as the source information. Then on page D-9 the nonlinear compressability of $SF_6$ is incorporated into the calculation to obtain a closer fit to the real gas properties.

Table D-2 shows the input data for a 100 kA operation with interruption at 28 milliseconds. This is one of several interrupting times that were calculated to assure adequate differential pressure for interruption. These calculations showed that for times up to 33 ms the differential pressure available at current zero increases with interrupting times. Figure D-4 shows the graphic printout of the circuit breaker operation with a 100 kA fault current.

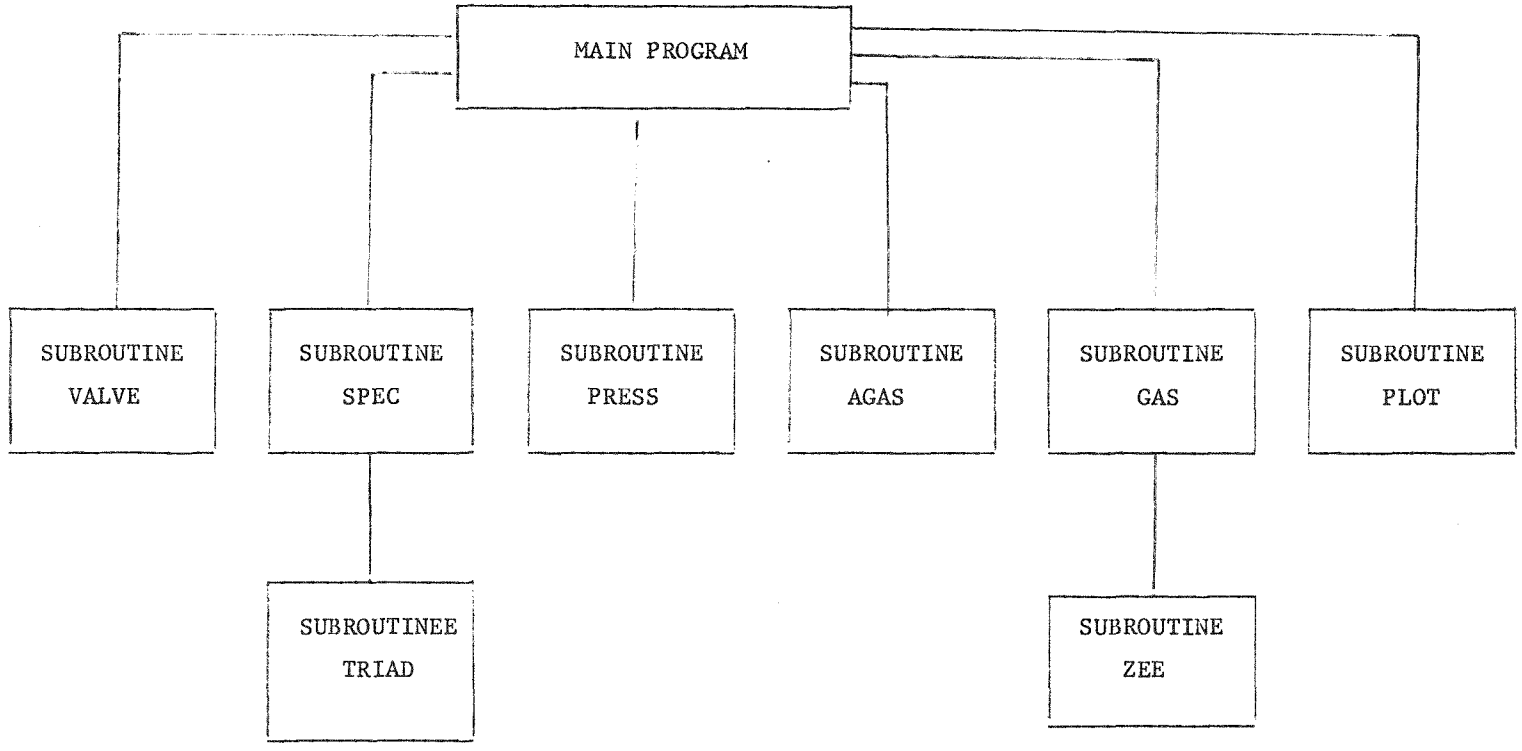


Figure D-1 Operational Scheme for Computer Model

TABLE D-1

COMPUTER PROGRAM FLOW CHART

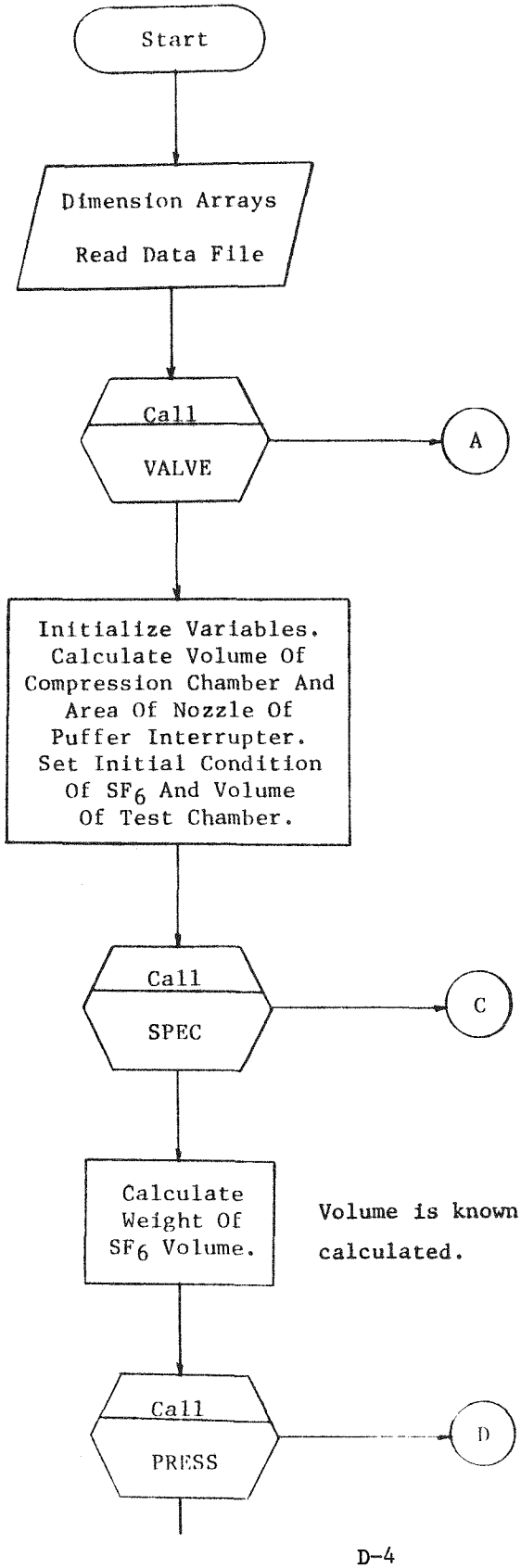

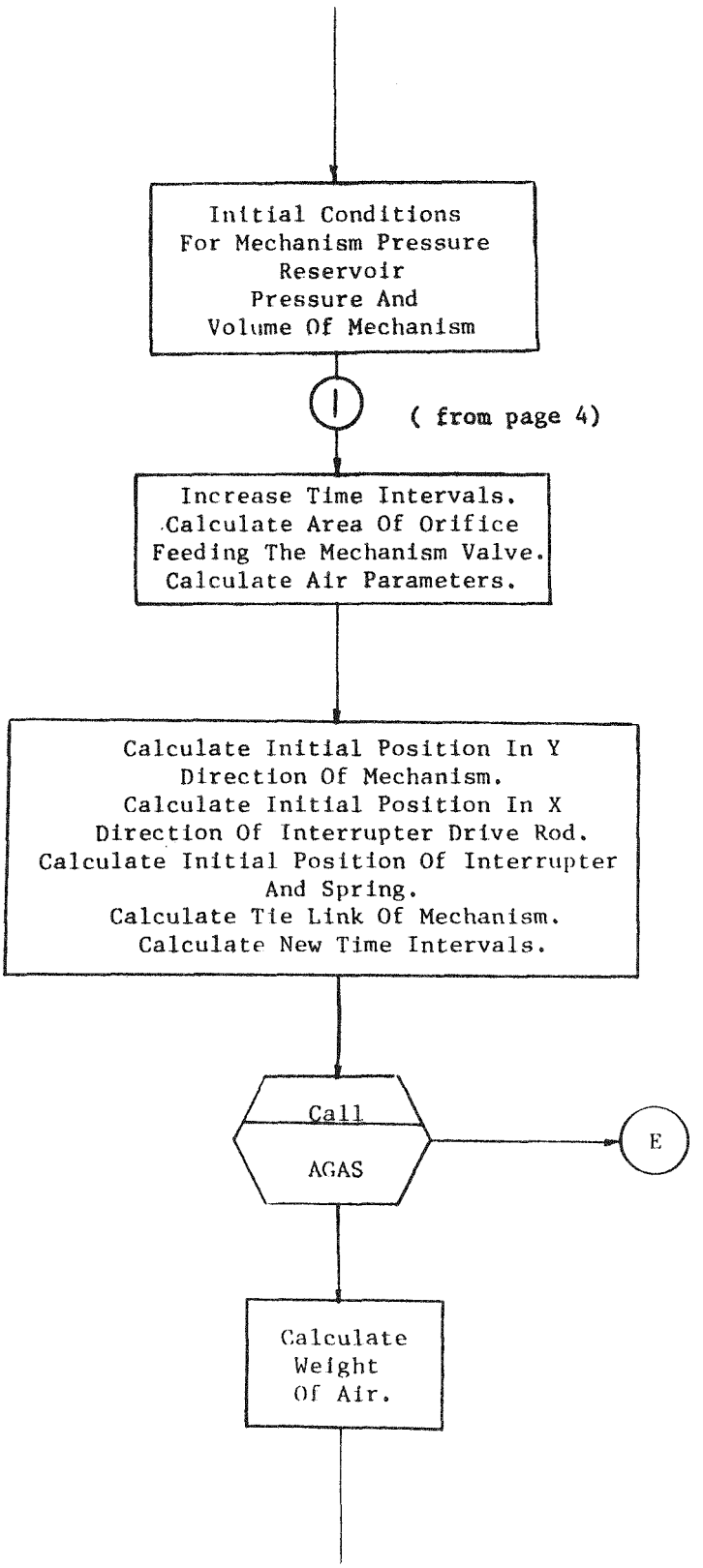


Calculates weight of air that flows from one chamber to another through an orfice due to pressure differential, over a fixed time interval (iteration)

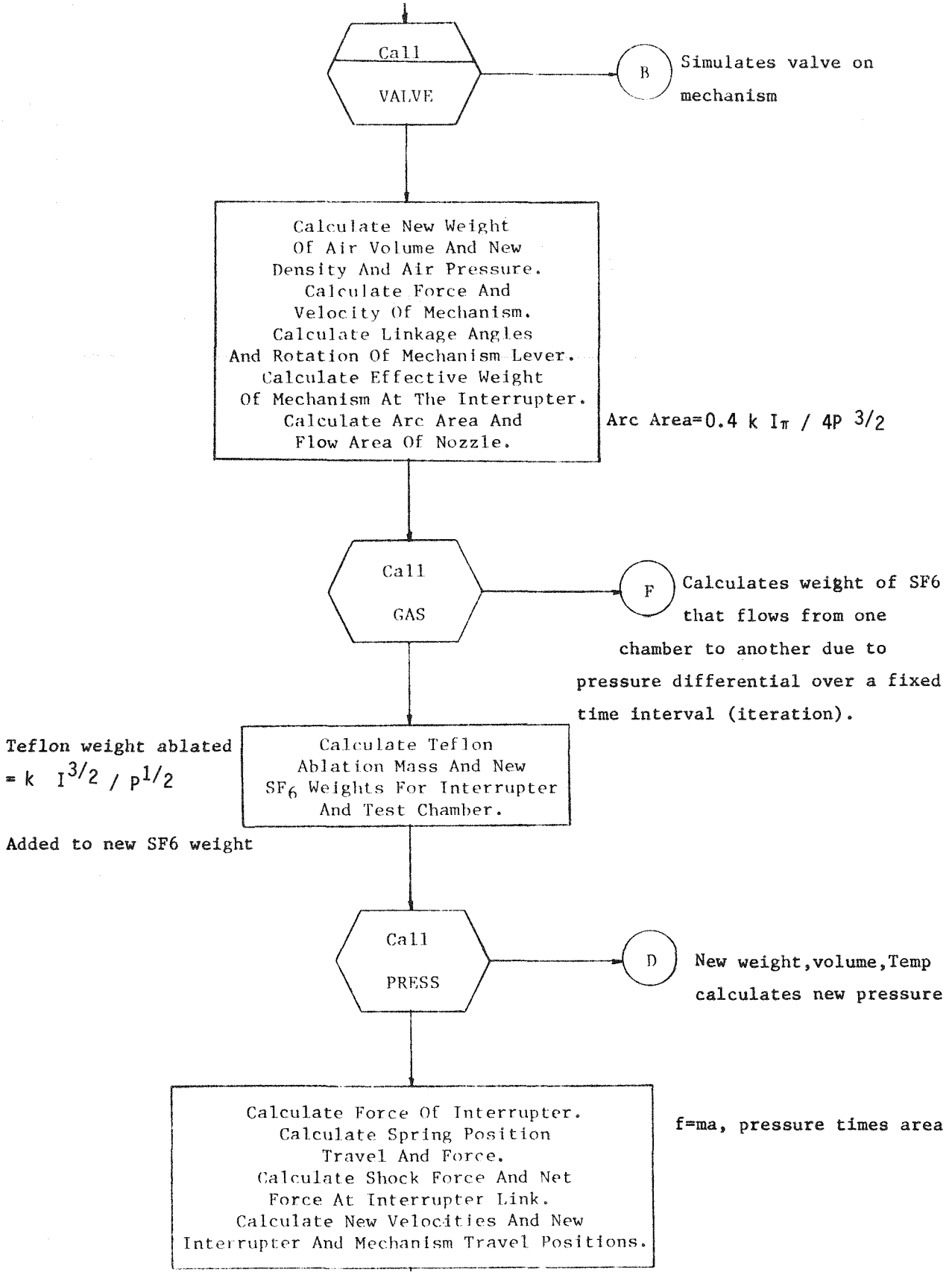
Call
VALVE
B
Simulates valve on mechanism
Calculate New Weight Of Air Volume And New Density And Air Pressure. Calculate Force And Velocity Of Mechanism. Calculate Linkage Angles And Rotation Of Mechanism Lever. Calculate Effective Weight Of Mechanism At The Interrupter. Calculate Arc Area And Flow Area Of Nozzle.
Arc Area=0.4 k Iπ / 4P 3/2
Call
GAS
F
Calculates weight of SF6 that flows from one chamber to another due to pressure differential over a fixed time interval (iteration).
Teflon weight ablated = k I3/2 / p1/2
Calculate Teflon Ablation Mass And New SF6 Weights For Interrupter And Test Chamber.
Added to new SF6 weight
Call
PRESS
D
New weight,volume,Temp calculates new pressure
Calculate Force Of Interrupter. Calculate Spring Position Travel And Force. Calculate Shock Force And Net Force At Interrupter Link. Calculate New Velocities And New Interrupter And Mechanism Travel Positions.
f=ma, pressure times area

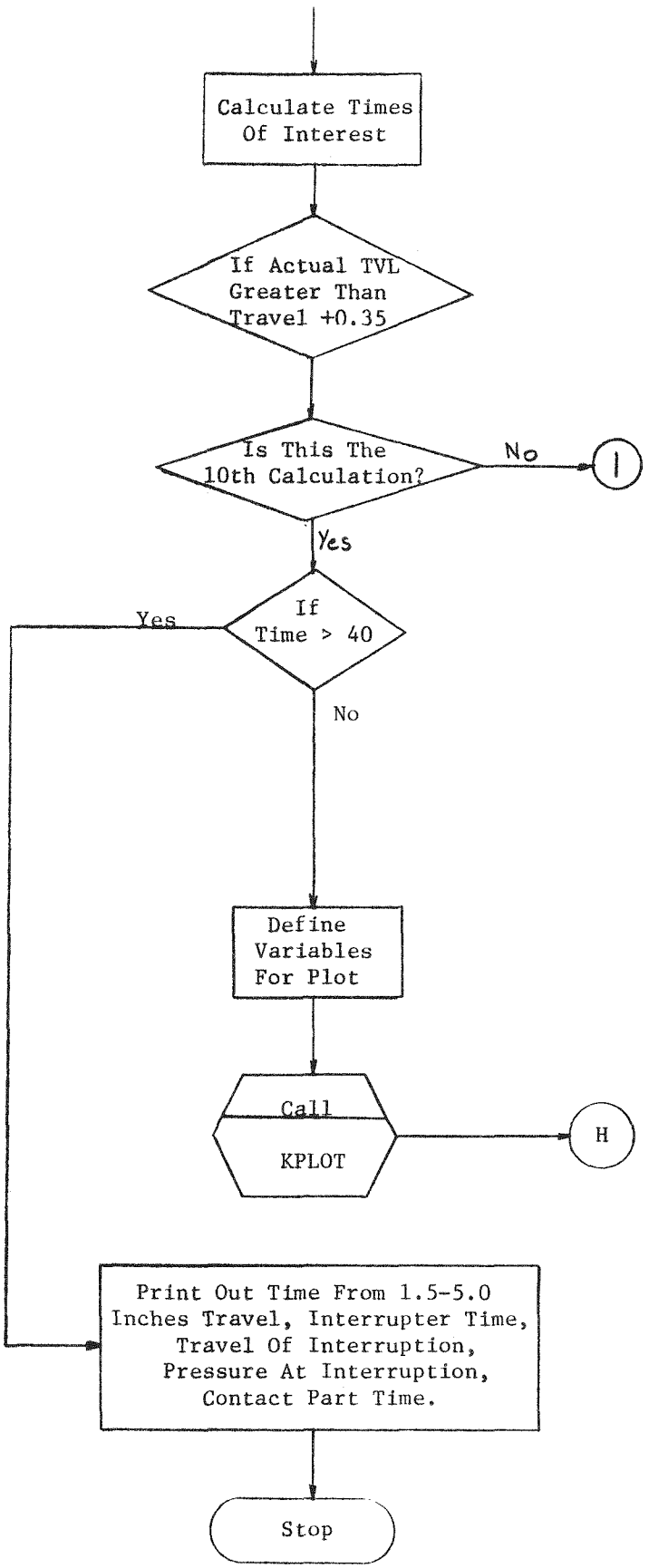
Calculate Times Of Interest
If Actual TVL Greater Than Travel +0.35
Is This The 10th Calculation?
No
1
Yes
If Time > 40
Yes
No
Define Variables For Plot
Call
KPLOT
H
Print Out Time From 1.5-5.0 Inches Travel, Interrupter Time, Travel Of Interruption, Pressure At Interruption, Contact Part Time.
Stop

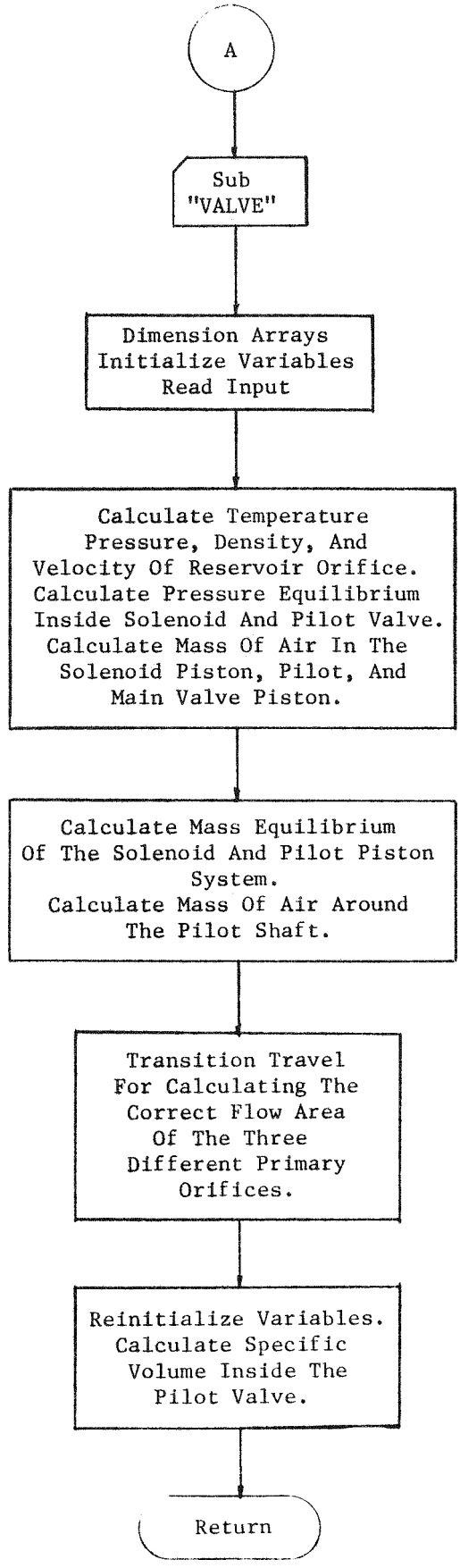
A
Sub "VALVE"
Dimension Arrays
Initialize Variables
Read Input
Calculate Temperature Pressure, Density, And Velocity Of Reservoir Orifice.
Calculate Pressure Equilibrium Inside Solenoid And Pilot Valve.
Calculate Mass Of Air In The Solenoid Piston, Pilot, And Main Valve Piston.
Calculate Mass Equilibrium Of The Solenoid And Pilot Piston System.
Calculate Mass Of Air Around The Pilot Shaft.
Transition Travel For Calculating The Correct Flow Area Of The Three Different Primary Orifices.
Reinitialize Variables.
Calculate Specific Volume Inside The Pilot Valve.
Return

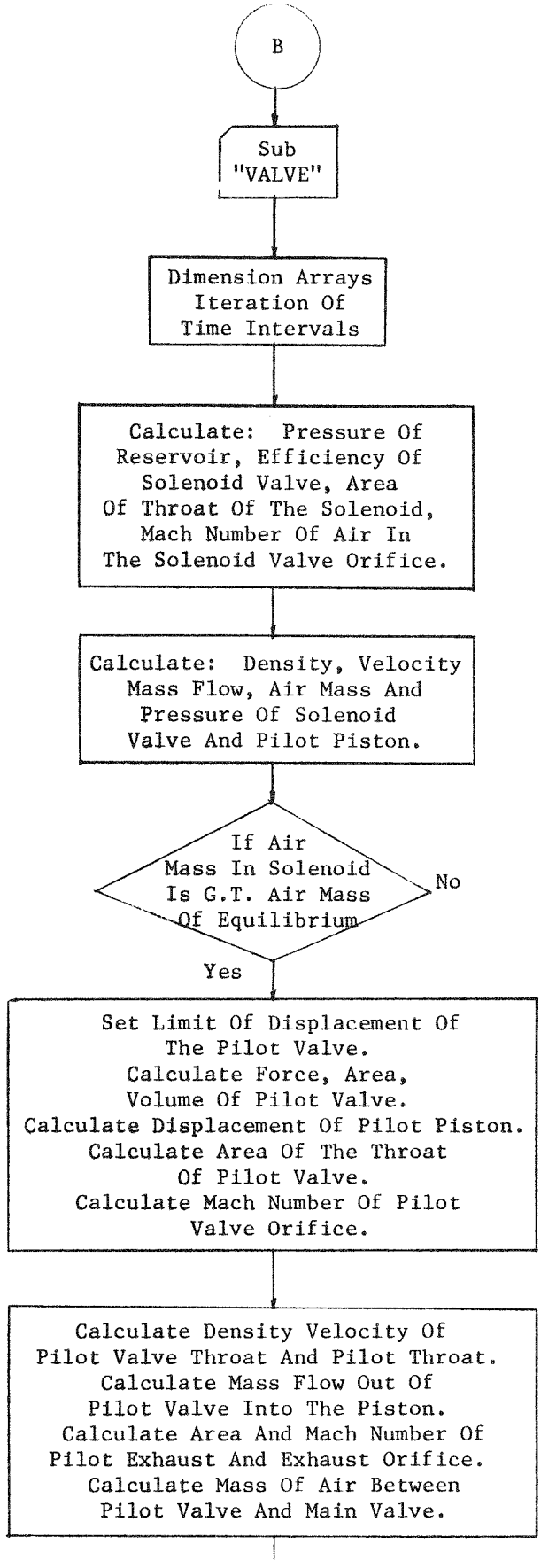
B
Sub "VALVE"
Dimension Arrays Iteration Of Time Intervals
Calculate: Pressure Of Reservoir, Efficiency Of Solenoid Valve, Area Of Throat Of The Solenoid, Mach Number Of Air In The Solenoid Valve Orifice.
Calculate: Density, Velocity Mass Flow, Air Mass And Pressure Of Solenoid Valve And Pilot Piston.
If Air Mass In Solenoid Is G.T. Air Mass Of Equilibrium
No
Yes
Set Limit Of Displacement Of The Pilot Valve. Calculate Force, Area, Volume Of Pilot Valve. Calculate Displacement Of Pilot Piston. Calculate Area Of The Throat Of Pilot Valve. Calculate Mach Number Of Pilot Valve Orifice.
Calculate Density Velocity Of Pilot Valve Throat And Pilot Throat. Calculate Mass Flow Out Of Pilot Valve Into The Piston. Calculate Area And Mach Number Of Pilot Exhaust And Exhaust Orifice. Calculate Mass Of Air Between Pilot Valve And Main Valve.

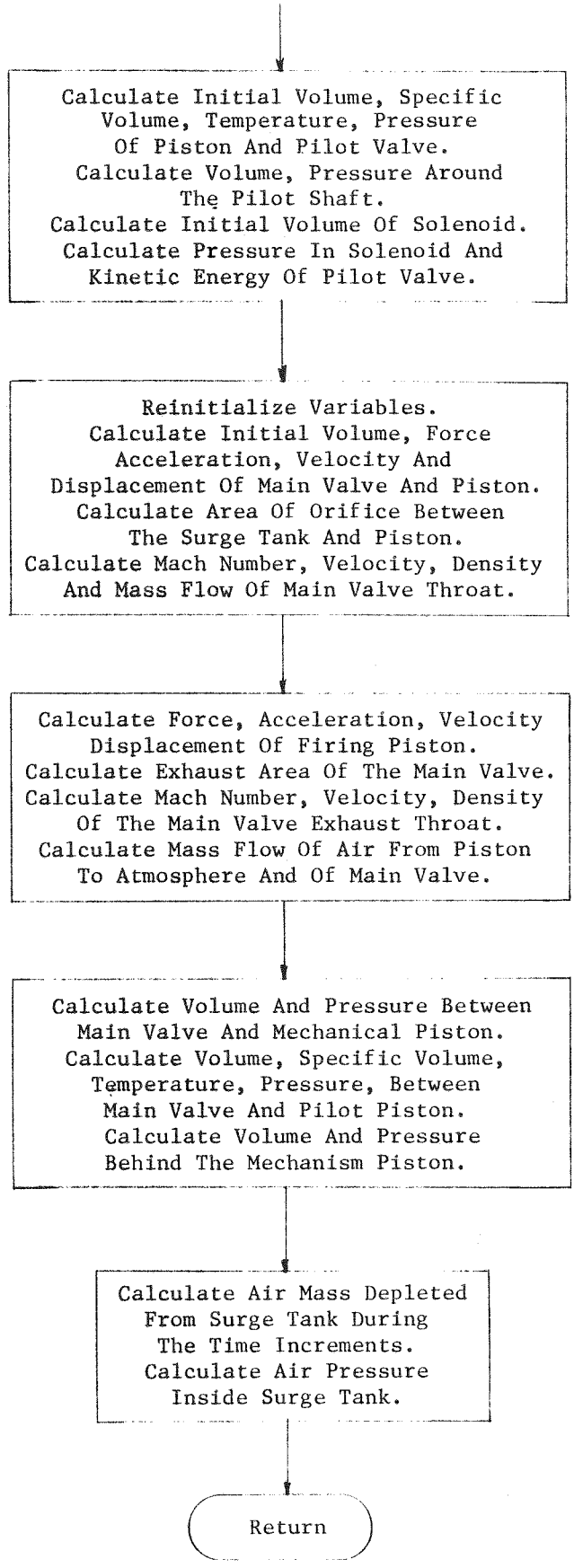
Calculate Initial Volume, Specific Volume, Temperature, Pressure Of Piston And Pilot Valve. Calculate Volume, Pressure Around The Pilot Shaft. Calculate Initial Volume Of Solenoid. Calculate Pressure In Solenoid And Kinetic Energy Of Pilot Valve.
Reinitialize Variables. Calculate Initial Volume, Force Acceleration, Velocity And Displacement Of Main Valve And Piston. Calculate Area Of Orifice Between The Surge Tank And Piston. Calculate Mach Number, Velocity, Density And Mass Flow Of Main Valve Throat.
Calculate Force, Acceleration, Velocity Displacement Of Firing Piston. Calculate Exhaust Area Of The Main Valve. Calculate Mach Number, Velocity, Density Of The Main Valve Exhaust Throat. Calculate Mass Flow Of Air From Piston To Atmosphere And Of Main Valve.
Calculate Volume And Pressure Between Main Valve And Mechanical Piston. Calculate Volume, Specific Volume, Temperature, Pressure, Between Main Valve And Pilot Piston. Calculate Volume And Pressure Behind The Mechanism Piston.
Calculate Air Mass Depleted From Surge Tank During The Time Increments. Calculate Air Pressure Inside Surge Tank.
Return

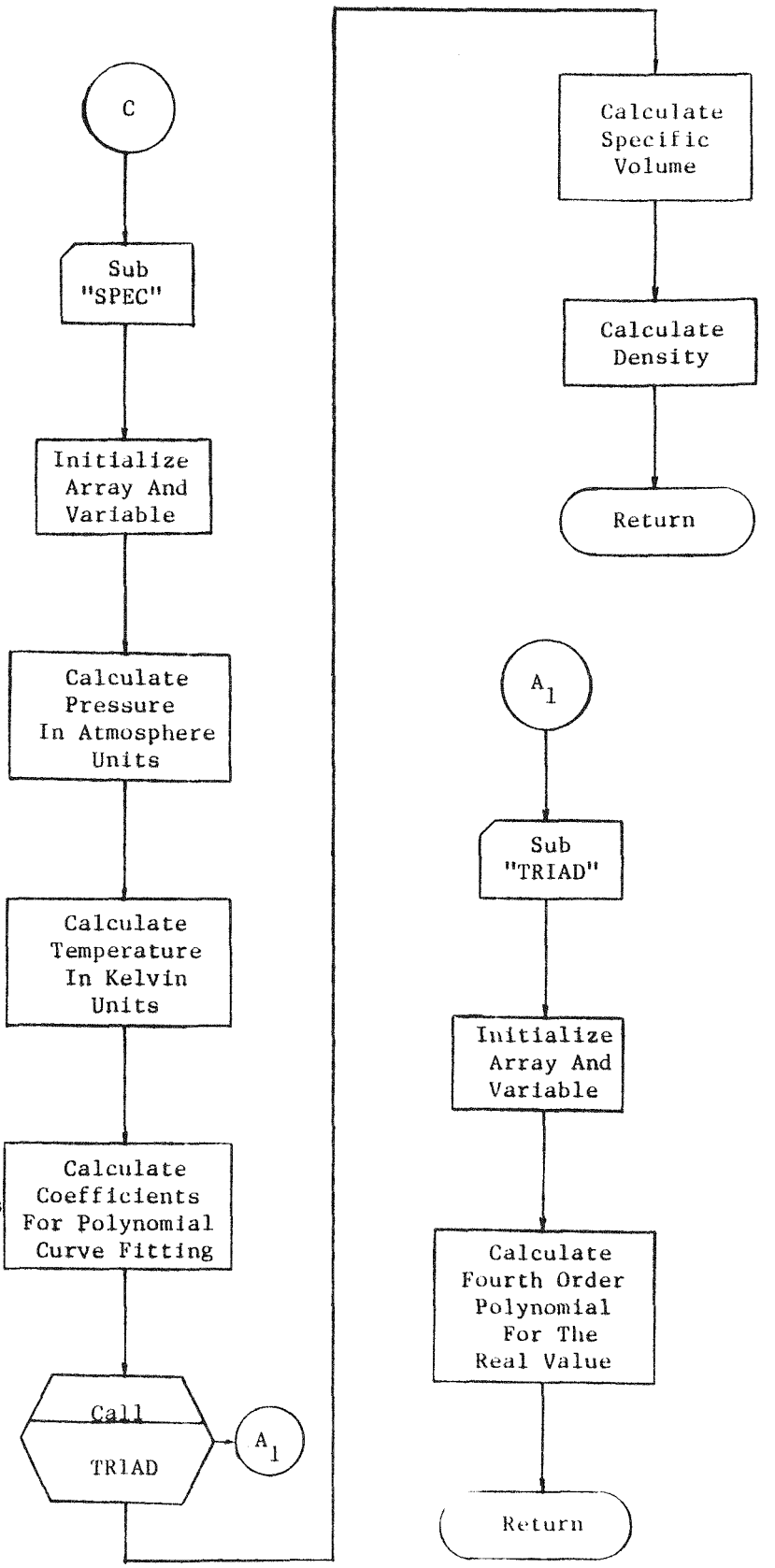


Equation for specific volume vs. Temp and Pres pressure.

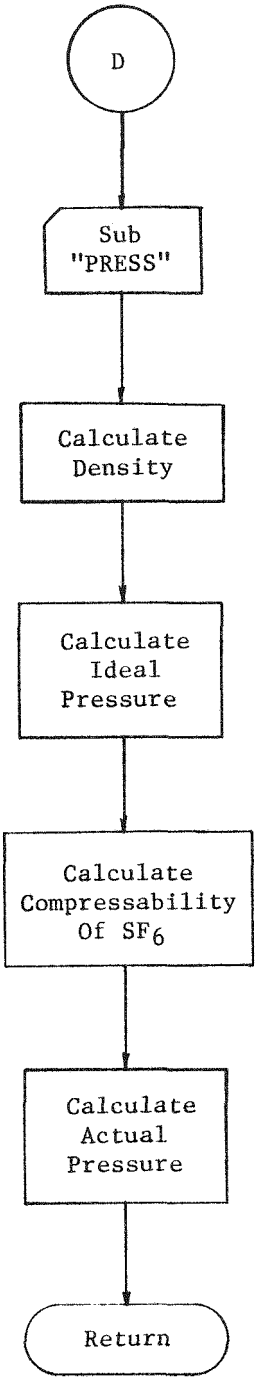
D
Sub "PRESS"
Calculate Density
Calculate Ideal Pressure
Calculate Compressability Of $SF_6$
Calculate Actual Pressure
Return

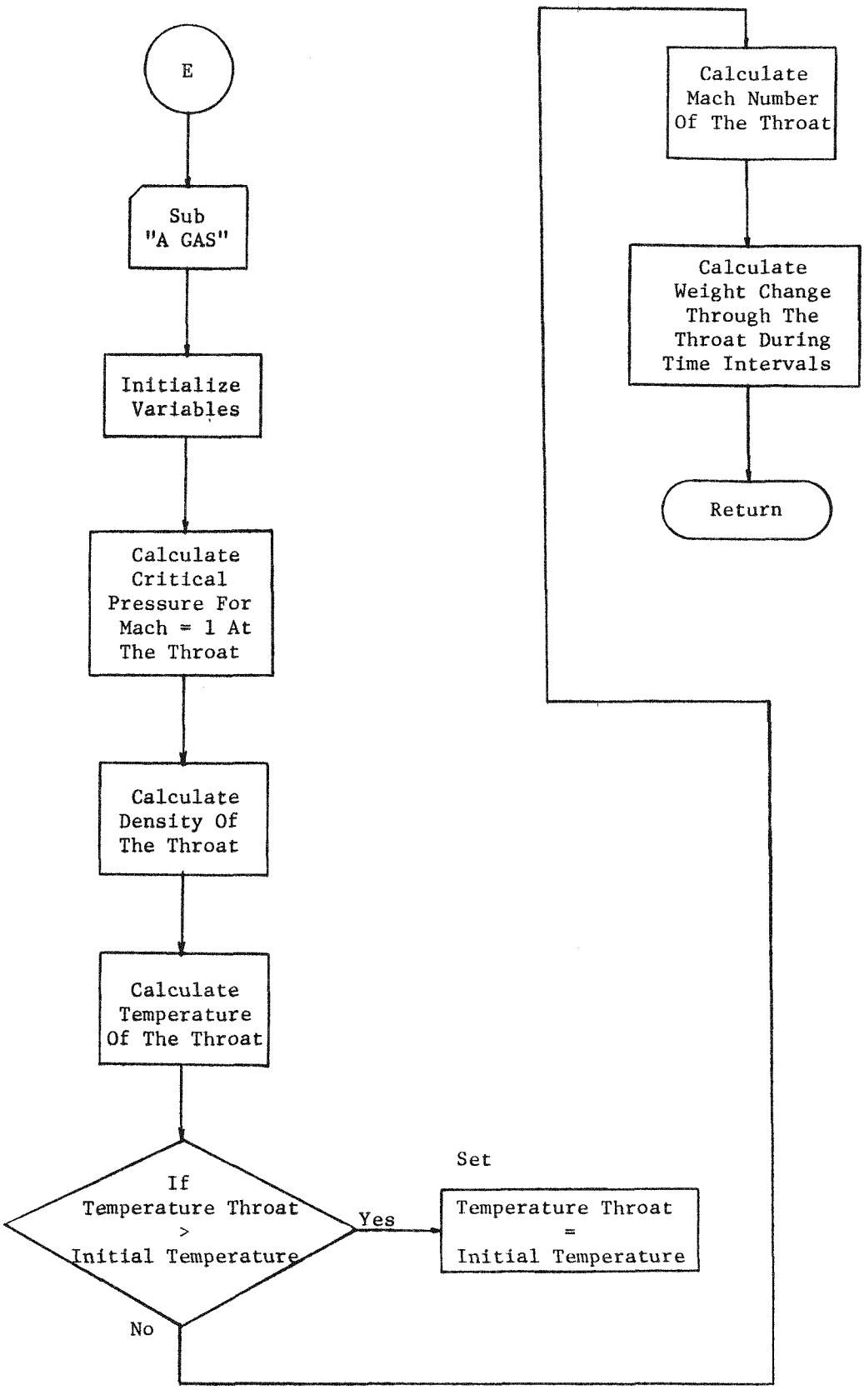
E
Sub "A GAS"
Initialize Variables
Calculate Critical Pressure For Mach = 1 At The Throat
Calculate Density Of The Throat
Calculate Temperature Of The Throat
If Temperature Throat > Initial Temperature
Yes
Set
Temperature Throat = Initial Temperature
No
Calculate Mach Number Of The Throat
Calculate Weight Change Through The Throat During Time Intervals
Return

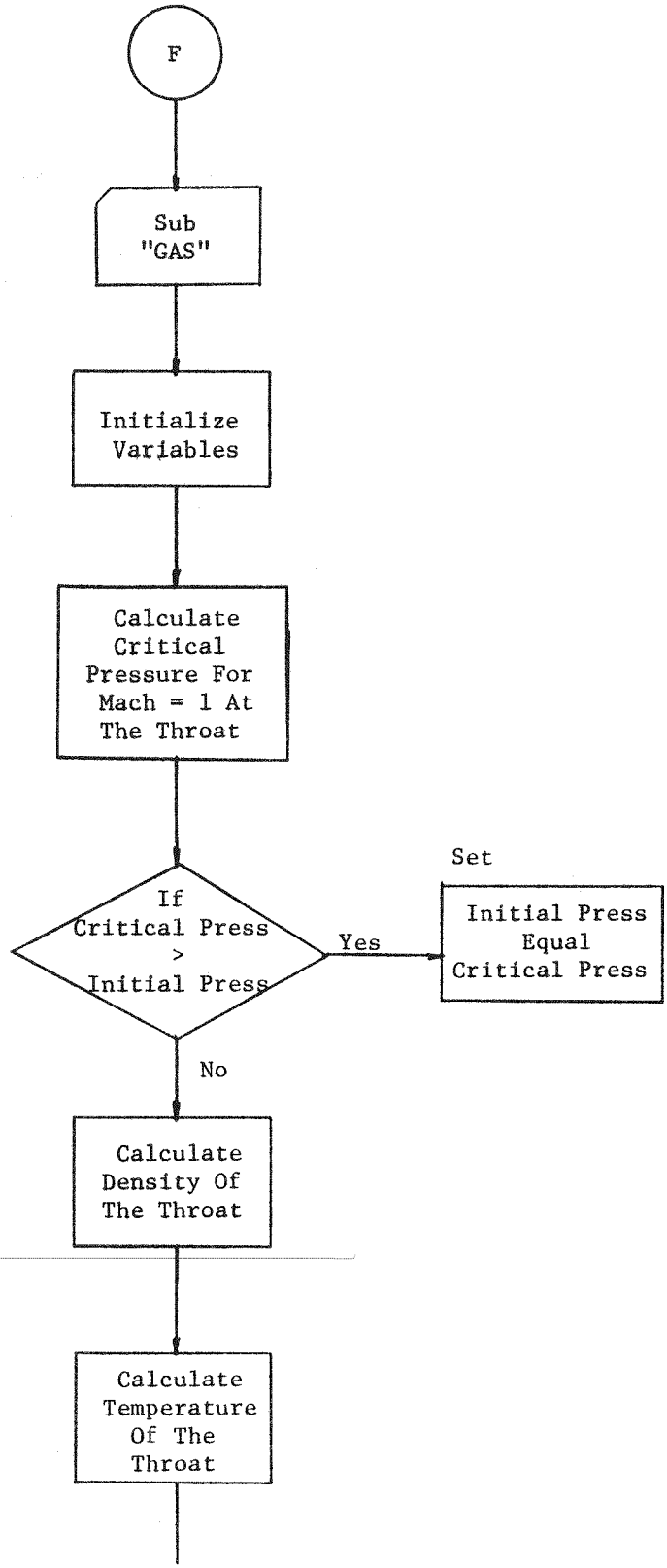
F
Sub "GAS"
Initialize Variables
Calculate Critical Pressure For Mach = 1 At The Throat
If Critical Press > Initial Press
Yes
Set
Initial Press Equal Critical Press
No
Calculate Density Of The Throat
Calculate Temperature Of The Throat

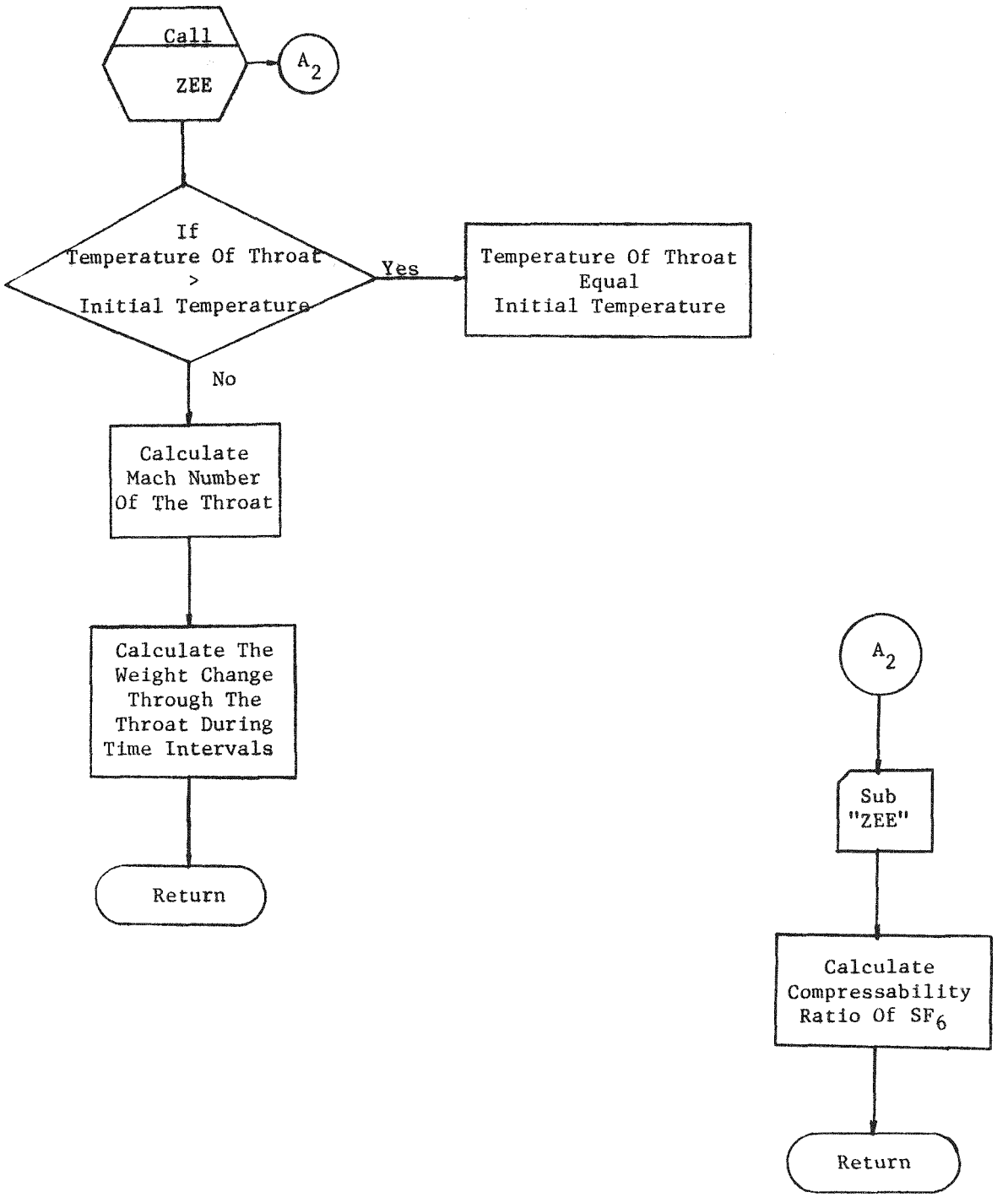
Call
ZEE
A2
If
Temperature Of Throat
>
Initial Temperature
Yes
Temperature Of Throat
Equal
Initial Temperature
No
Calculate
Mach Number
Of The Throat
Calculate The
Weight Change
Through The
Throat During
Time Intervals
Return
A2
Sub
"ZEE"
Calculate
Compressability
Ratio Of SF6
Return

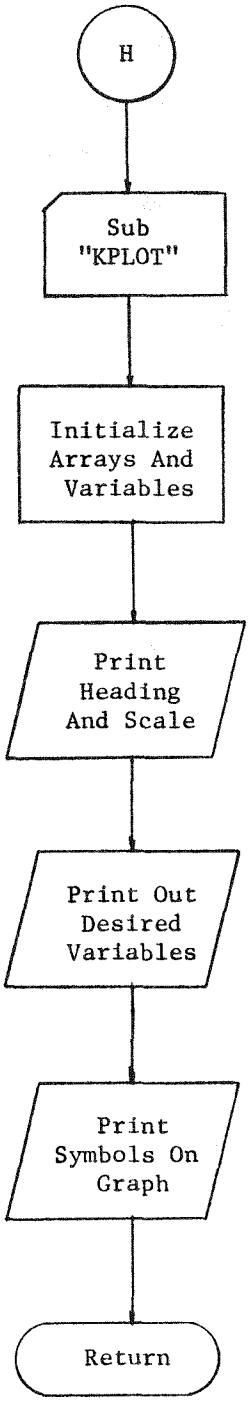
H
Sub "KPLOT"
Initialize Arrays And Variables
Print Heading And Scale
Print Out Desired Variables
Print Symbols On Graph
Return

TABLE D-2

COMPUTER PROGRAM FOR NO LOAD PUFFER CIRCUIT BREAKER OPERATION

```
 FEB  4 15:27  1982
SUPER PUFFER TEST MODEL-DUAL MECHANISM
REVISED BY ROSTRON/KOLOCOURIS  8-4-77
REVISED BY      :       :      6-20-78
CHANGE ANY BREAKER VARIABLES?  TYPE P TO CONTINUE.
*PAUSE*
($MAIN$)0+7
+P
READING VALVE DATA FILE /DATAV/ IN VALVE SPROG/
READING TRIP COIL CURRENT DATA FILE /DATAI/ IN VALVE SPROG
MODIFY VALVE DATA?
*PAUSE*
(VALVE)804+3
+P

CALC STEP,PLOT STEP                          =      0.2       1
MECHANISM WT., INTERRUPTER WT., LKG.WT.      =    85.00     75.00      90.
MECHANISM FRICTION, INTERRUPTER FRICTION     =   100.00    300.00
LINKAGE SLACK, SPRING CONSTANT               =     0.00 150000.00

DISTANCE BETWEEN LEVERS                      =    16.62
MECHANISM CRANK  -LENGTH,ANGLE               =     8.15     67.00
MECHANISM LEVER -LENGTH,ANGLE                =     4.45     41.00
MECHANISM TIE LINK,OFFSET - LENGTHS          =    10.60      3.30
INTERRUPTER LEVER -LENGTH,ANGLE              =     5.69     38.00
INTERRUPTER CRANK -LENGTH,ANGLE              =     4.28    104.00
SPRING LEVER -LENGTH,ANGLE                   =     3.60     48.00
SPRING FORCE -INITIAL, FINAL                 =  -500.00  -2000.00

SHOCK ABSORBER -Y POSITION,FORCE             =     0.75  30000.00
SHOCK LEVER -LENGTH,ANGLE                    =     4.45     42.00

MECH PRESSURE, RESERVIOR VOLUME              =   350.00   4000.00
SURGE TANK VOLUME, HOSE DIAMETER             =    50.00      2.00
MECH PISTON DIAMETER, CLEARANCE              =    10.00      0.25

PISTON DIA, INTERR TRAVEL                    =     9.75      6.50
ORIFICE COEFF, NOZZLE DIAMETER               =     1.00      1.50
CONTACT PART TIME, DEAD VOLUME               =     0.75     60.00
TEFLON ABLATION CONSTANT, ARR AREA COEFF     =     1.00    225.00
SF6 SPECIFIC HEAT RATIO, EXPONT,PRESSURE     =     1.13      0.10      70.
MECH PISTON ORIF AREA,ROD DIA                =     0.80      3.75
PISTON TRAVL,RELIEF AREA,PRESSURE            =     5.75      0.50      50.
CURRENT IN RMS, INTERRUPTING TIME            =     0.00     28.00
```

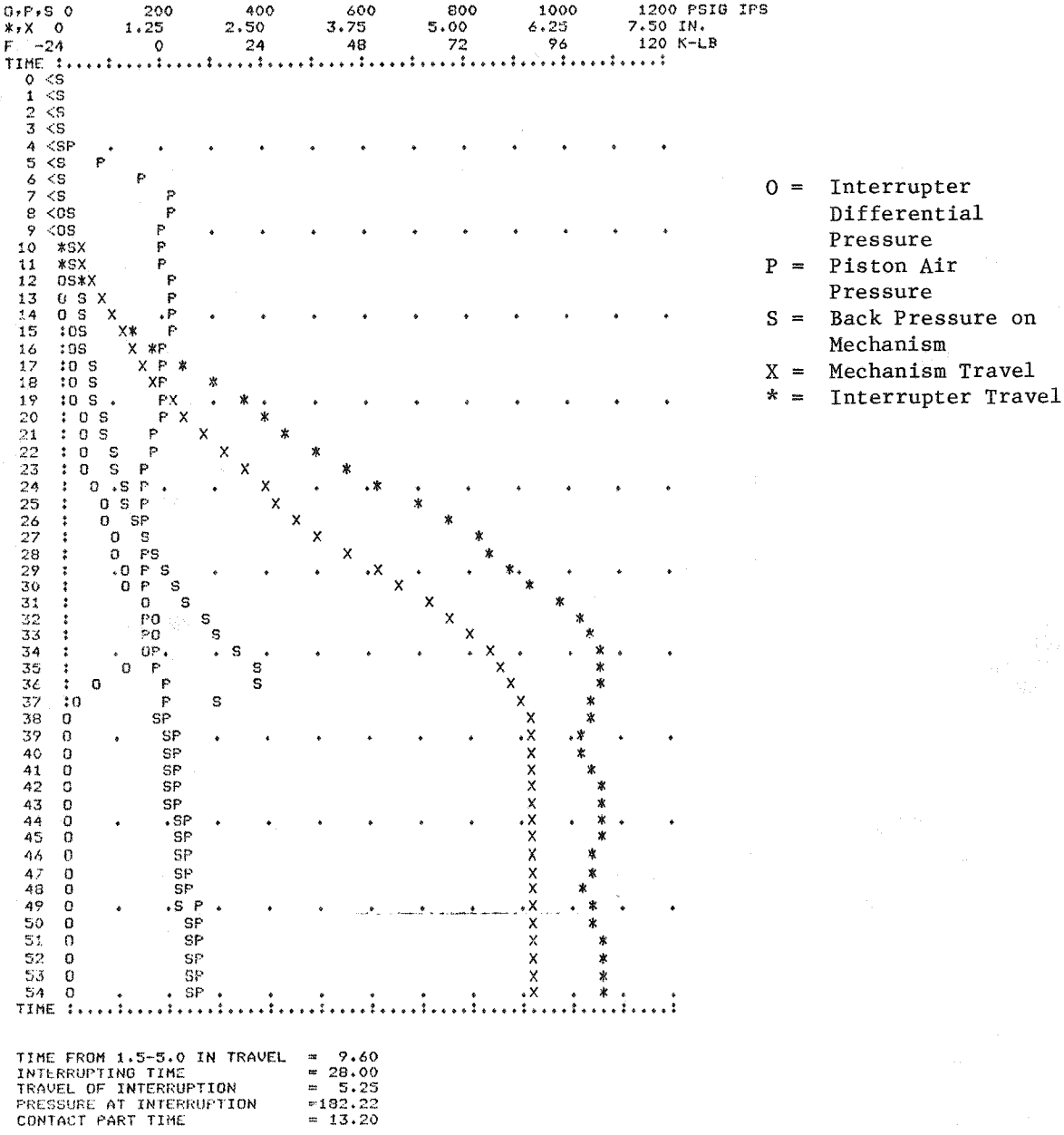


TIME FROM 1.5-5.0 IN TRAVEL = 9.60
INTERRUPTING TIME = 28.00
TRAVEL OF INTERRUPTION = 5.25
PRESSURE AT INTERRUPTION =182.22
CONTACT PART TIME = 13.20

Figure D-2 Computer Plot of No Load Operation of Puffer Circuit Breaker

TABLE D-3

COMPUTER PROGRAM FOR 100 kA PUFFER CIRCUIT BREAKER OPERATION

```
+P
READING VALVE DATA FILE /DATAV/ IN VALVE SPROG/
READING TRIP COIL CURRENT DATA FILE /DATAI/ IN VALVE SPROG
MODIFY VALVE DATA?
*PAUSE*
(VALVE)804+3
+P

CALC STEP,PLOT STEP                          =      0.2        1
MECHANISM WT., INTERRUPTER WT., LKG.WT.      =    85.00     75.00      90.
MECHANISM FRICTION, INTERRUPTER FRICTION     =   100.00    300.00
LINKAGE SLACK, SPRING CONSTANT               =     0.00 150000.00

DISTANCE BETWEEN LEVERS                      =    16.62
MECHANISM CRANK  -LENGTH,ANGLE               =     8.15     67.00
MECHANISM LEVER -LENGTH,ANGLE                =     4.45     41.00
MECHANISM TIE LINK,OFFSET - LENGTHS          =    10.60      3.30
INTERRUPTER LEVER -LENGTH,ANGLE              =     5.69     38.00
INTERRUPTER CRANK -LENGTH,ANGLE              =     4.28    104.00
SPRING LEVER -LENGTH,ANGLE                   =     3.60     48.00
SPRING FORCE -INITIAL, FINAL                 =  -500.00  -2000.00

SHOCK ABSORBER -Y POSITION,FORCE             =     0.75  30000.00
SHOCK LEVER -LENGTH,ANGLE                    =     4.45     42.00

MECH PRESSURE, RESERVIOR VOLUME              =   350.00   4000.00
SURGE TANK VOLUME, HOSE DIAMETER             =    50.00      2.00
MECH PISTON DIAMETER, CLEARANCE              =    10.00      0.25

PISTON DIA, INTERR TRAVEL                    =     9.75      6.50
ORIFICE COEFF, NOZZLE DIAMETER               =     1.00      1.50
CONTACT PART TIME, DEAD VOLUME               =     0.75     60.00
TEFLON ABLATION CONSTANT, ARR AREA COEFF     =     1.00    225.00
SF6 SPECIFIC HEAT RATIO, EXPONT,PRESSURE     =     1.13      0.10      70.
MECH PISTON ORIF AREA,ROD DIA                =     0.80      3.75
PISTON TRAVL,RELIEF AREA,PRESSURE            =     5.75      0.50      50.
CURRENT IN RMS, INTERRUPTING TIME            =   100.00     28.00
```

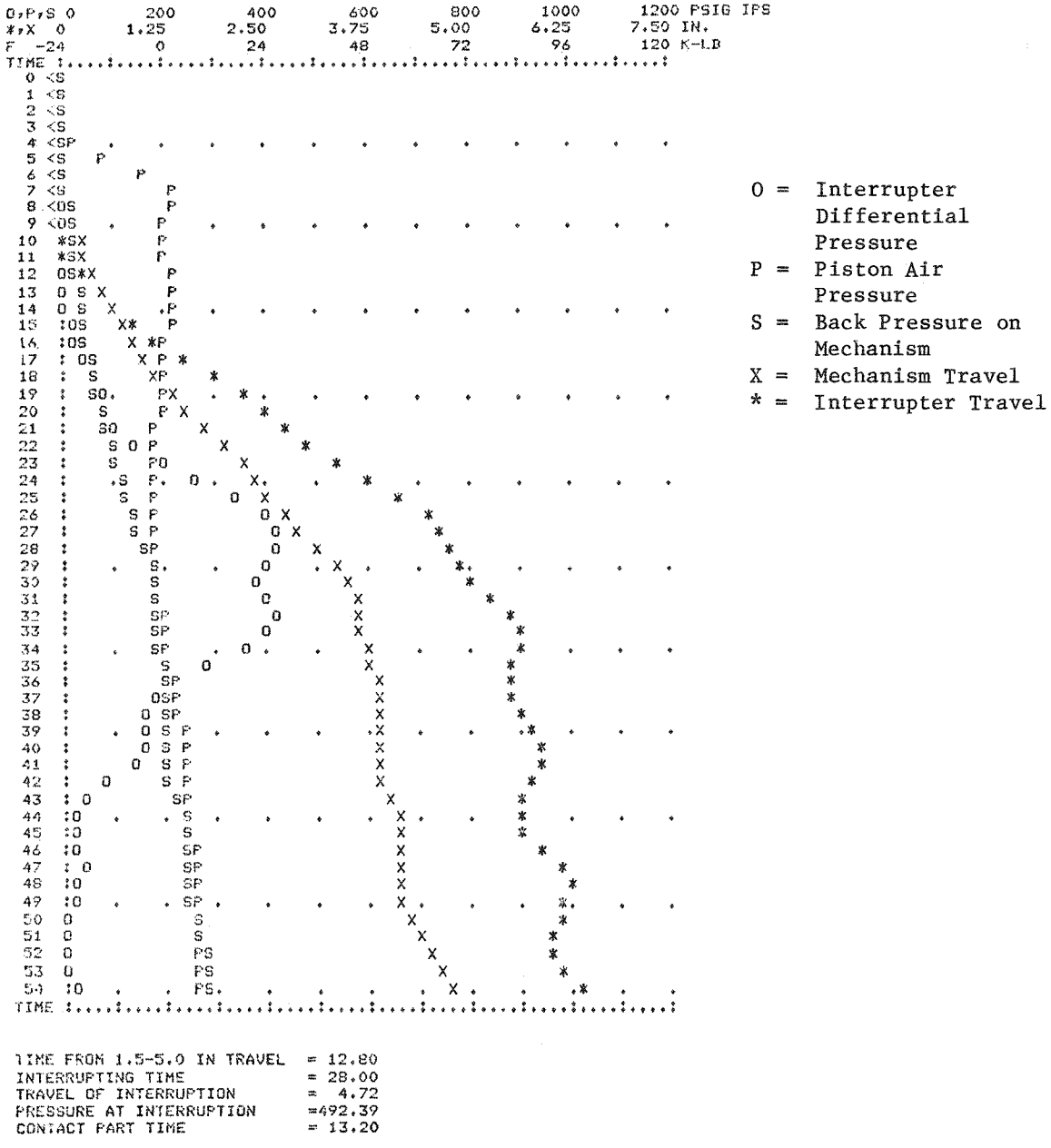


TIME FROM 1.5-5.0 IN TRAVEL = 12.80
INTERRUPTING TIME = 28.00
TRAVEL OF INTERRUPTION = 4.72
PRESSURE AT INTERRUPTION =492.39
CONTACT PART TIME = 13.20

Figure D-3 Computer Plot of 100 kA Puffer Circuit Breaker Operation

APPENDIX E

SCREEN COOLER DESIGN

## E.1 ENTRANCE COPPER SCREEN COOLER CALCULATIONS

### a. Estimates of Hot Gas Parameters

To provide the input conditions for the cooling plenum design, an estimate must be made for the mass flow rate and gas temperature at the entrance of the plenum. The assumptions made are:

- The mass flow rate is determined by the cold flow condition.
- The arc provides the energy to heat the gas.
- Gas generated from Teflon nozzle ablation is neglected.

The following parameters can be derived:

(a) mass flow rate = $1.57 \times 10^4$ g/s;
(b) arc energy per cycle of arcing = 10 J;
(c) gas temperature (100% arc energy deposition) = $2.1 \times 10^3$K

Since not all arc energy goes into heating the gas, we can only estimate, at best, the fraction of total arc energy absorbed by the nozzle, radiated away, and dissipated at the electrodes.

As an input for the cooling plenum design, we select a mass flow rate

$$m = 1.57 \times 10^4 \text{ g/s}$$

and an entrance temperature

$$T_g = 2000°K$$

### b. Heat Transfer Equations

Instead of having the screen located at the cooling plenum exit, full advantage of higher heat transfer from the gas to the copper screen can be realized by placing the screen at the entrance of the plenum where the gas temperature is higher. In order to keep the pressure drop to a minimum, the screen cooler is formed by rolling a long flat screen into a cylindrical shape with the flow parallel to the axis of the cylinder.

Differential equations describing the pressure drop, gas temperature, and screen temperature were derived (See Section 3). They are:

$$\frac{dP}{dx} = (Mm/A_{fr})^2 \quad fd\ (1 + n)^2\ /ptn^3 \qquad (4)$$

$$\frac{dT_g}{dx} = -2\ (\ MdSt/tn)\ (T_g - T_s) \qquad (5)$$

and

$$\frac{dT_s}{dt} = (4mC_gSt/A_{fr}dp_sC_s)\frac{1 + n}{n}\ (T_g - T_s) \qquad (6)$$

It is desirable to have a screen cooler design to give maximum gas temperature drop with minimum pressure drop. Using the Eqs. (4) and (5) we obtain

$$\frac{dt_g}{dP} = B\ ^2/(1 + n)^{2-b}$$

where B depends on the given screen size and gas parameters, and b relates the Reynolds to the Stanton number. In Section 3f, the value for b is determined to be -0.36.

We wish to maximize the function $dT_g/dP$ in our design. The conditions for maximum $dT_g/dP$ is

$$n = -2/b = 5.6$$

This result gives the guideline for winding for screen cooler for optimum gas temperature drop and pressure drop.

With the specified mass flow rate, m, and entrance gas temperature; and for a specific screen mesh, frontal area and length, screen and gas temperature as function of time and position con be obtained numerically by using the finite difference form of the heat transfer equations. Several screen mesh sizes and configurations were examined (see Appendix B-3). The 3-stack design with an overall length of 15 cm and diameter of 31.75 cm (12.5 in.) consisted of a 6 cm stack of 10 x 10 x .0245" screen as the first stack, 5 cm of 16 x 16 x .018" as the second, temperature rise at the end of one cycle of arcing with gas temperature at the screen exit of 1080°K. Here, the initial conditions were

$$T_s = T_g = 300°K$$

The initial screen temperature of 300°K is assumed applicable for the first full cycle of arcing. The time constant for temperature redistribution in the screen is given by

$$T = p_s C_s l^2/K$$

where l is the characteristic length of the temperature profile, and k, the thermal conductivity. For copper and l = 2 cm,

$$T = 3.5s$$

Consequently, it will take considerable time for the screen temperature profile to become more uniform. Therefore, it is desirable to avoid excessive local screen heating.

In Figure E-1, the screen temperature profiles are given for various arcing times. Near the end of the arcing cycle, the maximum screen temperature is 1050°K, and the distribution is rather uniform. Note also, it takes more than 10 ms for the hot gas to penetrate the entire screen cooler.

The gas temperature profile at the end of the arcing cycle is given by the solid line in Figure E-2. The exit gas temperature is 1300°K. Note that the first stack reduces the gas temperature by about 250°, the second by 400° and the third stack by 600°. Figure E-3 gives the exit gas temperature and pressure drop during the arcing cycle. The pressure drop rises to about 25 psi, the design criteria of 15-20 psi.

c. Cooling Plenum Volume Considerations

Knowing the exit gas temperature for the cooler, the volume can now be determined with the condition that the temperature of the gas discharged from the plenum be kept below 600°K.

d. Conclusions

Based on the expected arc energy and mass flow rate, the gas temperature at the entrance of the cooling plenum is estimated to be 1600-2000°K. Using these boundary conditions and the design requirements that the exit gas temperature is

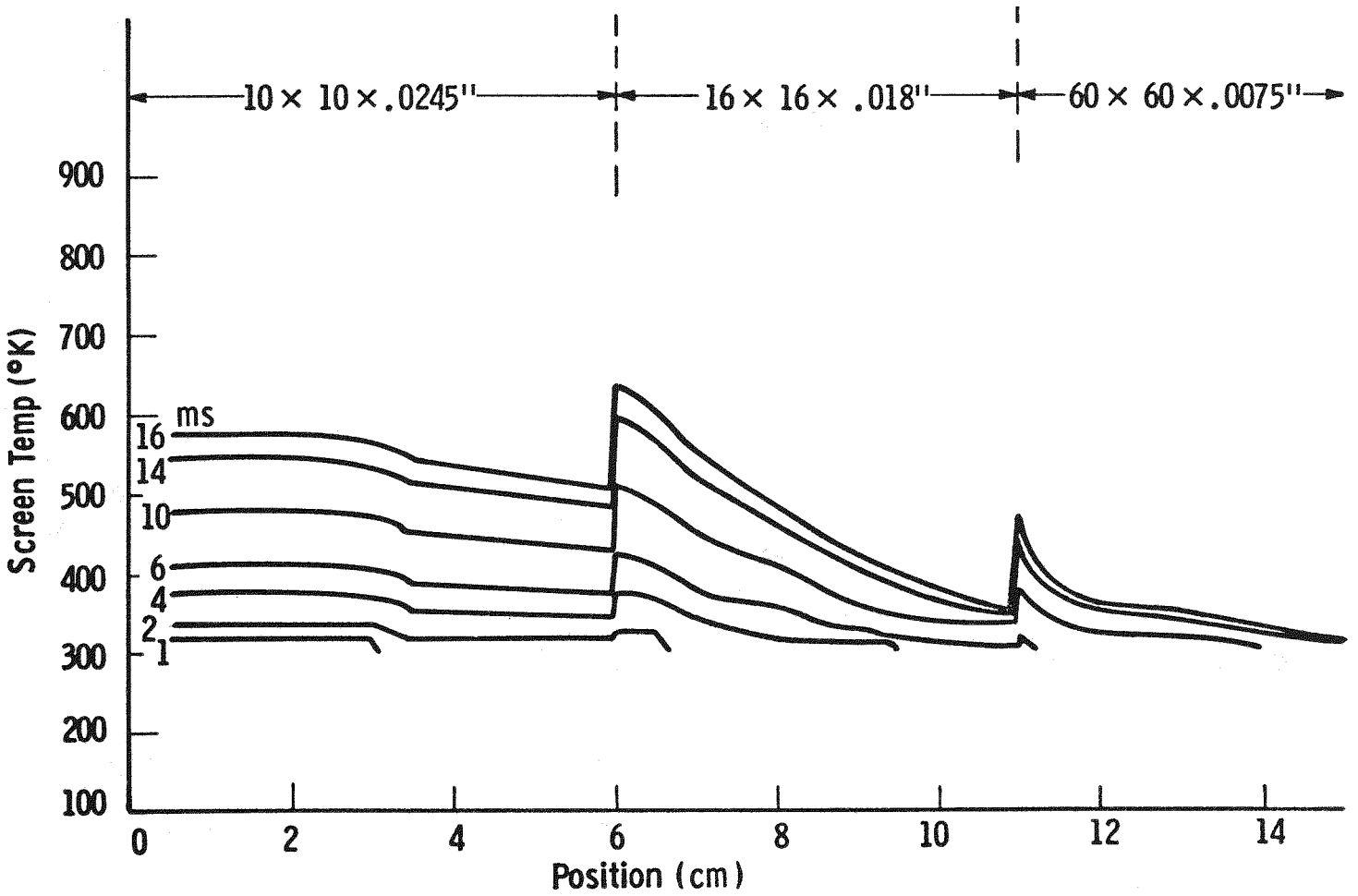


Figure E-1 Screen temperature vs. position for various arcing times

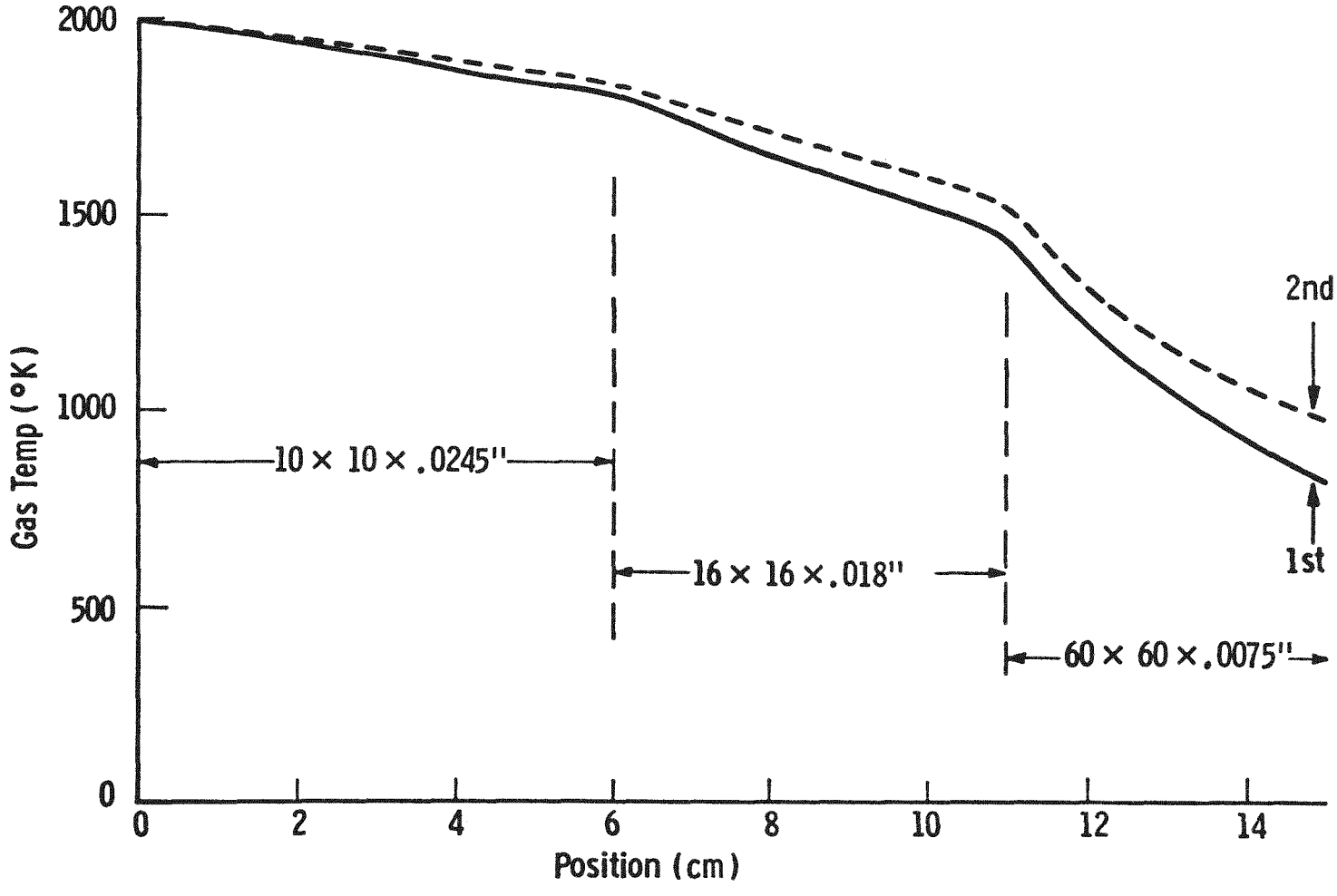


Figure E-2 Gas temperature profile at the end of the first and second arcing cycle

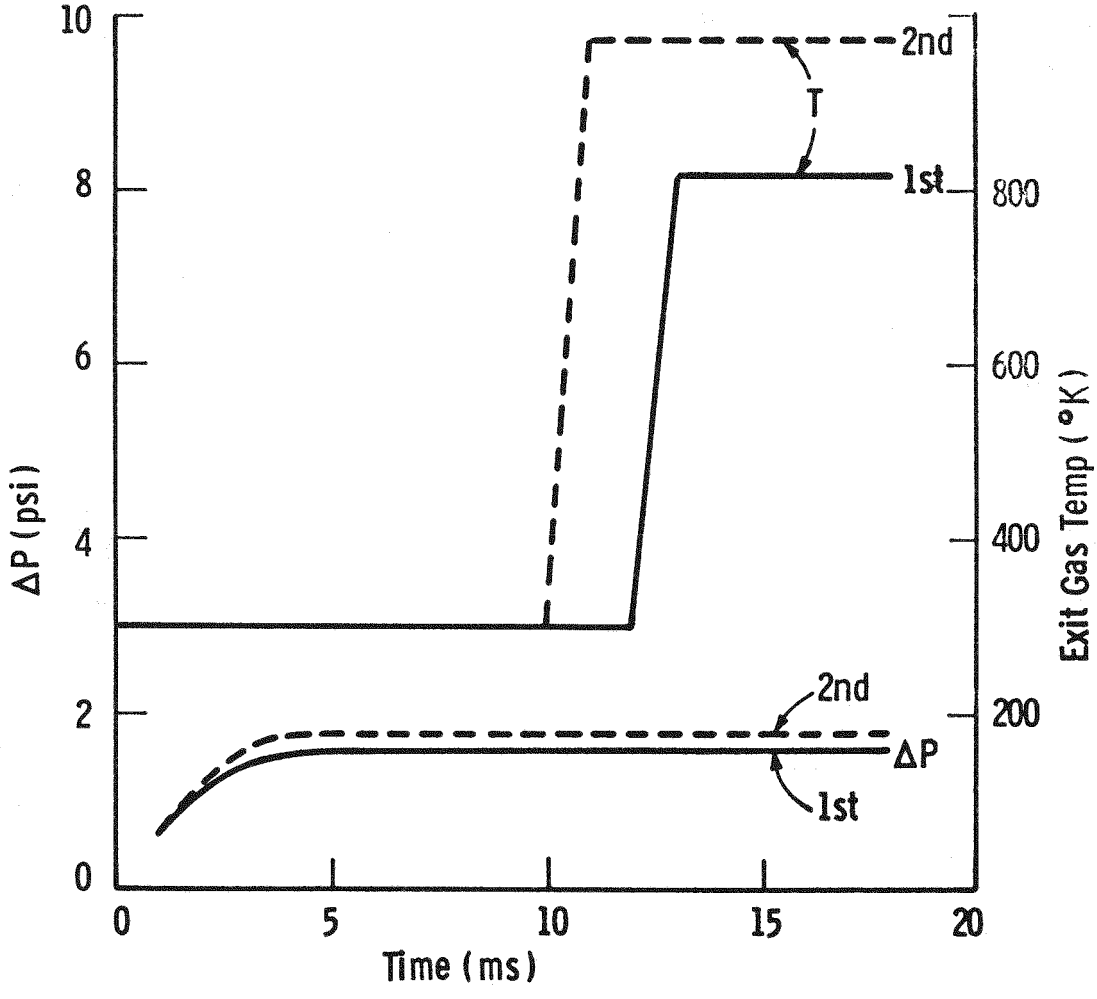


Figure E-3 Pressure drop across the entire cooler and exit gas temperature during the first and second arcing cycle

no higher than 600°K, and a pressure drop of less than 15-20 psi, calculations led to the following design; (a) a down stream cooling plenum volume of 2150 $in^3$ for a mixing fraction of 0.5 and 4230 $in^3$ for 0.2, and (b) at the entrance, a 3-stack coiled copper screen with a diameter of 31.8 cm (12.5 in.) and first stack is 6 cm long made from 10 x 10 x .0245" screen, second stack, 5 cm long made from 16 x 16 .018", and third stack, 4 cm long made from 60 x 60 x .0075" copper screen. For all stacks, the packing factor = 5.6. The calculation also showed that, (a) during one arcing cycle, maximum screen temperature 560-1050°K and screen cooler exit gas temperature is 920-1080°K.

## E.2 DERIVATION OF EXPRESSION FOR GAS AND SCREEN TEMPERATURE FOR SCREEN IN THE WINDOW OF COOLING PLENUM AND MIXING RATION CONSIDERATIONS.

The nomenclature used here is as defined in Section 3 the heat transfer from the gas to the screen is obtained from an energy balance:

$$\frac{dg}{dx} = p_g W \frac{dh}{dx} = AH \quad (T_g(x) - T_g(x, t))$$

with $h$ = gas enthalphy, $H$ = heat transfer coefficient,

$T_g$, $T_s$ = gas and screen temperature respectively.

Using the relationship between Stanton number, St, Reynolds number, Re, and Prandtl number, Pr, given by Keys and London[1] for different screens:

$$St = \frac{aRe^b}{Pr^c}$$

a, b and c being constants characterizing the screen, we arrive at the equation for the temperature drop across an arrangement

of $\frac{x}{d}$ layers of screen:

$$T_g(x) = T_s + (T_{gin} - T_s) \exp[-K_h x] \qquad (E\text{-}1)$$

with

$$K_h = \frac{a}{p} \left(\frac{d_h}{p}\right)^b \frac{1}{Pr^c} \left(\frac{pW}{u A_{fr}}\right)^b$$

$d_h$ being the hydraulic diameter of the screen. The screen temperature is a function of time, and an equation for it can be derived from a screen energy balance:

$$M_s C_s \frac{dT_s}{dt} = AH \left( T_g(x)_g - T_s(x) \right)$$

$M_s$, $C_s$ being screen mass and heat capacity, respectively. Integrating, we obtain:

$$T_s(t, x) = T_g(x) + (T_{sin} - T_g(x)) \exp\left(-\frac{t}{T}\right) \qquad \text{(E-2)}$$

with $$\frac{1}{T} = K_h \frac{C_p \, pW_d}{M_s \, C_s}$$

In order to obtain exact solutions for the gas temperature at the window exit, Equations E-1 and E-2 have to be combined. Additionaly, the initial temperature of the hot gas entering the screen has to be specified. An approximate value for this temperature can be obtained if a certian mixing of the hot gas entering the receptale with the cold gas in the receptacle is assumed. The enthalpy of the gas mixture is given by

$$h_m = \frac{Xm_h \, h_n}{Xm_h + p_c V_c}$$

where the subscripts h and c stand for hot and cold, respectively, and $V_c$ is the receptacle volume. The mixing ration X is introduced to allow for non-uniform mixing, and is defined as:

$$X = \frac{\text{fraction of hot gas mixing with certain fraction of cold gas}}{\text{fracton of cold gas}}$$

If, for example, the following mixing takes place:

50% of cold gas escapes unheated
20% mixes with 20% of the hot gas
20% mixes with 50% of the hot gas
10% mixes with 30% of the hot gas

The mixing ratio producing the highest mixing temperature

is $X = \frac{.3}{.1} = 3.$

Assuming uniform heating of the gas during one cycle at 50 kA, 1kV arc voltage, and an average mass flow rate of $1.13 \times 10^4$ g/s, given by the amount of gas displaced by the piston during one cycle, we determined the gas mixture temperature as function of the receptacle volume for several mixing ratios. The results are shown in Figure.

## E.3 DERIVATION OF HEAT TRANSFER EQUATIONS

### a. Nomenclature

| | |
|---|---|
| V | volume occupied by the coiled screen |
| L | length of screen when spread out |
| l | length of coiled screen |
| M | mesh size |
| d | wire diameter |
| t | screen thickness ( 2d) |
| N | number of screen layers in coil |
| A | total heat transfer area |
| $A_c$ | free flow area |
| D | coil diameter |
| $A_{fr}$ | frontal area = $D^2/4$ |
| a' | heat transfer area per unit volume |
| $4r_h$ | hydraulic diameter - $4A_c/A$ |
| a | spacing between layers |
| n | packing factor = a/t |
| p | porosity |
| $m_s$ | total screen mass of coil |
| f | flow friction factor |
| Re | Reynold number |
| Pr | prandtl number |
| St | Stanton number |
| u | viscosity |
| m | gas mass flow rate |
| $C_g$ | specific heat of gas |
| $C_s$ | specific heat of screen |

a. Nomenclature (Cont.)

| | |
|---|---|
| $P$ | pressure |
| $T_g$ | gas temperature |
| $T_s$ | screen temperature |

b. Relevant Relationships

(a) $N = D/2\ (a + t)$

(b) $L = \sum_{n=1}^{N} 2\ n\ (a + t) = (a + t)N^2 \quad N \quad 1$

$= A_{fr}/t\ (1 + n)$

(c) $A_c = A_{fr}$ - area blocked by layers

$= A_{fr} - tL$

$= A_{fr} n/(1 + n)$

(d) $p = A_c/A_{fr} = {}^{n}/(1 + n)$

(e) $a' = A/V = 2\,\pi dM/t(1 + n)$

(f) $4r_h = 4A_c 1\ /A$

$= 2nt/\pi dM$

(g) $m_s = \pi A_{fr} d^2 M\ p_s 1/2t(1 + n)$

(h) $Re = 4r_h \dot{m}/A_c u$

$= 2\ t\dot{m}(1 + n)/\pi dMA_{fr} u$

(i) $(St)\ (Pr)^2 = aRe^b$

c. Pressure Equation

Assumptions: neglect entrance effects, flow acceleration, and exit effect. The flow stream pressure drop due to core friction[2] is

$$P = (\dot{m}/A_c)\ ^2MfA/2p\ A_c$$

In the differential form,

$$dP/dx = (\dot{m}M/A_{fr})^2\,\pi fd(1 + n\ )^2/ptn^3 \qquad \text{(E-3)}$$

d. Heat Transfer Equations

Energy balance equations for screen

$$dQ/dt = m_sC_s dT_s/dt \qquad \text{(E-4)}$$

for gas

$$dQ/dt = -AH(T_g - T_s) \qquad \text{(E-5)}$$

and

$$dQ/dt = \dot{m}C_g \triangle T_g \qquad \text{(E-6)}$$

Combining E-4) and E-6 and with $H = mC_g\hat{S}t/A_c$

$$\triangle T_g = -2\ \ dMSt\triangle x\ (T_g - T_s)/tn$$

In differential form,

$$dT_g/dX = -2\pi Md(St)\ (T_g - T_s)/tn \qquad \text{(E-7)}$$

Combining (B-2) and (B-3),

$$dT_s/dt = AH(T_g - T_s)m_sC_s$$

Substituting the expressions for H and $m_s$,

$$dT_s/dt = 4\dot{m}C_gSt\ (1 + n)\ (T_g - T_s)/A_{fr}n\ dp_sC_s \qquad \text{(B-6)}$$

The equations E-3, E-6 and E-7 are the desired differential equation describing $T_g$, $T_s$ and P.

e. Empirical Screen Friction Factor and Relationship Between Re, St, and Pr Determination of f

The frictional factor, f, is not a strong function of Re for large Re ($10^3$). Approximately the coiled screen configuration by a pin-fin surface, we obtained the following values:

| | | | |
|---|---|---|---|
| n | = | 2 | f = .08 |
| n | = | 3 | f = .09 |

For our case of n = 5.6, we take f = 0.1.

f. Relationship Between Re, Pr, and St

Again using the pin-fin approximation, the following empirical relations can be written:

$$St = aRe^{b}/Pr^{c}$$

Experimental data showed that

| | | | | | | | |
|---|---|---|---|---|---|---|---|
| n = 1 | c = 2/3 | a = 0.1 | b = -0.36 |
| n = 2 | c = 2/3 | a = .23 | b = -0.37 |
| n = 3 | c = 2/3 | a = .26 | b = -0.35 |

For our case of = 5.6, take

c = 2/3 a = .3 and b = -.36

or $St = .3Re^{-.36}/Pr^{2/3}$

REFERENCES


1. Kays, W. M. and A. L. London, Compact Heat Exchanges, National Press, Palo Alto, CA, 1955.

2. Ibid., p. 21.

3. Ibid., p. 110-112.

APPENDIX F

# ANALYSIS OF PHOTOGRAPHIC ARC STUDIES AND RECOMMENDATIONS FOR FUTURE WORK

Photographic arc studies of double flow $SF_6$ arcs had been carried out by Westinghouse prior to the start of this project. This appendix describes the analysis of those studies, the development of important arc parameters for $SF_6$ interrupter design and the recommendations for further photographic arc studies. It was decided after the study of these results that more significant data could be obtained from the electrical testing of interrupters at currents close to the objectives of this project. Therefore no further photographic studies were carried out. Values of arc temperature, arc area and arc conductance obtained from these studies were used in the subsequent analysis of alternate interrupter designs.

## F.1 ARC COLUMN DECAY CHARACTERISTICS APPROACHING CURRENT ZERO

### Introduction

Since $SF_6$ gas-blast circuit breakers interrupt fault currents by rapidly developing sufficiently high column resistance so that appreciable current cannot flow after current zero, the characteristics of this process are of vital interest. Considerable information can be developed from the fast arc photographs described in this report combined with the electrical data.

A complete description of this process requires nearly instantaneous measurement of temperature profiles at several instants a few microseconds before and after current zero, such as has been done by Hermann et al., (1) for the upstream, high-pressure section of a 24 atmosphere nitrogen arc. Such information would be required in $SF_6$ arcs, and at downstream arc sections as well, and requires far more elaborate instrumentation techniques than we had in this non-spectrographic photographic study. However, some useful insights into the column decay behavior can be obtained without the time and expense this effort would require. A typical set of high speed two axis photographs of a 2000 Ampere arc is shown in Figure F-1. The views shown in each frame of the Figure, frame #1 for example, are respectively the front and top views of the arc.

Relation Between Arc Radiation and Electrical Conductivity

A complete and definitive study of radiation emission coefficients of $SF_6$ at 1 and 10 atm. pressure has recently been published by Liebermann and Lowke (2). Their data for total emissivity, $e_o$, and for the net emission coefficient for an isothermal cylinder of radius 0.1 cm, $e_n(0.1)$, are plotted against plasma electrical conductivity, c, in Figure F-2 for $SF_6$ at a pressure of 10 atm. Both are seen to vary approximately as $c^3$. However, much of this radiation is below 2000 A and strongly absorbed; the lines and continuum above 2000 A , which accounts for most of the escaping radiation and is recorded by the camera, rise much less rapidly with temperature (and thus with c) than the total radiation, as seen in Figure F-3. The effect on cascade arcs in $SF_6$ at 1 atm. pressure as observed by Hertz et al.,(3) is the most that the power radiated by the arc varies approximately linearly with arc current. Since the electric field varies relativly little(3) and the arc area expansion is limited by the cascade well, their data suggests approximate proprotionality to the first power of c.

The characteristics of isothermal arcs in 10 atm. of $SF_6$ are shown in Figure F-4 from Liebermann and Lowke, (2), with radiation as the only energy loss mechanism considered. The third frame before current zero in Run 8911 occurs when the current is about 200 Amperes, and the arc voltage about 2150 Volts. Entering Figure F-2 at 200 Amps, rising to the intersection of the R = 0.1 cm solid line and the 18,000°K temperature, a reasonable value for this current, we read a radiation loss field of 70 V/cm. The distance between electrodes is 17.15 cm (6-3/4 inches), which gives a 21.5 cm arc length if we assume 25% lengthening due to cork-screwing effects downstream of the nozzle throats as suggested by the photographs. Dividing the observed arc voltage by 21.5 cm arc length we obtain 100 V/cm as the measured average arc gradient for this frame. Thus radiation comprises 70% of the total loss, and may be presumed to be the dominant loss mechanism throughout the current range spanned by out photographs. Note that a slightly falling line through the above-mentioned point (200 Amps, 70 V/cm) in Figure F-2 describes (reading from right to left) an arc history consistent with available information as the current falls to zero: the arc radius falls so that falling area accounts for most of the current fall, the arc temperature falls slowly, and the electric field increases slowly. With the additional assumption that the fraction of total radiation that escapes the arc environment, varies little with current, the side-on observations represented by our arc photographs will yield information on the relative values of arc conductivity as the current falls to zero.

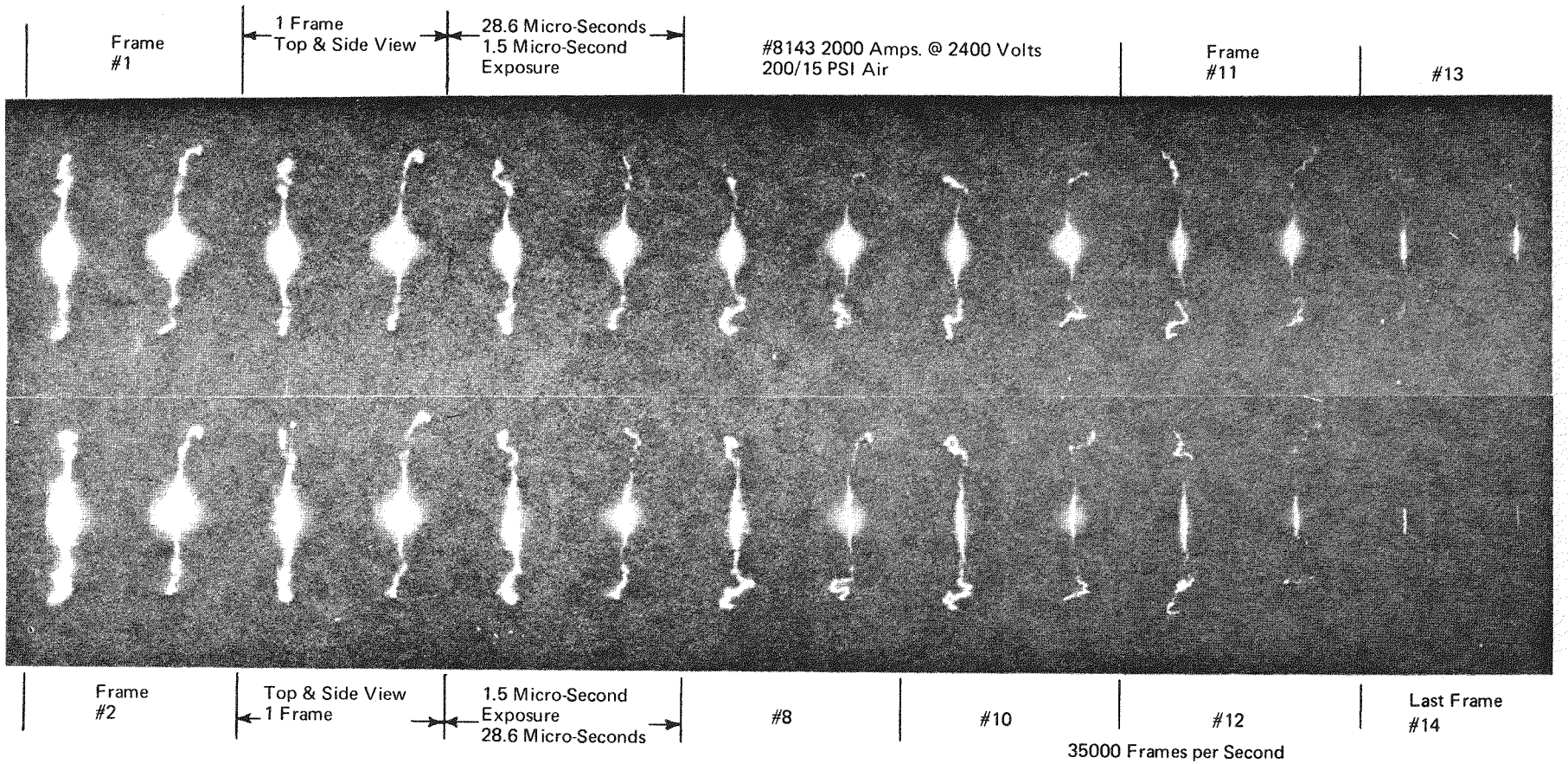


Figure F-1 Photos of the Arc with the Beckman and Whitley 350 Camera (Note: Consecutive frames alternate between top and bottom rows of frames seen below. Two are views per frame)

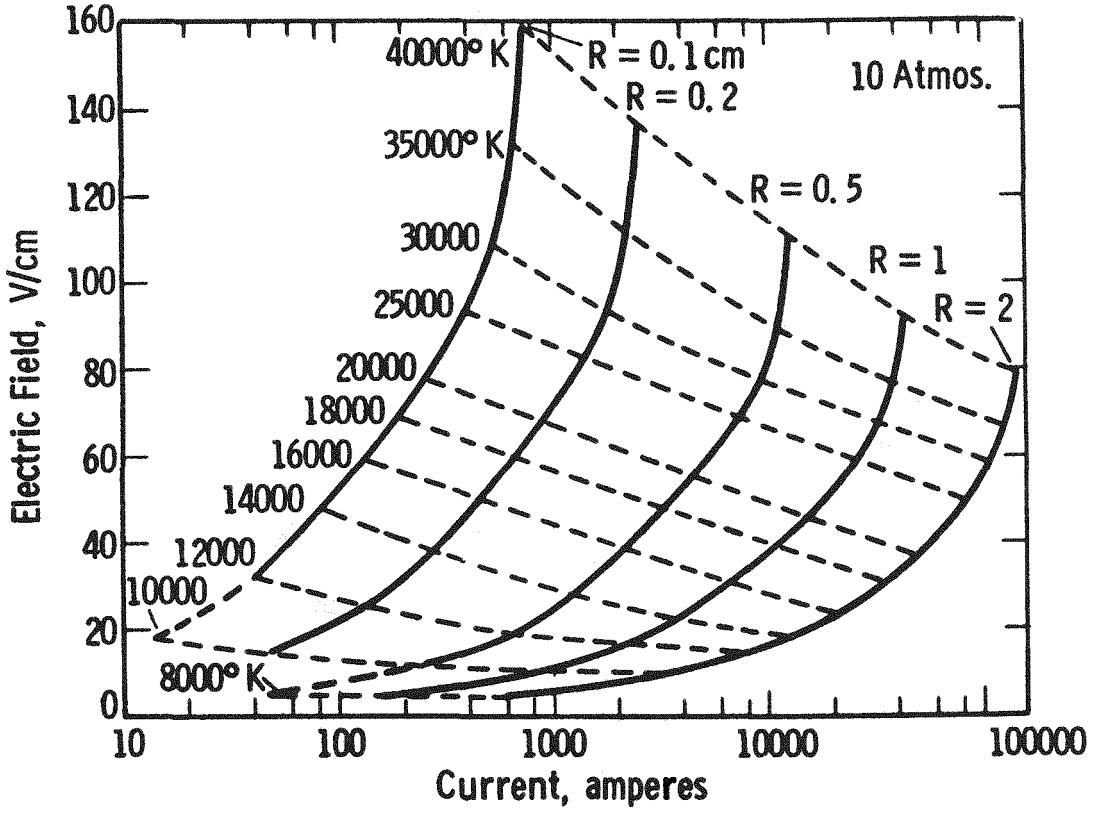


Figure F-2 Values of central temperature and electric field strength as a function of arc current and radius for a pressure of 10 atmospheres (Ref. 2).

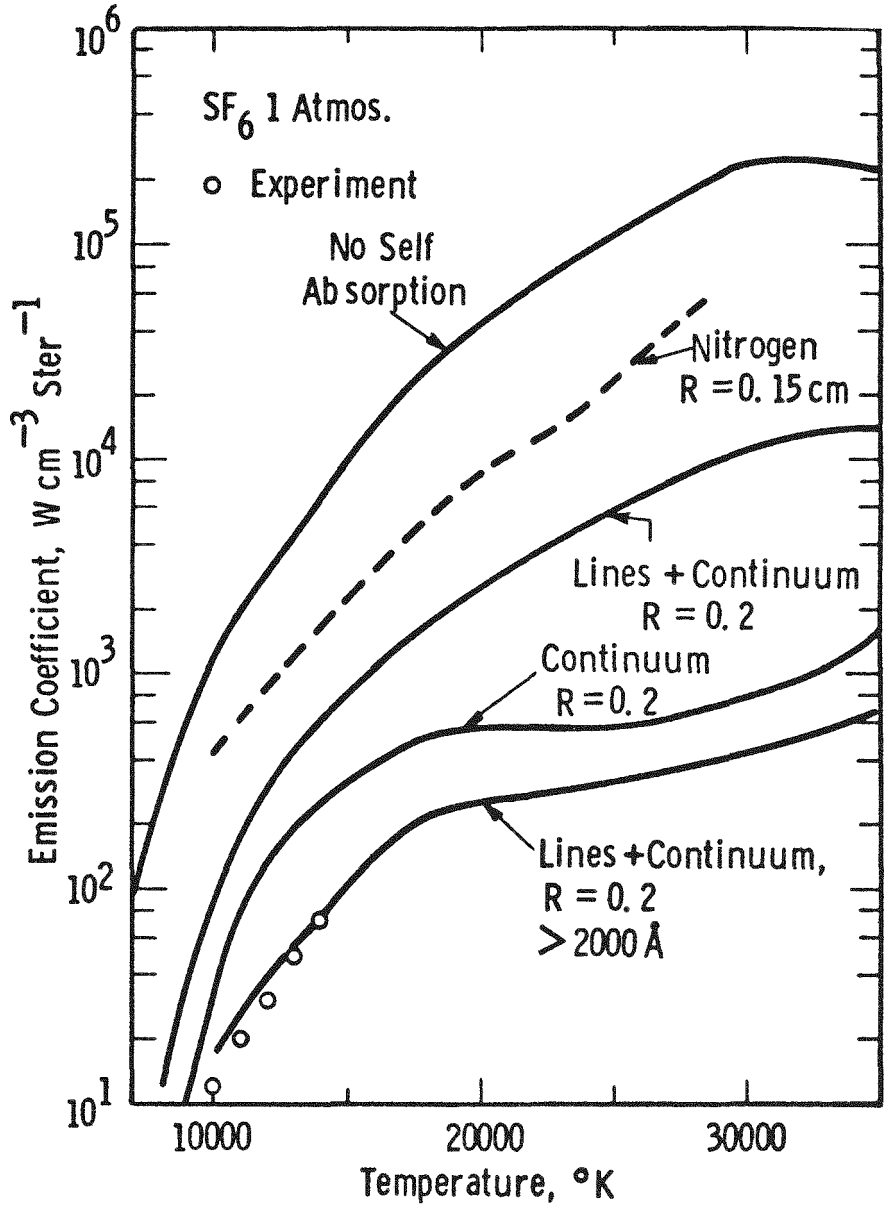


Figure F-3 Contribution of radiation from the continuum and 2000 Å to the total emission coefficient. Experimental points are for radiation 2000 R (Ref.2)

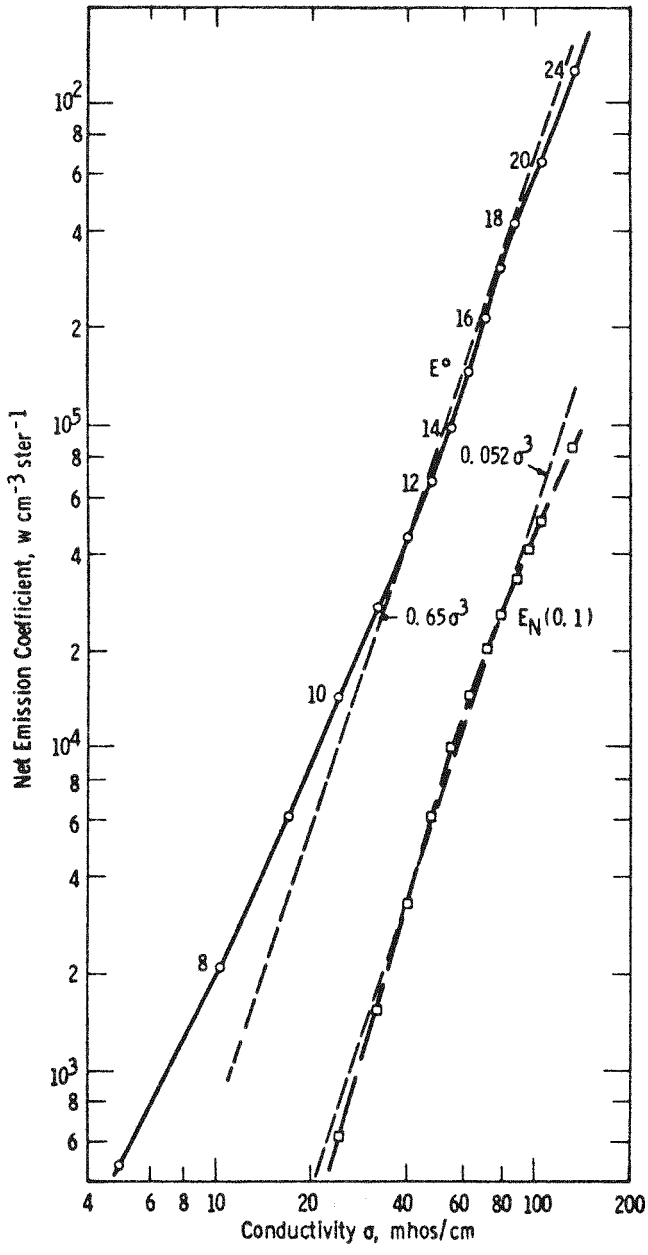


Figure F-4 Net emission coefficient for cylindrical isothermal plasmas of radius 0 ($E^o$) and 0.1 cm $E_N$ (0.1), 10 atm $SF_6$ (Lowke and Liebermann)

Microdensitometer Measurement of the Side-On Intensitites $J_o$ (X) and $J_1$ (X)

Three traverses were made across the arc in each of the last few frames before current zero, measuring the optical transmission T (X) of the film at a distance from arc center corresponding to X cm in the arc, with a Gaertner mass spectrometer photoplate comparator. One scan was made across the high pressure arc section between the nozzles, the other two across the left and the right downstream sections. The photomultiplier output was recorded on a strip chart while the arc image was driven past the slit at a constant, known speed, and the tranmission obtained directly by having adjusted the photomultiplier accelerating voltage to give a full scale reading with the film base, i.e. 100% transmission.

Using frames from Run 8916 with and without a neutral density filter rated 1.3, i.e. its insertion reduces light by a factor of $10^{1.3} = 20$, we were able to derive a calibration curve for the developing processing used with these films, which was consistent with the manufacturers specification for the Plus-X film used(4). It can be simply expressed with adequate accuracy as

$$J(X) = \frac{100}{T(X) - 0.3} - 3.5 \qquad \text{(F-1)}$$

where T(X) is the measured percent transmission at a distance X units from the arc axis, and the derived exposure is equated (in arbitrary units) to the side-on intensity at that value of X, since the frame exposure time is the same for all positions and frames. The constant 3.5 represents gross fog, higher than usual, apparently due to excessive light scattering inside the camera. The other constant 0.3 represents the upper limit in film density and corresponds to the value specified for 16 minutes developing time.

For each microdensitometer scan, T(X) was read at several values of X, and J(X) calculated by means of Eq. F-1. The results for the last four frames before current zero of Run 8911 are plotted against $r^2$, assumed equal to $X^2$, in Figure F-5

We plot J(X) vs $r^2$, rather than r or X, for two reasons. If J(X) is proportional to o(r), as we are suggesting, then the area under the J(X) vs $r^2$ curve will be proportional to the conductance of a unit length of the arc at the location. Secondly, the Abel transform(5) of a J(X) vs $X^2$ curve that is slightly concave upward, such as fits most sets of points in Figure F-5, is a straight line on the J(r) vs $r^2$ plot, i.e., triangular profile, with nearly the same base width as

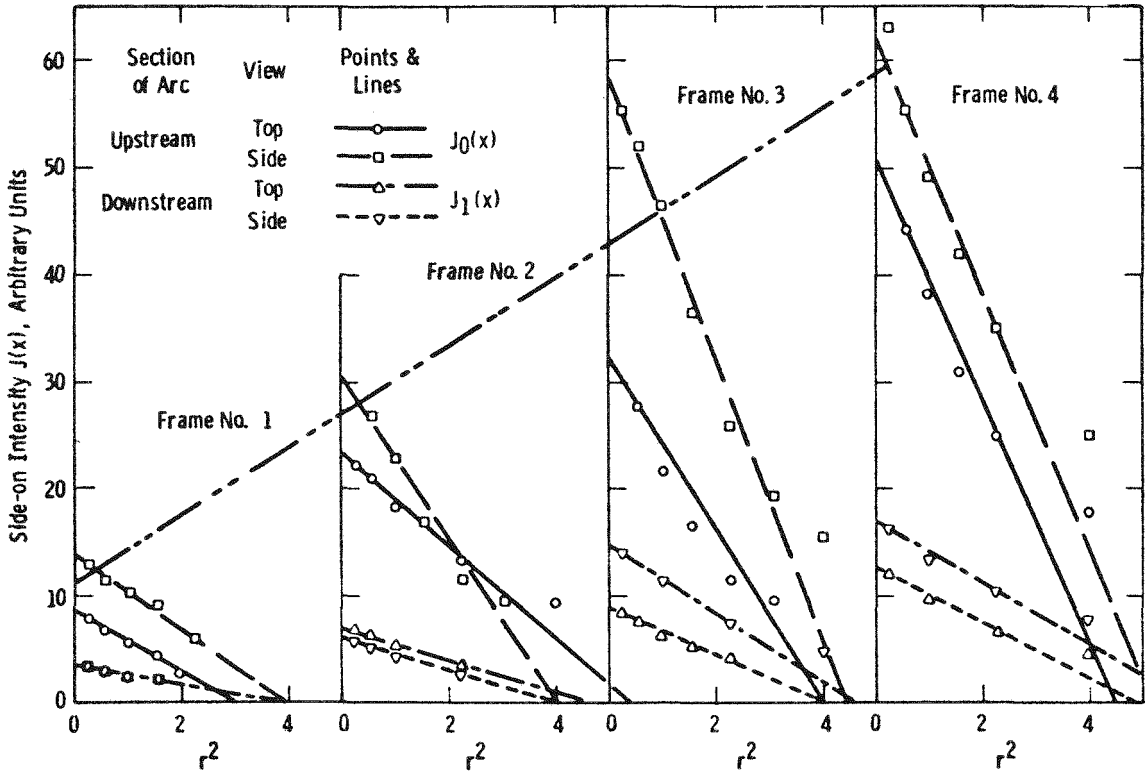


Figure F-5 Side-on Intensity Distribution for Frames no. 1 to 4 of run 8911

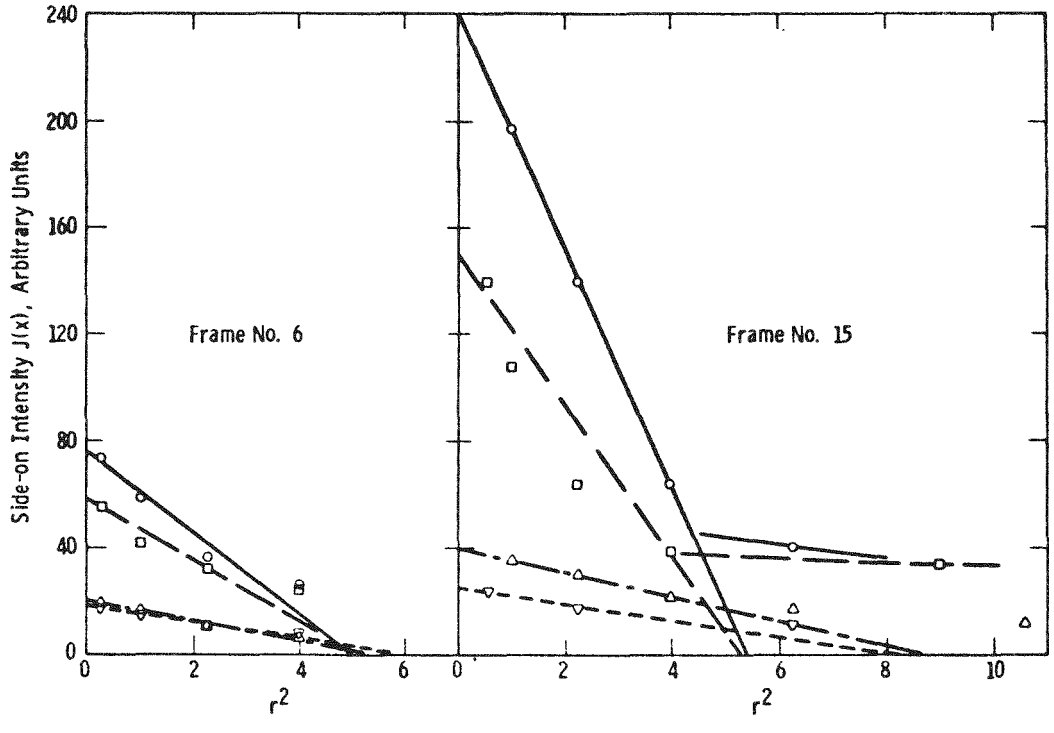


Figure F-6 Side-on intensity distribution for frames no. 6 and 15 of run 8911

the best triangular thru the J(X) vs $X^2$ points. This becomes a parabolic J(r) vs r distribution. Thus, at the present level of approximation, we draw the best line through the J(X) vs $X^2$ ($=r^2$) points, and consider it the same as the J(r) vs $r^2$ plot we would obtain if we did an Abel inversion calculation for each curve.

Straight lines fit the points reasonably well in each case in Figure F-5, with the side view generally giving greater axial intensity, J(0). The interval between frames in Run 8911 was 31.3 usec, the current slope (4700 A rms) was 2.50 A/us, so each successive frame (moving to the right in Figure F-5, although backwards in real time) was at a current greater by 78.4 Amps. The broken line through the average of top and side view $J_o$ (0) (the subscript "0" denoting the high pressure section of the arc between the nozzles) intersects the $r^2$ axis at 0.7 times one frame interval, fixing the current zero point and establishing the current for frame 1 as approximately 0.7 x 78.4 = 55 Amps. Reading the arc voltage at the time of each picture and dividing for arc conductance, we get the electrical data listed in Table F-1.

TABLE F-1

ELECTRICAL PARAMETERS FOR FRAMES OF RUN 8911

| Frame No. | 1 | 2 | 3 | 4 | 6 | 15 |
|---|---|---|---|---|---|---|
| Time before i = 0, usec | -22 | -53 | -84.5 | -116 | -178.5 | -460 |
| Current, i (t), A. | 55 | 133 | 212 | 290 | 447 | 1146 |
| Arc voltage, V (t), V. | 2620 | 2350 | 2150 | 2050 | 1850 | 1450 |
| Conductance, i (t)/V (t), mmhos | 21.0 | 56.7 | 98.5 | 141.5 | 241.5 | 790 |

The J(X) vs $r^2$ plots for frames 6 and 15 are shown in Figure F-6. For these frames the $J_o$ (0) values for top view are greater than those for the side view; the reason for the reversal is not known. There is more tailing at large $r^2$, like a radiating cloud around the arc, in frame 15 than any other.

In both Figures F-5 and F-6 for each frame, the left and right downstream scans are combined into a $J_1(X)$ for each view, top and side, to reduce the scatter of the data presented.

In general, the downstream sections were more variable due to turbulent snaking of the arc channels.

The intercept values $R_a^2$ vary less than expected with arc current. This appears to be mainly due to erroneously large arc images on the negative, apparently caused by imperfect focusing, the error being greatest at the lowest current. We have used arbitrary units for $r^2$ in all plots for this reason, and consider information on $R_a^2$ less reliable than on $J_o(0)$ and $J_1(0)$.

## F.2 ANALYSIS AND INTERPRETATION

An increase in the ratio of the downstream axial intensity, $J_1(0)$, to the upstream value, $J_o(0)$, as the current falls toward zero can be seen in Figures F-5 and F-6. In frame 15, $J_1(0)/J_o(0)$ is about 1/6, while in frame 1 it is about 1/3. This suggests a relatively increasing electric field downstream as the current falls, i.e., that the downstream arc section carry a larger share of the total arc voltage just before current zero than they do at higher currents. This agrees with the findings of the Brown Boveri group, that the arc section downstream of the throat increase in resistance before and after current zero at a rate considerably faster than does the high pressure arc section. They established that turbulence in the form of mm. scale eddies is the efficient heat transfer mechanism responsible for this rapid channel cooling in the downstream arc sections.

The central intensity values, $J_o(0)$ and $J_1(0)$, and the arc size intercepts, $R_a^2$ in arbitrary units, as read from Figures F-5 and F-6 are listed in Table F-2. A log-log plot of the $J_o(0)$ data vs arc conductance in Figure F-7 gives a slope of about 0.8. The $R_a^2$ data gives a slope of about 0.1, for a combined conductance per unit length (assuming as usual that c(r) is proportional to J(X)) varying as the total arc conductance to the 0.9 power. Even at over 1000 Amps, frame 15, the high pressure section of arc is more Mayr than Cassie, i.e., it loses conductance more through cooling than through area reduction.

Similar plots for the downstream data in Table II are shown in Figure F-8, and give slopes of 0.67 and 0.27 for $J_1(0)$ and $R_a^2$. The combined value, conductance per unit length, slope is about 0.95, greater than for the high pressure section as concluded previously. Both combined slopes are probably too low, partly because of the excessive $R_a^2$ at low currents resulting in under-estimating the $R_a^2$ slopes, and partly due to increasing arc lengthening due to turbulent looping as the current decreases.

TABLE F-2

ARC CENTRAL INTENSITIES AND $R_a^2$ VALUES

| | Frame No. | | 1 | 2 | 3 | 4 | 6 | 15 |
|---|---|---|---|---|---|---|---|---|
| Upstream | Conductance, mmhos | | 21.0 | 56.7 | 98.5 | 141.5 | 241.5 | 790 |
| | $J_o(0)$ | Top | 8.6 | 23.3 | 32.2 | 50.8 | 76 | 241 |
| | | Side | 13.7 | 30.5 | 58 | 62 | 58 | 150 |
| | $R_a^2$ | Top | 3.0 | 5.4 | 4.0 | 4.5 | 5.0 | 5.4 |
| | | Side | 4.0 | 4.0 | 4.4 | 5.2 | 5.1 | 5.3 |
| Downstream | $J_1(0)$ | Top | 3.5 | 6.8 | 8.9 | 12.5 | 20 | 40 |
| | | Side | 3.5 | 6.0 | 14.7 | 16.9 | 18.5 | 25 |
| | $R_a^2$ | Top | 3.7 | 4.0 | 4.0 | 4.9 | 5.3 | 8.7 |
| | | Side | 3.7 | 4.0 | 4.6 | 5.9 | 6.0 | 8.0 |

Microdensitometer scans were taken for 5 frames of Run 8916, at 10,700 Amps rms current and 36 usec between exposure. There was an unexplained difference in $J_o(0)$ and $J_1(0)$ trends between the odd numbered frames and the even numbered ones, as if some unexplained light absorption were occurring on one path and not on the other one. The profiles showed much more tailing than those of Run 8911, i.e., the intensity fell very slowly with $r^2$ beyond the central peak. No further analysis seem justified because of these problems.

## F.3 SUMMARY AND RECOMMENDATIONS

By taking microdensitometer scans of the arc photograph negatives approaching current zero, information on the relative rate of decay of the high-pressure and downstream arc sections can be obtained. It has been shown that side-on light intensity is essentially proportional to the local arc conductivity, so that information on the arc temperature profile can also be obtained.

In order to justify continuing this work, several improvements should be made:

1. The interval between pictures should be reduced an order of magnitude if possible, to about 3 usec, so that changes in the arc column close to current zero can be studied;

2. The focus must be sharpened and the amount of light scattering inside the camera greatly reduced;

3. The size of the arc cross section image on the negative should be increased by framing one (or both) downstream section, so that more accurate radial determinations may be made.

The projected difficulty and cost of carrying out these recommendations was so large that it was decided that more valuable information could be obtained in less time at less expense by making tests of a full scale model interrupter at currents near the objective (120 kA) of this project.

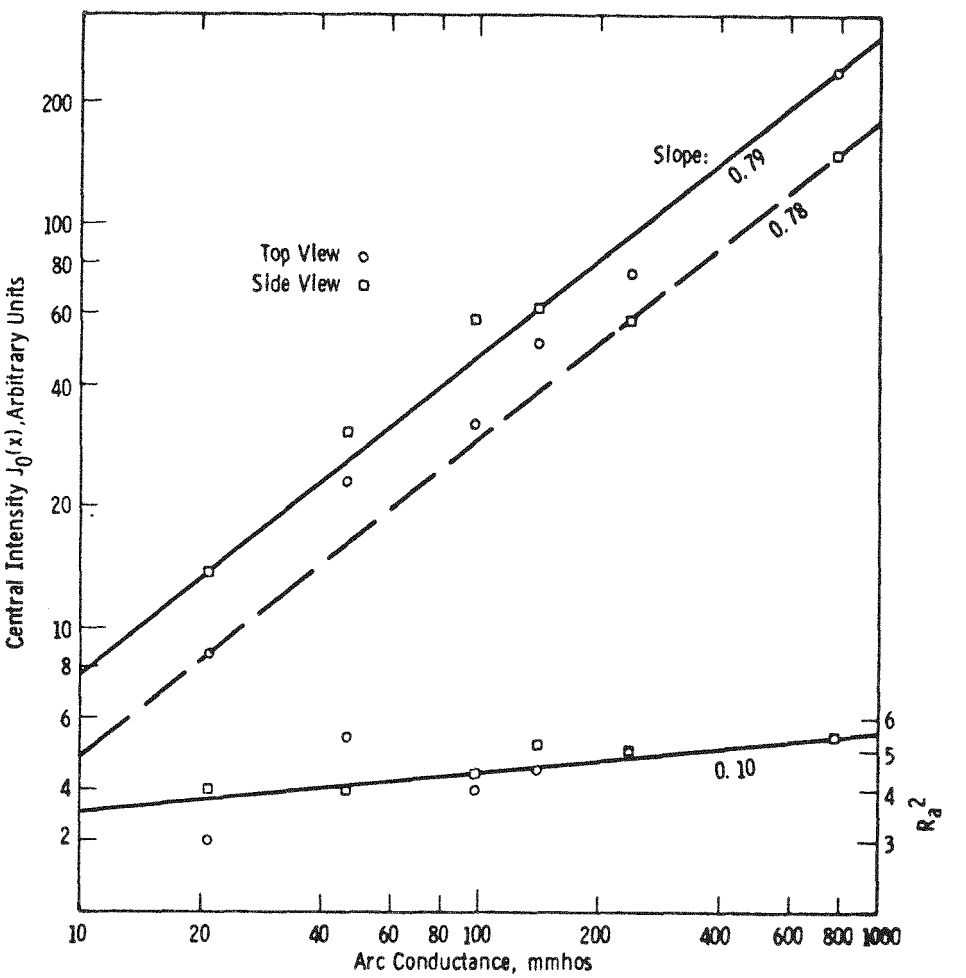


Figure F-7 Central Intensity J(0) and square of arc radius vs arc conductance, high pressure section, film 8911

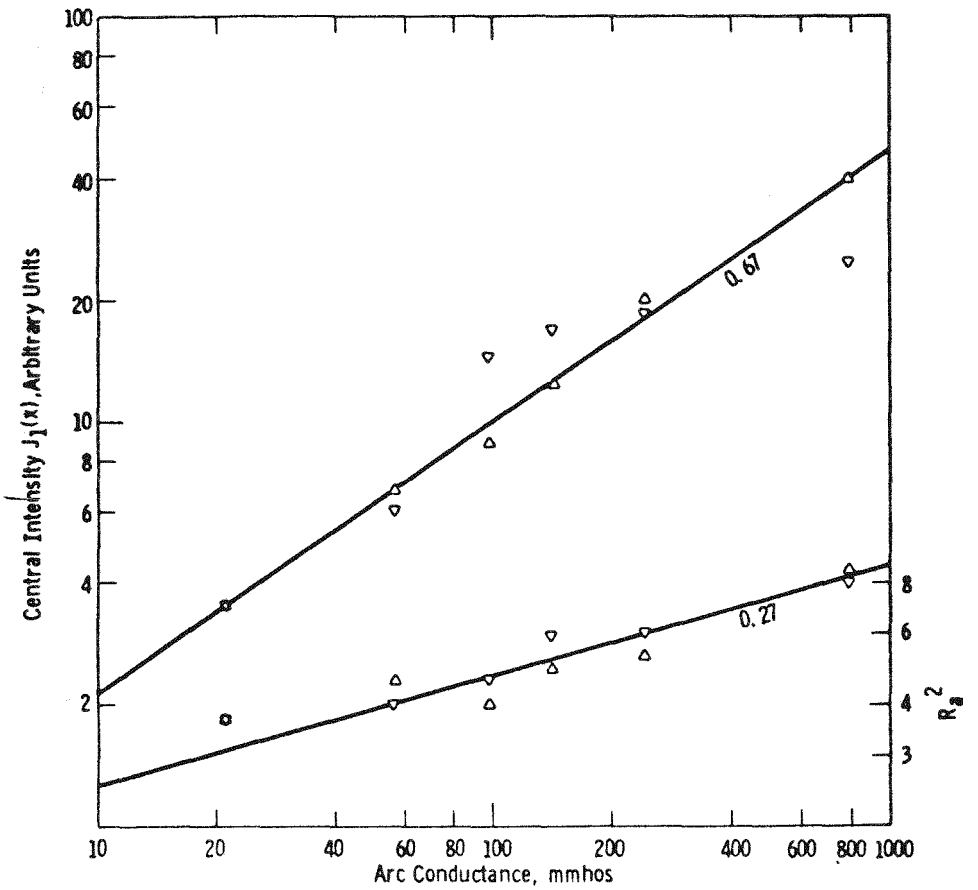


Figure F-8 Central Intensity J (0) and square of arc radius vs arc conductance average of left and right low pressure sections, film 8911

REFERENCES


1. W. Herman, L. Niemeyer, and E. Schade, "The Transient Behavior of Axially Blown High Pressure Arcs", Gas Discharges, IEE Conference Publication #118, Sept. 1974.

2. R. W. Liebermann and J. J. Lowke, "Radiation Emission Co-efficients for Sulfur Hexafluoride Arc Plasmas", J. Quant. Spectroscopy and Radiative Transfer, scheduled for December, 1975.

3. W. Hertz, H. Motschmann and H. Wittel, "Investigations of the Properties of $SF_6$ as and Arc Quenching Medium", Proc. IEEE 59, 485-92, (1971).

4. Eastman, Kodak Plus-X Pan Film Emulsion Characteristics, DS 12-13.

5. R. N. Bracewell, "Strip Integration in Radio Astronomy", Austral. J. Phys. 9, 198 (1956). See the fourth row from the top of Fig. 2, some Abel transforms, Page 204.